Oguz Akin
Editor

Atlas of Gynecologic Oncology Imaging

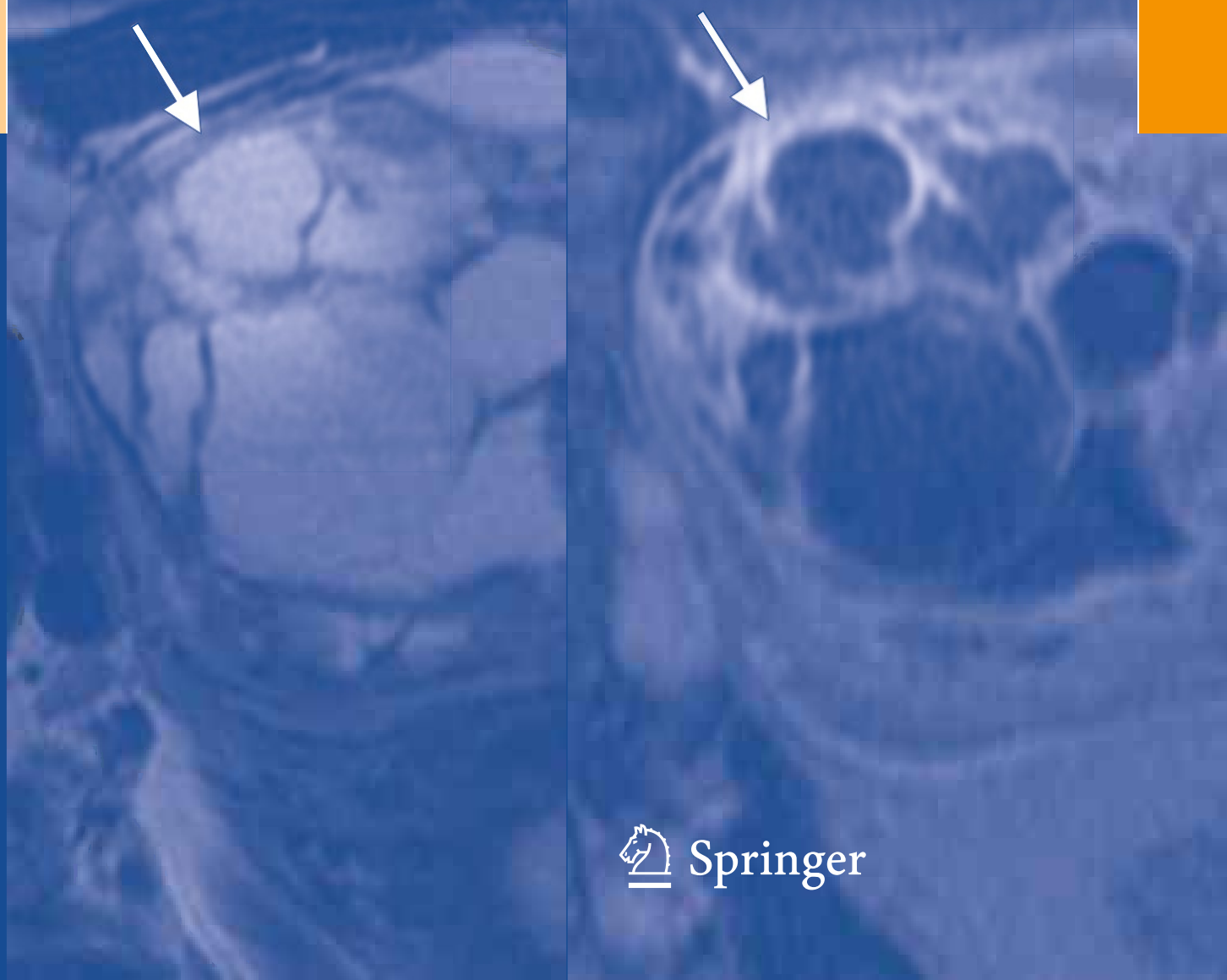

Springer

Atlas of Oncology Imaging

For further volumes:
http://www.springer.com/series/8759

Oguz Akin
Editor

Atlas of Gynecologic Oncology Imaging

Springer

Editor
Oguz Akin, MD
Weill Medical College of Cornell University
New York, NY
USA

Department of Radiology
Body Imaging Service
Memorial Sloan-Kettering Cancer Center
New York, NY
USA

ISBN 978-1-4614-7211-7 ISBN 978-1-4614-7212-4 (eBook)
DOI 10.1007/978-1-4614-7212-4
Springer New York Heidelberg Dordrecht London

Library of Congress Control Number: 2013949540

Printed on acid-free paper

Springer is part of Springer Science+Business Media (www.springer.com)

Foreword

Progress in cancer imaging is as relentless as the pounding of the waves against the seashore. New techniques are constantly being added to the imaging armamentarium, and more and more imaging biomarkers relevant to clinical decision-making are being discovered. As a result, the radiologist's job is daily becoming both more important and more challenging. This *Atlas of Gynecologic Oncology Imaging* will be of value to radiologists and referring physicians of all experience levels who seek to harness the growing powers of imaging for the benefit of patients.

Perhaps the most unique strength of this *Atlas* is that it was written entirely by gynecologic imaging specialists who are members of the gynecologic oncology disease management team at Memorial Sloan-Kettering Cancer Center (MSKCC). The text thus presents a coherent view of the roles of standard and cutting-edge imaging techniques in gynecologic oncology, developed in an institution with a multidisciplinary, team approach to cancer care.

Covering all modern cross-sectional modalities (CT, MRI, US, and PET), the *Atlas* presents a rich array of images culled from MSKCC's ample selection of straightforward and challenging cases. It depicts normal anatomy as well as common gynecological tumors. For each type of cancer, primary staging and recurrence patterns are illustrated. Also discussed is the integration of findings from different, yet complementary, imaging modalities. For every cancer, at every stage of management, the authors list the pertinent findings to include in the radiology report. Throughout, the focus is on using imaging to inform the clinical decision-making.

New York, NY, USA — Hedvig Hricak, MD, PhD, Dr hc
New York, NY, USA — Richard R. Barakat, MD

Contents

Contributors

Asim Afaq, MD Department of Radiology, Memorial Sloan-Kettering Cancer Center, New York, NY, USA

Oguz Akin, MD Weill Medical College of Cornell University, New York, NY, USA

Department of Radiology, Body Imaging Service, Memorial Sloan-Kettering Cancer Center, New York, NY, USA

Irene A. Burger, MD Department of Radiology, University Hospital Zurich, Zurich, Switzerland

Pier Luigi Di Paolo, MD Department of Radiology, Memorial Sloan-Kettering Cancer Center, New York, NY, USA

Yulia Lakhman, MD Department of Radiology, Body Imaging Section, Memorial Sloan-Kettering Cancer Center, Evelyn H. Lauder Breast Center, New York, NY, USA

Duan Li, MD Department of Radiology, Memorial Sloan-Kettering Cancer Center, New York, NY, USA

Weining Ma, MD Department of Radiology, Memorial Sloan-Kettering Cancer Center, New York, NY, USA

Department of Radiology, NewYork-Presbyterian Hospital/Weill Cornell Medical Center Diagnostic Radiology, New York, NY, USA

Neeta Pandit-Taskar, MD Department of Radiology, Memorial Sloan-Kettering Cancer Center, New York, NY, USA

Harpreet K. Pannu, MD Department of Radiology, Memorial Sloan-Kettering Cancer Center, New York, NY, USA

Hebert Alberto Vargas, MD Department of Radiology, Memorial Sloan-Kettering Cancer Center, New York, NY, USA

Ovarian Cancer

1

Hebert Alberto Vargas, Pier Luigi Di Paolo,
Asim Afaq, and Oguz Akin

1.1 Anatomy, Histology, and Imaging Techniques

The ovaries are paired pelvic organs typically found below the bifurcation of the common iliac vessels lateral to the uterus (Table 1.1). They are responsible for hormone secretion and the production of female reproductive cells. Histologically, the ovaries are composed of follicles embedded in a mesh of stroma formed of connective tissue and spindle cells and covered by a layer of surface epithelium (Table 1.2). Abnormal proliferation of any of the tissue types can result in both benign and malignant ovarian tumors.

Ovarian cancer is the most lethal of all gynecologic tumors [1]. It is a genetically heterogeneous disease with a poor prognosis; and despite advances in technology and chemotherapeutic agents, the mortality from ovarian cancer has remained stable for the past 50 years [1]. Although it is sensitive to platinum-based chemotherapy, the 5-year survival for patients with advanced disease is only 30 % [1, 2]. The high mortality reflects advanced stage at presentation, including spread to serosal surfaces, abdominal or pelvic lymph nodes, and parenchymal metastases, as well as a high tendency for recurrence.

The standard of care for patients with newly diagnosed advanced ovarian cancer is comprehensive staging laparotomy and primary surgical cytoreduction followed by adjuvant chemotherapy [3]. The use of neoadjuvant chemotherapy followed by interval debulking surgery as a suitable alternative option has also been proposed [4]. The location and extent of location of peritoneal spread dictates the feasibility of cytoreductive surgery and predicts the likelihood of optimal primary cytoreduction.

Multiple imaging modalities have a role in the evaluation of the ovaries, including ultrasound, CT, MRI, and positron emission tomography (PET) (Table 1.3). In patients presenting with symptoms or findings on clinical examination suggestive of pelvic pathology, the main role of imaging is to distinguish ovarian origin from pathologies from adjacent organs (*e.g.*, uterus or bowel) and to identify features that allow discrimination between benign and malignant ovarian tumors. In patients with ovarian cancer, imaging is used to identify the presence and extent of regional and distant spread of the disease, and serves as a "road map" to surgery. Following treatment, imaging is also used to identify potential sites of recurrence when this is clinically suspected. Ultimate diagnosis usually requires histologic confirmation, but interpretation of imaging findings in the context of other patient characteristics such as age, menopausal status, personal and family history, clinical examination, and tumor markers such cancer antigen 125 (CA 125) allows the formulation of an appropriate differential diagnosis and guides patient management.

H.A. Vargas, MD • P.L. Di Paolo, MD • A. Afaq, MD
Department of Radiology, Memorial Sloan-Kettering Cancer Center, 1275 York Avenue, Room C278, New York, NY 10065, USA
e-mail: vargasah@mskcc.org; dipaolop@mskcc.org; asimafaq@doctors.org.uk

O. Akin, MD (✉)
Weill Medical College of Cornell University, New York, NY, USA

Department of Radiology, Body Imaging Service, Memorial Sloan-Kettering Cancer Center, 1275 York Avenue, New York, NY 10065, USA
e-mail: akino@mskcc.org

O. Akin (ed.), *Atlas of Gynecologic Oncology Imaging*, Atlas of Oncology Imaging,
DOI 10.1007/978-1-4614-7212-4_1,

Table 1.1 Ovarian anatomy

Feature	Comments
Usual anatomic relationships	Anterior: obliterated umbilical artery
	Posterior: ureter
	Superior: external iliac vessels
Anatomic location	Location of the ovaries varies, depending on multiple factors:
	Pregnancy may cause permanent displacement of the normal ovaries
	Supporting ligaments may be lax or absent (*e.g.*, after hysterectomy):
	Suspensory ligament: connects the superior pole of the ovary to the pelvic sidewall
	Ovarian ligament: attaches the lower pole of the ovary to the uterus
	Mesovarium: attaches the ovary to the broad ligament. Contains the neurovascular bundle
Ovarian vessels	Dual arterial supply: ovarian arteries from aorta and ovarian branches of uterine artery (arises from the internal iliac artery)
	Right ovarian vein drains directly into the inferior vena cava
	Left ovarian vein drains into left renal vein
Ovarian nerves	Superior group: from the intermesenteric nerves and renal plexus
	Middle group: from the superior hypogastric plexus or hypogastric nerve
	Inferior group: from the inferior hypogastric plexus (pelvic plexus)

Table 1.2 Ovarian histology

Layer	Features
Surface epithelium	Outermost layer, formed of simple cuboidal cells covering the ovarian surface
	Derived from the mesoderm (similar to the mesothelium of the peritoneum)
	Site of origin of most ovarian tumors
Cortex	Comprises most of the ovary during reproductive age
	Contains ovarian follicles (including follicular cells, granulosa cells, and oocytes)
Medulla	Innermost layer
	Highly vascular; fed by branches of the ovarian vessels

Table 1.3 Imaging techniques used for evaluation of the ovaries

Technique	Main use	Advantages	Disadvantages
Ultrasound	First-line evaluation of ovarian pathology	Readily available Cost-effective Usually well tolerated	Operator-dependent
CT	Staging of ovarian cancer Evaluation of incidentally detected lesions	Fast Reproducible More widely available than MRI	Involves ionizing radiation Soft tissue resolution is not as good as ultrasound or MRI
MRI	Characterization of lesions indeterminate on ultrasound or CT	Superb soft tissue resolution No ionizing radiation	More expensive and less readily available than ultrasound or CT
PET/CT	Staging of ovarian cancer Evaluation of ovarian cancer recurrence	Depicts function in addition to anatomy	Ionizing radiation from both the PET and CT components

CT computed tomography, *MRI* magnetic resonance imaging, *PET* positron emission tomography

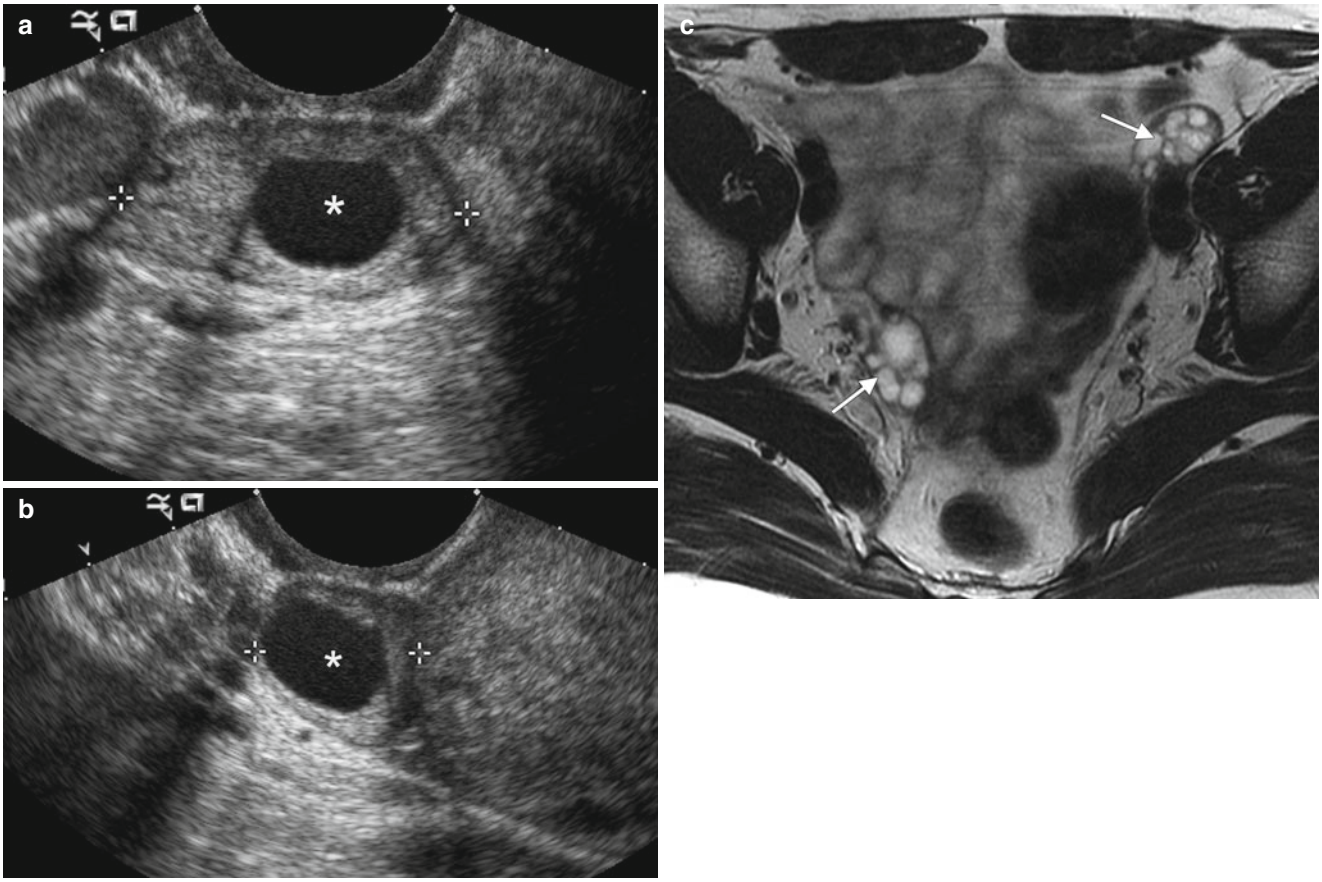

Fig. 1.1 Normal ovaries. The size of the ovaries and the presence and size of follicles vary depending on the patient's age and menopausal status. Immature follicles are usually smaller than 1 cm, but normal ovaries may contain follicles up to 3 cm in size. With the advent of high-resolution imaging, the ovaries are now frequently identified in postmenopausal women. The normal fallopian tubes are not routinely seen because of their small size and tortuous course. On ultrasound, the ovaries are typically isoechoic to muscle, and the normal follicles are hypoechoic. These images, from a 40-year-old patient, present longitudinal (**a**) and transverse (**b**) two-dimensional ultrasound views of the normal right ovary containing a physiologic follicle (*asterisk*). On T1-weighted MR images, the ovaries display homogeneous, low to intermediate signal intensity, whereas on T2-weighted MR images, the follicles become hyperintense compared with the surrounding stroma. This T2-weighted MR image (**c**) shows the normal appearance of the ovaries in a 34-year-old premenopausal woman (*arrows*). In postmenopausal women, the ovaries typically appear as predominantly solid structures with a relative increase in stromal tissue and may contain small T2-hyperintense follicles, although dysfunctional cysts up to several centimeters in size may also be encountered

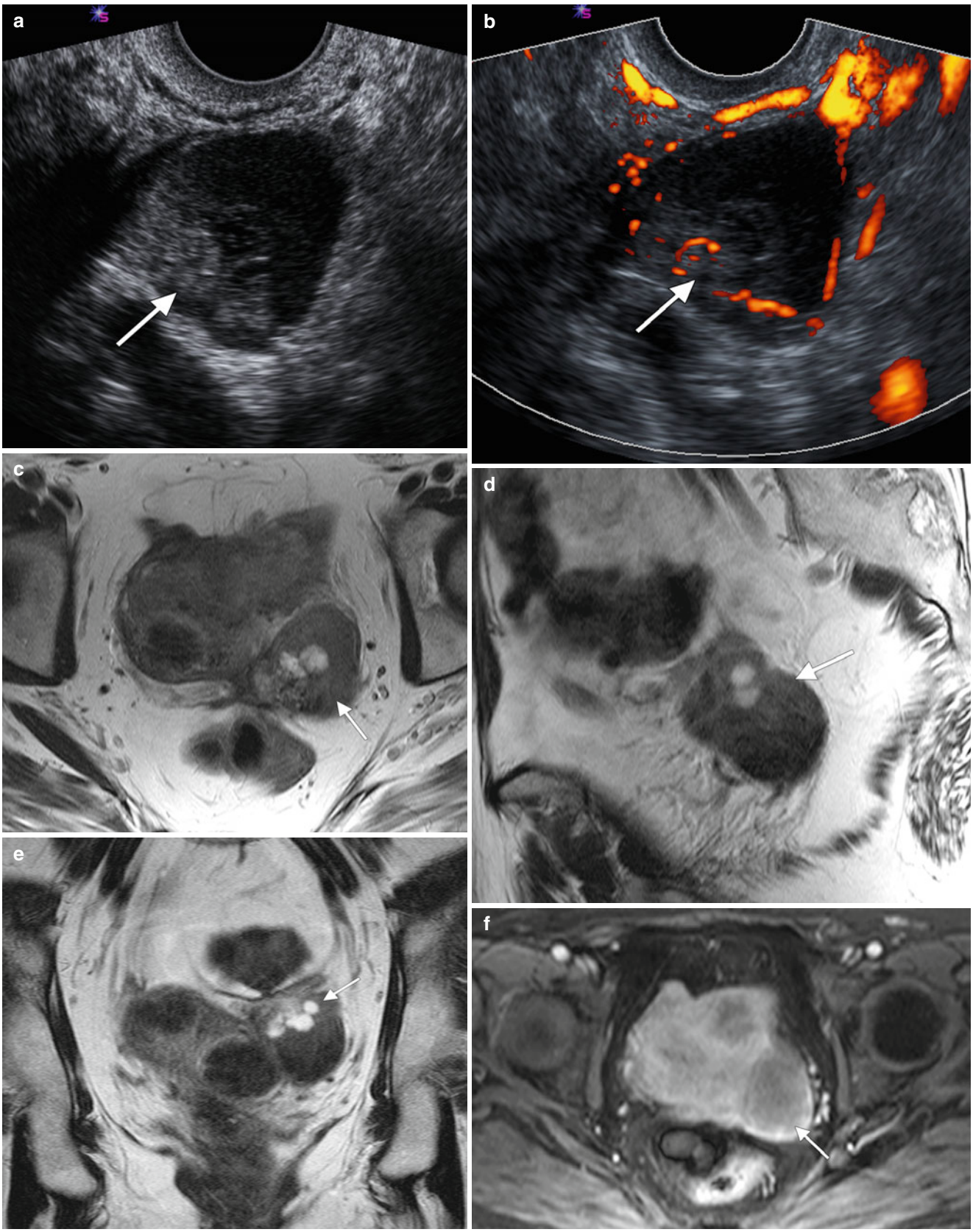

Fig. 1.2 Ultrasound is usually the modality of choice for initial evaluation of suspected adnexal lesions. The other imaging modalities are reserved for the assessment of ultrasound-indeterminate lesions or the staging of suspected ovarian cancer. These are representative images from a 60-year-old woman with weight loss and mild abdominal discomfort. Two-dimensional (**a**) and color Doppler (**b**) ultrasound images demonstrate a complex solid/cystic mass with internal vascularity (*arrows*). Axial (**c**), sagittal (**d**), and coronal (**e**) T2-weighted images and a fat-suppressed T1-weighted image following intravenous gadolinium (**f**) showed that the mass arises from the left ovary (*arrows*) and has cystic and enhancing solid components. Benign uterine leiomyomas were also demonstrated. Pathology showed endometrioid adenocarcinoma of the left ovary

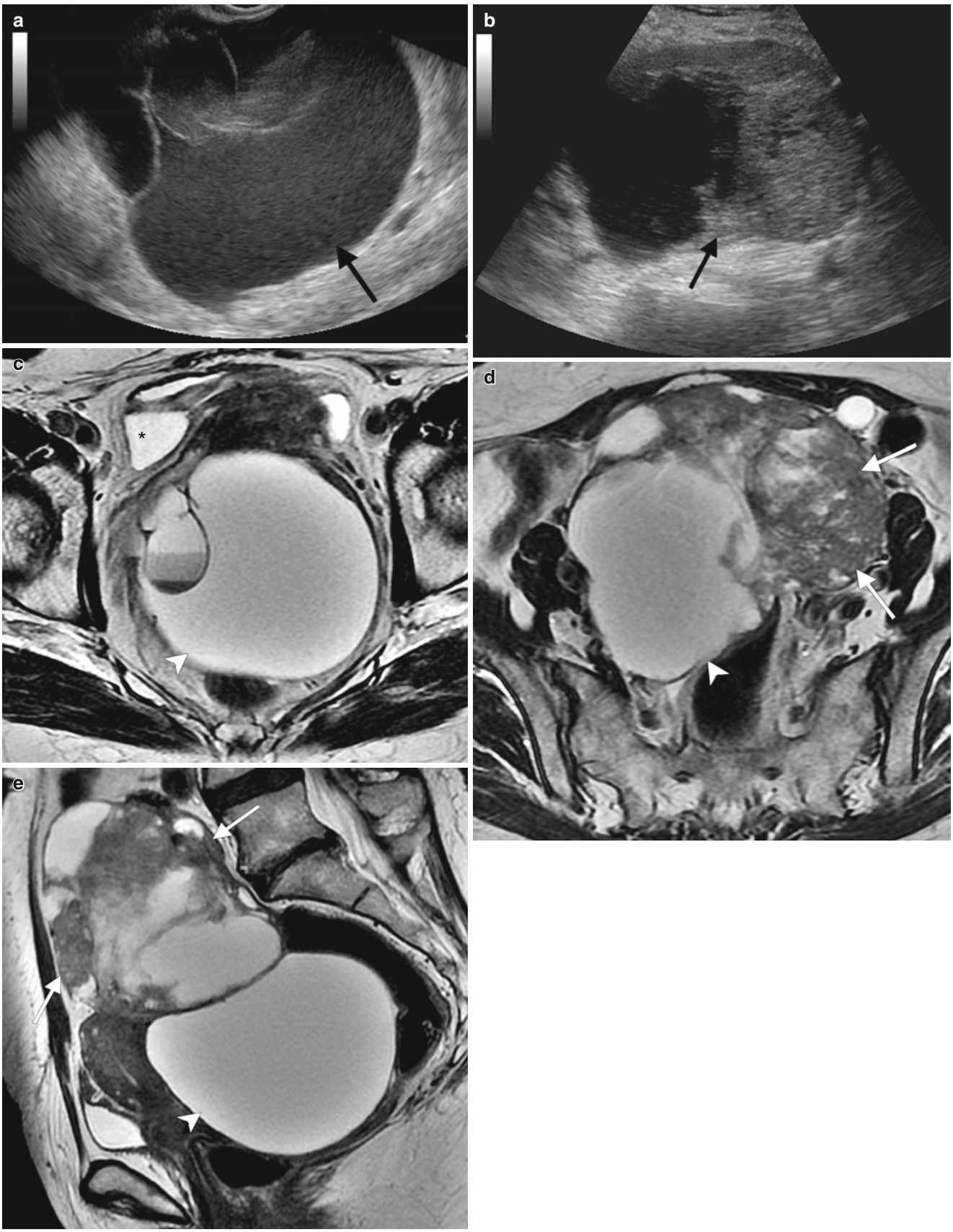

Fig. 1.3 MRI can be used for further characterization of masses detected by ultrasound, as shown by these representative images from a 67-year-old woman who self-palpated a "lump" in her lower abdomen. Two-dimensional transabdominal ultrasound images (**a**, **b**) showed a large, complex pelvic mass, but its exact origin and relation to adjacent organs was difficult to evaluate because of its large size. Axial (**c**, d) and sagittal (**e**) T2-weighted images showed the large, central pelvic mass containing solid components (*arrows*) and cystic components (*arrowheads*). Some of the cystic components demonstrate fluid-fluid layering (*asterisk*), probably owing to hemorrhage. There is mass effect on the uterus and bladder, which are displaced anteriorly. Pathology showed high-grade serous ovarian carcinoma

1.2 Benign Ovarian Pathology

Follicular and corpus luteum cysts are common in women of reproductive age (Tables 1.4 and 1.5). Follicular cysts result from failure of the normal ovarian follicle to rupture or regress. The corpus luteum develops from an ovarian follicle following ovulation. It secretes progesterone, and is essential for establishing and maintaining pregnancy. If the ovum is not fertilized, the corpus luteum regresses spontaneously after one or two menstrual cycles. Hemorrhage into a corpus luteum cyst can produce a complex appearance that changes over time depending on the stage of clot evolution. Cysts larger than 3 cm in size should be followed up on ultrasound to ensure resolution. A summary of ultrasound features used to predict whether ovarian tumors are benign or malignant are presented in Table 1.6.

Table 1.4 Imaging features of benign ovarian tumors

Lesion	Ultrasound	T1WI	T2WI	T1+C	Other
Follicular cyst	Anechoic, thin-walled, unilocular cyst	Low	High	None	Should be followed up to ensure resolution
Corpus luteum cyst	Cystic lesion May contain clot "Ring of fire" on Doppler	Low	High	None	Lack of enhancement differentiates clot from solid nodule
Mature teratoma	Fat-fluid level/"white balls"/"tip of iceberg" appearance	High	Variable	None	Low signal on fat-suppressed sequences
Endometrioma	Simple/complex cyst, low-level echoes Low-level echoes	High	Variable	None	No fat suppression Appearance influenced by iron content (from hemorrhage)
Fibrotic tumors	Solid lesions	Low	Low	Delayed enhancement	May be associated with pleural effusion (Meigs syndrome) Some secrete hormones
Tubo-ovarian abscess	May be solid, cystic, or complex	Low	Heterogeneous high with adjacent fat stranding or edema	Thick, enhancing walls	Usually present as a complication of pelvic inflammatory disease in young women
Serous cystadenoma	Unilocular cyst	Low	High	None	Can be indistinguishable from follicular cysts on imaging
Mucinous cystadenoma	Multilocular cyst	Low	High	None	May contain thin septations

T1+C T1 with contrast, *T1WI* T1-weighted image, *T2WI* T2-weighted image

Table 1.5 Imaging criteria used to differentiate benign versus malignant ovarian masses[a]

Criteria	Benign	Malignant
Primary criteria		
Cyst	Simple	Papillary projection
Number of septae	<3	≥3
Wall/septal thickness (mm)	<3	≥3
Solid component	Homogeneous	Heterogeneous with necrosis or hemorrhage
Size (cm)	<4	≥4
Ancillary criteria		
Ascites	Absent	Present
Peritoneal/omental deposits	Absent	Present
Lymph nodes	No enlarged lymph nodes	Enlarged lymph nodes

[a]These criteria apply to ultrasound, CT, and MRI

Table 1.6 Positive predictive value of simple ultrasound features used to predict whether ovarian tumors are benign or malignant[a]

Ultrasound feature	Positive predictive value (%)
For predicting benign histology	
Unilocular	99
Presence of solid components, of which largest solid component has largest diameter <7 mm	100
Presence of acoustic shadows	95
Smooth multilocular tumor with largest diameter <100 mm	99
No blood flow	98
At least one feature	96
For predicting malignant histology	
Irregular solid mass	96
Presence of ascites	97
≥ 4 papillary projections	88
Irregular multilocular solid mass measuring ≥10 cm	84
Strong Doppler blood flow	88
At least one feature	87

[a]If both benign and malignant features are present, the result is inconclusive and a second-stage test (*e.g.*, MRI) is recommended [6]

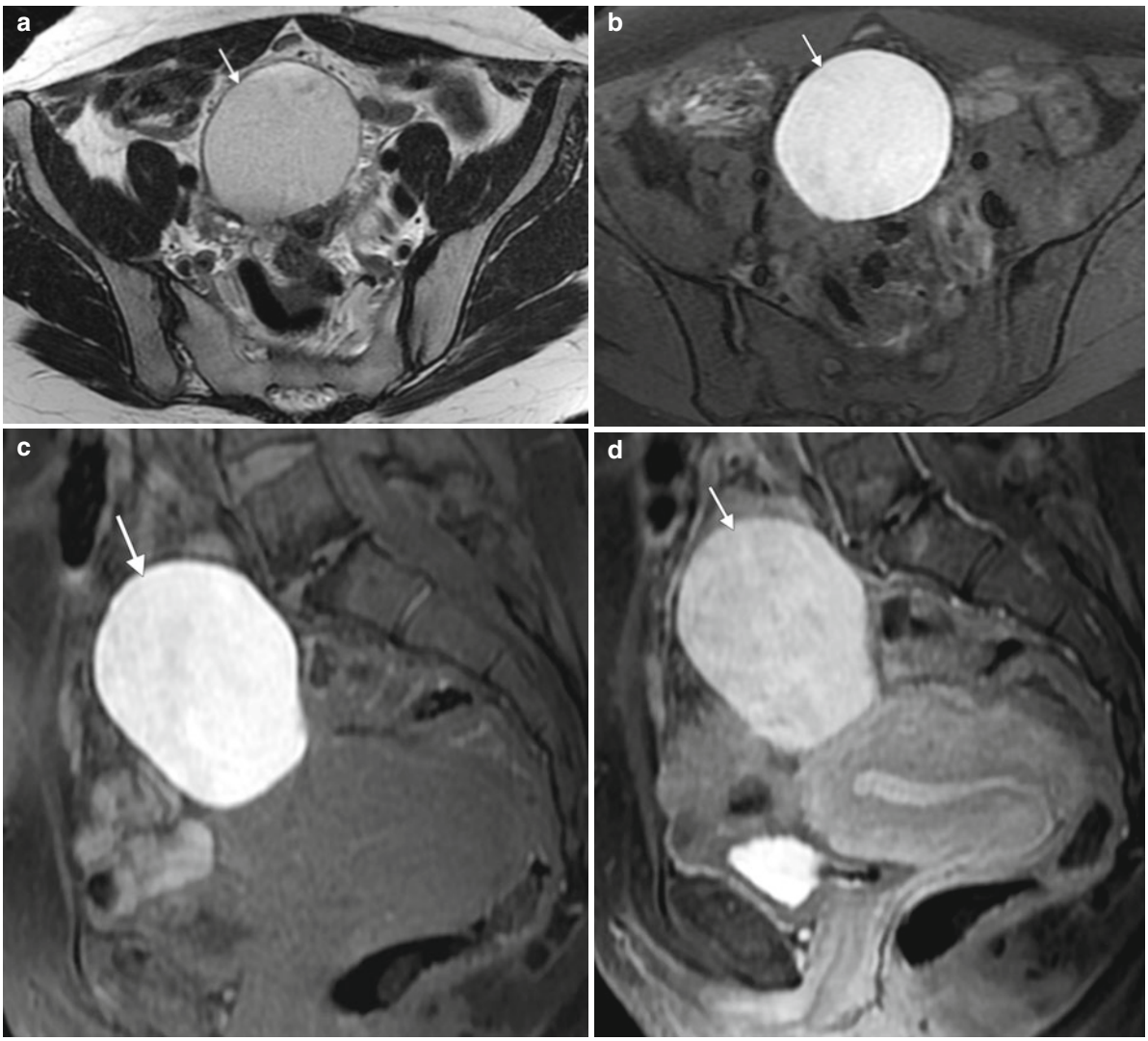

Fig. 1.4 Endometriosis and endometrioma. Endometriosis refers to the presence of endometrial glandular tissue outside of the uterus. Common locations include the ovary, uterine ligaments, fallopian tube, rectovaginal septum, pouch of Douglas, bladder wall, uterovesical fold, and umbilicus. Ovarian involvement results in the development of endometriomas, which are cystic lesions containing blood products. These images are from a 36-year-old woman with a family history of ovarian cancer and an ovarian lesion identified on screening ultrasound. An axial T2-weighted image (**a**) demonstrates a homogeneous, well-defined, hyperintense lesion arising from the right ovary. Fat-suppressed axial (**b**) and sagittal T1-weighted images before (**c**) and after (**d**) intravenous gadolinium show the lesion to be T1-hyperintense without fat suppression. This appearance is consistent with endometrioma

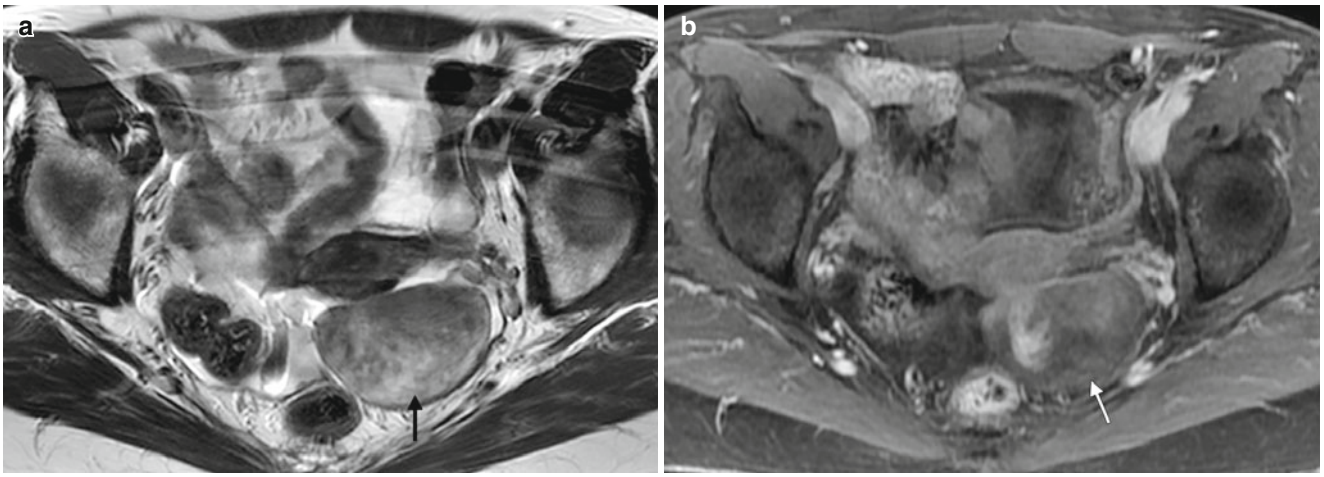

Fig. 1.5 Fibrotic tumors of the ovary. Fibromas, thecomas, and fibrothecomas are fibrotic tumors of sex-cord stromal origin that account for approximately 5 % of all ovarian tumors. They are usually asymptomatic and typically are detected in middle-aged women during routine gynecologic examination. Because of their solid appearance on imaging, they may mimic pedunculated uterine leiomyomas and even malignant ovarian tumors. They are associated with ascites in 15 % of cases and with pleural effusion (Meigs syndrome) in 1 %. Thecomas may be associated with endometrial thickening (due to estrogen secretion) or hirsutism and amenorrhea (due to androgen secretion). These images are from a 51-year-old woman with an adnexal mass. An axial T2-weighted MR image (**a**) and an axial fat-suppressed T1-weighted, contrast-enhanced MR image (**b**) demonstrate a well-defined, heterogeneous but predominantly T1- and T2-hypointense lesion in the left adnexal region. Pathology showed a fibrothecoma

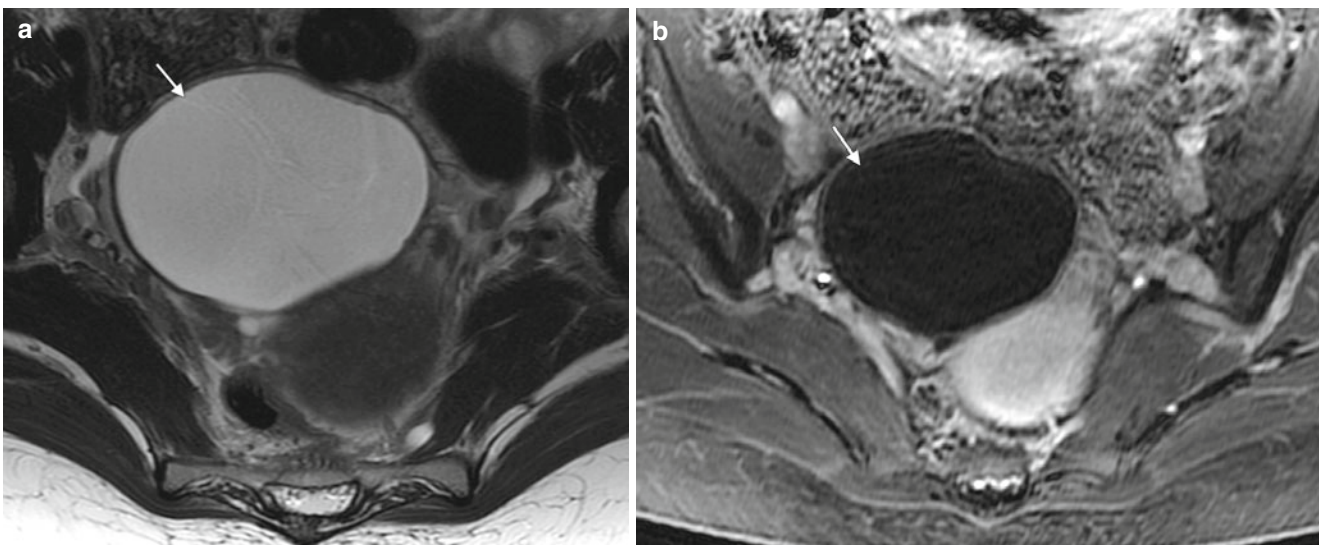

Fig. 1.6 Benign epithelial tumors. Benign types of serous and mucinous tumors are common (together accounting for about 50 % of benign ovarian neoplasms), whereas benign forms of endometrioid and clear cell tumors are exceptionally rare. Serous cystadenomas are the most common benign epithelial tumors. They can occur at any age, with a peak incidence in the fourth and fifth decades, and are bilateral in about 20 % of cases [5]. They can be indistinguishable from follicular cysts on imaging. However, unlike follicular cysts, serous cystadenomas remain unchanged (and may even increase in size) over subsequent menstrual cycles. The cyst wall may contain small solid nodules. Mucinous cystadenomas are the second most common benign epithelial tumors. They are bilateral in only 2–3 % of cases. Classically, they have been associated with a "stained glass" appearance on MRI owing to variable signal intensities of the different loculi containing proteinaceous or mucinous fluid and hemorrhage. These representative images are from a 34-year-old woman with a history of multiple ovarian serous cystadenoma resections. An axial T2-weighted image (**a**) and an axial fat-suppressed T1-weighted image following intravenous gadolinium (**b**) demonstrate a large cystic lesion arising from the right ovary (*arrows*). No solid or enhancing components were identified. Pathology confirmed the diagnosis of recurrent ovarian serous cystadenoma

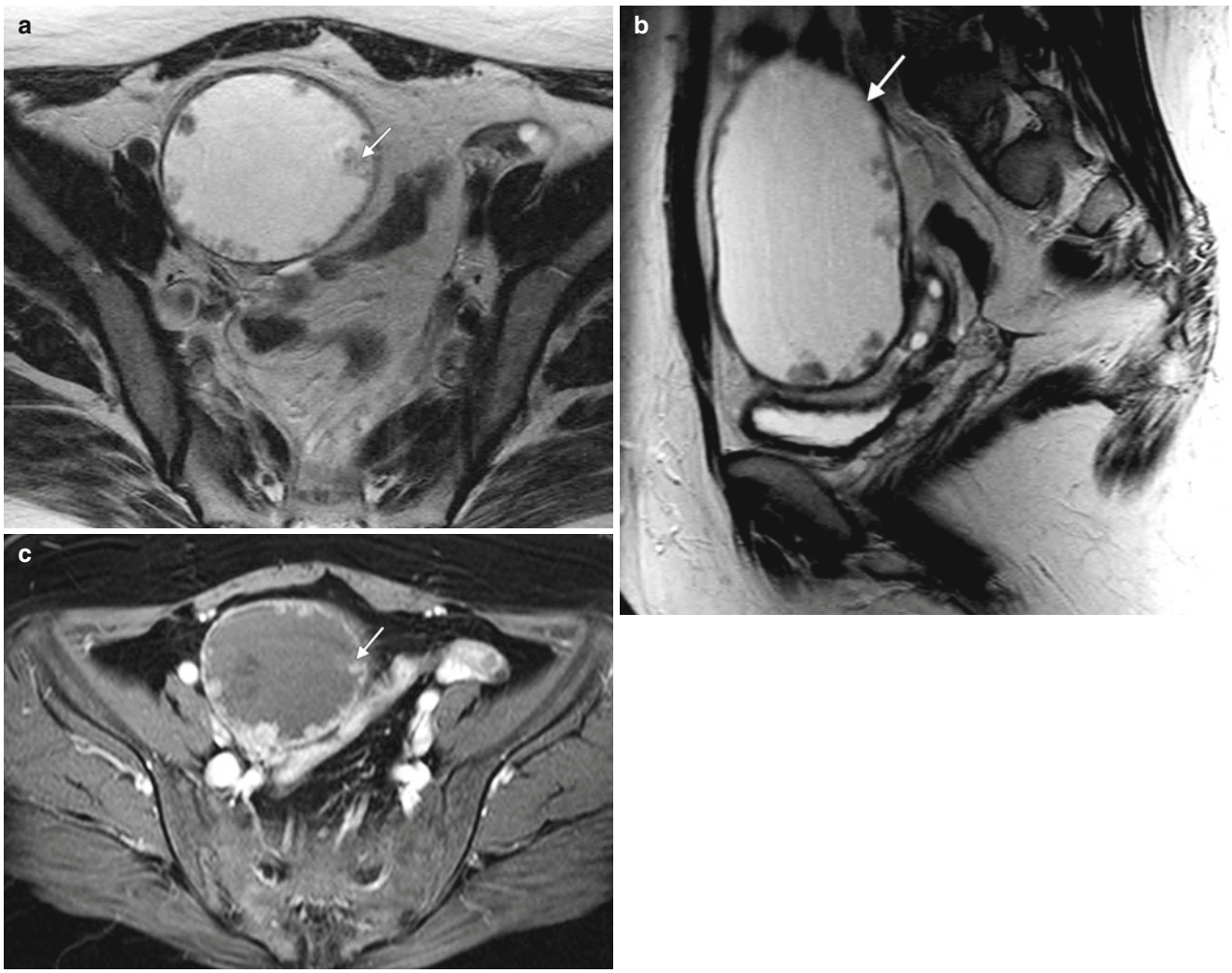

Fig. 1.7 Borderline ovarian tumors. Depending on their pathologic features and clinical behavior, epithelial ovarian tumors can be classified as benign, borderline, or malignant. Borderline tumors have some or all of the features of a malignant tumor but no stromal invasion. They behave clinically in a more aggressive way than a benign neoplasm but have a better prognosis than an invasive malignancy. The tumor shown in these images was proven by pathology to be a serous borderline ovarian tumor of low malignant potential, occurring in a 41-year-old woman. Axial (**a**) and sagittal (**b**) T2-weighted images and a fat-suppressed axial T1-weighted image after intravenous gadolinium (**c**) demonstrated a predominantly cystic pelvic mass arising from the right ovary (*arrows*) with several peripheral enhancing solid nodules

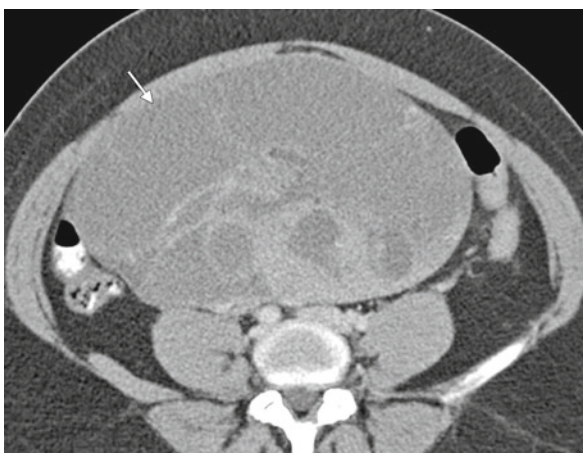

Fig. 1.8 Borderline ovarian mucinous tumor of low malignant potential in a 38-year-old woman with abdominal distention and a palpable abdominal mass. This axial CT image of the pelvis following intravenous contrast demonstrates a large, predominantly cystic mass with some peripheral solid components and irregular septations (*arrow*)

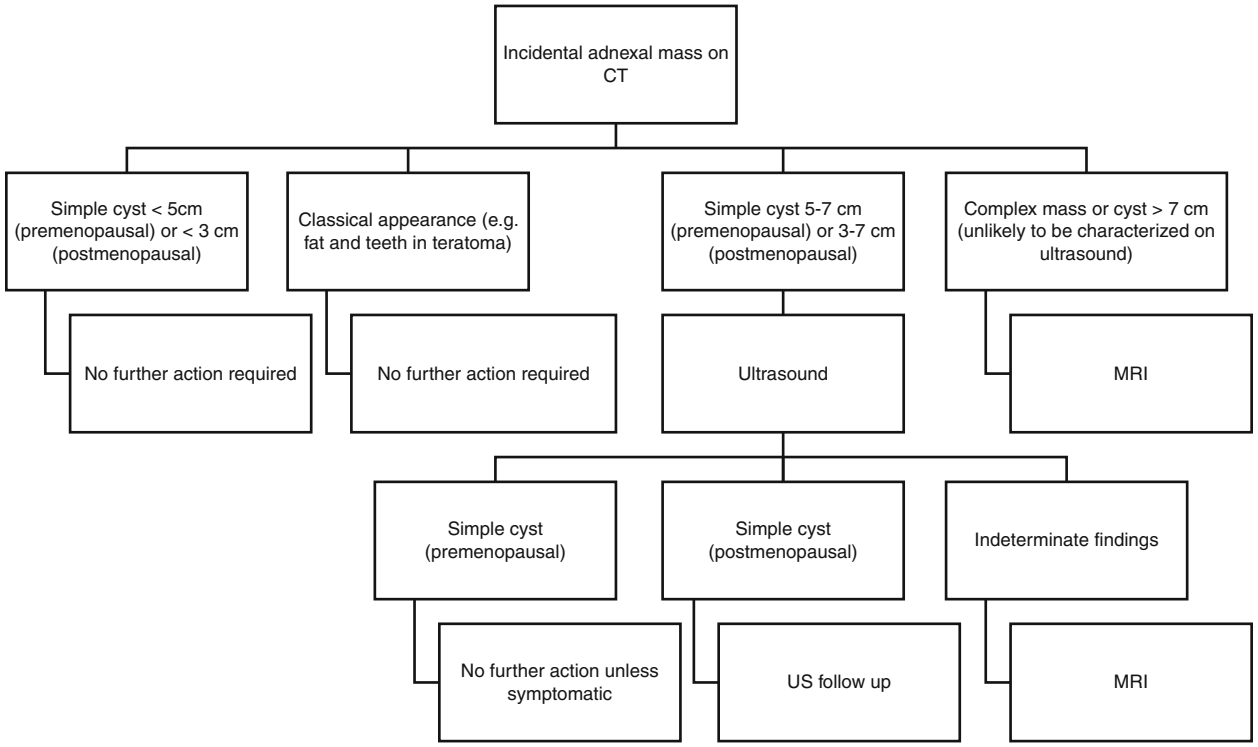

Fig. 1.9 Management of ovarian lesions incidentally detected on CT scans. *US* ultrasound (Adapted from Spencer and Gore [7] and Levine et al. [8])

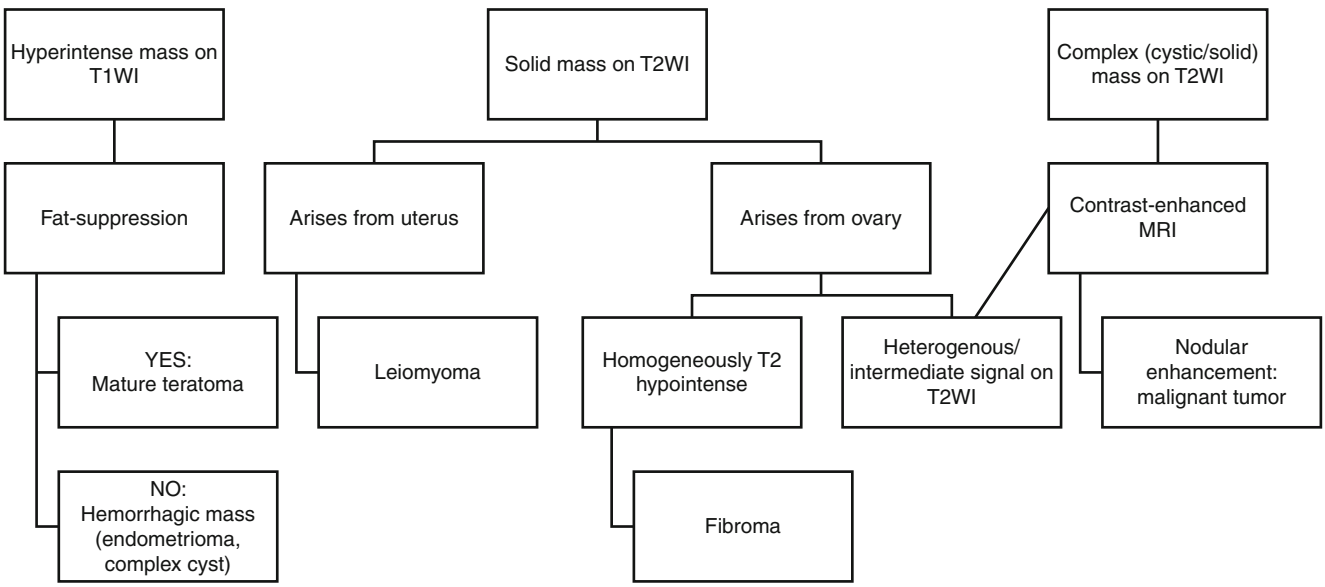

Fig. 1.10 Decision tree for the MRI evaluation of the ultrasound indeterminate mass. *T1WI* T1-weighted image, *T2WI* T2-weighted image (Adapted from Spencer et al. [9])

1.3 Malignant Ovarian Tumors

Table 1.7 lists the histologic subtypes of ovarian cancer. A large majority of these neoplasms are of epithelial origin, but nonepithelial tumors may also occur.

Table 1.7 Histologic subtypes of ovarian cancer

Subtype	Prevalence and further information
Epithelial origin (90 %)	
Serous cystadenocarcinomas	Most common histologic subtype of ovarian cancer (50 % of cases). Often bilateral
Mucinous cystadenocarcinomas	Represent about 20–30 % of ovarian cancer histologies. Tend to occur in older women. Larger in size and more often unilateral, these usually have a better prognosis than serous counterparts. Associated with pseudomyxoma peritonei
Endometrioid carcinomas	Third most common type of ovarian cancer. Arise from the surface epithelium. Up to 30 % are bilateral. Associated with endometriosis, endometrial hyperplasia, and endometrial cancer. Prognosis is usually better than either mucinous or serous carcinomas
Clear cell carcinomas	Represent about 5–10 % of ovarian cancers. Also associated with endometriosis. Bilateral in up to 20 % of cases
Sertoli-Leydig cell tumors	Rare sex cord–stromal ovarian tumors, representing <0.5 % of all ovarian neoplasms. They are the most common virilizing ovarian tumors. The average age at presentation is 25 years, and 75 % of cases occur before 30 years of age
Nonepithelial origin (10 %)	
Malignant germ cell tumors	In adults, germ cell tumors are relatively rare. However, in children and adolescents, 30 % of tumors of germ cell origin are malignant. Subtypes include dysgerminomas, immature teratomas, endodermal sinus tumors, embryonal carcinomas, choriocarcinomas, and malignant mixed germ cell tumors
Mixed/undifferentiated ovarian tumors	Usually metastatic at the time of presentation; associated with very poor prognosis
Ovarian metastases	Most commonly from the gastrointestinal tract, breast, lung, contralateral ovary, endometrium, melanoma, or pancreas. Imaging usually cannot distinguish between primary and metastatic ovarian neoplasms

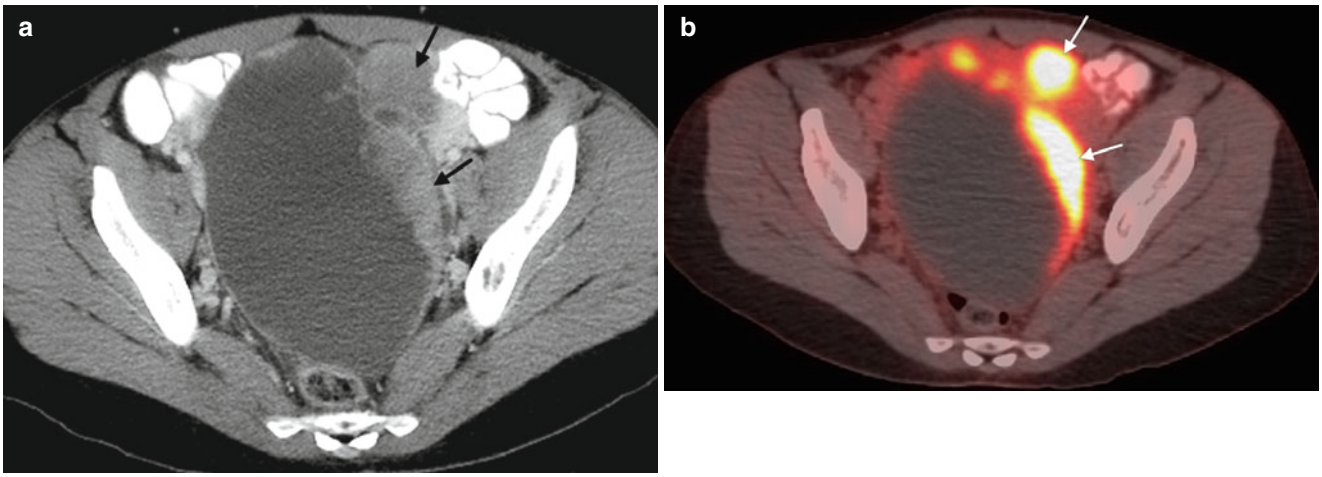

Fig. 1.11 46-year-old woman with abdominal pain and distention. Axial CT (**a**) and fused fluorodeoxyglucose–positron emission tomography (FDG-PET) and CT (**b**) of the pelvis following oral and intravenous contrast enhancement demonstrate a large cystic mass in the central pelvis with peripheral, enhancing hypermetabolic solid components (*arrows*). Pathology demonstrated high-grade, serous ovarian carcinoma

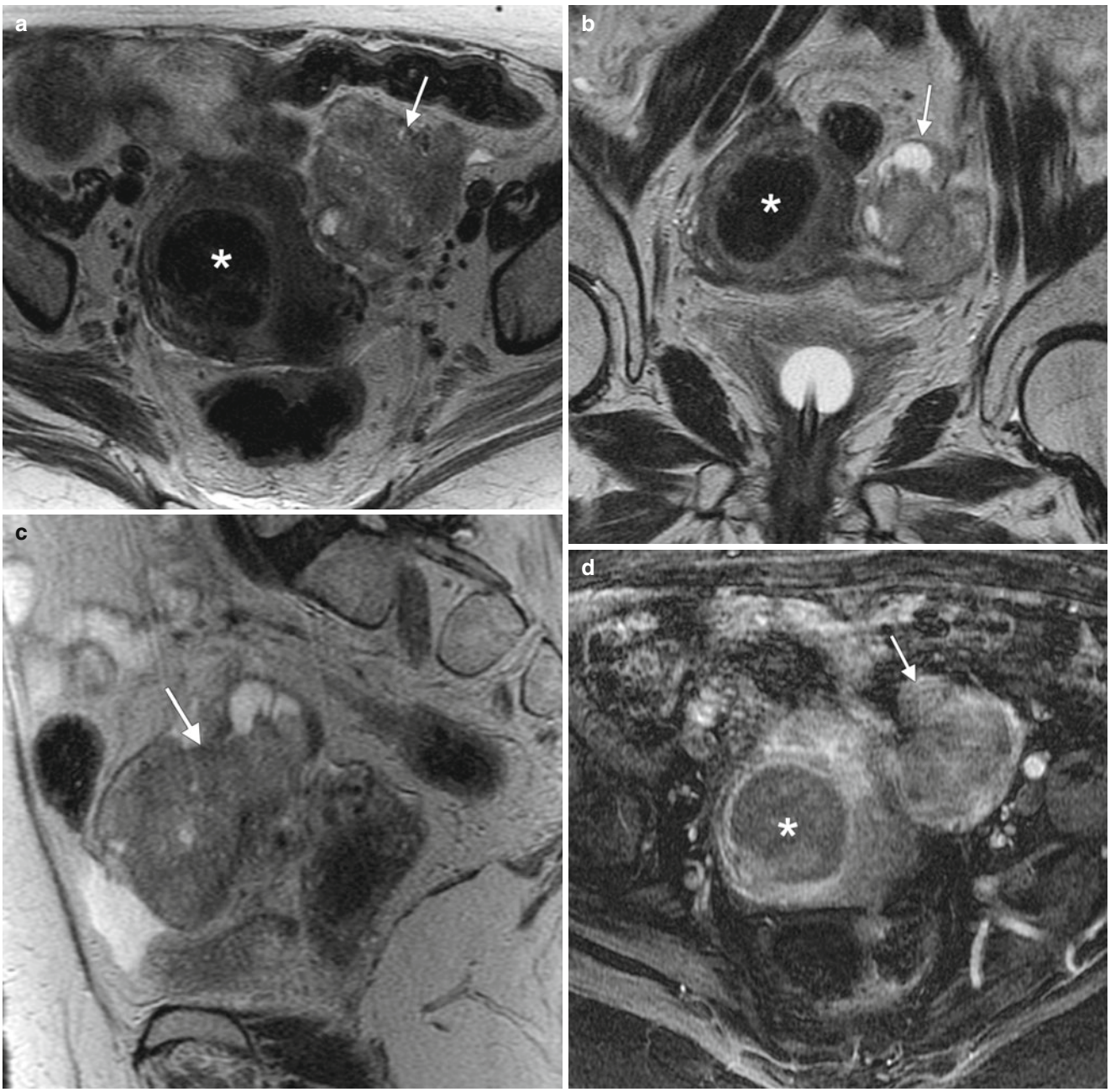

Fig. 1.12 75-year-old woman complaining of bloating and abdominal swelling. Axial (**a**), coronal (**b**), and sagittal (**c**) T2-weighted MR images and a fat-suppressed, axial T1-weighted image after intravenous gadolinium (**d**) demonstrate a predominantly solid, enhancing mass with some cystic components (*arrows*). Pathology was consistent with high-grade serous carcinoma with anaplastic features. A uterine fibroid is also shown (*asterisk*)

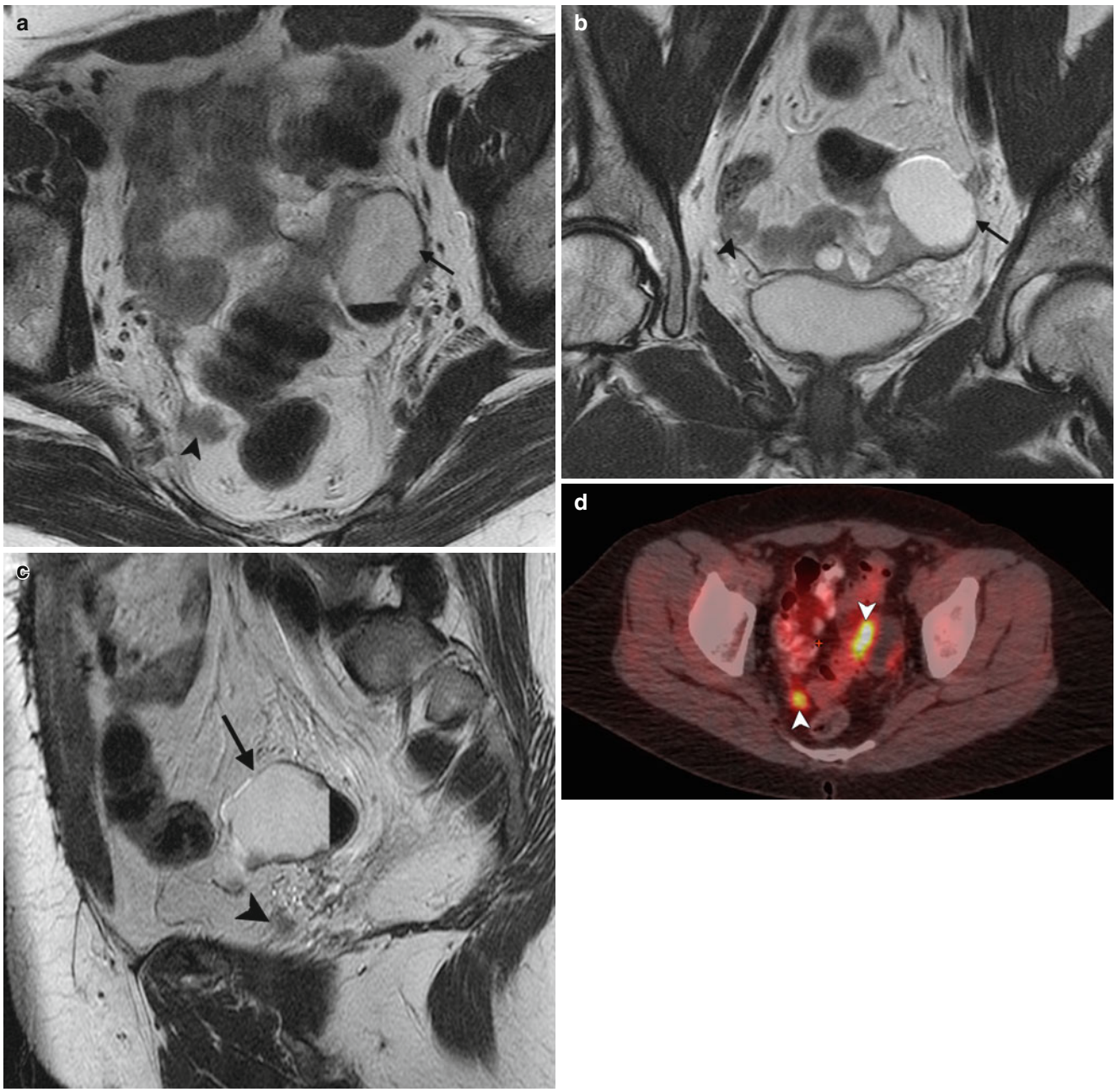

Fig. 1.13 46-year-old woman who consulted her general practitioner for nausea, vomiting, and abdominal fullness. Axial (**a**), coronal (**b**), and sagittal (**c**) T2-weighted MR images demonstrated a mixed solid/cystic left adnexal mass (*arrows*) and multiple serosal deposits (*arrowheads*). The serosal deposits demonstrated hypermetabolic activity on a fused positron emission tomography (PET) and CT image (**d**). Pathology demonstrated papillary serous ovarian carcinoma

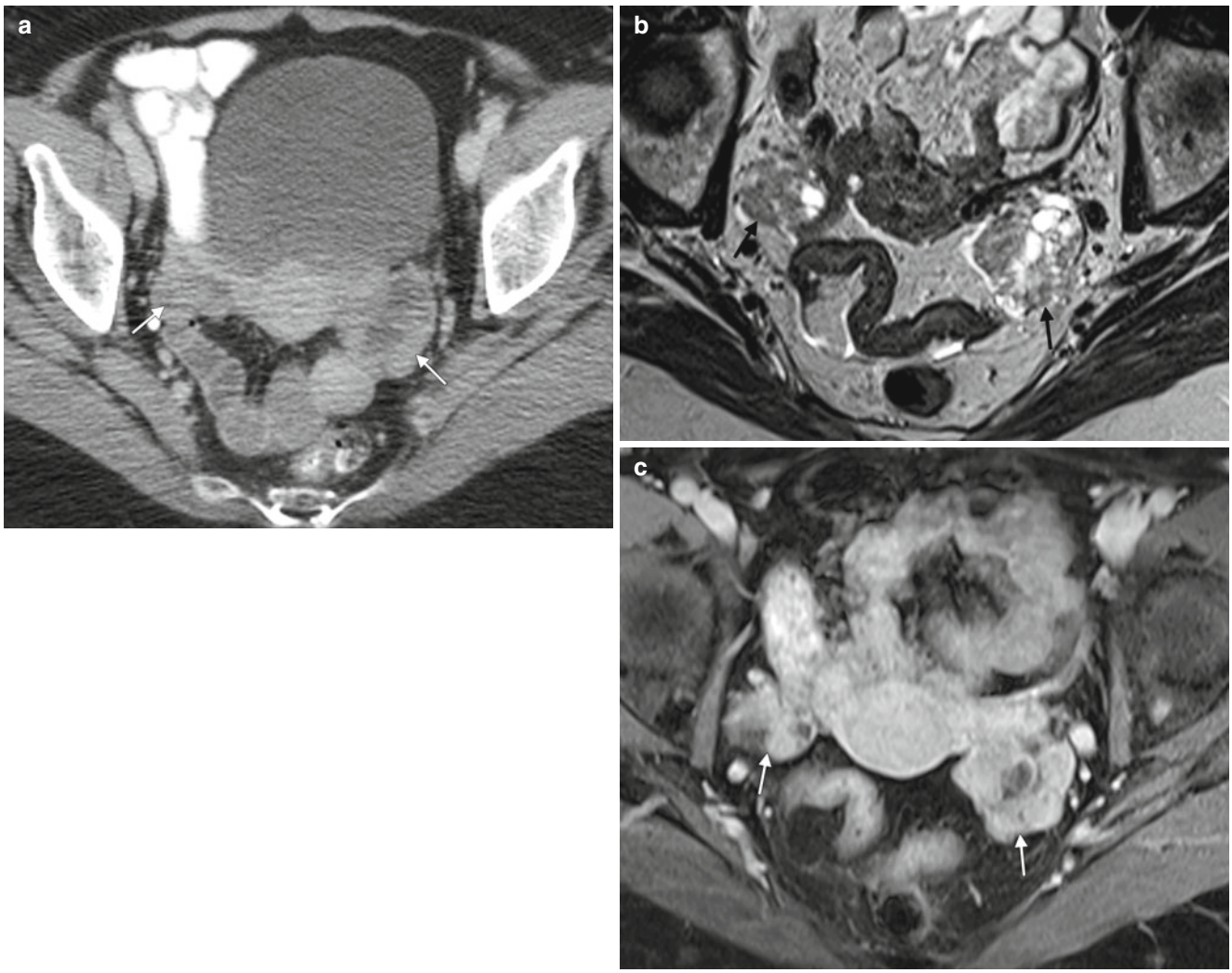

Fig. 1.14 60-year-old woman with a family history of *BRCA*-related breast and ovarian cancer who presented for further evaluation of sonographically detected left ovarian cancer. An axial contrast-enhanced CT scan (**a**), an axial T2-weighted MR image (**b**), and an axial, fat-suppressed T1-weighted MR image following intravenous gadolinium (**c**) show heterogeneous bilateral ovarian masses with mixed solid, cystic, and enhancing components. Pathology demonstrated a high-grade serous ovarian carcinoma

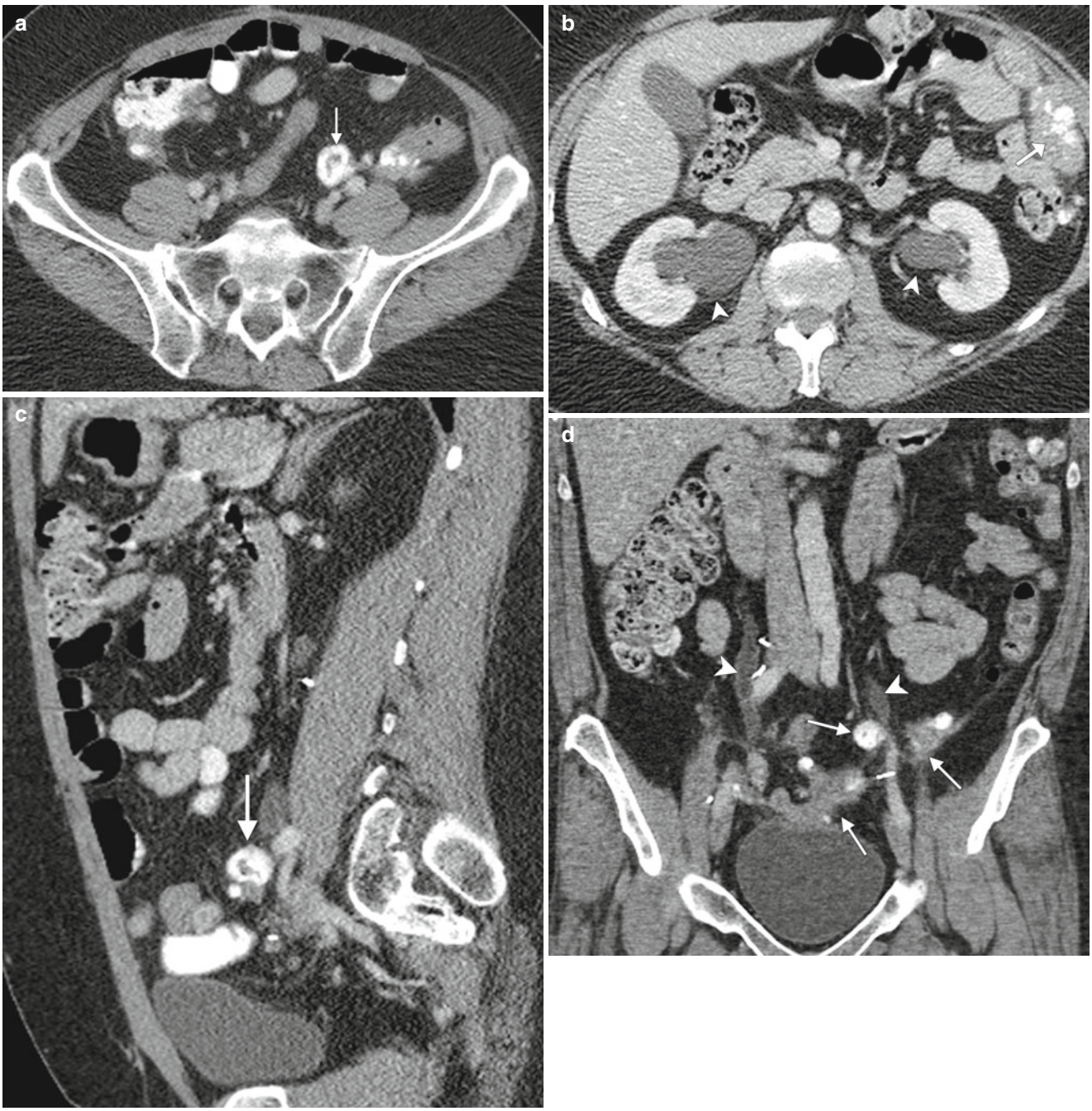

Fig. 1.15 44-year-old woman with low-grade, papillary serous ovarian carcinoma. Axial (**a**, **b**), sagittal (**c**), and coronal (**d**) contrast-enhanced CT scans demonstrate calcified peritoneal deposits (*arrows*) and bilateral hydronephrosis and hydroureter (*arrowheads*)

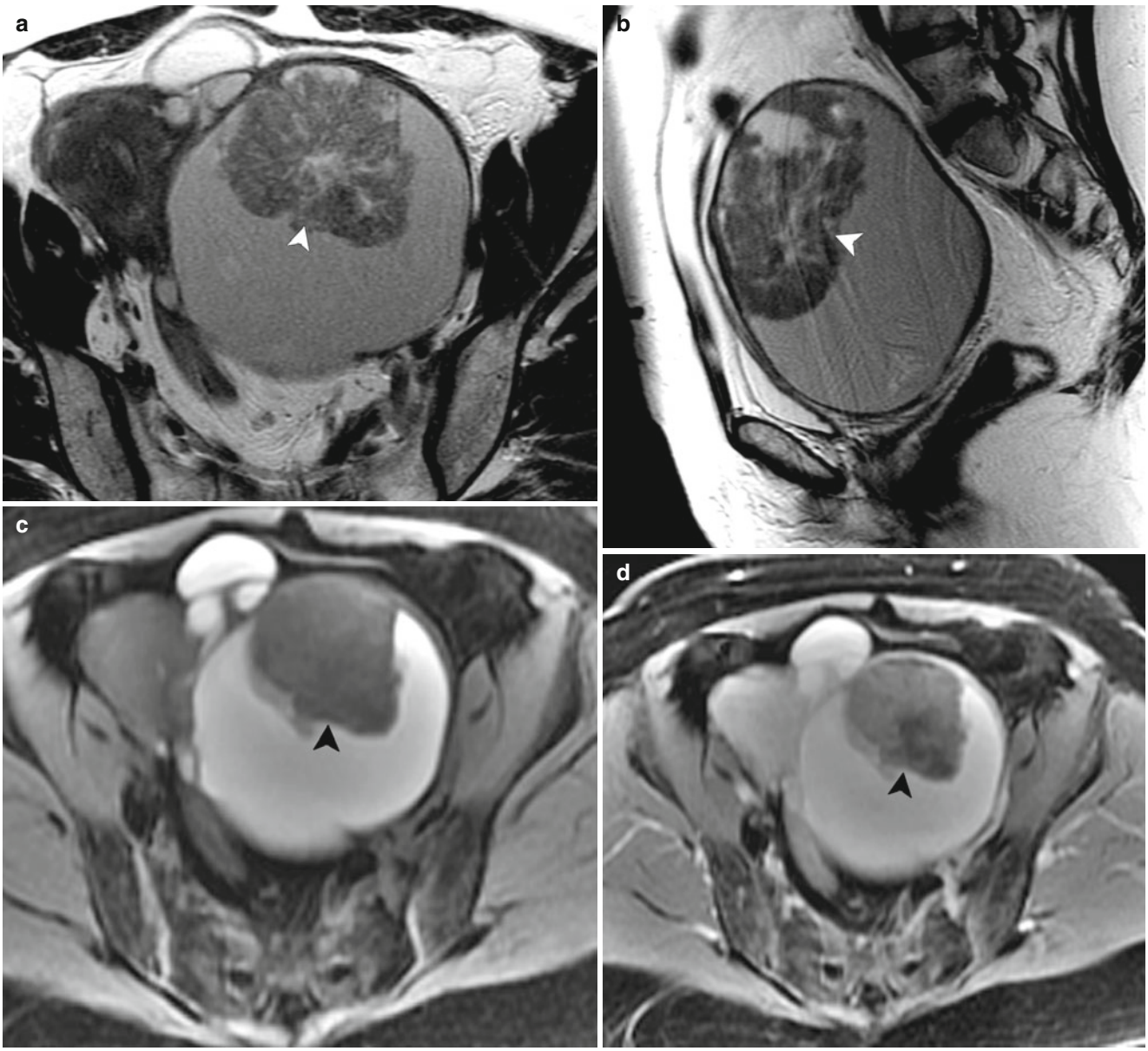

Fig. 1.16 61-year-old woman undergoing evaluation for postmenopausal bleeding. T2-weighted axial (**a**) and sagittal (**b**) MR images and fat-suppressed T1-weighted MR images before (**c**) and after (**d**) the administration of intravenous gadolinium showed a heterogeneous, enhancing solid nodule (*arrowheads*) arising from a T1-hyperintense cystic mass. Pathology showed an ovarian endometrioid adenocarcinoma arising from an endometrioma

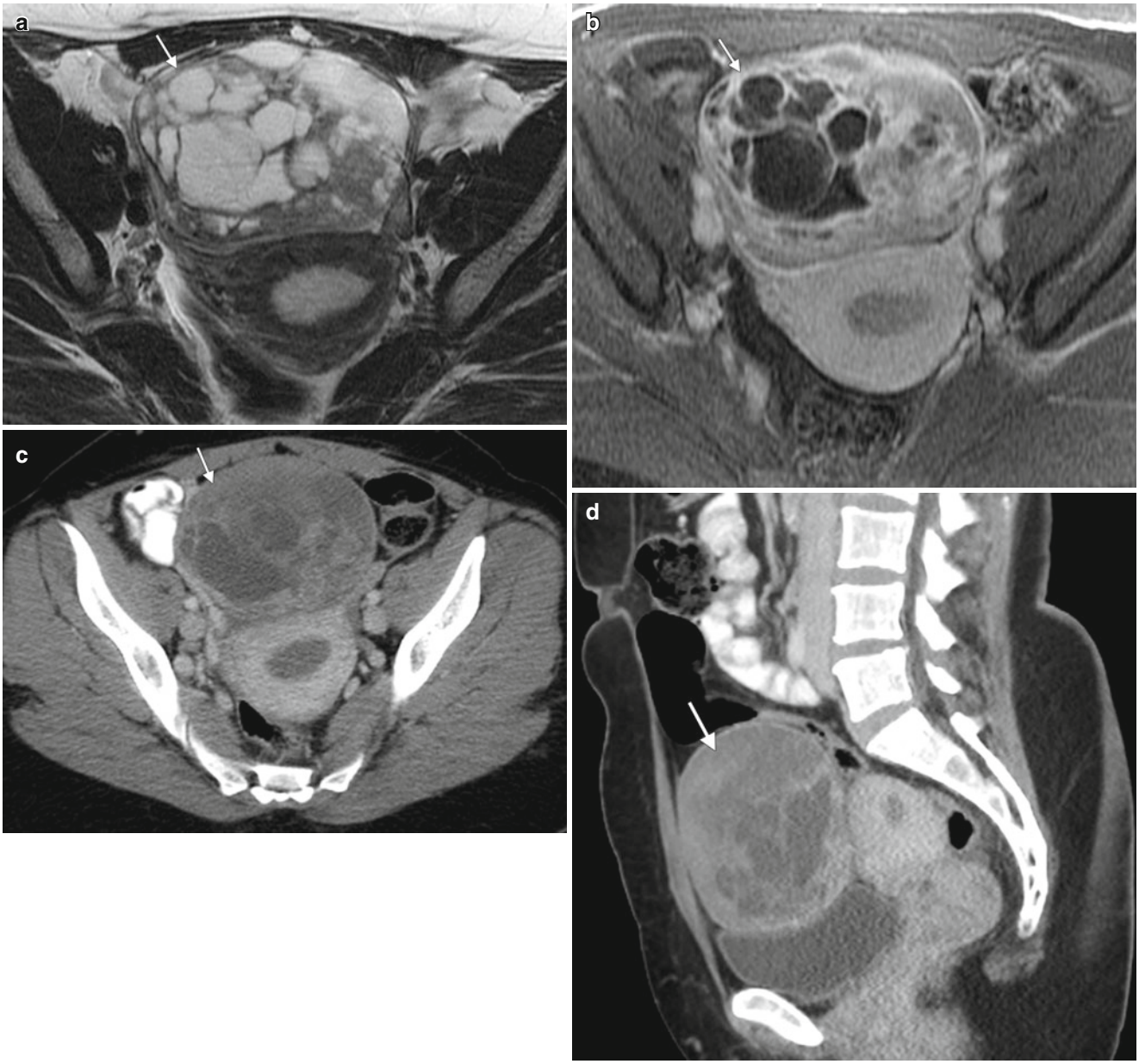

Fig. 1.17 46-year-old woman with granulosa cell ovarian cancer. An axial T2-weighted MR image (**a**) and an axial fat-suppressed T1-weighted image following intravenous gadolinium (**b**) as well as axial (**c**) and sagittal (**d**) contrast-enhanced CT scans demonstrate a heterogeneous, mixed cystic/solid mass (*arrows*) with enhancing nodules and thick septations. Also note endometrial hyperplasia (*asterisk*), frequently associated with hormone secretion due to granulosa cell tumors

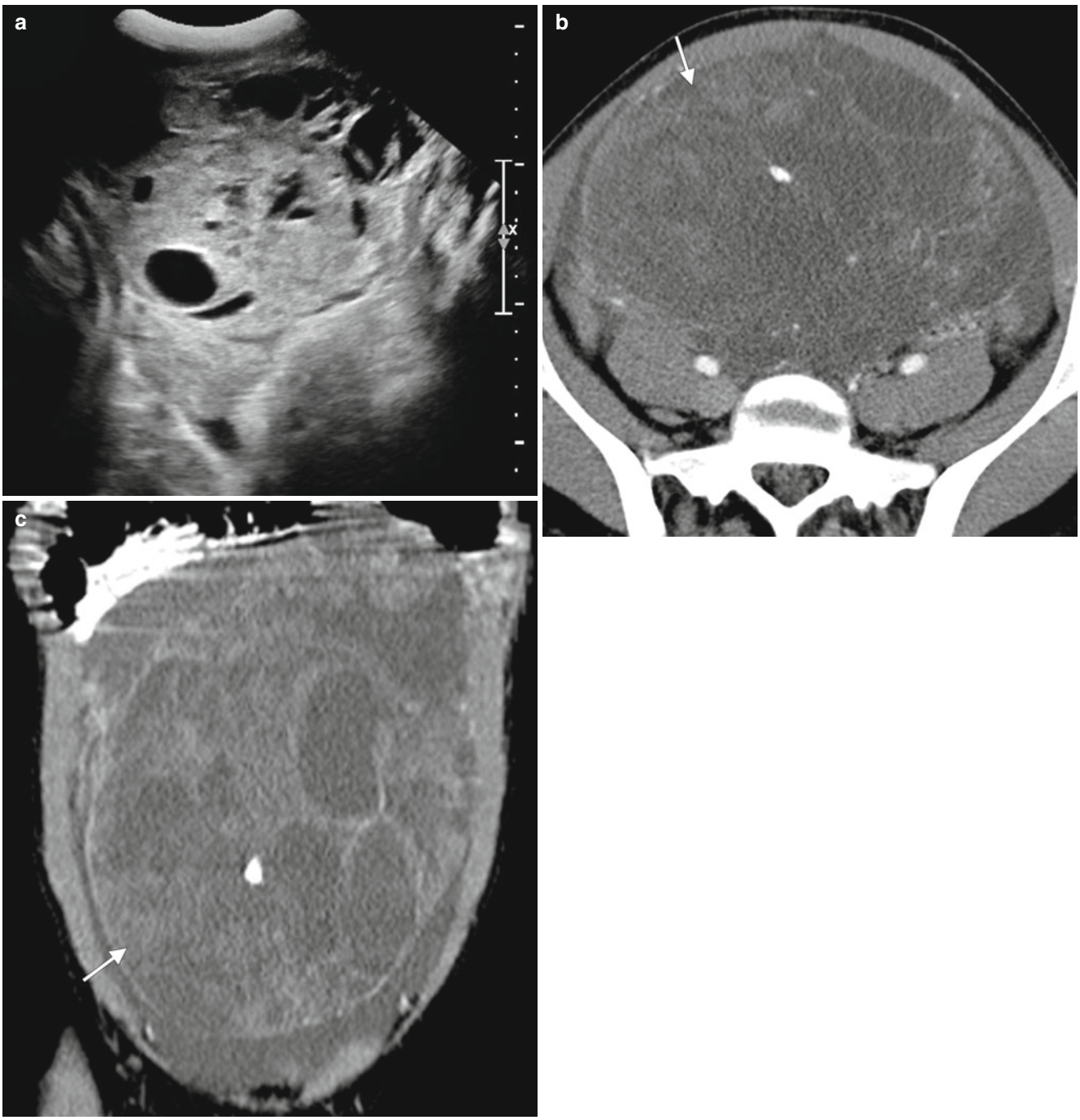

Fig. 1.18 15-year-old girl with abdominal pain. A two-dimensional ultrasound image (**a**) showed a large, mixed cystic/solid mass in the central abdomen. Axial (**b**) and sagittal (**c**) CT scans following intravenous contrast demonstrate a large, mixed cystic and solid abdominopelvic mass with punctate areas of calcification. A pathology specimen demonstrated an intermediate to poorly differentiated Sertoli-Leydig cell tumor

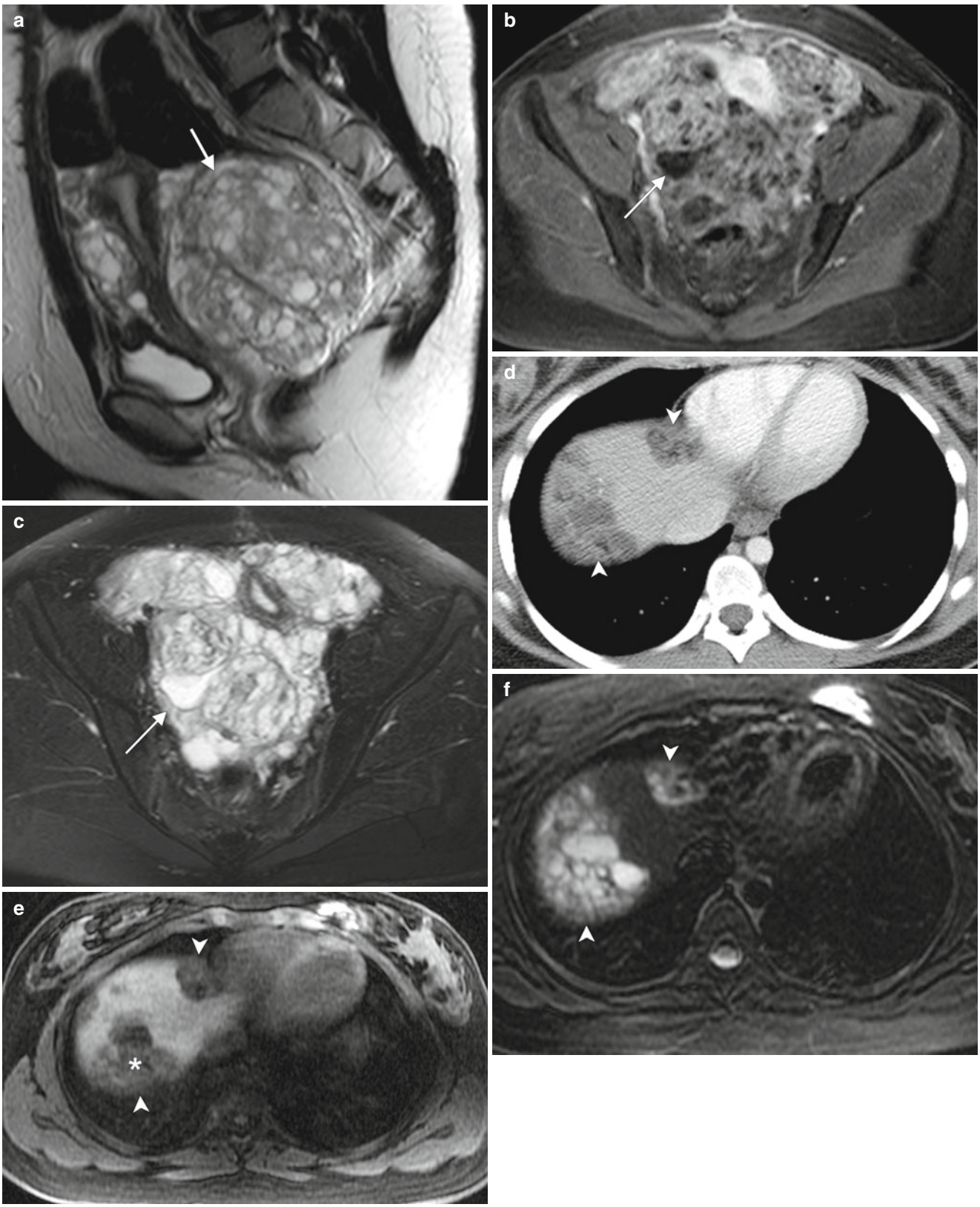

Fig. 1.19 14-year-old girl with metastatic malignant teratoma. A sagittal T2-weighted MR image (**a**), an axial, fat-suppressed T1-weighted image of the pelvis after intravenous gadolinium (**b**), and an axial fat-suppressed T2-weighted image (**c**) demonstrate a large, heterogeneous central pelvic mass (*arrows*). An axial contrast-enhanced CT scan (**d**), axial fat-suppressed T1-weighted MR image (**e**), a T2-weighted MR image (**f**), and in-phase (**g**) and out-of-phase (**h**) T1-weighted images of the upper abdomen demonstrate multiple liver lesions (*arrowheads*). Note the T1-hyperintense components within the primary and metastatic lesions in the abdomen and pelvis (*asterisks*)

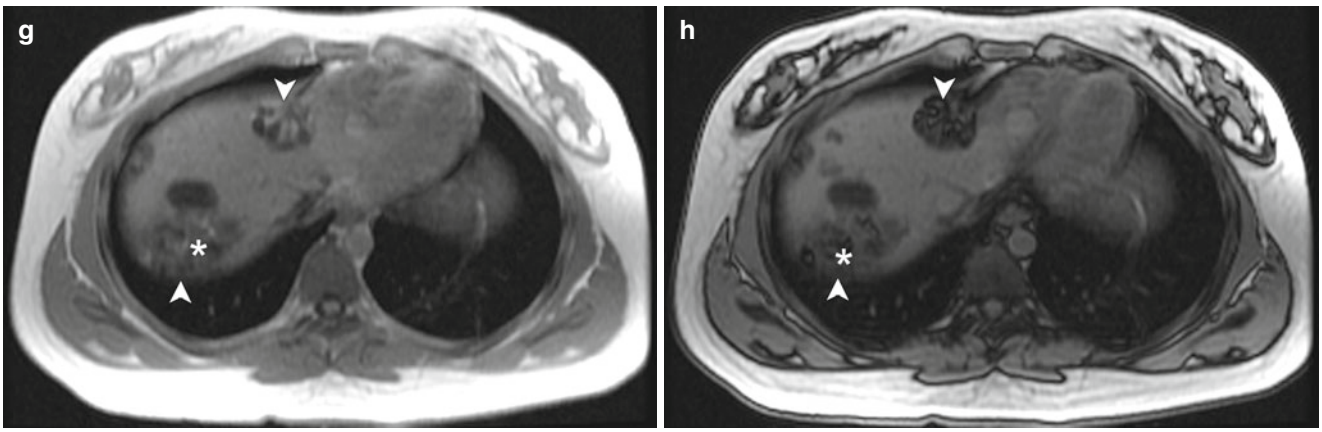

Fig. 1.19 (continued)

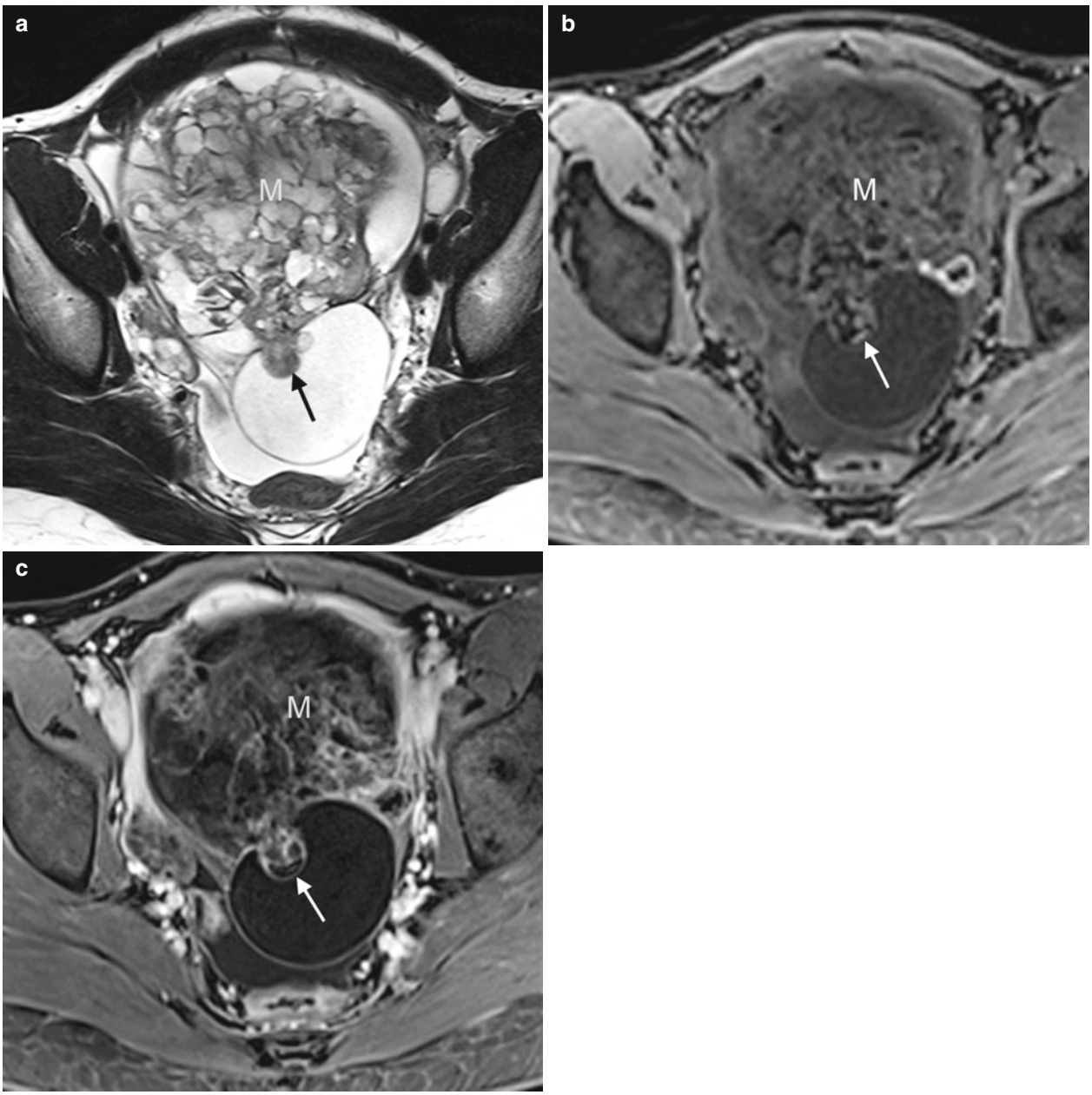

Fig. 1.20 16-year-old girl with pelvic pain. Axial T2-weighted MR image (**a**) and fat-suppressed axial T1-weighted images before (**b**) and after (**c**) the administration of intravenous gadolinium demonstrate a mixed cystic and solid mass (*M*) with thick, heterogeneous septations and enhancing solid nodules (*arrows*). Pathology was consistent with an immature teratoma

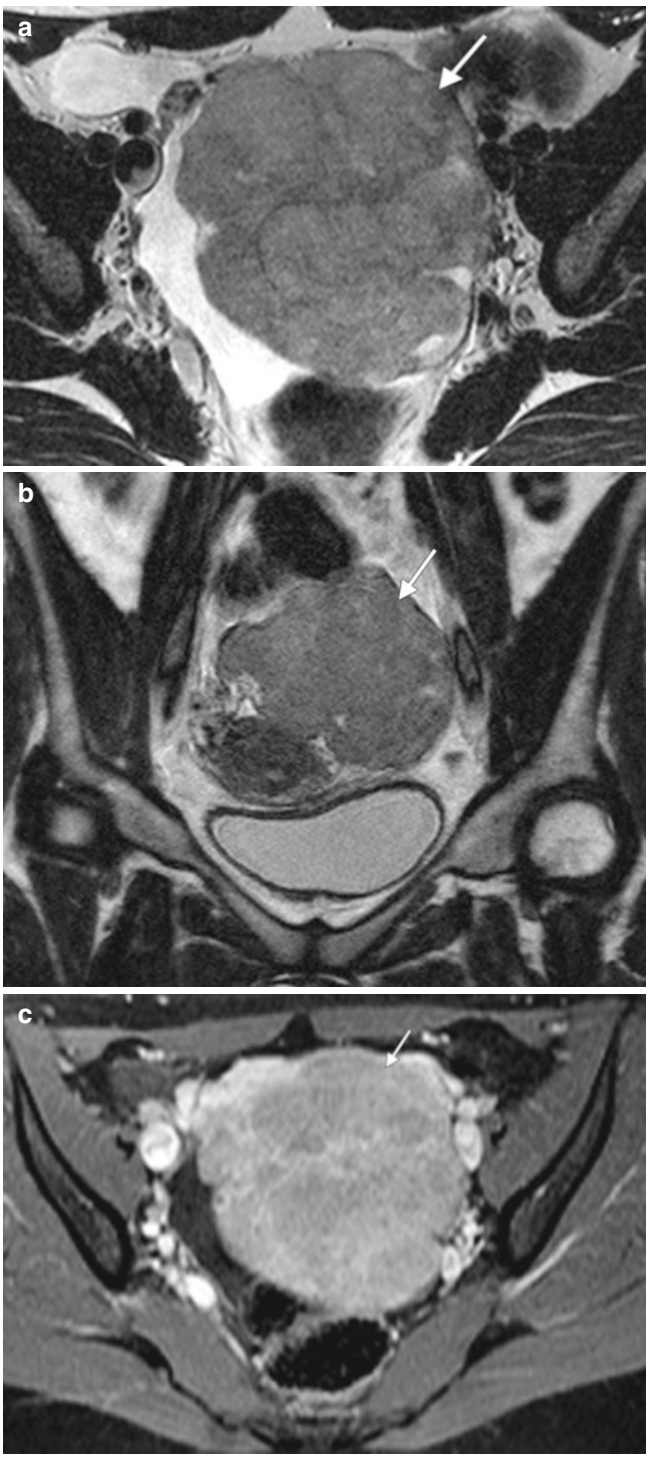

Fig. 1.21 27-year-old woman who presented with dyspareunia. Axial (**a**) and coronal (**b**) T2-weighted MR images and an axial, fat-suppressed T1-weighted image following intravenous gadolinium (**c**) demonstrate a heterogeneous, predominantly solid, enhancing pelvic mass (*arrows*). Pathology showed an ovarian dysgerminoma

Fig. 1.22 This coronal CT scan shows diffuse abdominal and pelvic masses consistent with tumor recurrence in a 57-year-old woman. One year earlier, she had been treated with chemotherapy for carcinosarcoma (also known as malignant mixed Müllerian tumor or MMMT) of the left ovary

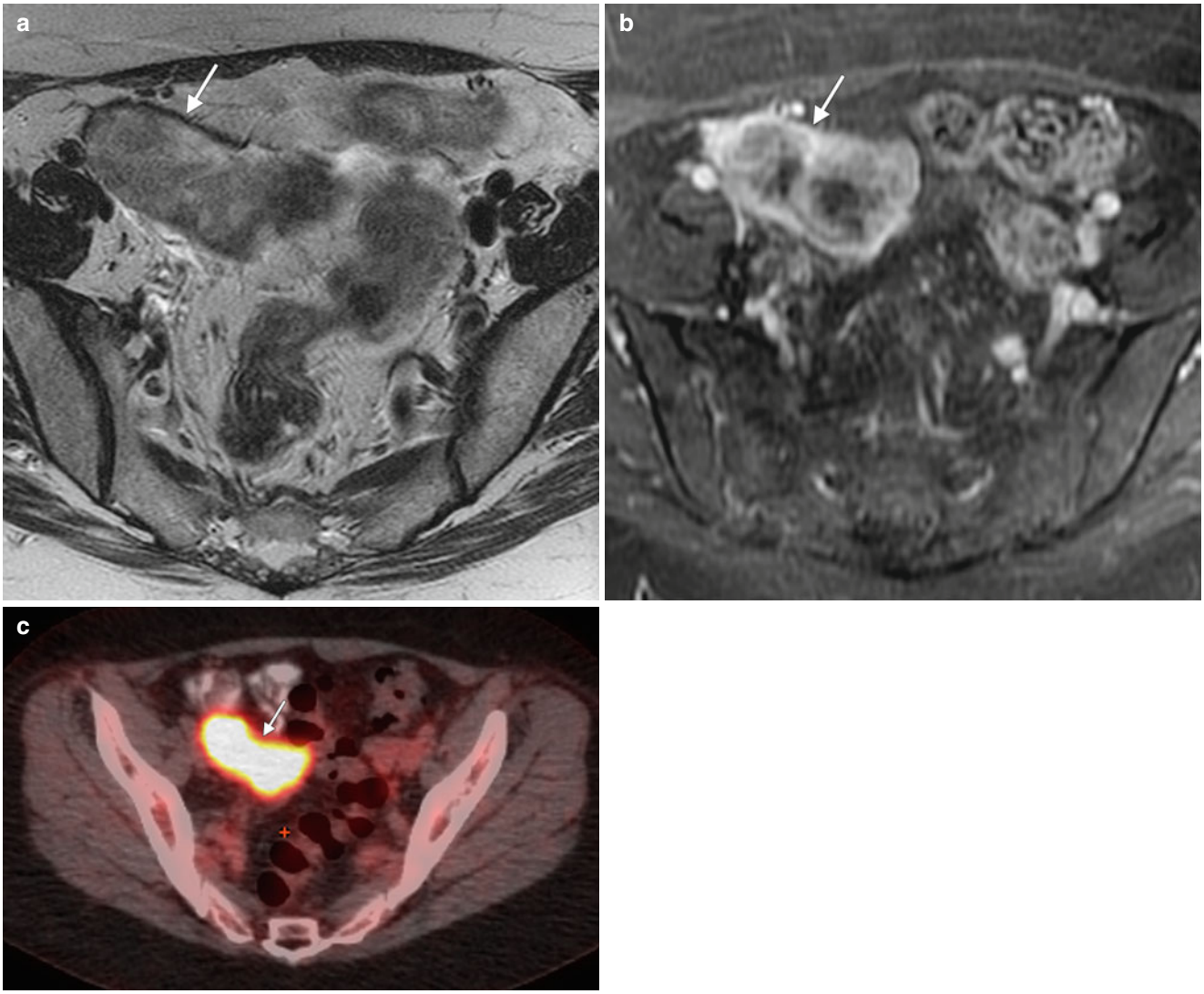

Fig. 1.23 Metastases to the ovary in a 45-year-old woman with a history of colon cancer are seen on imaging performed because of rising tumor markers. An axial T2-weighted MR image (**a**), a fat-suppressed T1-weighted image after intravenous gadolinium (**b**), and a fused (PET/CT) image (**c**) demonstrate a right ovarian mass (*arrows*). Pathology confirmed metastatic adenocarcinoma consistent with a colonic primary tumor

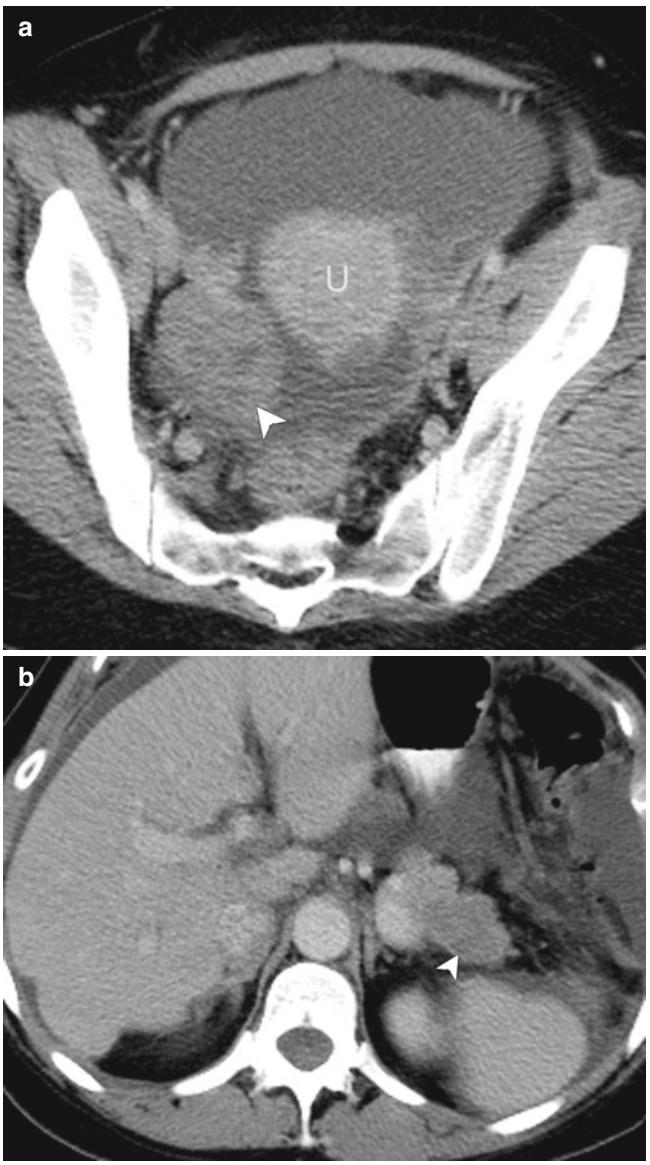

Fig. 1.24 Right adnexal, mixed solid/cystic mass (*arrow*) was identified on a contrast-enhanced CT scan of the pelvis (**a**) in a 44-year-old woman. The uterus (*U*) is also shown. An axial CT image of the upper abdomen (**b**) also demonstrated a pancreatic tail mass (*arrowhead*). Specimens from hysterectomy and bilateral salpingo-oophorectomy were consistent with metastatic adenocarcinoma. Immunohistochemistry findings supported an upper gastrointestinal or pancreatic primary tumor

1.4 Ovarian Cancer Staging

Regardless of the histologic subtype, ovarian cancer is staged according to the American Joint Committee on Cancer TNM criteria [10] or the International Federation of Gynecology and Obstetrics (FIGO) staging [11] (Table 1.8).

Table 1.8 Staging of ovarian cancer[a]

TNM category[b]	FIGO category[c]	Ovary
T1	I	Tumor confined to ovaries
T1a	Ia	Tumor confined to one ovary, capsule intact
T1b	Ib	Tumor confined to both ovaries, capsule intact
T1c	Ic	Tumor present on the surface of one or both ovaries; capsule ruptured; malignant ascites (positive peritoneal washings)
T2	II	Tumor involving one or both ovaries with pelvic extension
T2a	IIa	Extension and/or metastasis to the uterus or tubes
T2b	IIb	Extension to other pelvic tissue
T2c	IIc	Tumor either stage IIa or IIb but present on surface of one or both ovaries; or capsule ruptured; or malignant ascites (positive peritoneal washings)
T3 and/or N1	III	Tumor involving one or both ovaries with peritoneal implants outside the pelvis or positive retroperitoneal or inguinal nodes
T3a	IIIa	Tumor limited to the true pelvis with negative lymph nodes but with histologically confirmed microscopic peritoneal metastases
T3b	IIIb	Peritoneal metastases, none >2 cm in diameter; negative lymph nodes
T3c and/or N1	IIIc	Abdominal implants >2 cm in diameter or positive retroperitoneal or inguinal nodes
M1	IV	Distant metastases

[a]Regardless of histologic subtype
[b]American Joint Committee on Cancer TNM criteria [10]
[c]International Federation of Gynecology and Obstetrics [11]

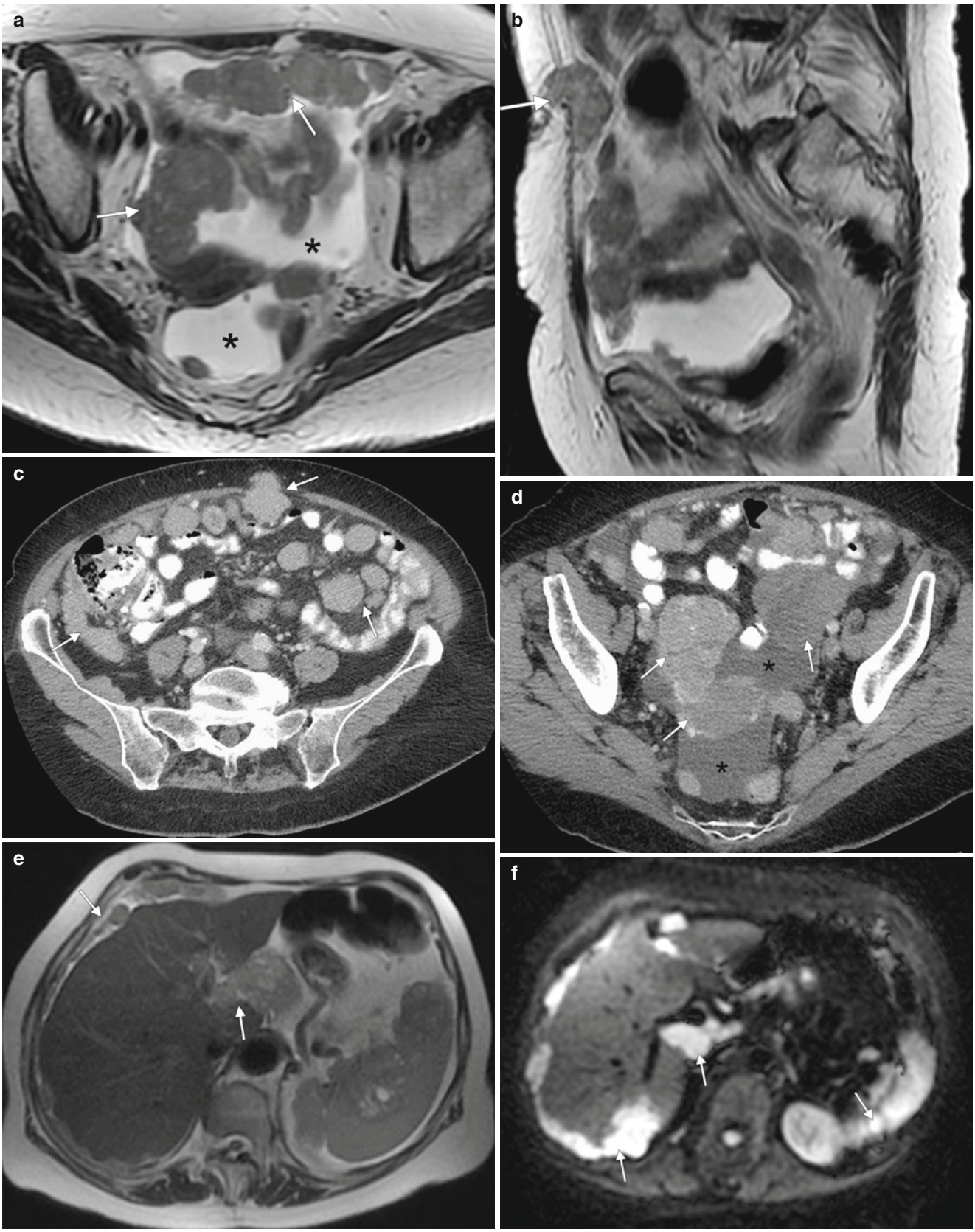

Fig. 1.25 73-year-old woman with ovarian cancer. Axial (**a**) and sagittal (**b**) T2-weighted images of the pelvis, axial contrast-enhanced CT scans of the pelvis (**c**, **d**), and a fat-suppressed T2-weighted MR image (**e**) and a diffusion-weighted MR image (**f**) of the upper abdomen demonstrate diffuse peritoneal carcinomatosis including implants in the umbilicus, liver, spleen, and pelvis (*arrows*). Ascites is also present (*asterisks*)

Fig. 1.26 The usefulness of imaging in the assessment of complications from ovarian cancer can be seen in this example of a 54-year-old woman with high-grade papillary serous carcinoma of the ovary presenting with bowel obstruction. This coronal CT scan demonstrates dilated bowel loops secondary to diffuse serosal metastatic deposits (*arrows*). Ascites is also present (*asterisks*)

1.5 Role of Imaging in Ovarian Cancer Staging

The role of imaging is better established and more widely accepted in the staging of ovarian cancer than in other gynecologic malignancies. Table 1.9 lists the imaging features that are important for staging and should be included in the radiology report. Although CT and MRI have similar accuracy when used for this purpose, CT is most commonly performed [13, 14]. MRI is particularly useful in patients with contraindications to enhanced CT, including pregnancy, renal impairment, and allergy to iodinated contrast [15]. Intraperitoneal dissemination is the most common route of spread of ovarian cancer. Peritoneal implants may occur anywhere in the peritoneal cavity. The most common sites include the pouch of Douglas, paracolic gutters, the surface of the small and large bowel, the greater omentum, the surface of the liver, and the subphrenic space. MRI is very sensitive (95 %) in detecting peritoneal metastases, which appear as nodular or plaquelike enhancing soft tissue masses showing delayed enhancement following intravenous gadolinium [16]. The detection of small implants is facilitated when they are surrounded by ascites. MRI is also useful in differentiating between subcapsular liver implants and parenchymal liver metastasis, which alters staging and therapy [17]. Preliminary reports have also shown that diffusion-weighted MRI (DW-MRI) may be helpful for detecting the extent of peritoneal disease. On conventional T1-weighted images (T1WI), T2WI, and fat-suppressed T1WI, small serosal implants invaginated within peritoneal reflections are often obscured by adjacent structures. DW-MRI depicts deposits on the visceral peritoneum as foci of high signal intensity against a background of suppressed signal from surrounding ascites, bowel contents, and fat, making them more conspicuous.

Table 1.9 Information to include in the radiology report for ovarian cancer staging

Stage	Parameter	Information to report
T stage	Size	3 Dimensions
	Location	Unilateral vs bilateral
	Characteristics	Complex masses, septations, papillary projections, enhancing nodules, necrosis
	Local extent	Involvement of adjacent organs (*e.g.*, bowel, bladder)
		Location and size of peritoneal implants influence staging (*see* Table 1.8)
		Metastatic deposits in potentially nonresectable sites should be specifically mentioned
N stage	Size	2 Dimensions in the axial plane
	Regional nodes	Para-aortic
		Common, internal, and external iliac (including obturator)
		Inguinal
M stage	Location	Parenchymal liver, lung, skeletal metastases
		Nonregional lymph nodes, above the renal hilum
	Peritoneal deposits	Included in the T stage and do not affect M stage
Other	Ascites	Comment on volume (mild, moderate, large), simple vs complex
		The presence of ascites does not affect staging unless malignant cells are present
		Malignant pleural effusion is M1
		Benign pleural effusion does not impact staging, but size of pleural effusion correlates with outcomes [12]

1.6 Posttreatment Assessment and Recurrence

The mainstay of ovarian cancer response assessment is based on serial measurements of serum CA 125 in combination with morphologic evaluation using CT, MRI, or both [18, 19]. The limitations of CA 125 as a tumor marker are well known. Normal values do not exclude the presence of disease, and elevated values usually indicate recurrence but cannot establish its location or extent [20–22]. Imaging is comparable to laparotomy but superior to serum CA 125 in the detection of residual or recurrent peritoneal and serosal implants in women who have been treated for ovarian cancer [16, 23]. Imaging is also used to evaluate for the presence of features that would preclude secondary cytoreduction, such as pelvic side wall invasion (suspected when the tumor lies within 3 mm of the pelvic side wall or when the iliac vessels are surrounded or distorted by tumor) and osseous invasion from an adjacent pelvic side wall recurrence. This evaluation is extremely relevant because the previously advocated "second look surgery" (surgical re-exploration following initial surgery and the completion of chemotherapy in patients without clinical evidence of recurrent tumor) is no longer part of standard clinical practice. Imaging diagnosis of recurrence may obviate a second laparotomy, because secondary cytoreduction is only justified if resection with no residual tumor is possible.

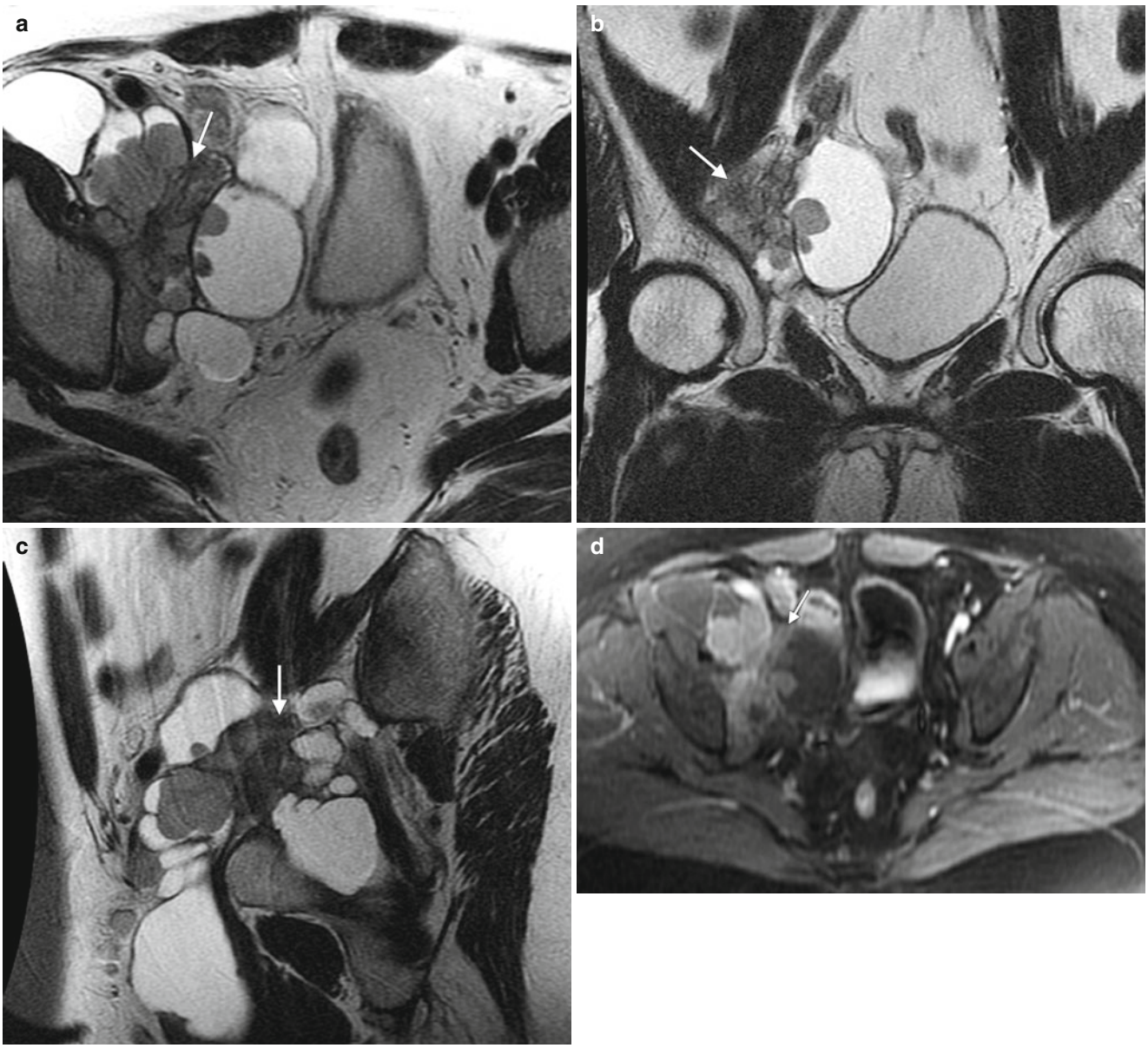

Fig. 1.27 Raised CA 125 prompted a pelvic MRI examination in this 53-year-old woman with a history of well-differentiated ovarian cystadenocarcinoma of low malignant potential; 5 years earlier, she underwent radical hysterectomy and bilateral salpingo-oophorectomy. Axial (**a**), coronal (**b**), and sagittal (**c**) T2-weighted MR images and a fat-suppressed, axial T1-weighted image after intravenous gadolinium (**d**) demonstrated an enhancing mixed cystic and solid mass (*arrows*) in the right hemipelvis with involvement of the right pelvic sidewall consistent with cancer recurrence

1.7 Primary Fallopian Tube Carcinoma

Imaging plays a key role in the detection and characterization of adnexal masses. Ovarian and fallopian tube lesions display a myriad of imaging findings, which are dependent on the tissue type present. Knowledge of such features can enable a definitive diagnosis in certain cases, or at least can help to narrow the differential diagnosis. Imaging also allows local staging and detection of metastatic and recurrent disease, thus helping to formulate an individualized patient management plan.

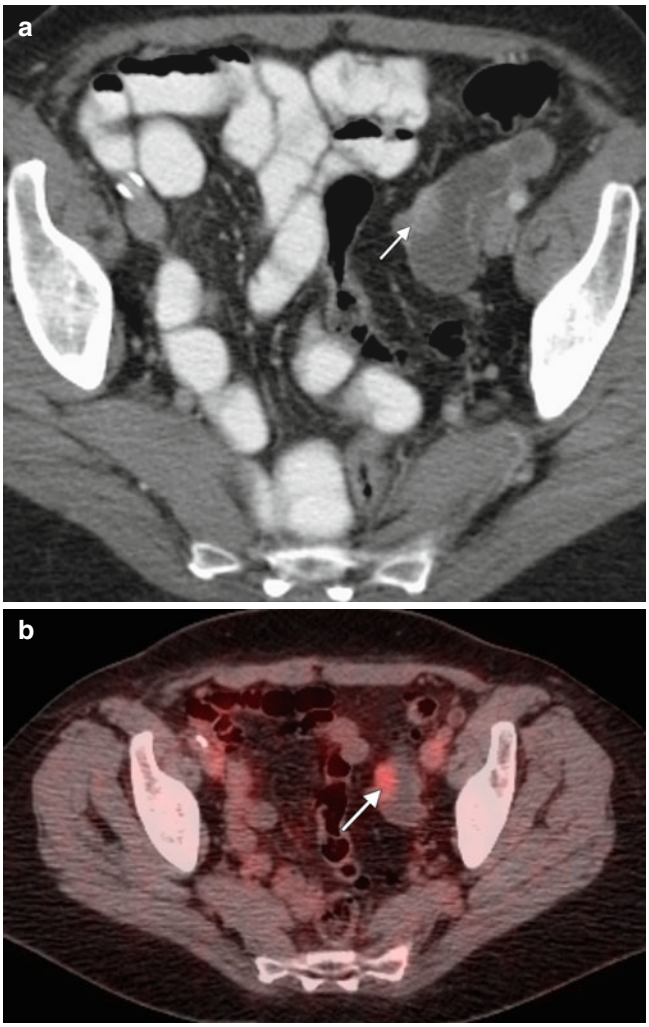

Fig. 1.28 The tubal origin of a primary adnexal tumor is occasionally apparent on imaging. In this case, a 67-year-old woman was found to have bilateral pulmonary nodules and thoracic lymphadenopathy incidentally detected on CT scans. A supraclavicular lymph node biopsy showed metastatic adenocarcinoma of Müllerian origin. Axial contrast enhanced CT (**a**) and fused FDG-PET/CT (**b**) of the pelvis demonstrated left hydrosalpinx containing enhancing mural nodules (*arrows*)

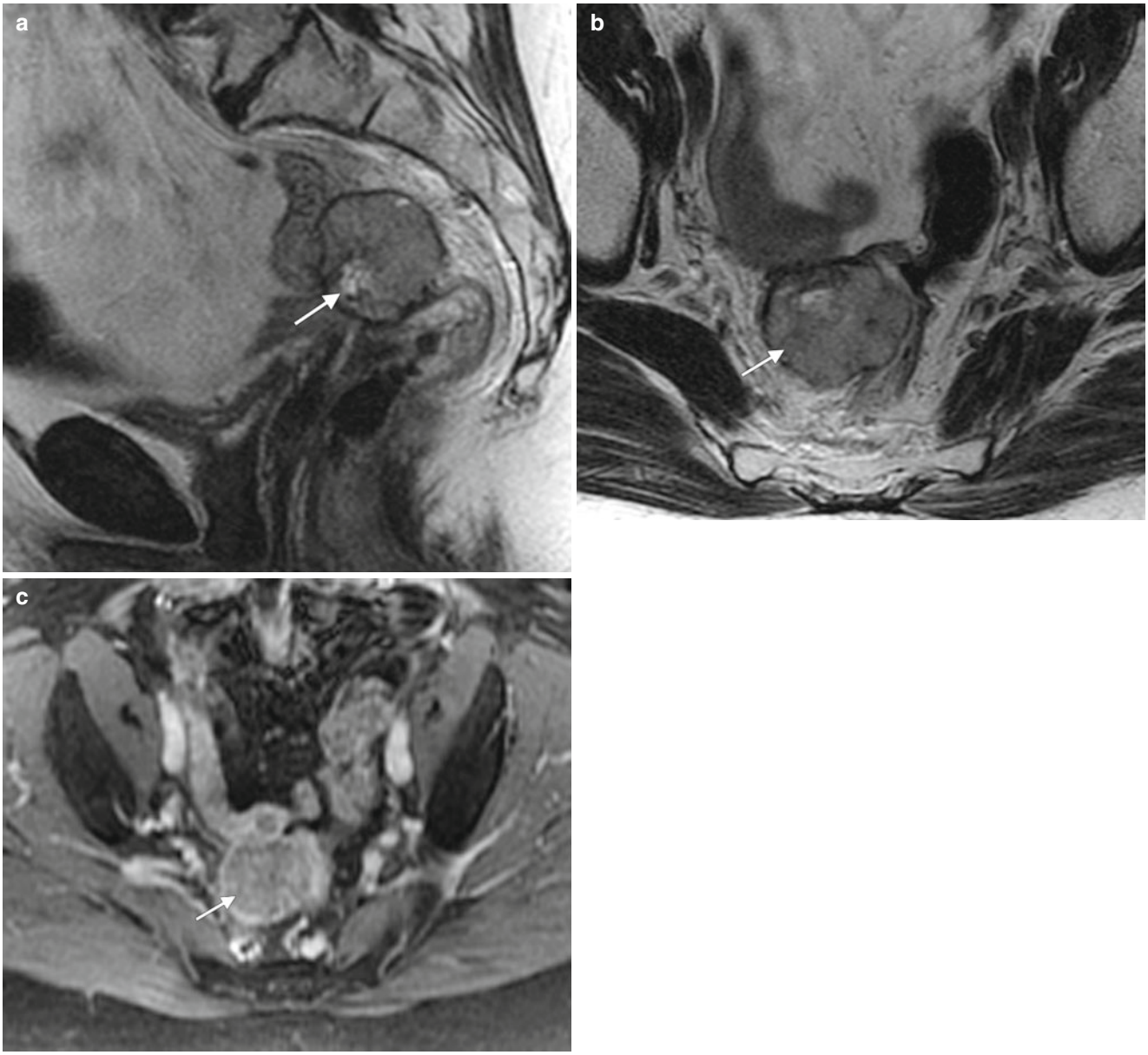

Fig. 1.29 Fallopian tube carcinoma staging and recurrence. The pattern of spread and sites of recurrence are similar to those of primary ovarian cancer. These representative images are from a 62-year-old woman who underwent a radical hysterectomy and bilateral salpingo-oophorectomy for primary fallopian tube carcinoma 4 years earlier. Axial (**a**) and sagittal (**b**) T2-weighted MR images and a fat-suppressed axial T1-weighted image after intravenous gadolinium (**c**) demonstrate a heterogeneously enhancing mass (*arrows*) in the right superolateral aspect of the vaginal cuff, inseparable from adjacent sigmoid and small bowel loops. The patient underwent surgical resection, and pathology showed recurrent high-grade serous carcinoma

References

1. Siegel R, Ward E, Brawley O, Jemal A. Cancer statistics, 2011: the impact of eliminating socioeconomic and racial disparities on premature cancer deaths. CA Cancer J Clin. 2011;61:212–36. doi:10.3322/caac.20121.
2. Omura GA, Brady MF, Homesley HD, et al. Long-term follow-up and prognostic factor analysis in advanced ovarian carcinoma: the Gynecologic Oncology Group experience. J Clin Oncol. 1991;9:1138–50.
3. Ramirez I. The role of surgery in the management of epithelial ovarian cancer. Cancer Control. 2011;18:22–30.
4. Vergote I, Trope CG, Amant F, et al. Neoadjuvant chemotherapy or primary surgery in stage IIIC or IV ovarian cancer. N Engl J Med. 2010;363:943–53. doi:10.1056/NEJMoa0908806.
5. Jung SE, Lee JM, Rha SE, Byun JY, Jung JI, Hahn ST. CT and MR imaging of ovarian tumors with emphasis on differential diagnosis. Radiographics. 2002;22:1305–25.
6. Timmerman D, Ameye L, Fischerova D, et al. Simple ultrasound rules to distinguish between benign and malignant adnexal masses before surgery: prospective validation by IOTA group. BMJ. 2010;341:c6839. doi:10.1136/bmj.c6839.
7. Spencer JA, Gore RM. The adnexal incidentaloma: a practical approach to management. Cancer Imaging. 2011;11:48–51. doi:10.1102/1470-7330.2011.0008.
8. Levine D, Brown DL, Andreotti RF, et al. Management of asymptomatic ovarian and other adnexal cysts imaged at US Society of Radiologists in Ultrasound Consensus Conference Statement. Radiology. 2010;256:943–54. doi:10.1148/radiol.10100213.
9. Spencer JA, Forstner R, Cunha TM, Kinkel K. ESUR guidelines for MR imaging of the sonographically indeterminate adnexal mass: an algorithmic approach. Eur Radiol. 2010;20:25–35.
10. Edge SB, Byrd DR, Compton CC, Fritz AG, Greene FL, Trotti A, editors. AJCC cancer staging manual. 7th ed. New York: Springer; 2010.
11. FIGO Committee on Gynecologic Oncology. Current FIGO staging for cancer of the vagina, fallopian tube, ovary, and gestational trophoblastic neoplasia. Int J Gynaecol Obstet. 2009;105:3–4.
12. Mironov O, Ishill NM, Mironov S, et al. Pleural effusion detected at CT prior to primary cytoreduction for stage III or IV ovarian carcinoma: effect on survival. Radiology. 2011;258:776–84.
13. Tempany CM, Zou KH, Silverman SG, Brown DL, Kurtz AB, McNeil BJ. Staging of advanced ovarian cancer: comparison of imaging modalities–report from the Radiological Diagnostic Oncology Group. Radiology. 2000;215:761–7.
14. Coakley FV. Staging ovarian cancer: role of imaging. Radiol Clin North Am. 2002;40:609–36. doi:10.1007/s00330-010-1886-4.
15. Forstner R, Sala E, Kinkel K, Spencer JA. ESUR guidelines: ovarian cancer staging and follow-up. Eur Radiol. 2010;20:2773–80.
16. Ricke J, Sehouli J, Hach C, Hanninen EL, Lichtenegger W, Feliz R. Prospective evaluation of contrast-enhanced MRI in the depiction of peritoneal spread in primary or recurrent ovarian cancer. Eur Radiol. 2003;13:943–9. doi:10.1148/radiol.2482070371.
17. Akin O, Sala E, Moskowitz CS, et al. Perihepatic metastases from ovarian cancer: sensitivity and specificity of CT for the detection of metastases with and those without liver parenchymal invasion. Radiology. 2008;248:511–7. doi:10.1148/radiol.10100162.
18. Rustin G, Tuxen M. Use of CA 125 in follow-up of ovarian cancer. Lancet. 1996;348(9021):191–2. doi:S0140673696240292 [pii].
19. Tuxen MK, Soletormos G, Dombernowsky P. Tumor markers in the management of patients with ovarian cancer. Cancer Treat Rev. 1995;21:215–45.
20. Folk JJ, Botsford M, Musa AG. Monitoring cancer antigen 125 levels in induction chemotherapy for epithelial ovarian carcinoma and predicting outcome of second-look procedure. Gynecol Oncol. 1995;57:178–82. doi:10.1006/gyno.1995.1121.
21. Patsner B, Orr Jr JW, Mann Jr WJ, Taylor PT, Partridge E, Allmen T. Does serum CA-125 level prior to second-look laparotomy for invasive ovarian adenocarcinoma predict size of residual disease? Gynecol Oncol. 1990;38:373–6. doi:10.1016/0090-8258(90)90076-W [pii].
22. Rubin SC, Hoskins WJ, Hakes TB, et al. Serum CA 125 levels and surgical findings in patients undergoing secondary operations for epithelial ovarian cancer. Am J Obstet Gynecol. 1989;160:667–71.
23. Low RN, Duggan B, Barone RM, Saleh F, Song SY. Treated ovarian cancer: MR imaging, laparotomy reassessment, and serum CA-125 values compared with clinical outcome at 1 year. Radiology. 2005;235:918–26.

Endometrial Cancer

2

Hebert Alberto Vargas, Pier Luigi Di Paolo,
Asim Afaq, and Oguz Akin

2.1 Anatomy, Histology, and Physiology

The uterus is the most common site of cancer in the female genital tract [1, 2]. Most uterine cancers in the United States arise from the endometrium, which is the innermost layer of the uterine corpus and constitutes the lining of the uterine cavity (Table 2.1). The endometrium is an integral component of the female reproductive system, undergoing cyclic changes in response to intricate variations in circulating levels of sex hormones, which ultimately result in the development of a local environment optimal for the implantation and subsequent development of an embryo (Table 2.2). Shifting trends with an apparent increase in incidence of endometrial cancer across the world probably reflect changes in the prevalence of established risk factors, namely obesity, low parity, late menarche, early menopause, and increasing age [3]. Most patients present at an older age than patients with cervical cancer. The typical clinical scenario is vaginal bleeding in a postmenopausal female. Prognosis depends on a number of factors: the most important is the depth of myometrial invasion by tumor, but other factors include stage, lymphovascular invasion, histologic grade, and lymph node status. If detected at an early stage, endometrial cancer is potentially curable [4]. Diagnosis is made on the basis of clinical suspicion with pathological confirmation from transvaginal biopsy or curettage of the endometrial cavity. Imaging has little role in the diagnosis of the primary tumor, but it is helpful for staging newly diagnosed cancer and detecting recurrence following endometrial cancer treatment (Table 2.3).

H.A. Vargas, MD (✉) • P.L. Di Paolo, MD • A. Afaq, MD
Department of Radiology,
Memorial Sloan-Kettering Cancer Center,
1275 York Avenue, Room C278, New York, NY 10065, USA
e-mail: vargasah@mskcc.org; dipaolop@mskcc.org;
asimafaq@doctors.org.uk

O. Akin, MD (✉)
Weill Medical College of Cornell University,
New York, NY, USA

Department of Radiology, Body Imaging Service,
Memorial Sloan-Kettering Cancer Center,
1275 York Avenue, New York, NY 10065, USA
e-mail: akino@mskcc.org

O. Akin (ed.), *Atlas of Gynecologic Oncology Imaging*, Atlas of Oncology Imaging,
DOI 10.1007/978-1-4614-7212-4_2, © Springer Science+Business Media New York 2014

Table 2.1 Uterine zonal anatomy and histology

Layer	Histology	Features relevant to imaging
Endometrium	Single-layer columnar epithelium resting on a layer of connective tissue that varies in thickness throughout the menstrual cycle	Thickness varies throughout menstrual cycle (thinnest just after menstruation and gradual thickening over the cycle)
Myometrium	Smooth muscle layer; the innermost aspect, the "junctional zone," constitutes the interface between the myometrium and endometrium	May appear indistinct or shrink during menstruation; the junctional zone may thicken (paralleling changes in endometrial thickness, but to a lesser degree) and mimic uterine pathology (e.g., adenomyosis)
Perimetrium	Serosal layer covering the dorsal and ventral aspects of the uterus	

Table 2.2 Factors affecting endometrial thickness

Factor	Comments
Physiologic	In premenopausal women, endometrial cavity is thinnest just after menstruation and gradually thickens over the menstrual cycle
Hormone replacement therapy	Biopsy is warranted if endometrial thickness is >8 mm if the patient is asymptomatic or ≥5 mm in the presence of postmenopausal bleeding
Endometrial hyperplasia/polyp	Imaging cannot differentiate endometrial hyperplasia or polyps from stage IA endometrial cancer; the most helpful feature to exclude cancer is the absence of myometrial or cervical invasion

Table 2.3 Imaging techniques used for evaluation of the endometrium

Technique	Main use	Advantages	Disadvantages
Ultrasound	First-line evaluation of uterine pathology	Readily available Cost-effective Usually well tolerated	Operator-dependent Limited accuracy in staging endometrial cancer
CT	Staging of endometrial cancer	Fast Reproducible More widely available than MRI	Involves ionizing radiation Contrast resolution is not as good as ultrasound or MRI
MRI	Most accurate for local staging (*e.g.*, depth of myometrial invasion) and evaluation of recurrence	Superb contrast resolution No ionizing radiation	More expensive and less readily available than ultrasound or CT
Positron emission tomography (PET)	Evaluation of metastatic disease	Depicts both anatomy and function Whole-body evaluation	Radiation from both CT and PET component of the examination

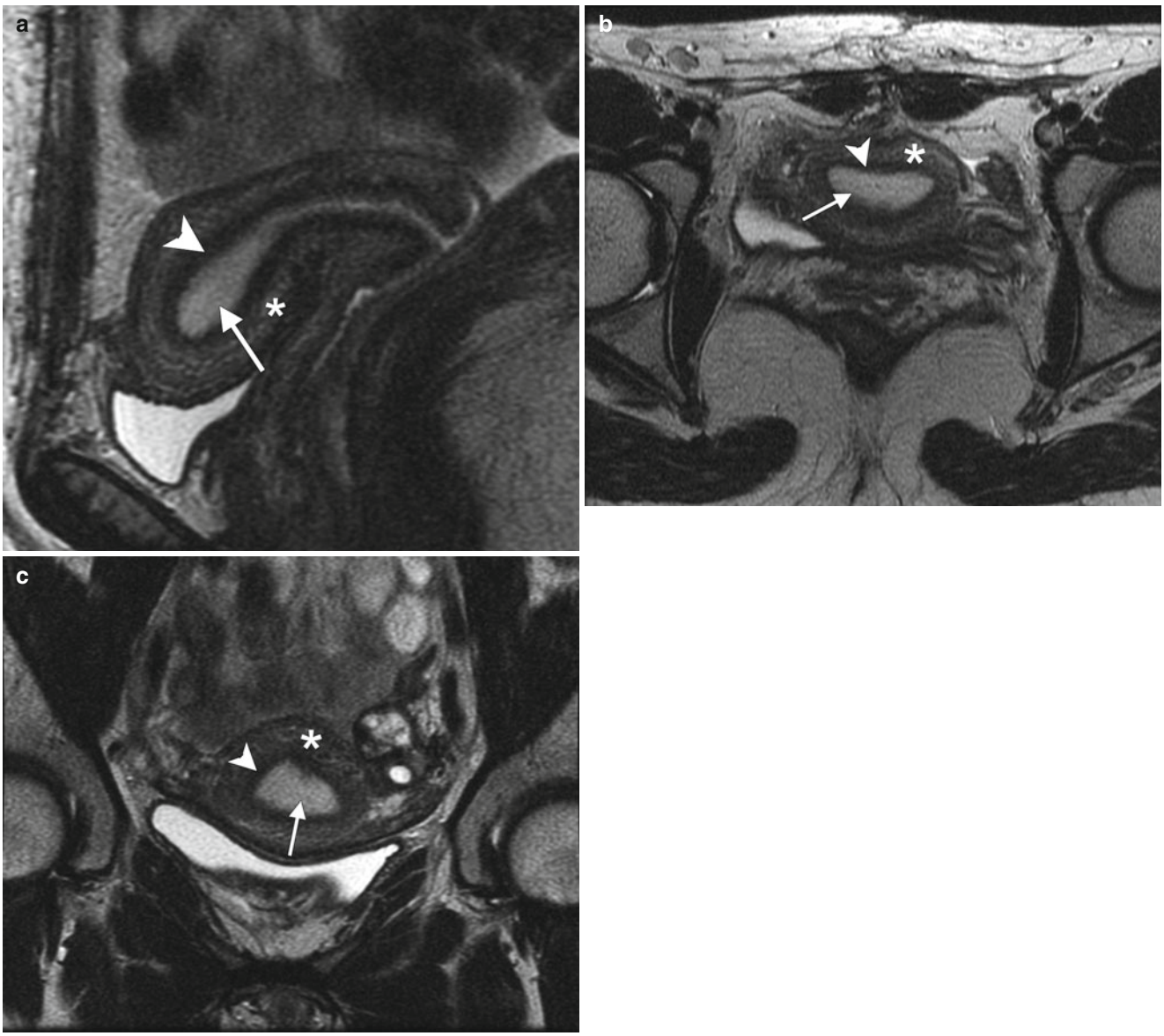

Fig. 2.1 Zonal anatomy of the normal uterus. T2-weighted sagittal (**a**), axial (**b**), and coronal (**c**) images demonstrate the normal uterine zonal anatomy in a premenopausal woman, including the endometrium (*arrows*), junctional zone (*arrowheads*), and outer myometrium (*asterisks*)

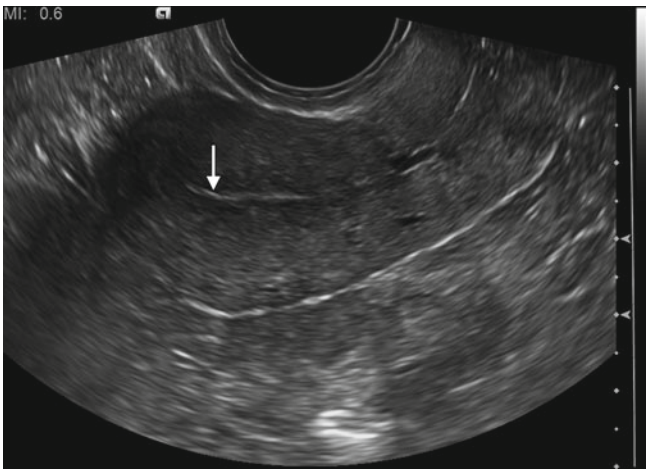

Fig. 2.2 Longitudinal 2-D transvaginal ultrasound image of the normal endometrium (*arrow*). The hallmark of endometrial cancer on imaging is thickening of the endometrial cavity. Varying size cutoffs have been proposed: the prevalence of endometrial cancer has been reported to be 0.6 % when the endometrial thickness is <5 mm, compared with 19 % when the endometrial thickness is 5 mm or more [5]. However, endometrial thickening may be present in many physiologic and benign conditions

2.2 Benign Uterine Pathology

Benign pathologies to be considered in symptomatic women include adenomyosis, leiomyomata (fibroids), and intravenous leiomyomatosis.

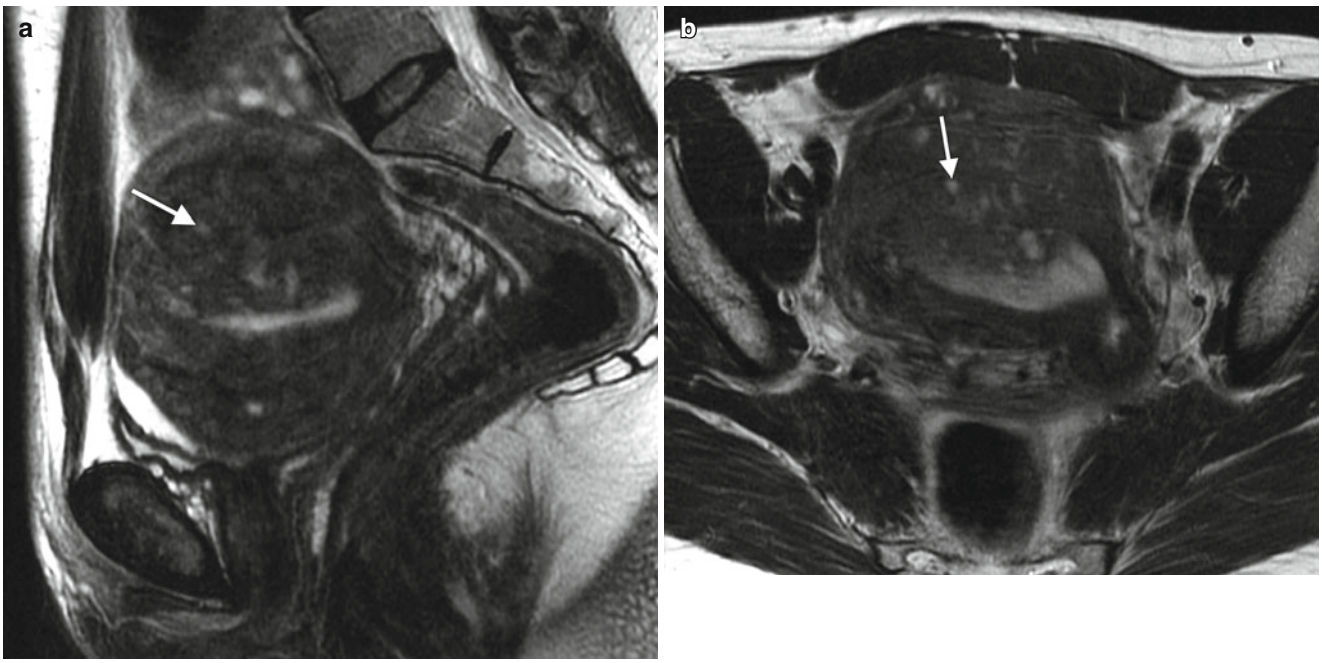

Fig. 2.3 Adenomyosis is the term used for the presence of endometrial glands within the myometrium. The most common imaging findings are thickening of the junctional zone (>12 mm on the midsagittal plane on T2-weighted MRI has an accuracy of 85 % and specificity of 96 % [6]) and the presence of "microcysts" in the myometrium measuring 3–7 mm. *Pitfall*: Physiologic myometrial contractions may simulate the presence of adenomyosis. The use of antiperistaltic medication or repeat imaging a few minutes after the initial acquisition have been proposed as methods to circumvent this issue, as myometrial contractions should subside and adenomyosis persists following such maneuvers. These representative images show a 45-year-old premenopausal woman with severe menstrual cramps and menorrhagia. Sagittal (**a**) and axial (**b**) T2-weighted images demonstrate a thickened junctional zone with multiple punctate cystic spaces (*arrows*) consistent with adenomyosis

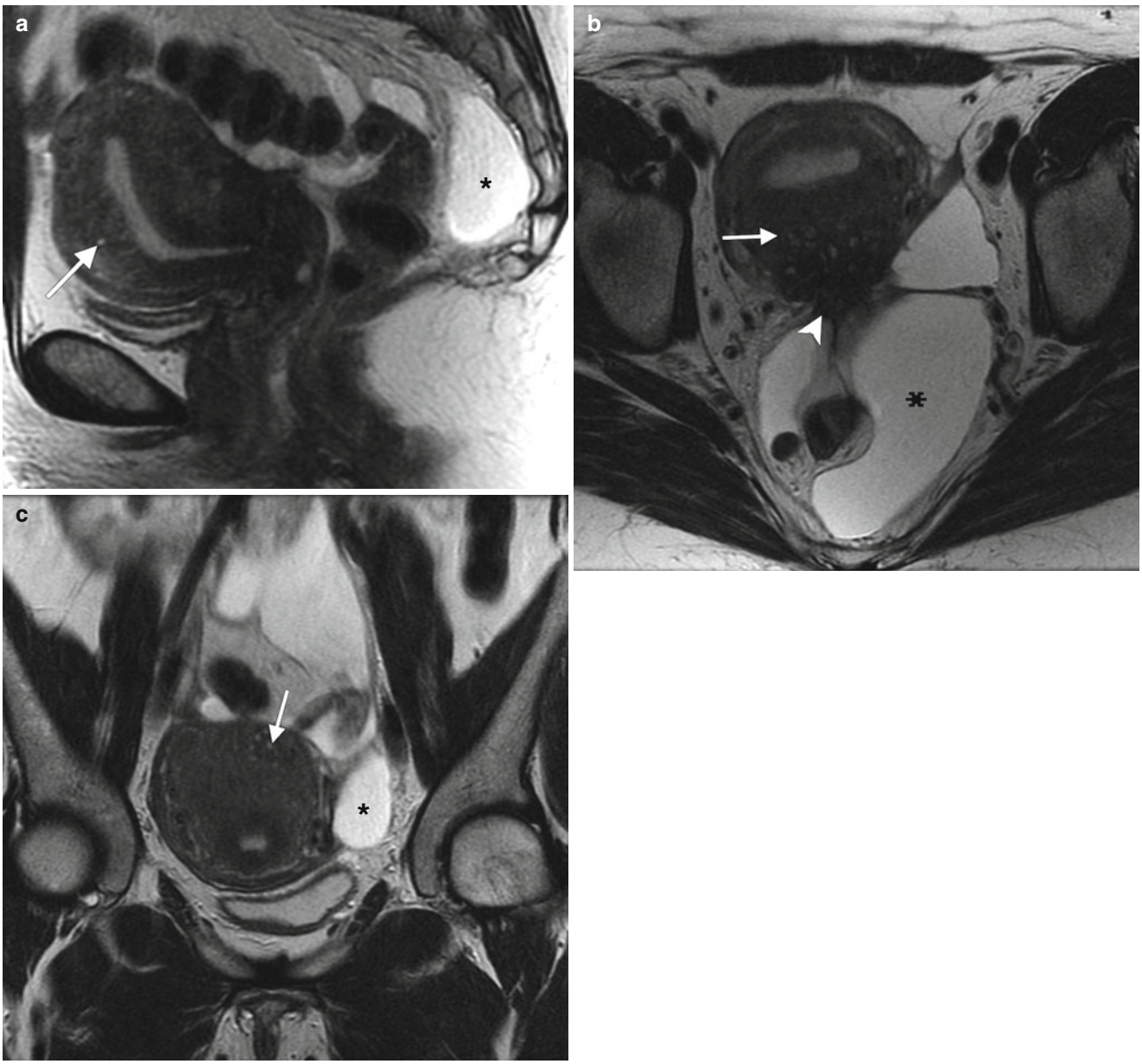

Fig. 2.4 42-year-old woman with a history of appendectomy and myomectomy for dysfunctional uterine bleeding. Sagittal (**a**), axial (**b**), and coronal (**c**) T2-weighted MR images demonstrate thickening of the junctional zone with small T2-hyperintense spaces (*arrows*) consistent with adenomyosis. There is also retraction and tethering of the soft tissues along the posterior uterine wall (*arrowhead*) suspicious for endometriosis. A multiloculated cystic structure (*asterisks*) conforming to the shape of the pelvis probably represents a peritoneal inclusion cyst

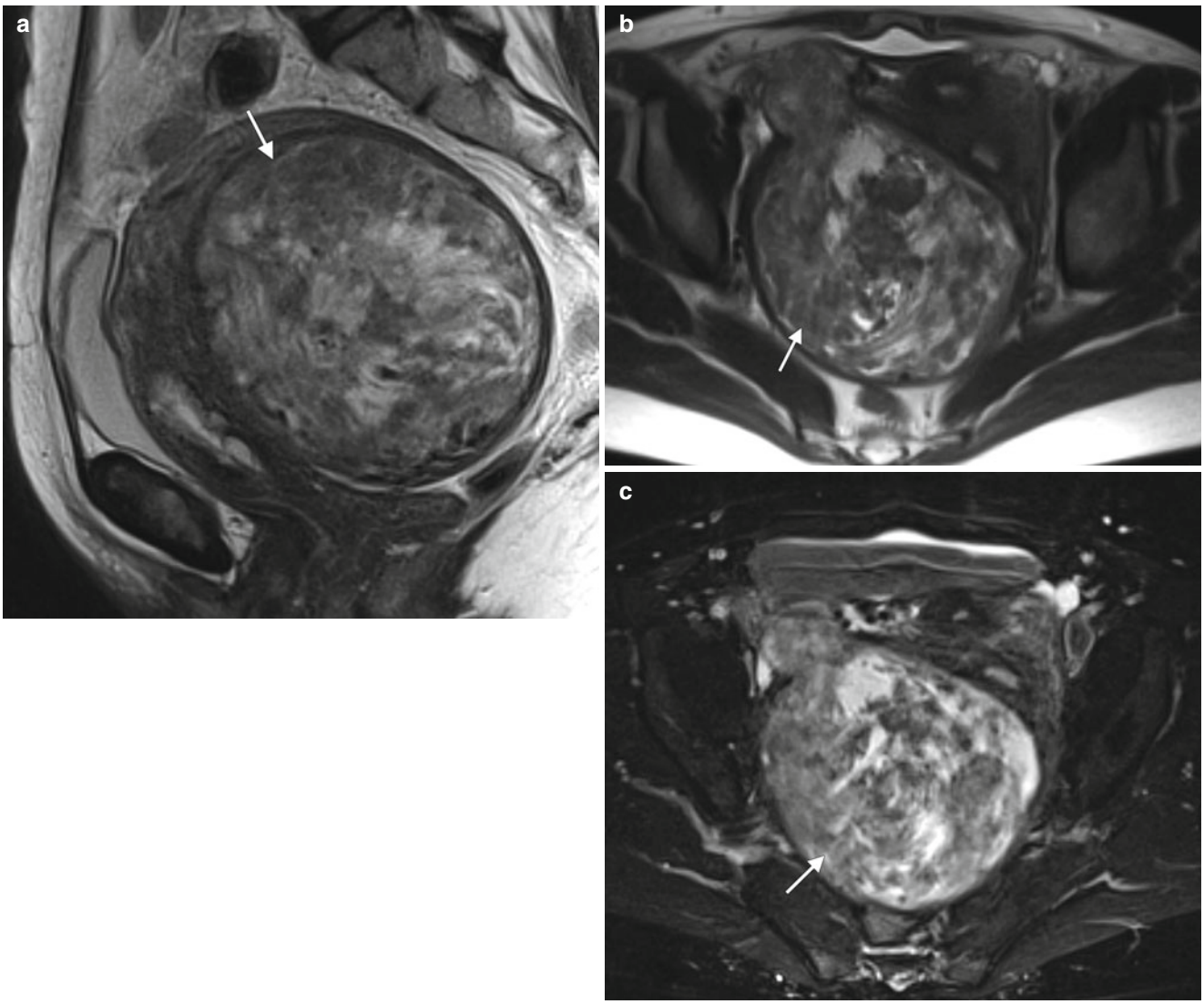

Fig. 2.5 Uterine leiomyomata (fibroids) are the most common tumors in women. They are benign masses originating from the myometrium. Symptoms vary and are related to the size and location of the tumor. The most common symptoms are menorrhagia, pelvic pressure (pain, increased urinary frequency), and infertility. These representative MR images are from a 51-year-old woman with pelvic pressure and dyspareunia. Sagittal (**a**) and axial (**b**) T2-weighted images and fat-suppressed T1-weighted images following the intravenous administration of gadolinium (**c**) demonstrate a heterogeneously enhancing myometrial mass (*arrows*). The patient underwent a hysterectomy for symptom control. Pathology confirmed the diagnosis of uterine leiomyoma

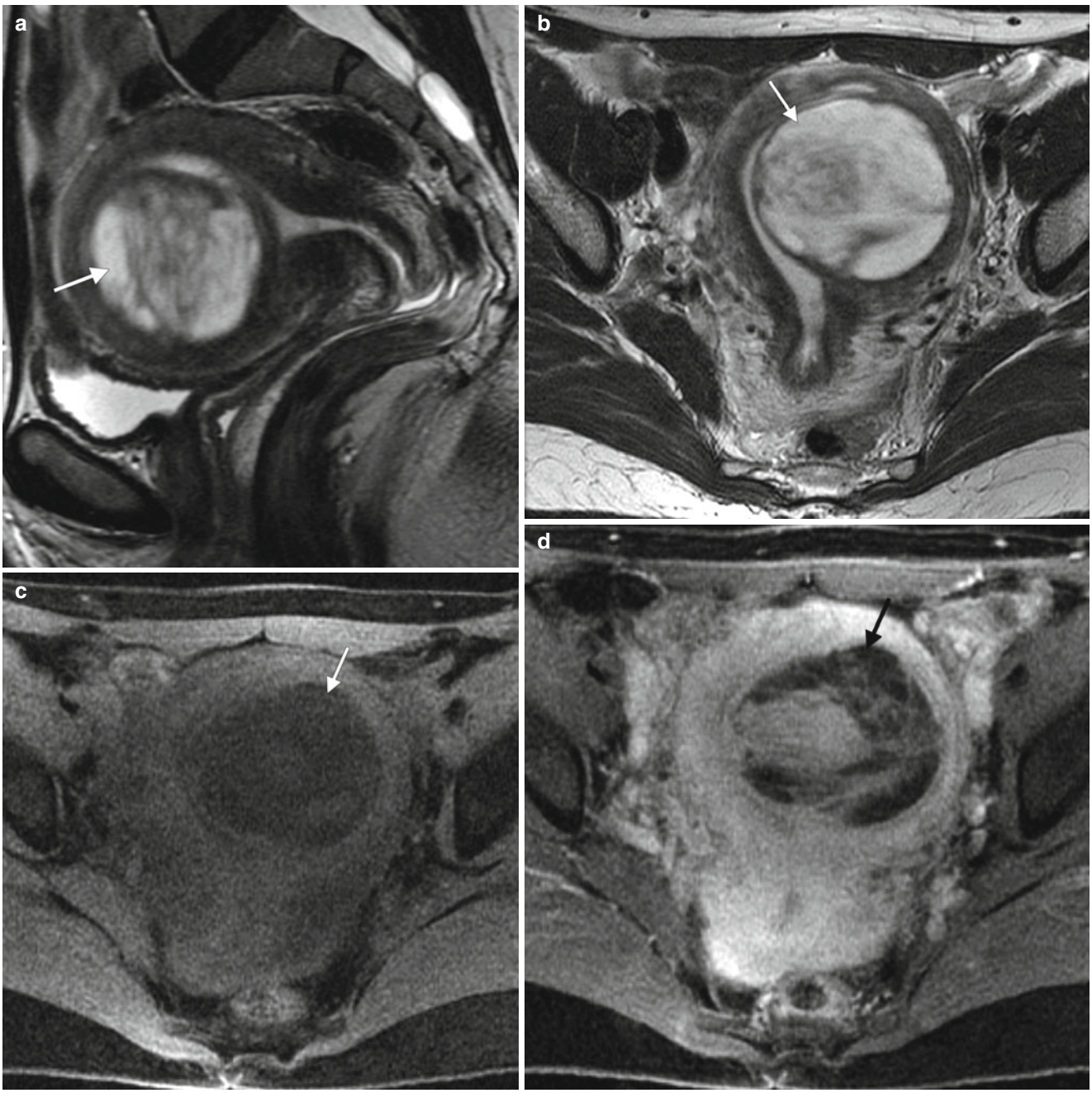

Fig. 2.6 The appearance of uterine leiomyomas is variable. These images show a 44-year-old woman with worsening menometrorrhagia over 3 years. Sagittal (**a**) and axial (**b**) T2-weighted MR images and axial fat-suppressed T1-weighted images before intravenous gadolinium (**c**) and after gadolinium (**d**) demonstrate a predominantly cystic, well-circumscribed, submucosal myometrial mass in the left uterine body (*arrows*) with enhancing septations. Pathology showed a degenerating leiomyoma with hydropic changes

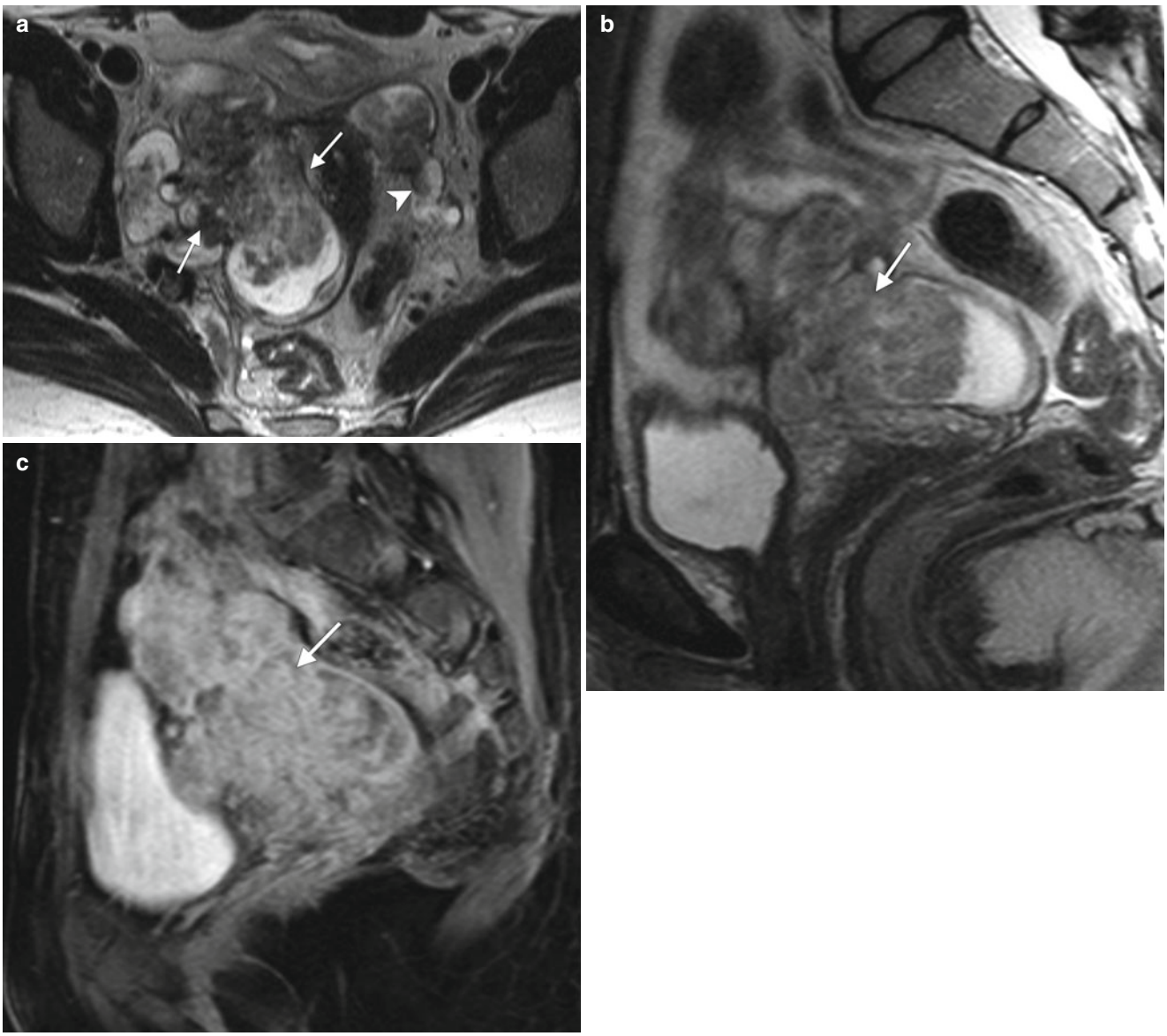

Fig. 2.7 Intravenous leiomyomatosis is a rare form of uterine leiomyomatosis, usually presenting in premenopausal women. It is characterized by intravascular extension of nodular masses composed histologically of benign smooth muscle. Enhancing tumors may extend to uterine, gonadal, and iliac veins, inferior vena cava, and heart and pulmonary vasculature. This pathology is estrogen-dependent, and long-term prognosis is very good after resection. Below are representative images from a 44-year-old woman with multiple previous uterine myomectomies. Axial (**a**) and sagittal (**b**) T2-weighted MR images and a sagittal fat-suppressed, T1-weighted image following intravenous administration of gadolinium (**c**) demonstrate multiple, bilateral, heterogeneously enhancing masses in the pelvis (*arrows*). Coronal (**d**) and sagittal (**e**) contrast-enhanced CT scans demonstrate tumor extension into the right common iliac vein and inferior vena cava (*arrowheads*). Pathology confirmed the diagnosis of benign leiomyomata with intravenous leiomyomatosis

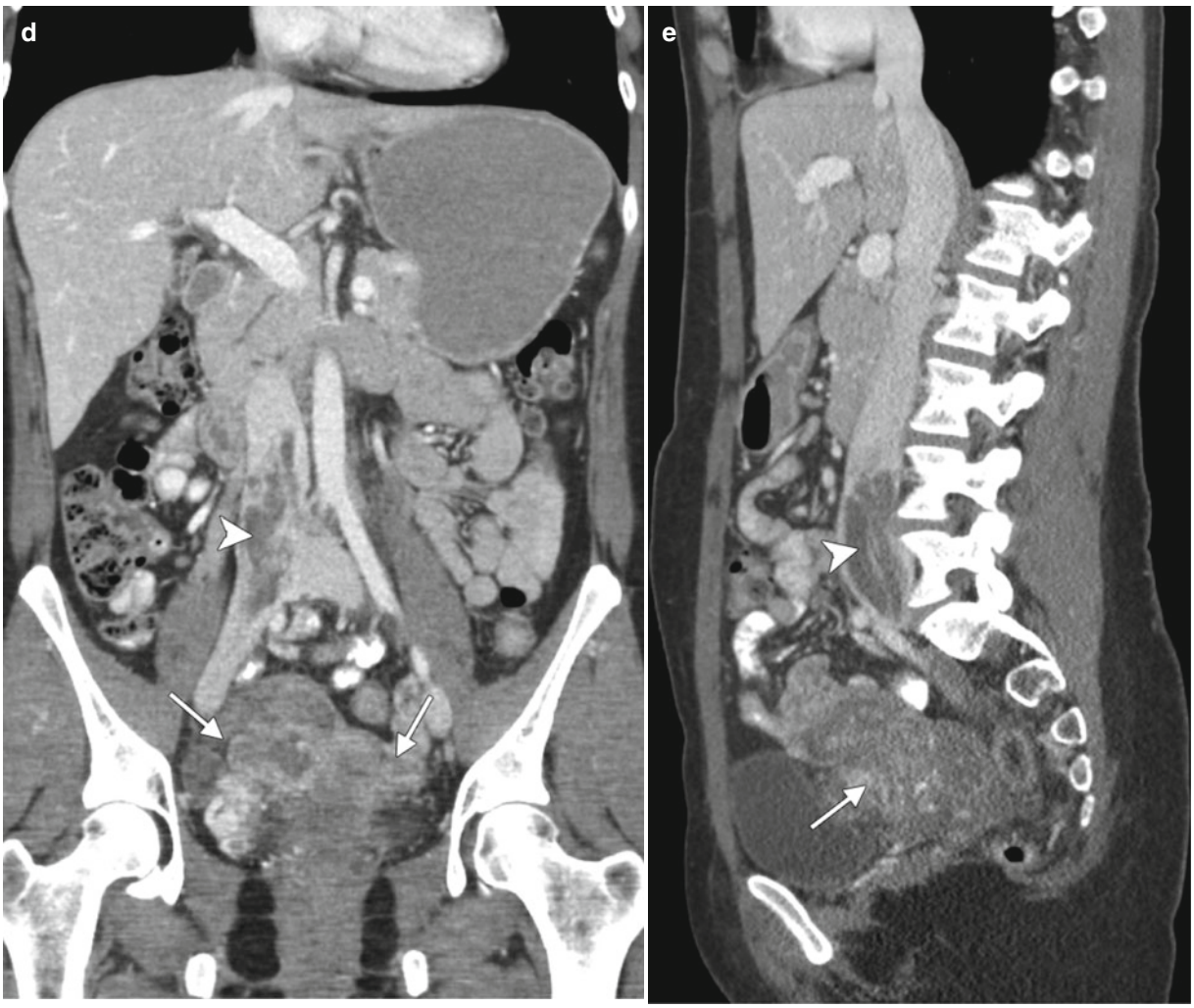

Fig. 2.7 (continued)

2.3 Malignant Uterine Pathology

The histologies of endometrial cancer (Table 2.4) are reflected in changed MRI signal characteristics (Table 2.5). The prognosis is suggested by the staging system of the International Federation of Gynecology and Obstetrics (FIGO) (Tables 2.6 and 2.7). Imaging findings that should be included in the radiology report are presented in Table 2.8.

Table 2.4 Endometrial cancer histologies

Histology	Prevalence (%)
Endometrioid adenocarcinoma	85
Serous adenocarcinoma	10
Clear cell adenocarcinoma	<5
Uterine sarcomas Leiomyosarcoma Endometrial stromal sarcoma Carcinosarcoma (malignant mixed müllerian tumor)	<1

Table 2.5 Typical MRI signal characteristics of endometrial cancer in relation to normal endometrium and normal myometrium

Imaging type	Characteristics of endometrial cancer
Relative to endometrium	
T1WI	Isointensity
T2WI	Intermediate signal intensity
T1WI+C	Earlier enhancement
Relative to myometrium	
T1WI	Variable intensity
T2WI	Hyperintensity
T1WI+C	Less and more delayed enhancement[a]
Diffusion-weighted MRI	Hyperintensity (hypointensity on ADC map)

ADC apparent diffusion coefficient, *T1WI* T1-weighted imaging, *T1WI+C* T1-weighted imaging with contrast enhancement, *T2WI* T2-weighted imaging

[a]Maximum contrast between hyperintense myometrium and hypointense endometrial tumor occurs 50–120 s after contrast medium administration; this is the most important phase for accurate assessment of the depth of myometrial invasion. Delayed-phase images obtained 3–4 min after contrast medium administration are useful in evaluating for cervical stromal invasion (FIGO stage II). The presence of an intact enhancing cervical mucosa excludes stromal invasion

Table 2.6 Endometrial cancer staging, International Federation of Gynecology and Obstetrics (FIGO), 2009

FIGO stage	Description	5-Year overall survival (%) [4]
IA	Tumor confined to the uterus, no or <50 % myometrial invasion	85
IB	Tumor confined to the uterus, ≥50 % myometrial invasion	
II	Cervical stromal invasion	75
IIIA	Tumor invades serosa or adnexa	45
IIIB	Vaginal and/or parametrial involvement	
IIIC1	Pelvic lymph node involvement	
IIIC2	Para-aortic lymph node involvement	
IVA	Tumor invasion of bladder mucosa and/or bowel mucosa	25
IVB	Distant metastases	

Adapted from Pecorelli [7]

Table 2.7 Key changes in the 2009 FIGO Staging System for Endometrial Cancer

FIGO 2009	FIGO 1988
Stage IA: myometrial invasion = none OR < 50 % Stage IB: myometrial invasion ≥50 %	Stage IA: myometrial invasion = none Stage IB: myometrial invasion = <50 % Stage IC: myometrial invasion ≥50 %
Stage II: cervical stromal invasion (without subgrouping in stage IIA or IIB). Tumors with endocervical glandular invasion are considered stage I tumors	Stage IIA: endocervical glandular invasion Stage IIB: cervical stromal invasion
Stage IIIC is divided into: Stage IIIC1: pelvic lymph node involvement Stage IIIC2: para-aortic lymph node involvement	Stage IIIC: any lymphadenopathy (pelvic or retroperitoneal)

FIGO International Federation of Gynecology and Obstetrics.

Table 2.8 Information to include in the radiology report

Finding	Details
Myometrial invasion <50 % vs ≥50 %	Differentiation between no myometrial invasion and <50 % myometrial invasion is not necessary, as it does not affect staging
Cervical stromal and/or vaginal invasion	Present vs absent
Extrauterine extension	Adnexae, bladder, rectum
N stage	Regional nodes: para-aortic, common, internal and external iliac (including obturator) regions
Metastases	Liver and lung most common locations

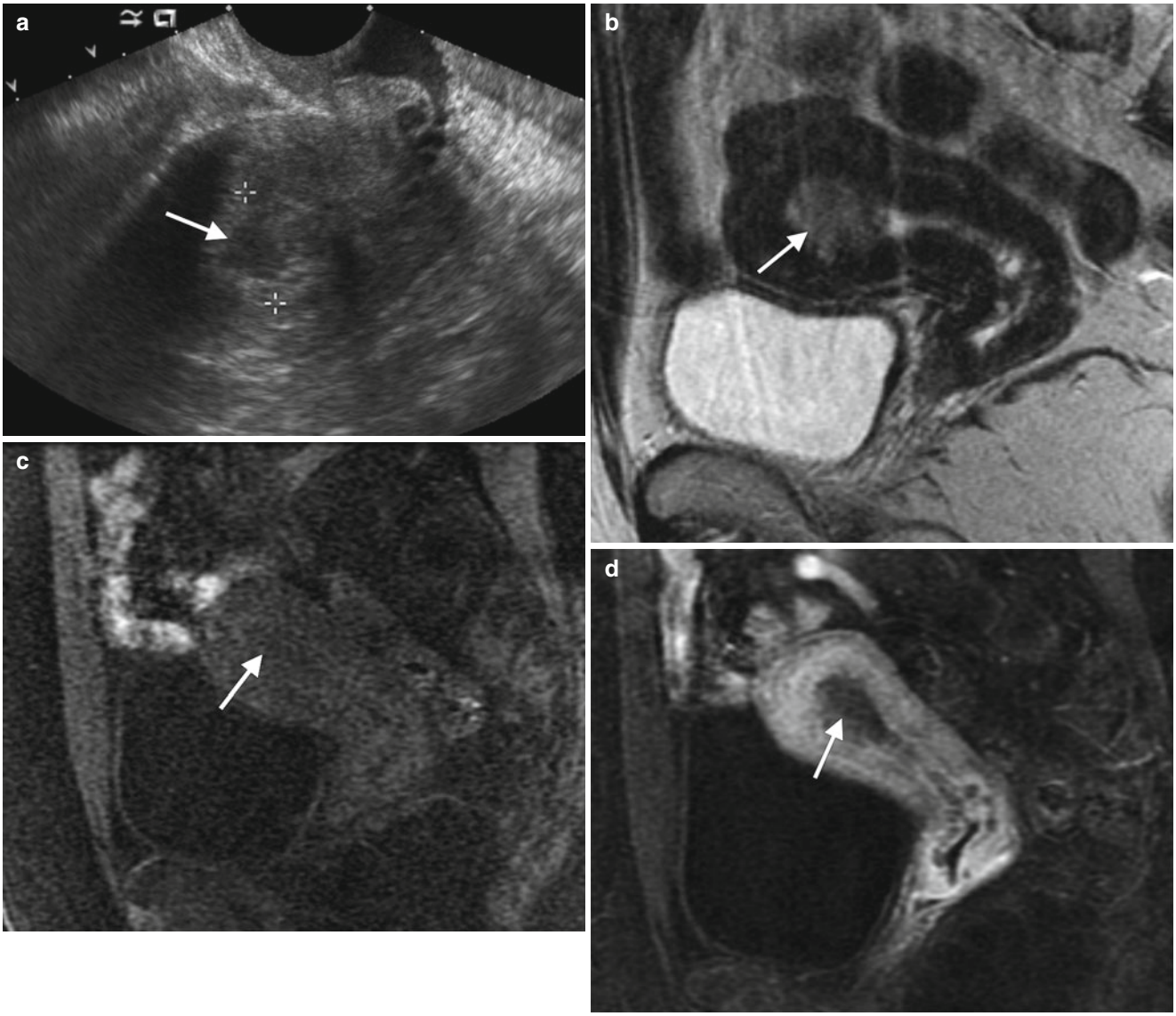

Fig. 2.8 Endometrial thickening is the hallmark of endometrial cancer. This 64-year-old woman with a history of breast cancer underwent a screening gynecologic evaluation, and ultrasound (**a**) revealed a thickened endometrial cavity (20 mm). A sagittal T2-weighted MR image (**b**) and sagittal fat-suppressed T1-weighted images before (**c**) and after (**d**) the administration of intravenous gadolinium revealed a soft tissue endometrial mass with superficial myometrial invasion (*arrows*). Pathology showed an endometrioid adenocarcinoma of the endometrium

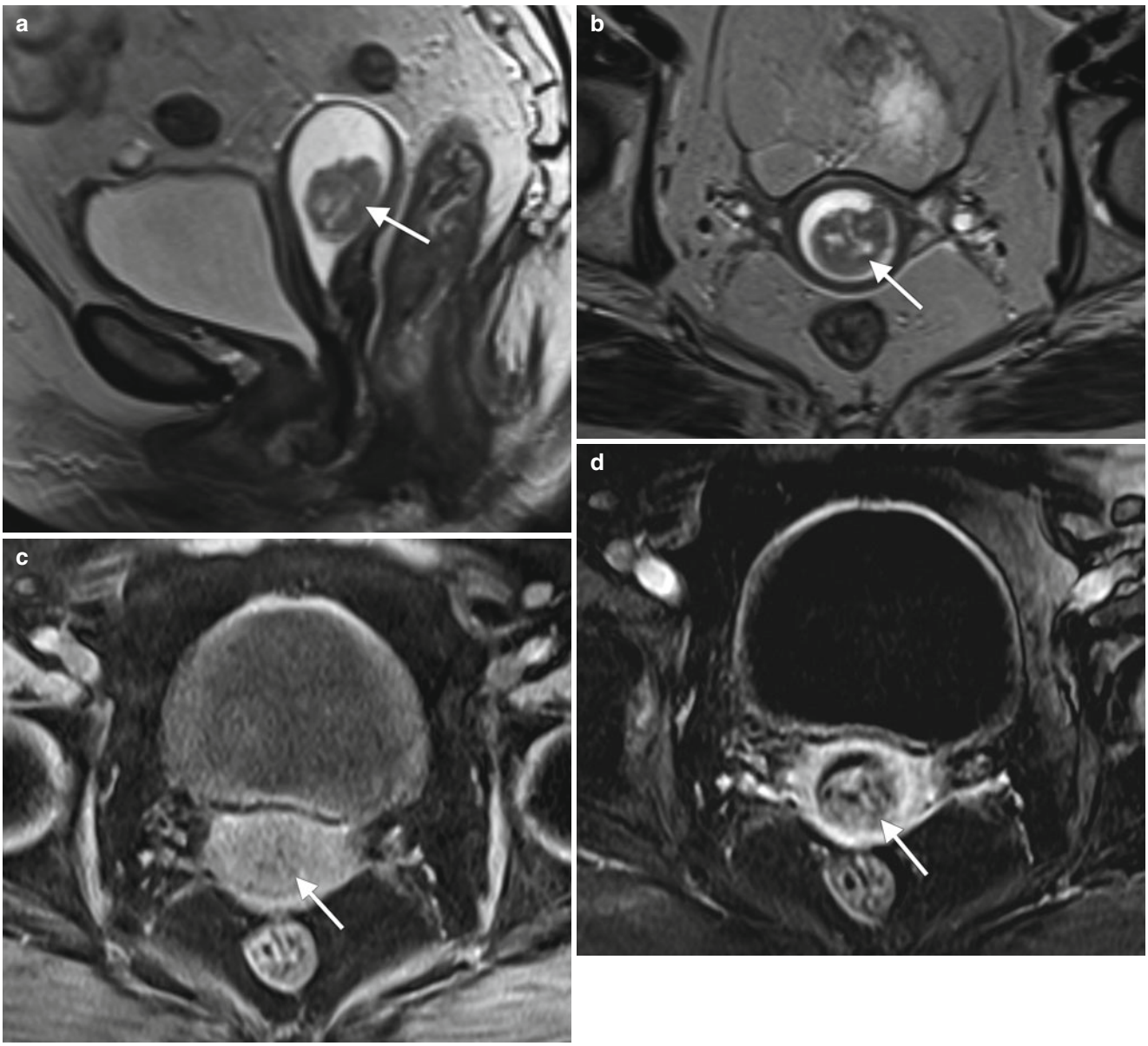

Fig. 2.9 FIGO stage IA endometrial cancer in a 65-year-old postmenopausal patient with vaginal spotting. Sagittal (**a**) and axial (**b**) T2-weighted MR images and axial, fat-suppressed T1-weighted images before (**c**) and after (**d**) intravenous gadolinium demonstrate an enhancing soft tissue endometrial mass (*arrows*) with uninterrupted enhancement of the subendometrial stripe, which indicates absence of myometrial invasion. The endometrial cavity is distended, probably due to cervical stenosis

Fig. 2.10 FIGO stage IA endometrial cancer in a 39-year-old premenopausal woman with menorrhagia. Sagittal (**a**), axial (**b**), and coronal (**c**) T2-weighted MR images, an axial apparent diffusion coefficient map derived from diffusion-weighted MRI (**d**), and fused PET/CT images (**e**, **f**) demonstrate a hypermetabolic soft tissue tumor (*arrows*) expanding the endometrial cavity. The adjacent myometrium is compressed but not invaded. An exophytic leiomyoma is also present (*arrows*). Pathology showed a grade 1 endometrioid adenocarcinoma and confirmed the absence of myometrial invasion

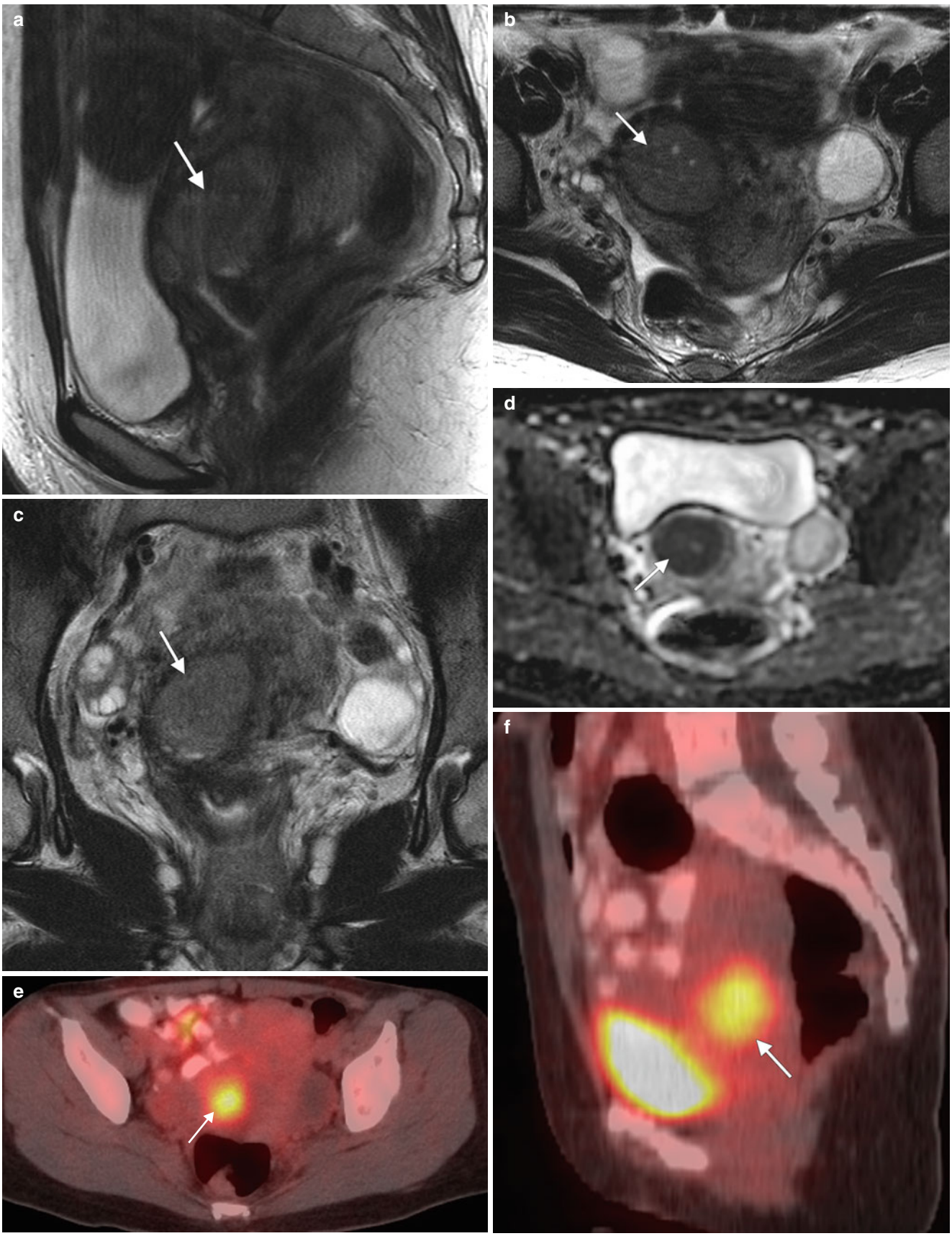
a
b
c
d
e
f

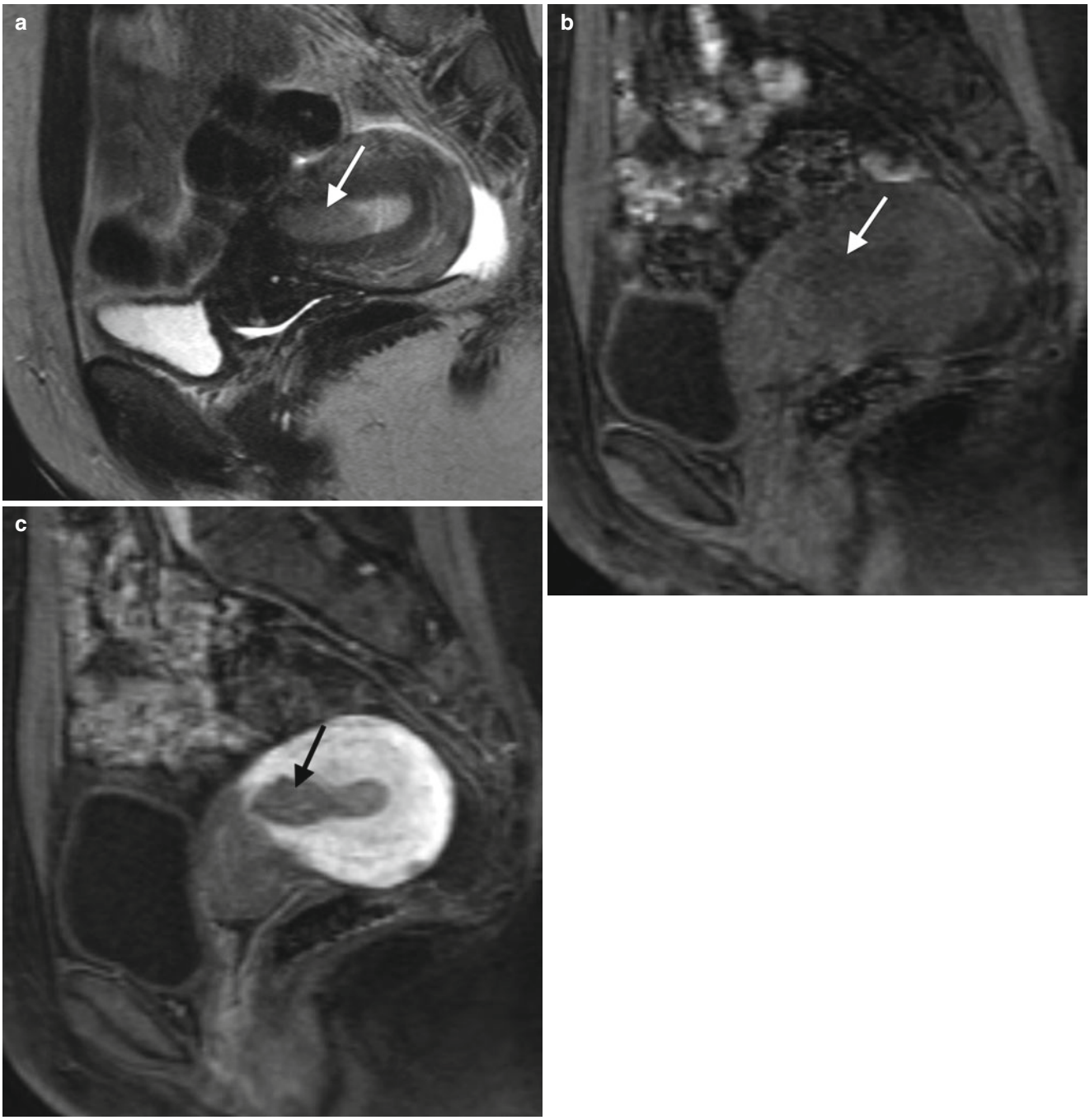

Fig. 2.11 FIGO stage IA endometrial cancer in a 37-year-old woman with vaginal bleeding between menstrual periods. A sagittal T2-weighted MR image (**a**) and fat-suppressed sagittal T1-weighted images before (**b**) and after (**c**) intravenous gadolinium demonstrate an endometrial mass with minimal irregularity at the endometrium-myometrium interface, probably representing superficial myometrial invasion. Pathology showed endometrioid adenocarcinoma

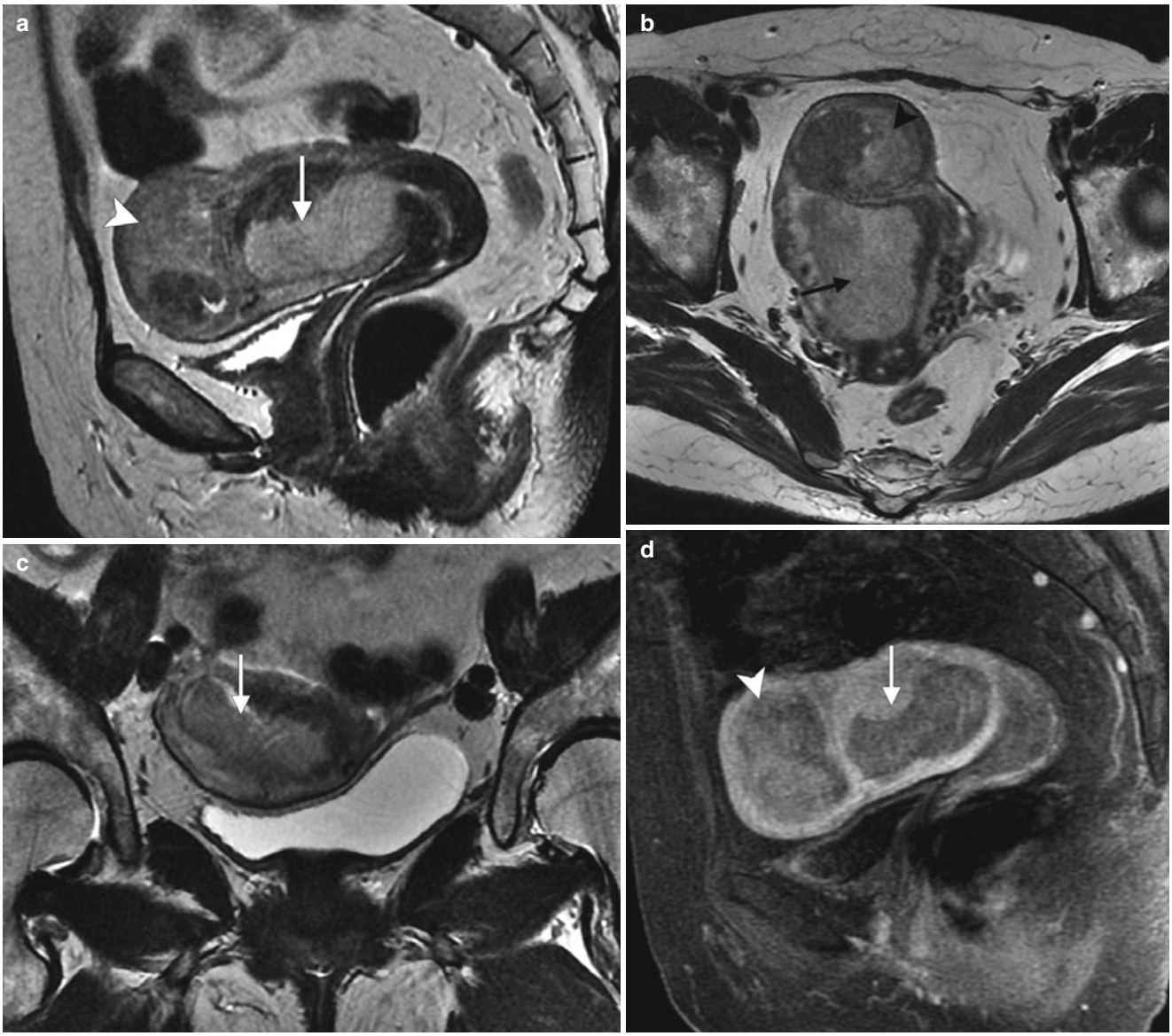

Fig. 2.12 FIGO stage IB endometrial cancer in a 66-year-old woman presenting with postmenopausal vaginal bleeding. Sagittal (**a**), axial (**b**), and coronal (**c**) T2-weighted MR images and a sagittal, fat-suppressed T1-weighted image following intravenous gadolinium (**d**) demonstrate a soft tissue mass centered on the endometrial cavity (*arrows*) with deep (>50 %) myometrial invasion. A benign leiomyoma (*arrowheads*) is also shown. Pathology was consistent with endometrioid adenocarcinoma

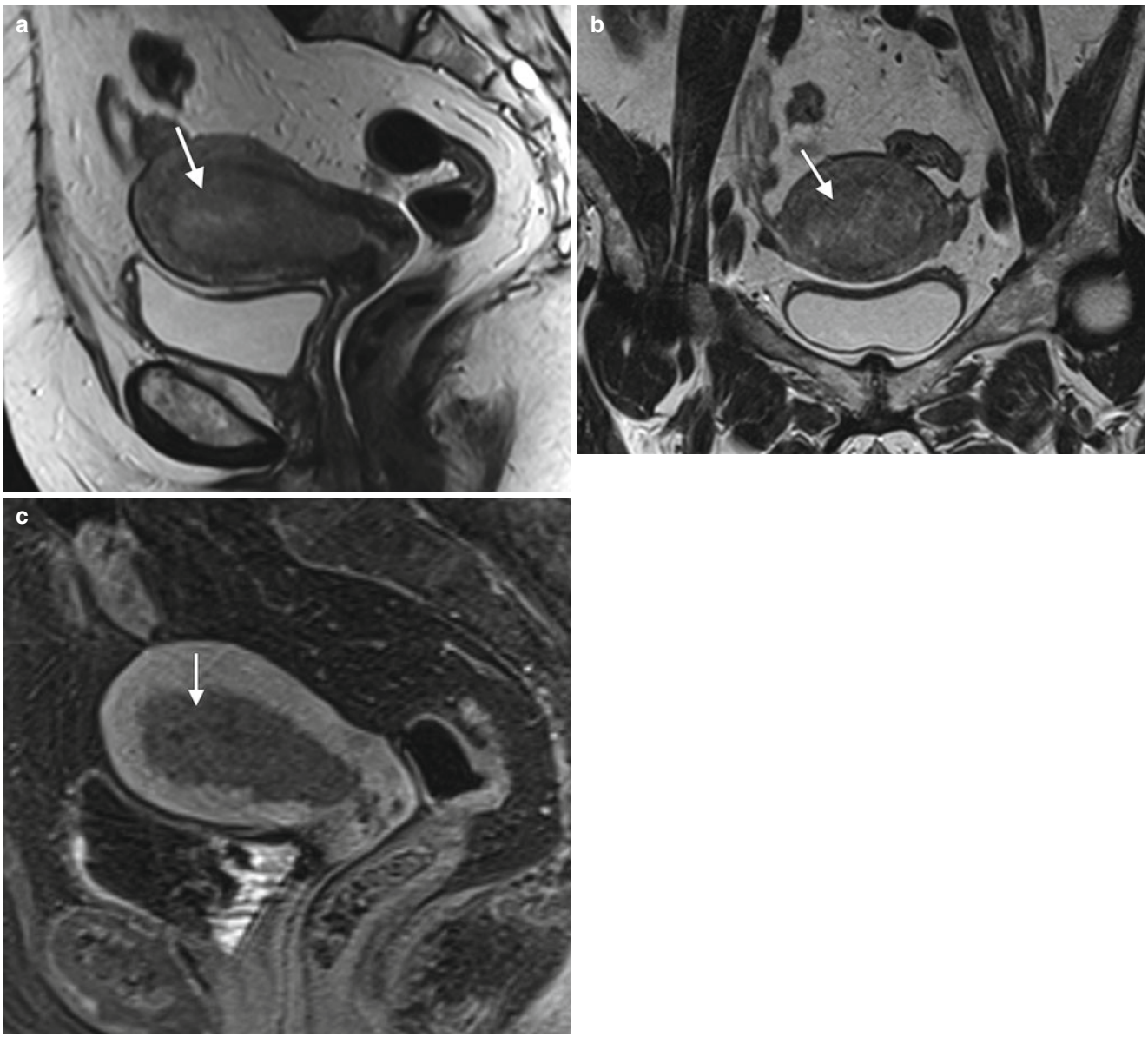

Fig. 2.13 FIGO stage IB endometrial cancer in a 66-year-old woman with postmenopausal vaginal bleeding. Axial (**a**) and oblique coronal (**b**) T2-weighted MR images and a sagittal, fat-suppressed T1-weighted image following intravenous gadolinium (**c**) demonstrate an endometrial soft tissue mass (*arrows*) with deep (>50 %) myometrial invasion. Pathology showed endometrioid adenocarcinoma

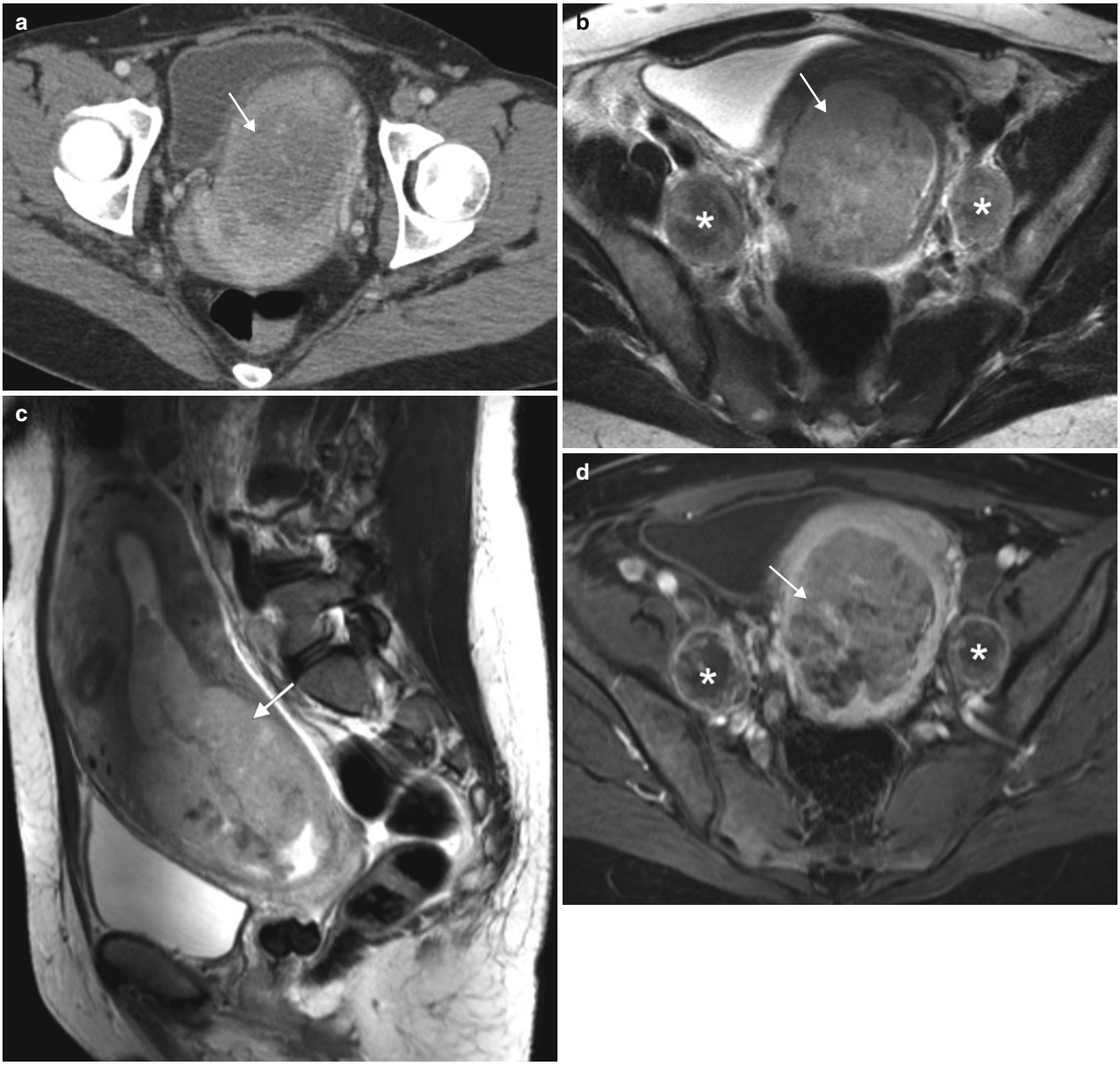

Fig. 2.14 51-year-old woman presenting with vaginal discharge and crampy abdominal pain. An axial, contrast-enhanced CT scan (**a**) demonstrated a heterogeneously enhancing uterine mass. Axial (**b**) and sagittal (**c**) T2-weighted MR images and fat-suppressed axial (**d**) and sagittal (**e**) T1-weighted images following intravenous gadolinium demonstrate a heterogeneously enhancing endometrial mass with deep myometrial invasion (>50 %) (*arrows*). Bilateral metastatic pelvic lymph node involvement is also shown (*asterisks*). Pathology showed an undifferentiated carcinoma with a minor, well-differentiated endometrioid adenocarcinoma component

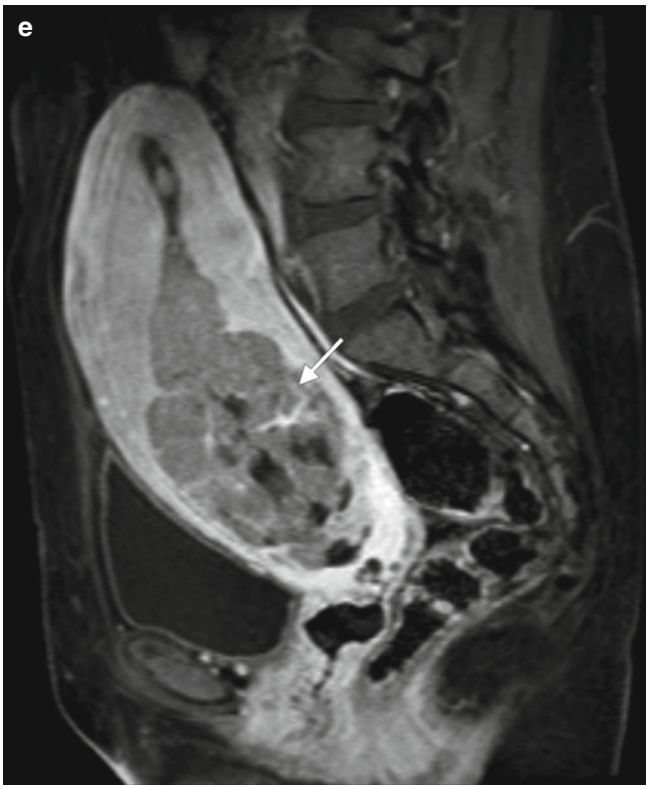

Fig. 2.14 (continued)

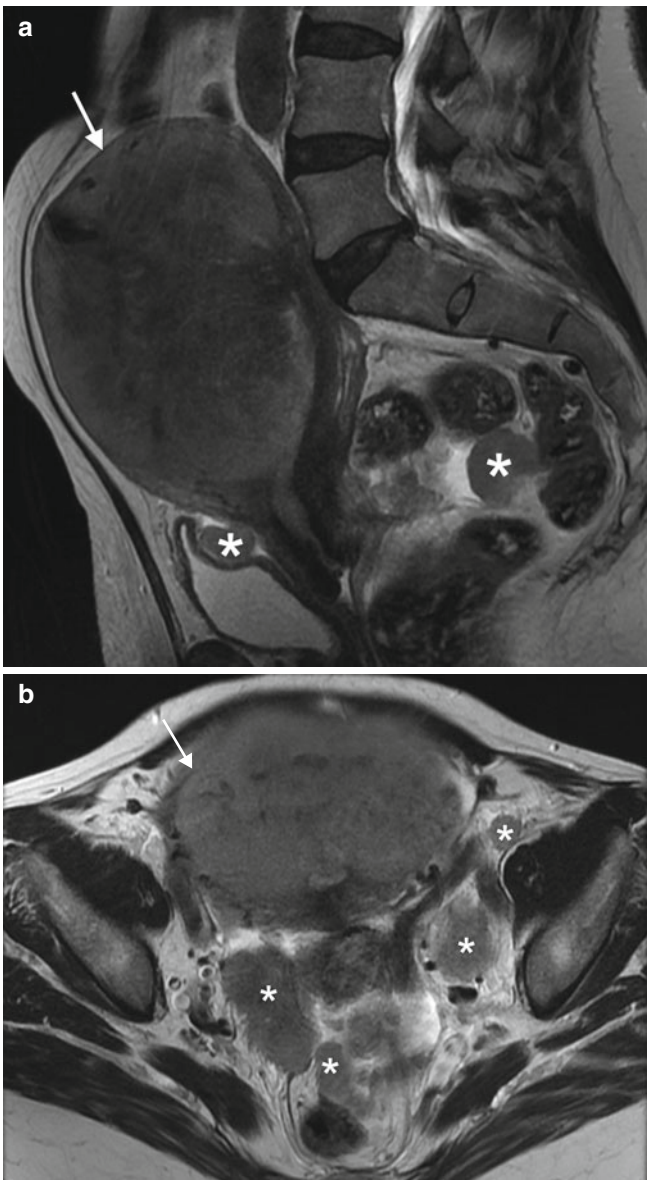

Fig. 2.15 FIGO stage III endometrial cancer in a 52-year-old woman complaining of increasing abdominal girth and irregular perimenopausal vaginal bleeding. Sagittal (**a**), axial (**b**), and coronal (**c**) T2-weighted MR images and a sagittal, fat-suppressed T1-weighted image following intravenous gadolinium (**d**) demonstrate a large, heterogeneously enhancing endometrial mass extending to the serosa (*arrows*). Bilateral metastatic involvement of pelvic nodes is also present (*asterisks*). Pathology was reported as undifferentiated endometrial adenocarcinoma

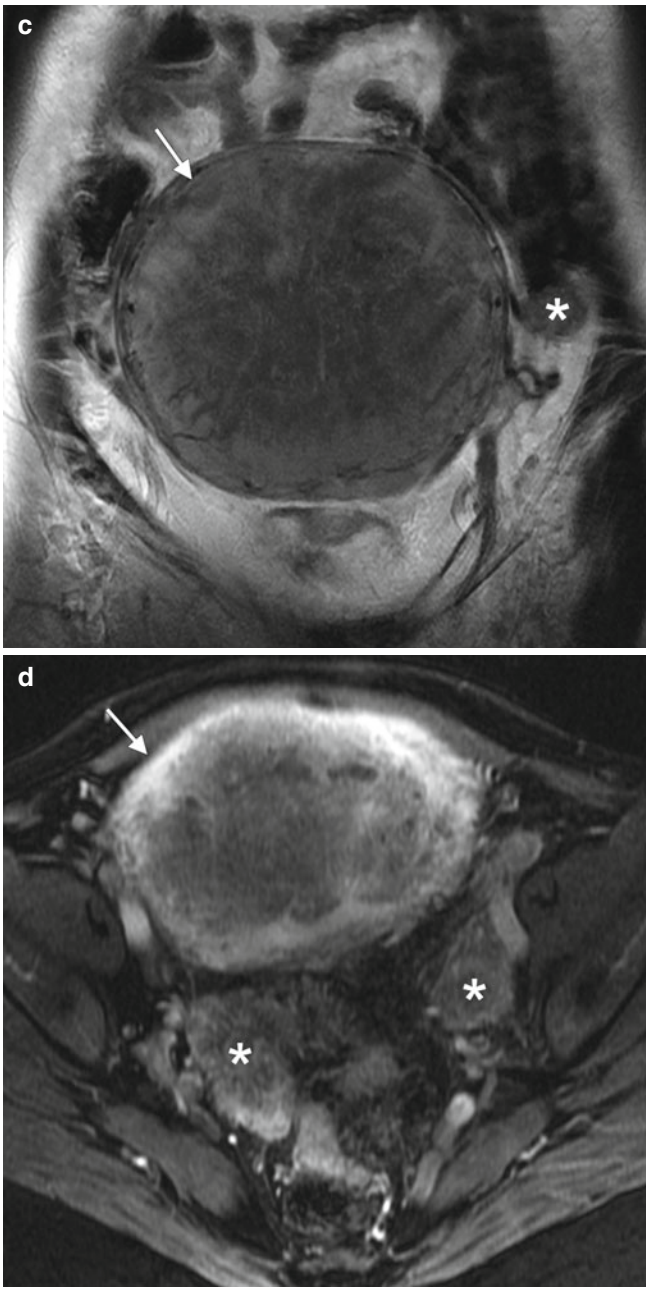

Fig. 2.15 (continued)

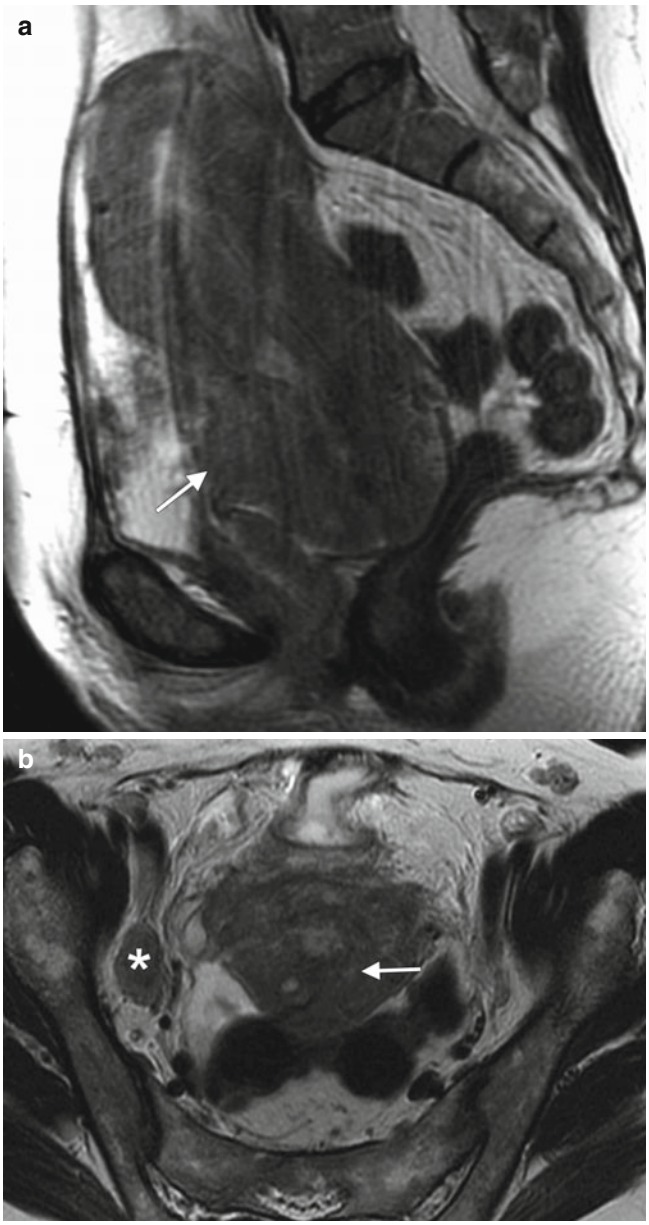

Fig. 2.16 FIGO stage III endometrial cancer in a 49-year-old woman with menorrhagia. Sagittal (**a**) and axial (**b**) T2-weighted MR images and an axial, fat-suppressed T1-weighted image following intravenous gadolinium (**c**) demonstrate a heterogeneous endometrial mass (*arrows*) with extension beyond the uterine serosa and ovarian metastasis (*asterisks*). An axial T1-weighted MR image (**d**) shows a T1-hypointense lesion (*arrowhead*) suspicious for metastasis

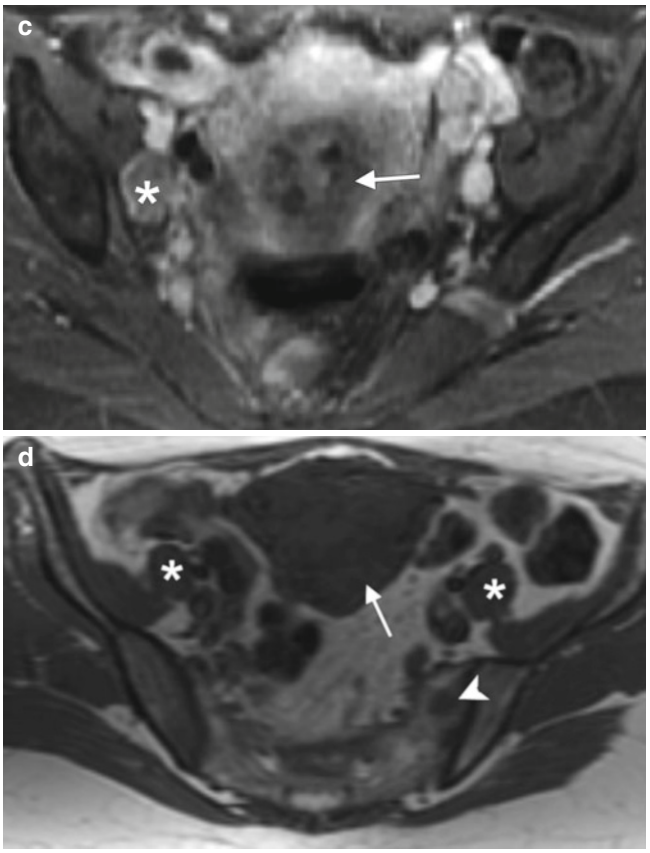

Fig. 2.16 (continued)

2.4 Uterine Sarcomas

Uterine sarcomas are rare forms of tumors arising from the mesenchymal or stromal elements of the uterus. The most common types of uterine sarcomas are leiomyosarcomas, carcinosarcomas (also called malignant mixed müllerian tumors [MMMTs]) and endometrial stromal sarcomas. They are aggressive tumors, and even when detected early in the disease course, they have a worse prognosis than the much more common epithelial endometrial carcinomas. Overall 5-year survival for uterine sarcomas ranges from 17.5 to 54.7 % [8], compared with 5-year survival rates of up to 83 % for endometrial cancer [1]. For stage I tumors alone, the 5-year survival rate for leiomyosarcoma is only about 51 %, compared with 96 % for endometrial cancer [1, 9].

Carcinosarcomas are staged according to the 2009 FIGO staging criteria for endometrial carcinomas. For the first time, the 2009 FIGO staging system provided separate staging criteria for leiomyosarcomas and endometrial stromal sarcomas and adenosarcomas. The main differences from the staging of epithelial endometrial cancers include the use of tumor size (as opposed to depth of myometrial invasion) for defining stage I disease, replacing cervical involvement with extrauterine extension for defining stage II disease, and replacing serosal and vaginal involvement with involvement of the omentum and other abdominal tissues for defining stage IIIA and IIIB disease.

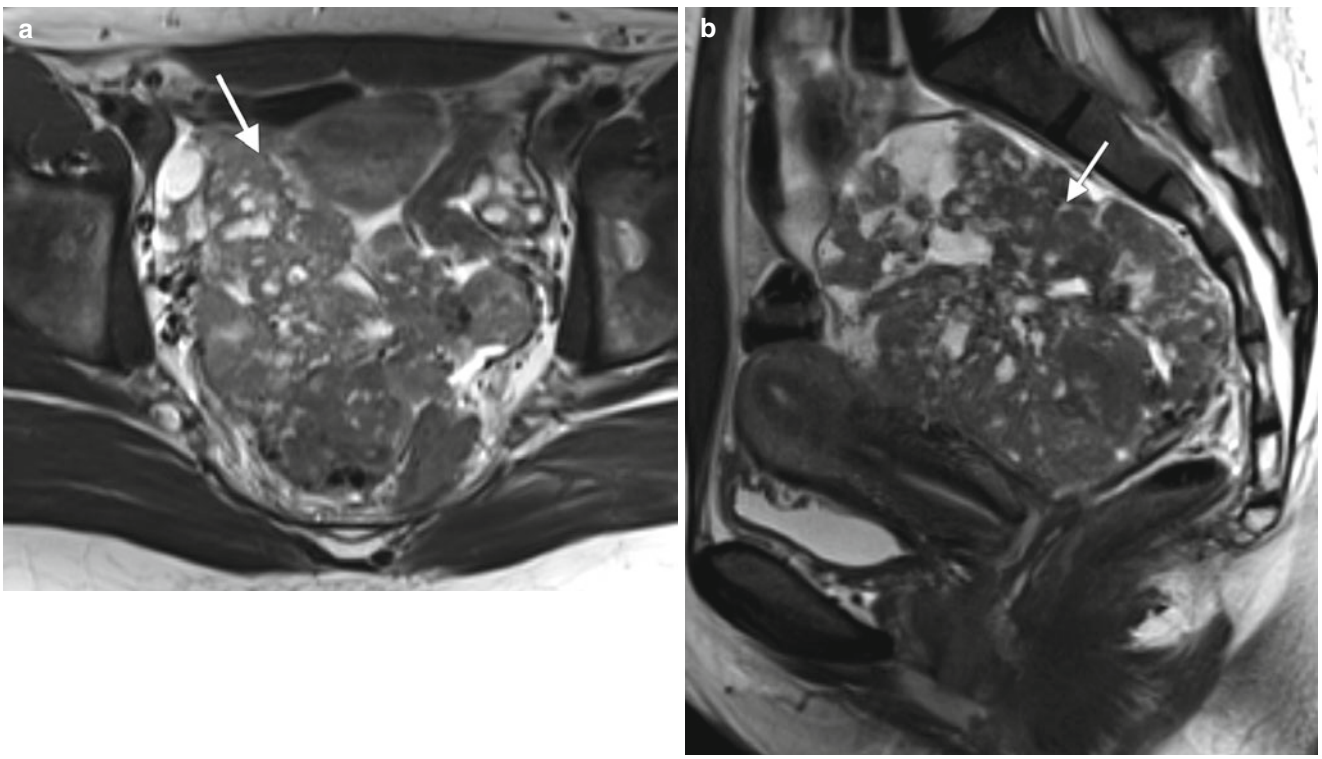

Fig. 2.17 High-grade leiomyosarcoma in a 37-year-old woman with a history of menorrhagia and multiple submucosal uterine leiomyomas resected hysteroscopically 3 years earlier. Axial (**a**), sagittal (**b**), and coronal (**c**) T2-weighted MR images and a sagittal, fat-suppressed T1-weighted image following intravenous gadolinium (**d**) demonstrate a loculated, heterogeneous, partially necrotic pelvic mass arising from the posterior aspect of the uterus and displacing the rectum posteriorly

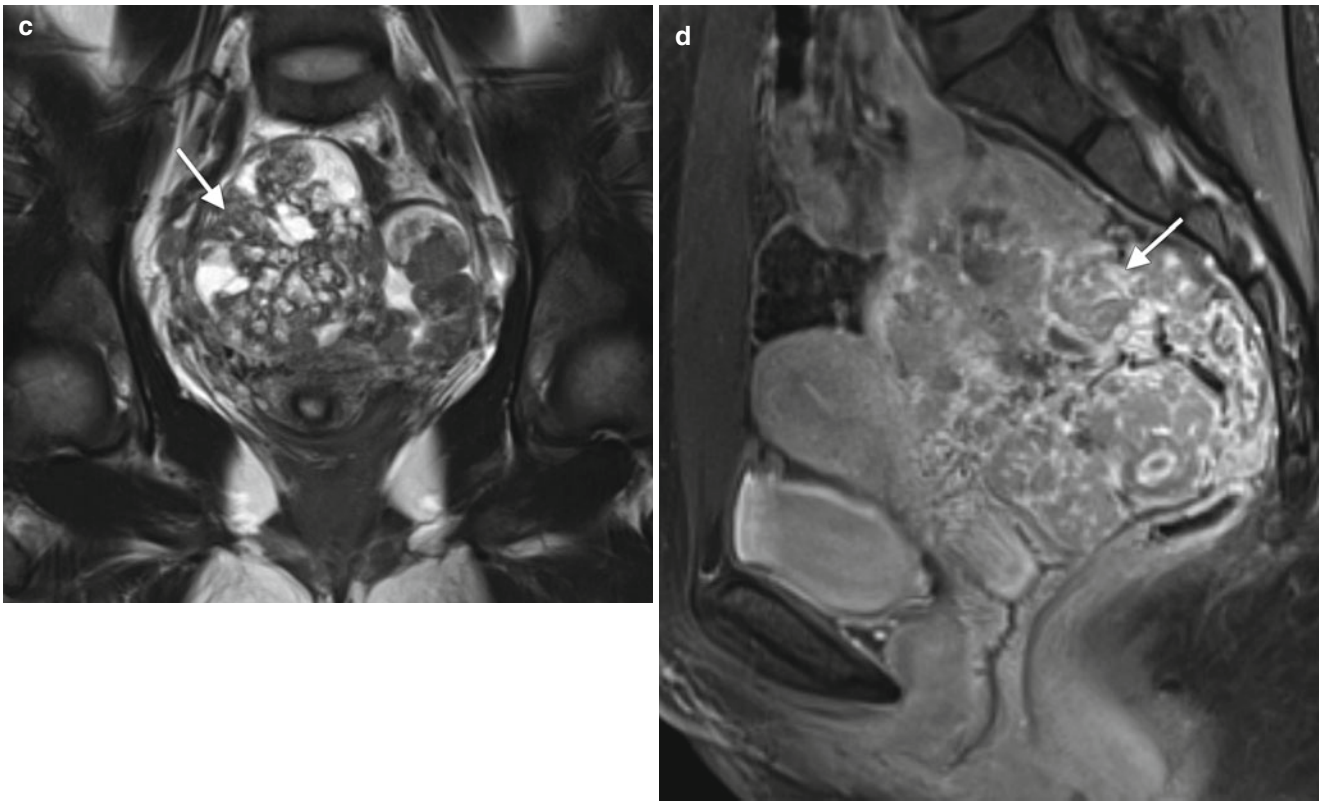

Fig. 2.17 (continued)

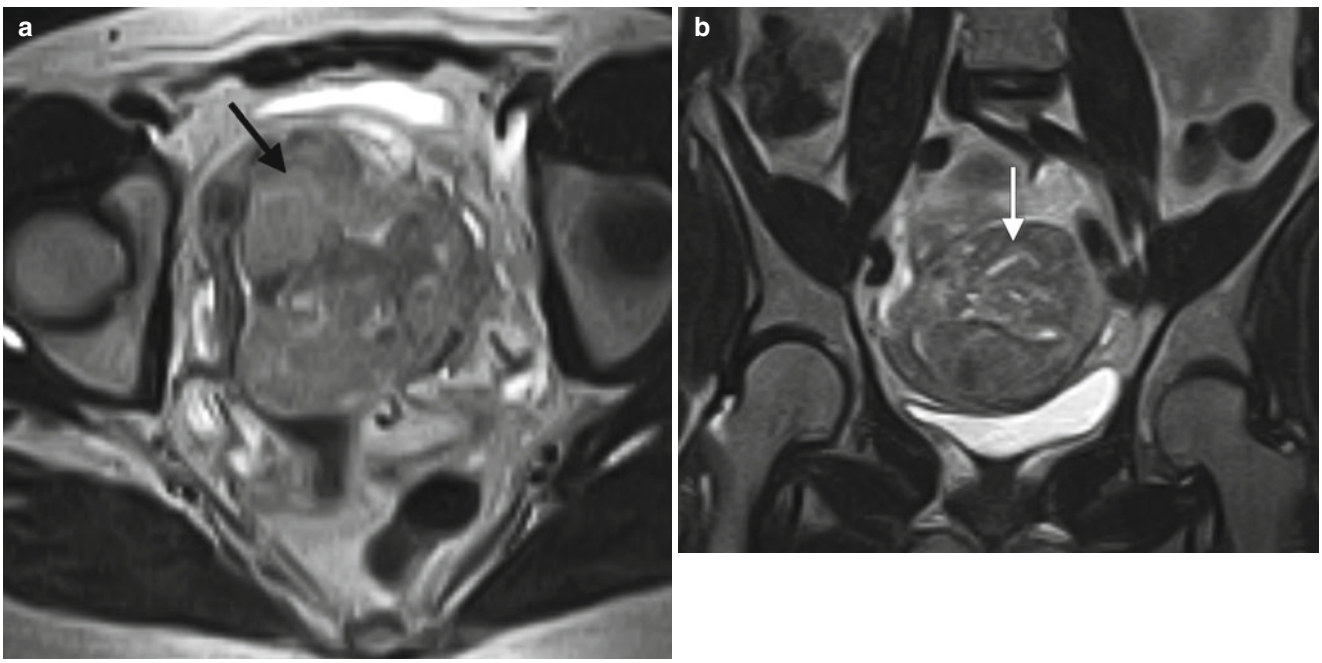

Fig. 2.18 High-grade epithelioid leiomyosarcoma in a 53-year-old woman with pelvic pain. Axial (**a**) and coronal (**b**) T2-weighted MR images, an axial fat-suppressed T1-weighted image following intravenous gadolinium (**c**), and an axial T1-weighted image (**d**) demonstrate a heterogeneously enhancing myometrial mass (*arrows*). Pathology showed a high-grade epithelioid leiomyosarcoma

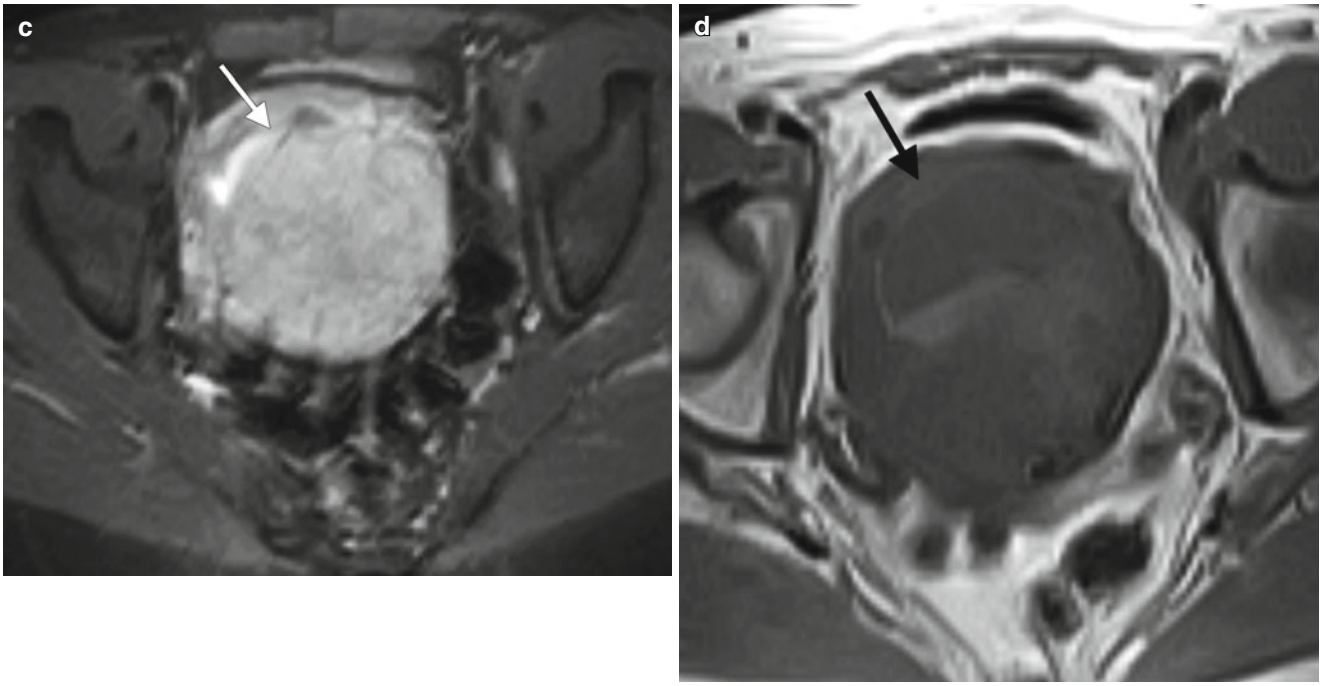

Fig. 2.18 (continued)

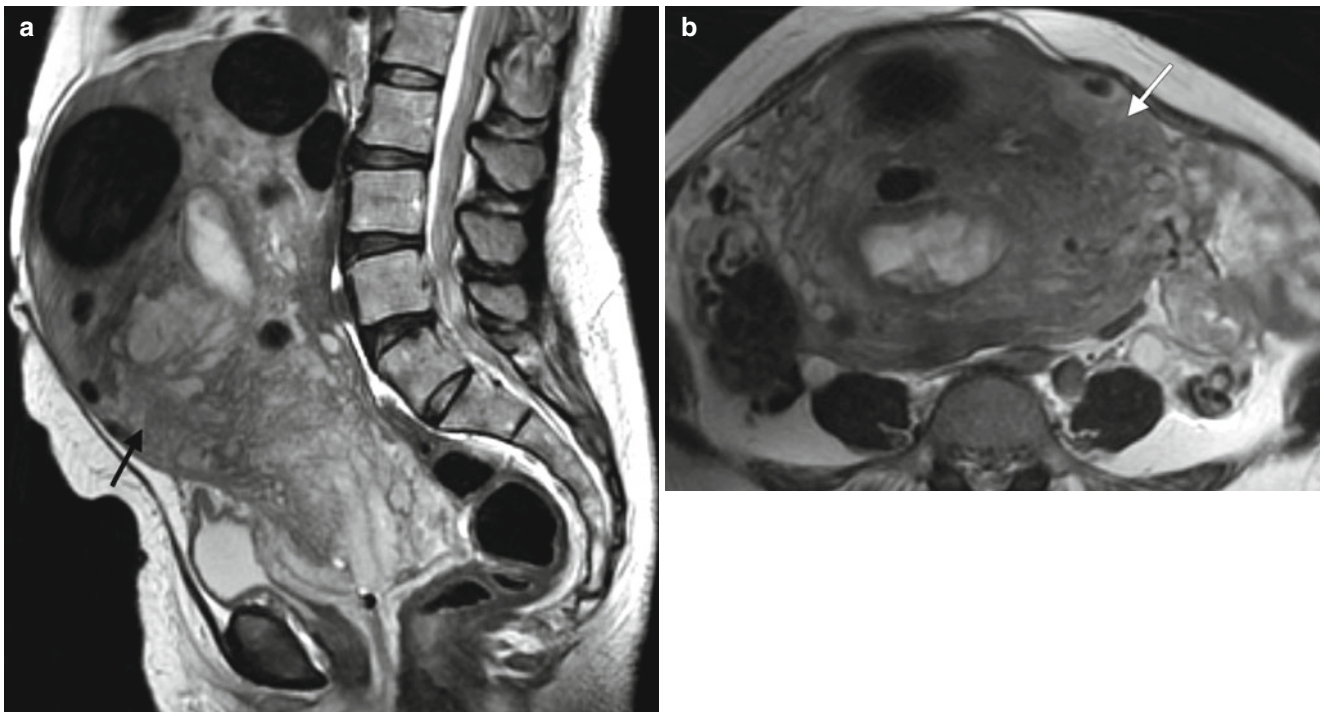

Fig. 2.19 Endometrial stromal sarcoma in a 58-year-old woman with postmenopausal vaginal bleeding. Sagittal (**a**) and axial (**b**) T2-weighted MR images demonstrate a large, heterogeneous mass (*arrows*) with mixed solid and cystic components involving the endometrium and myometrium and extending beyond the uterine serosa, with involvement of both ovaries. Pathology showed an endometrial stromal sarcoma

2.5 Endometrial Cancer Treatment and the Role of Lymphadenectomy

Endometrial cancer is staged and treated surgically. Surgery includes radical hysterectomy and bilateral salpingo-oophorectomy. Lymphadenectomy for early-stage (stage I) endometrial cancer remains controversial. Two large, prospective, multicenter studies investigated whether pelvic lymphadenectomy could improve the survival of women with early-stage endometrial cancer. Both studies reported no benefit in overall or recurrence-free survival in the patients randomized to lymphadenectomy [10, 11]. The recent SEPAL study (Survival Effect of Para-aortic Lymphadenectomy in endometrial cancer) showed that pelvic and para-aortic lymphadenectomy improves outcome in patients with an intermediate or high risk of recurrent disease [12]. Adjuvant treatment with chemotherapy, radiotherapy, or both is performed for women with stage III and IV endometrial cancer, although certain subgroups of women with earlier-stage disease may also benefit [13].

Endometrial cancers presenting in premenopausal women (about 20 % of all endometrial cancers) require special consideration. Some advocate ovarian preservation for this patient population in order to prevent surgical menopause [13]. However, these patients are at risk of synchronous and metachronous ovarian neoplasms. For women who wish to retain fertility, uterine preservation by medical treatment with a progestational agent can also be considered [13].

2.6 Endometrial Cancer Recurrence

The most common site of endometrial cancer recurrence is the vaginal cuff. The treatment of choice for women who have a relapse at the vaginal cuff after surgery is radiation, with 2-year survival after an isolated recurrence at the vaginal cuff being as high as 75 % [14, 15]. However, patients with recurrent endometrial cancer constitute a highly heterogeneous population that includes women presenting with widespread disease (in whom palliation constitutes the mainstay of treatment) in addition to those presenting with isolated vaginal cuff recurrences. As such, treatment is highly individualized. Surgery, radiation, chemotherapy, and hormonal therapy are all used for recurrent endometrial cancer.

The typical patient with endometrial cancer is a postmenopausal woman presenting with vaginal bleeding, although up to 20 % of cases occur in premenopausal women. The hallmark of endometrial cancer on imaging is thickening of the endometrial stripe. Endometrial cancer is staged and treated surgically. Imaging provides important prognostic information, such as depth of myometrial invasion by tumor and lymph node involvement, and thus contributes to an individualized treatment approach.

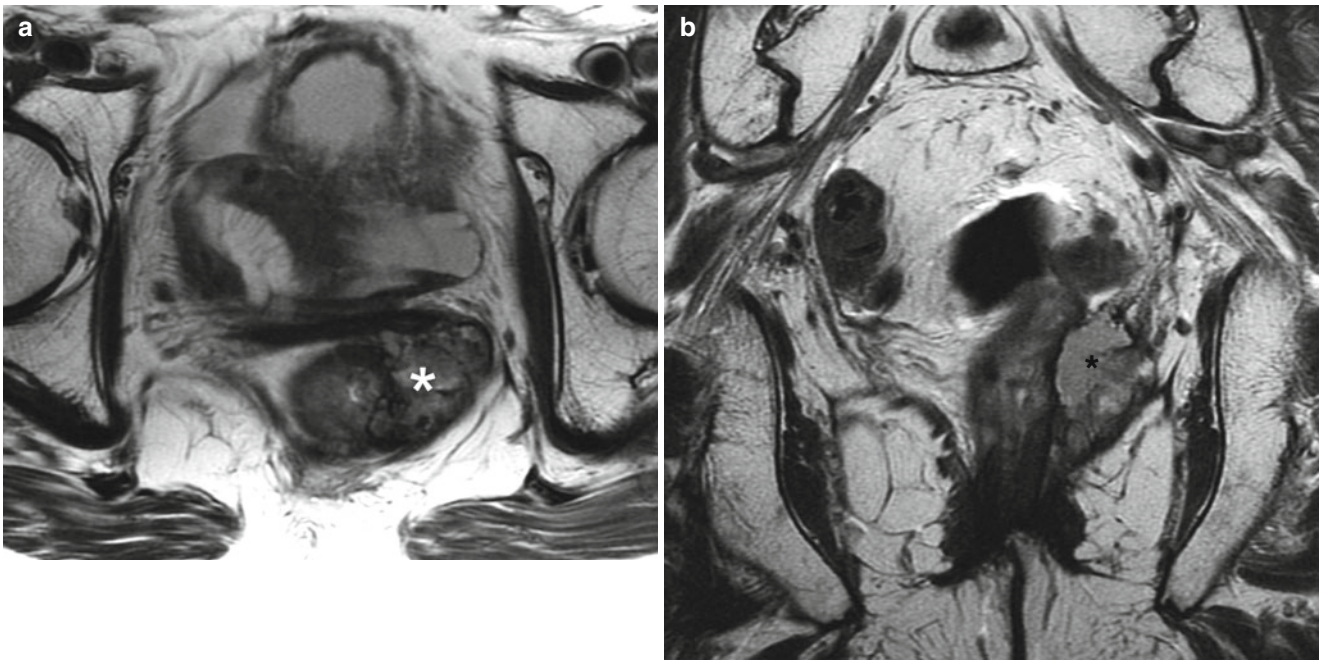

Fig. 2.20 This 72-year-old woman had a history of endometrioid endometrial adenocarcinoma treated with radical hysterectomy, bilateral salpingo-oophorectomy, and adjuvant chemotherapy 10 years earlier. Axial (**a**), coronal (**b**), and sagittal (**c**) T2-weighted MR images and an axial, fat-suppressed T1-weighted image following intravenous gadolinium (**d**) demonstrate a partially necrotic left pelvic tumor (*asterisks*) abutting the vagina with probable invasion of the rectal wall and left levator ani muscle. The soft tissue demonstrates hypermetabolic activity (*arrows*) on a fused FDG-PET scan of the pelvis (**e**). Axial (**f**) and coronal (**g**) contrast-enhanced CT scans of the upper abdomen demonstrate a perihepatic implant (*arrowheads*)

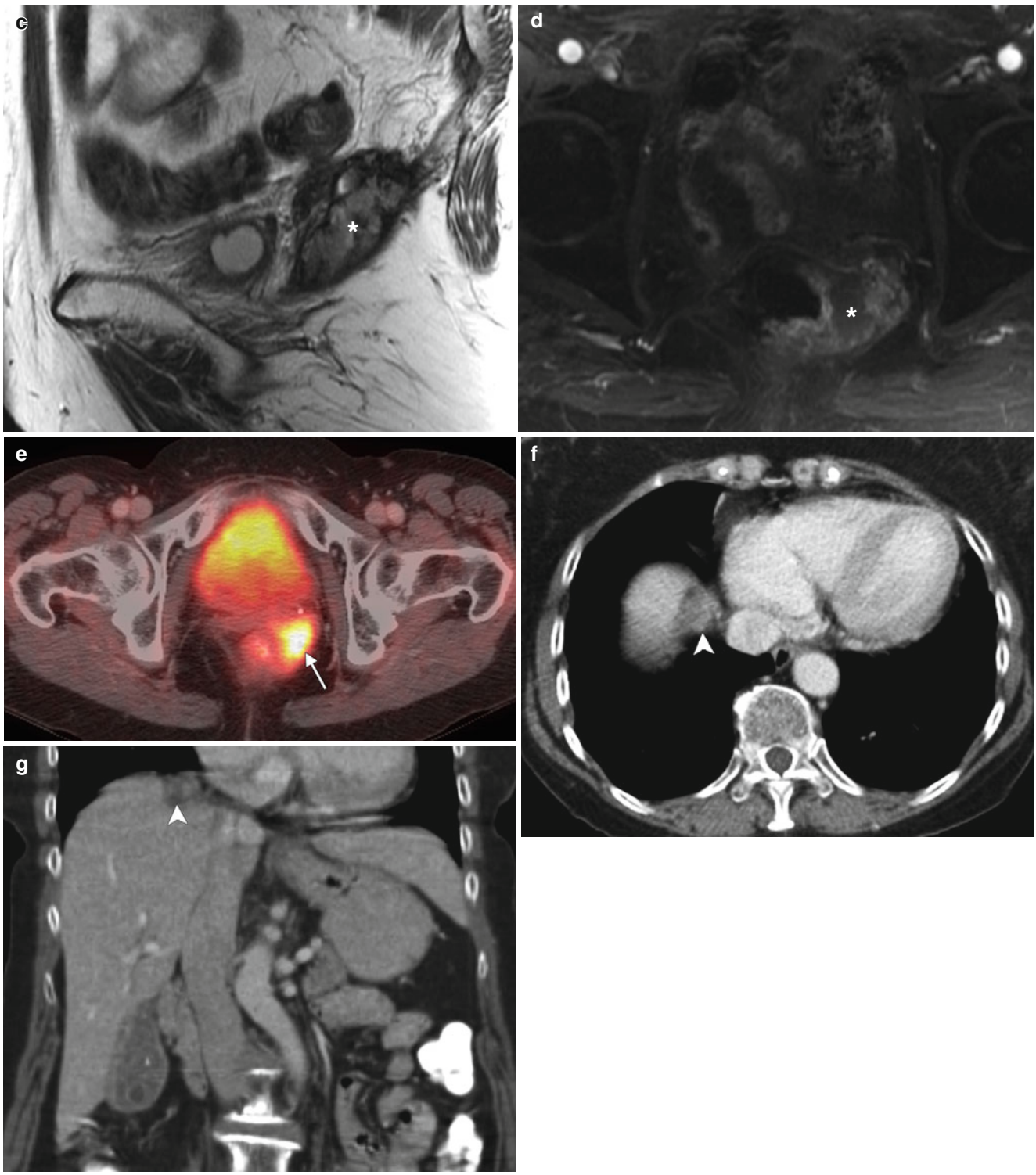

Fig. 2.20 (continued)

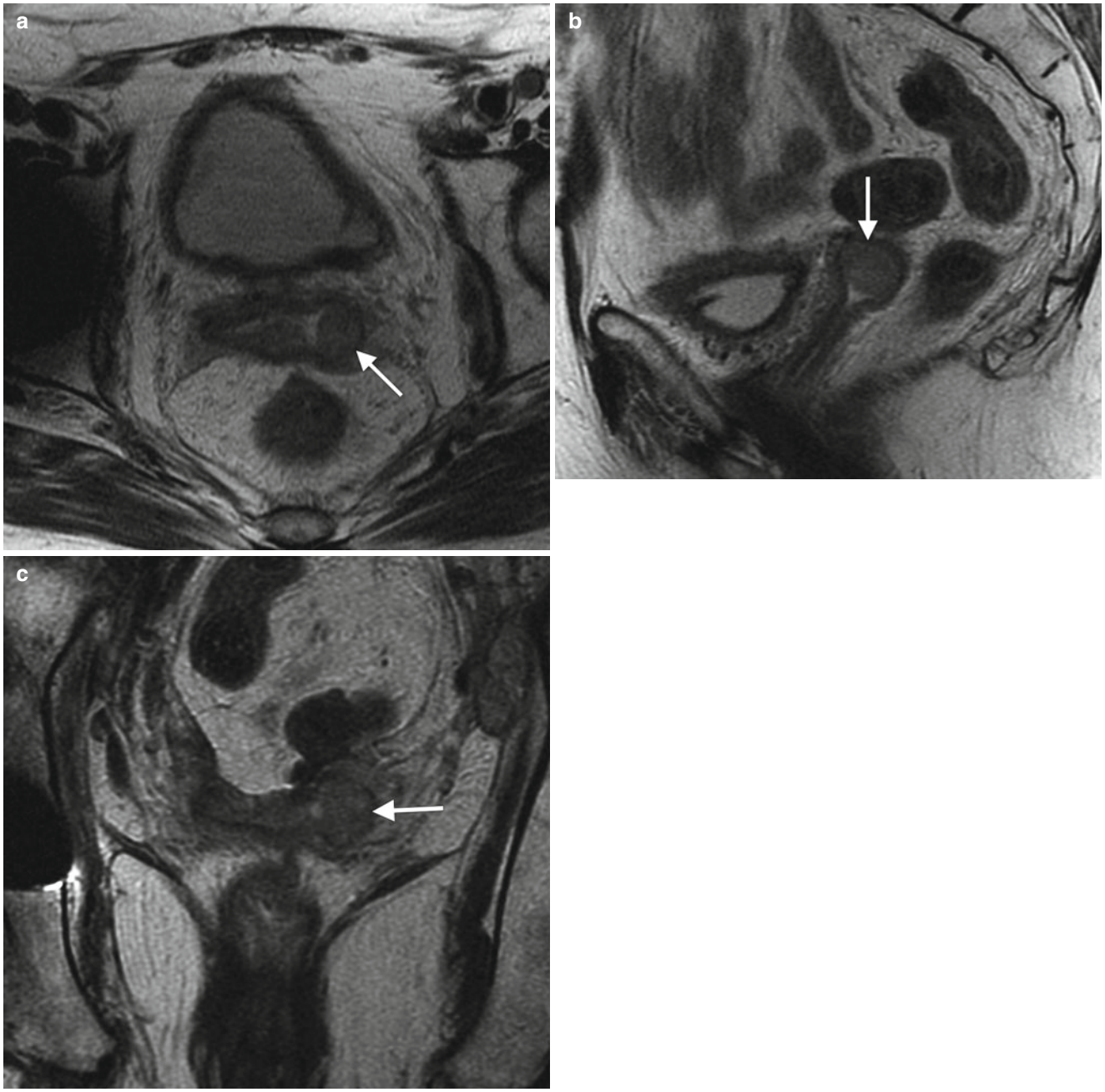

Fig. 2.21 This 68-year-old woman had a history of clear cell adenocarcinoma of the endometrium, which was treated with adjuvant chemotherapy followed by radical hysterectomy and bilateral salpingo-oophorectomy 2 years earlier. Axial (**a**), sagittal (**b**), and coronal (**c**) T2-weighted MR images demonstrate a soft tissue mass in the left aspect of the vaginal cuff (*arrows*) consistent with cancer recurrence

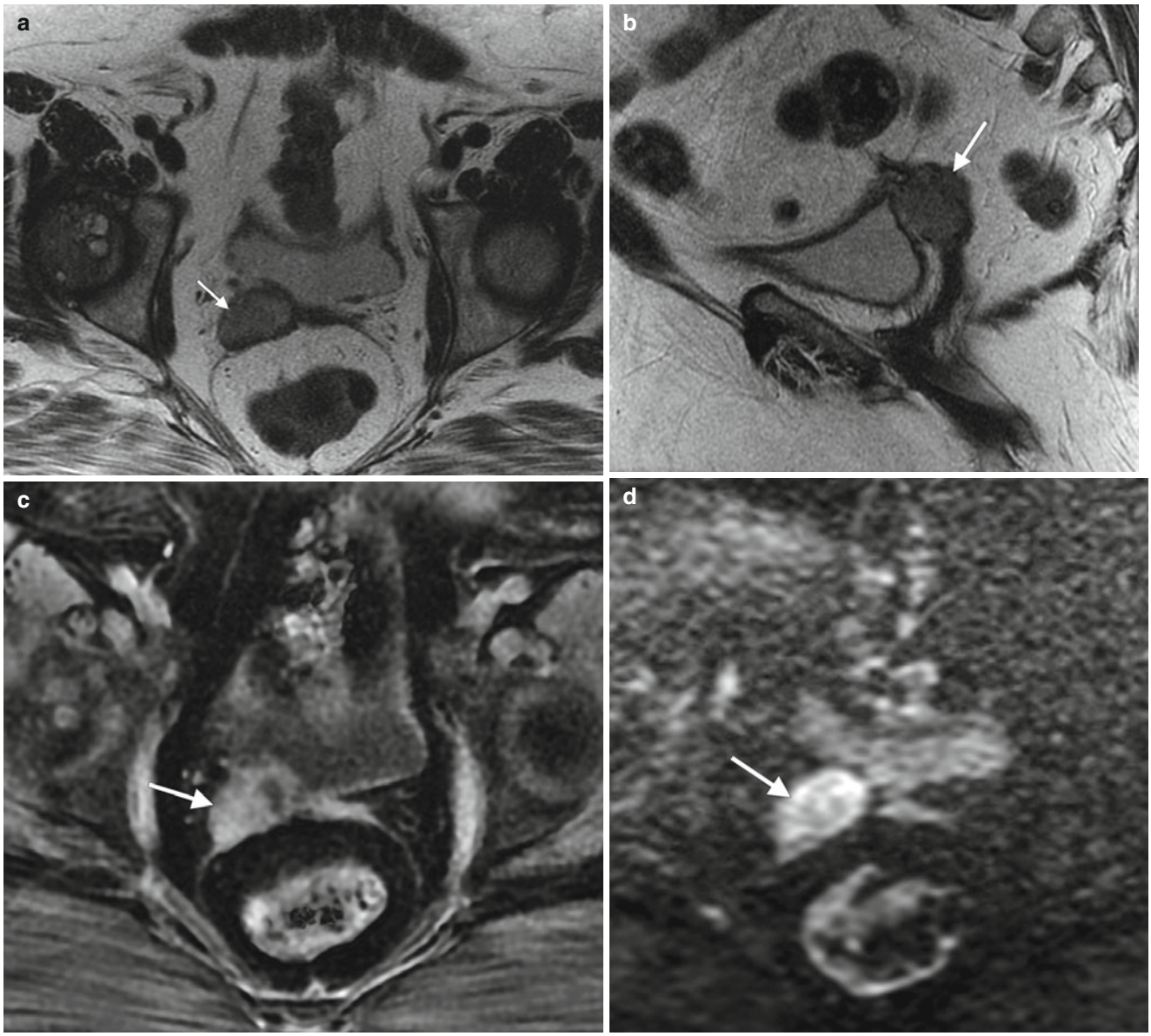

Fig. 2.22 This 53-year-old woman had a history of stage IA endometrioid adenocarcinoma of the endometrium, which was treated with radical hysterectomy and bilateral salpingo-oophorectomy 2 years earlier. Axial (**a**) and sagittal (**b**) T2-weighted MR images, an axial, fat-suppressed T1-weighted image following intravenous gadolinium (**c**), and an axial diffusion-weighted MR image (b = 300) (**d**) demonstrate a soft tissue mass in the right side of the vaginal cuff (*arrows*) consistent with cancer recurrence. The tumor abuts the posterior bladder wall and anterior mesorectal fascia

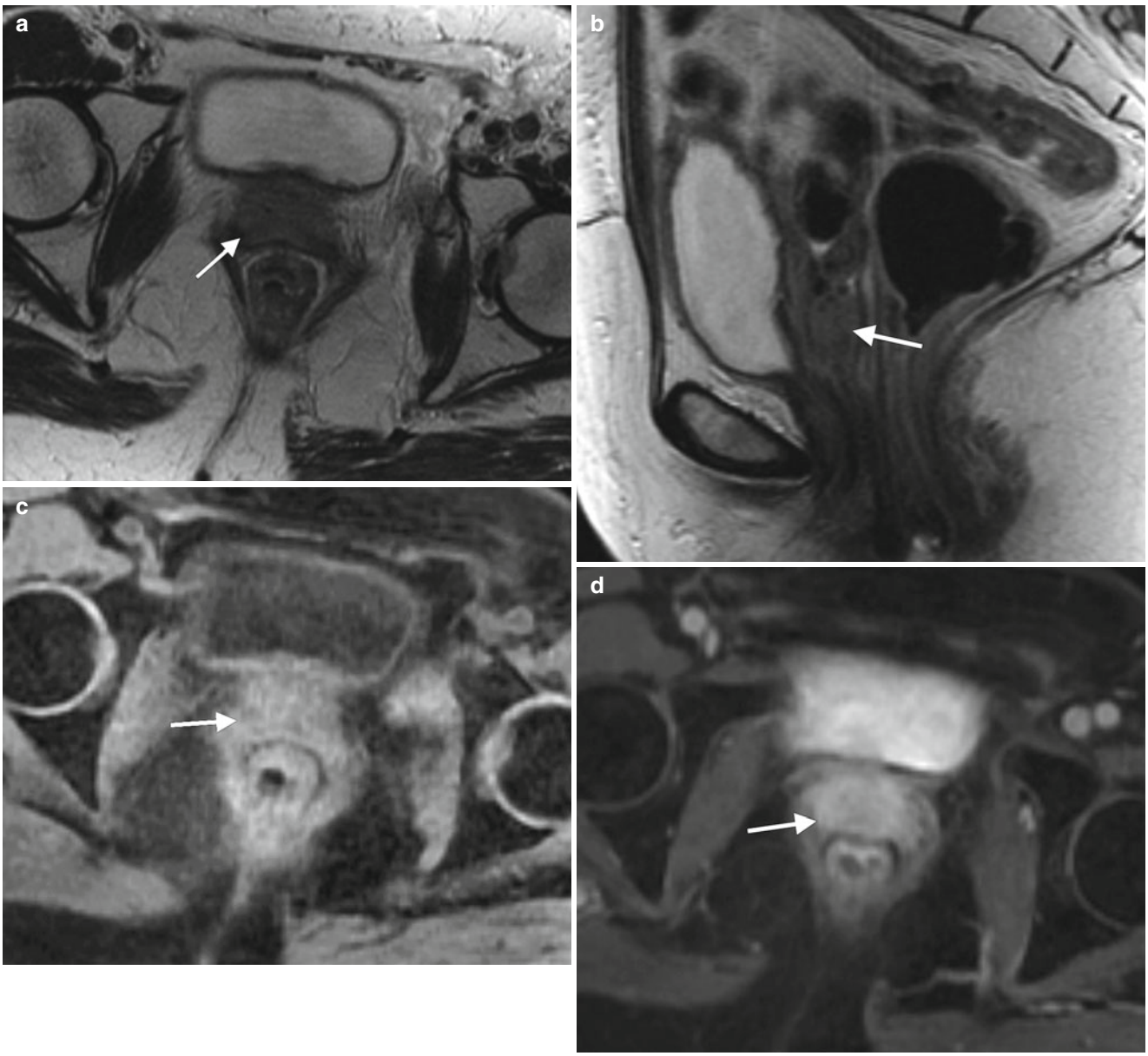

Fig. 2.23 This 59-year-old woman had a history of stage IIIC endometrioid adenocarcinoma of the endometrium, treated with radical hysterectomy and bilateral salpingo-oophorectomy 9 months earlier. Axial (**a**) and sagittal (**b**) T2-weighted MR images and axial, fat-suppressed T1-weighted images before (**c**) and after (**d**) intravenous gadolinium demonstrate a soft tissue mass in the vaginal cuff (*arrows*) consistent with cancer recurrence

References

1. Siegel R, Naishadham D, Jemal A. Cancer statistics, 2012. CA Cancer J Clin. 2012;62:10–29. doi:10.3322/caac.20138.
2. Jemal A, Bray F, Center MM, Ferlay J, Ward E, Forman D. Global cancer statistics. CA Cancer J Clin. 2011;61:69–90. doi:10.3322/caac.20107.
3. Bray F, dos Santos Silva I, Moller H, Weiderpass E. Endometrial cancer incidence trends in Europe: underlying determinants and prospects for prevention. Cancer Epidemiol Biomarkers Prev. 2005;14:1132–42. doi:10.1158/1055-9965.epi-04-0871.
4. Saso S, Chatterjee J, Georgiou E, Ditri AM, Smith JR, Ghaem-Maghami S. Endometrial cancer. BMJ. 2011;343:d3954. doi:10.1136/bmj.d3954.
5. Gull B. Transvaginal ultrasonography of the endometrium in women with postmenopausal bleeding: is it always necessary to perform an endometrial biopsy? Am J Obstet Gynecol. 2000;182:509–15.
6. Novellas S, Chassang M, Delotte J, et al. MRI characteristics of the uterine junctional zone: from normal to the diagnosis of adenomyosis. Am J Roentgenol. 2011;196:1206–13. doi:10.2214/ajr.10.4877.
7. Pecorelli S. Revised FIGO staging for carcinoma of the vulva, cervix, and endometrium. Int J Gynaecol Obstet. 2009;105:103–4.
8. Koivisto-Korander R. Clinical outcome and prognostic factors in 100 cases of uterine sarcoma: experience in Helsinki University Central Hospital 1990-2001. Gynecol Oncol. 2008;111:74–81. doi:10.1016/j.ygyno.2008.06.002.
9. Abeler VM. Uterine sarcomas in Norway. A histopathological and prognostic survey of a total population from 1970 to 2000 including 419 patients. Histopathology. 2009;54:355–64.
10. Panici PB, Basile S, Maneschi F, et al. Systematic pelvic lymphadenectomy vs no lymphadenectomy in early-stage endometrial carcinoma: randomized clinical trial. J Natl Cancer Inst. 2008;100:1707–16. doi:10.1093/jnci/djn397.
11. ASTEC Study Group, Kitchener H, Swart AM, Qian Q, Amos C, Parmar MK. Efficacy of systematic pelvic lymphadenectomy in endometrial cancer (MRC ASTEC trial): a randomised study. Lancet. 2009;373:125–36. doi: 10.1016/s0140-6736(08)61766-3.
12. Todo Y, Kato H, Kaneuchi M, Watari H, Takeda M, Sakuragi N. Survival effect of para-aortic lymphadenectomy in endometrial cancer (SEPAL study): a retrospective cohort analysis. Lancet. 2010;375:1165–72. doi:10.1016/s0140-6736(09)62002-x.
13. Wright JD. Contemporary management of endometrial cancer. Lancet. 2012;379:1352–60. doi:10.1016/s0140-6736(12)60442-5.
14. Creutzberg CL, van Putten WLJ, Koper PC, et al. Survival after relapse in patients with endometrial cancer: results from a randomized trial. Gynecol Oncol. 2003;89:201–9. doi:10.1016/s0090-8258(03)00126-4.
15. Huh WK, Straughn Jr JM, Mariani A, et al. Salvage of isolated vaginal recurrences in women with surgical stage I endometrial cancer: a multiinstitutional experience. Int J Gynecol Cancer. 2007;17:886–9.

Cervical Cancer

3

Irene A. Burger and Yulia Lakhman

3.1 Epidemiology

Cervical carcinoma is the second most common cancer in women in developing countries and the seventh most common cancer in the developed countries. Nearly 80 % of cases occur in less developed countries [1].

The American Cancer Society estimates that 12,170 new cases of invasive cervical carcinoma will be diagnosed in the United States in 2012 and about 4,220 women will die from their disease [2]. Cervical cancer mortality in the United States has declined by almost 70 % between 1955 and 1992 thanks to the introduction and increasing use of screening with a Pap smear.

In the United States, the median age at diagnosis is 47 years of age, and nearly half of cases are diagnosed before the age of 35. However, women over 55 years of age contribute disproportionately to cervical cancer mortality, primarily as a consequence of more advanced disease at the time of diagnosis [3].

3.2 Risk Factors

Cervical carcinoma is the first malignancy for which a direct relation between a viral infection and cancer was proposed [4]. It is thought that a woman must be infected with human papillomavirus (HPV) before she develops cervical cancer and two-thirds of all cervical cancers are caused by HPV 16 and 18 [3, 5].

I.A. Burger, MD
Department of Radiology, University Hospital Zurich,
Ramistrasse 100, Zurich 8091, Switzerland
e-mail: irene.burger@usz.ch

Y. Lakhman, MD (✉)
Department of Radiology, Body Imaging Section,
Memorial Sloan-Kettering Cancer Center,
Evelyn H. Lauder Breast Center, 300 East 66 Street,
Room 703, New York, NY 10065, USA
e-mail: lakhmany@mskcc.org

Table 3.1 Risk factors associated with cervical cancer

Infection with certain types of HPV, particularly HPV 16 and 18
Early age at first sexual intercourse
Multiple sexual partners
Genital warts
Immunosuppression
HIV-positive status
Smoking
Long-term use of oral contraceptives

Infection with HPV is common, and in most people it is either suppressed or cleared by cell-mediated immunity within 1–2 years. Less than 10 % of new infections progress to persistent infections and precancerous lesions [3]. Invasive cancers develop slowly over many years and decades in a minority of women with precancerous lesions, with the peak incidence at about 35–55 years of age.

Additional risk factors associated with the development of cervical cancer include sexual activity starting at a young age, a high total number of sexual partners, and a history of genital warts. Patients who receive immunosuppressive agents and those who are HIV positive are also at increased risk. Cigarette smoking is another independent risk factor for development of cervical dysplasia and invasive cancer. Tobacco-specific carcinogens can bind to and damage cellular DNA, possibly cooperating with HPV in producing malignant transformation. Finally, long-term oral contraceptive use has been associated with increased risk for cervical cancer.

Risk factors associated with cervical cancer are summarized in Table 3.1.

3.3 Anatomy

The cervix is narrower and more cylindrical than the uterine corpus and bulges into the vagina. The portion projecting into the vagina is referred to as the portio vaginalis or

O. Akin (ed.), *Atlas of Gynecologic Oncology Imaging*, Atlas of Oncology Imaging
DOI 10.1007/978-1-4614-7212-4_3, © Springer Science+Business Media New York 2014

ectocervix. The external os (the opening between the cervix and the vagina) is marked histologically by the squamocolumnar junction. The internal os (the opening between the cervix and uterine isthmus) is less clearly demarcated, and it is indicated histologically by the change from cervical fibrous stroma and endocervical mucosa to the mixed histology of the isthmus, which is intermediate between uterine and cervical tissue. The internal os is delineated anatomically by narrowing of the uterine contour and by the entry level of the uterine vessels.

The cervix is supported by multiple ligaments: anteriorly (pubocervical and paired uterovesical ligaments); posteriorly (paired uterosacral ligaments); laterally (paired cardinal ligaments forming the parametria—cellular connective tissue). The parametrium is found adjacent to the lateral margins of the uterus, where the peritoneum reflects to form the broad ligaments. The uterine vessels pass through the lateral parametrium to reach the uterus at the level of the internal os. Parametrial tissue also contains the ureters, as well as many efferent lymphatics.

Table 3.2 Histological types of cervical cancer (WHO)

	Frequency (%)
Squamous cell carcinoma	85
Keratinizing	
Nonkeratinizing	
Spindle cell carcinoma	
Adenocarcinoma	10–12
Endocervical type	
Variant: adenoma malignum (minimal deviation carcinoma)	
Variant: villoglandular papillary adenocarcinoma	
Endometrioid adenocarcinoma	
Clear cell adenocarcinoma	
Serous adenocarcinoma	
Mesonephric adenocarcinoma	
Intestinal type (signet ring) adenocarcinoma	
Other epithelial tumors	
Adenosquamous carcinoma	
Adenoid cystic carcinoma	
Small cell carcinoma	
Undifferentiated carcinoma	
Metastatic tumors (breast, ovary, colon, lung, and direct spread of endometrial carcinoma)	

3.4 Diagnosis

Presentation

In developed countries most cases of cervical carcinoma are diagnosed in asymptomatic patients due to routine screening with a Pap smear. Symptomatic patients present with abnormal vaginal bleeding and occasional vaginal discomfort or malodorous discharge. In patients with advanced disease, symptoms may include flank pain due to hydronephrosis, hematuria due to bladder invasion, rectal bleeding, or other gastrointestinal symptoms.

Histology

Cervical cancer arises from the squamocolumnar junction, which migrates over the years from the ectocervix in young women into the endocervical canal in older women. Therefore, exophytic tumors are typical for young women whereas endophytic tumors are more characteristic for older women.

Squamous cell carcinoma is the most common histologic subtype, responsible for 85 % of primary cervical cancers. Adenocarcinomas account for about 10–12 % of cases, but their incidence is on the rise in more developed countries. It is explained by the fact that adenocarcinoma in situ (the precursor lesion) is detected much less efficiently by Pap smear screening than preinvasive squamous lesions (squamous dysplasia and cervical intraepithelial neoplasia [CIN]). Clear cell carcinoma is a rare subtype of adenocarcinoma accounting for about 5 % of adenocarcinomas of the cervix. In the past, many cases were associated with in-utero exposure to diethylstilbestrol [6]. However, since its use in pregnancy was banned in 1971, the number of cases associated with this drug has diminished. Other uncommon histologic subtypes are adenosquamous carcinomas and small-cell carcinomas. Histologic types of carcinoma found in cervix (World Health Organization [WHO] classification) are summarized in Table 3.2.

3.5 Staging

Clinical Staging

Once the tissue diagnosis of invasive cervical carcinoma is established, the patient is staged. The International Federation of Gynecology and Obstetrics (FIGO) system, last revised in 2009, is the most widely used staging system for cervical carcinoma (Table 3.3) [7]. The FIGO staging of cervical carcinoma is clinical and does not rely on either surgical or pathologic findings. This allows uniformity of staging for all patients worldwide, which is of particular importance as

Table 3.3 2009 FIGO staging for cervical carcinoma [7]

Stage I	**The carcinoma is strictly confined to the cervix (extension to the corpus would be disregarded)**
IA	Invasive carcinoma, which can be diagnosed only by microscopy, with deepest invasion ≤5 mm and the largest extension ≥7 mm
IA1	Measured stromal invasion of ≤3 mm in depth and extension of ≤7 mm
IA2	Measured stromal invasion of >3 mm and not >5 mm with an extension of not >7 mm
IB	Clinically visible lesions limited to the cervix uteri or preclinical cancers greater than stage IA
IB1	Clinically visible lesion ≤4 cm in greatest dimension
IB2	Clinically visible lesion >4 cm in greatest dimension
Stage II	**Cervical carcinoma invades beyond the uterus but not to the pelvic wall or to the lower third of the vagina**
IIA	Without parametrial invasion
IIA1	Clinically visible lesion ≤4 cm in greatest dimension
IIA2	Clinically visible lesion >4 cm in greatest dimension
IIB	With obvious parametrial invasion
Stage III	**The tumour extends to the pelvic wall and/or involves lower third of the vagina and/or causes hydronephrosis or non-functioning kidney**
IIIA	Tumour involves lower third of the vagina, with no extension to the pelvic wall
IIIB	Extension to the pelvic wall and/or hydronephrosis or nonfunctioning kidney
Stage IV	**The carcinoma has extended beyond the true pelvis or has involved (biopsy proven) the mucosa of the bladder or rectum. A bullous edema, as such, does not permit a case to be allotted to Stage IV**
IVA	Spread of the growth to adjacent organs
IVB	Spread to distant organs

Table 3.4 Procedures permitted for FIGO staging of cervical cancer

Physical examination	Palpation of lymph nodes
	Vaginal examination
	Rectovaginal examination with or without anesthesia
Radiologic studies	Chest radiograph
	Skeletal radiograph
	Intravenous pyelogram
	Barium enema
Procedures	Cervical biopsy
	Cervical conization
	Hysteroscopy
	Colposcopy
	Endocervical curettage
	Cystoscopy
	Proctoscopy
Other studies (not allowed for assignment of clinical staging)	Computed tomography
	Magnetic resonance imaging
	Positron emission tomography with fluorodeoxyglucose
	Ultrasonography
	Bone scanning
	Lymphangiography
	Laparoscopy

cervical carcinoma is most prevalent in countries where surgical and diagnostic resources are limited.

For small early-stage tumors (stage IA and IB1), stage is assigned after measurement of the depth and width of tumor invasion on cone biopsy, pelvic examination for clinically assessment of tumor size, or both. For more advanced tumors, pelvic examination under anesthesia is sometimes necessary for the parametrial assessment. Additional tests permitted for FIGO staging are summarized in Table 3.4 and are restricted to imaging modalities available in most countries.

It is well known that clinical staging of cervical carcinoma is associated with significant inaccuracies compared to surgical staging, with an error rate up to 32 % in patients with stage IB disease and up to 65 % in patients with stage III disease [8]. The main difficulty is accurate clinical estimation of the tumor size in craniocaudal plane, assessment of parametrial and pelvic side wall invasion, and evaluation of lymph node metastases.

Although revised FIGO staging system does not allow the results of CT, MRI, or positron-emission tomography (PET or PET CT) to influence the clinical stage, the committee does encourage the use of these imaging techniques, if available, to more accurately assess important prognostic factors as tumor size, parametrial and pelvic side wall invasion, adjacent organ invasion, and lymph node status [7, 9, 10].

3.6 Management

Treatment options are summarized in Table 3.5 [5, 11].

3.7 Imaging

- Cervical cancer is typically detected clinically (Pap smear and/or physical examination)
- Imaging
  - Evaluation of extent of disease
  - Radiation therapy planning
  - Monitoring treatment response
  - Detection of tumor recurrence
  - Guidance prior to and during interventional procedures

Table 3.5 Treatment algorithm for cervical cancer

Stage	Clinical features	Treatment
IA1	If desires fertility preservation	Observation after cone biopsy with negative margins OR Simple hysterectomy OR
	If lymphovascular invasion	Radical trachelectomy or radical hysterectomy + pelvic lymphadenectomy
IA2	If desires fertility preservation	Radical trachelectomy + pelvic lymphadenectomy ± para-aortic lymph node sampling OR Radical hysterectomy + pelvic lymphadenectomy ± para-aortic lymph node sampling OR Radiotherapy
IB1 and IIA1	If desires fertility preservation, stage IB1 only and tumor is <2 cm	Radical trachelectomy + pelvic lymphadenectomy ± para-aortic lymph node sampling OR Radical hysterectomy + pelvic lymphadenectomy ± para-aortic lymph node sampling OR Radiotherapy
IB2 and IIA2		Chemoradiotherapy OR Radical hysterectomy + pelvic lymphadenectomy + para-aortic lymph node sampling OR Chemoradiotherapy ± adjuvant hysterectomy
IIB and IIIA		Chemoradiotherapy
IVA		Chemoradiotherapy OR Primary pelvic exenteration
IVB		Palliative chemotherapy OR Chemoradiotherapy

Table 3.6 Role of US, CT, MRI, PET-CT in initial staging of cervical cancer [12–14]

Ultrasonography (US)	
Transabdominal US	**No role in evaluating local extent**; may be used to detect hydronephrosis **Similar accuracy to MRI for tumor detection and parametrial evaluation**
Transrectal (TRUS) US	BUT **Operator dependent** **Narrow field of view (FOV)** yields no information regarding nodal status
Computed tomography (CT)	**Inferior to MRI in local staging of early-stage cervical cancer** Limited soft tissue contrast accounts for poor detection of small tumors, parametrial invasion, and early invasion of the rectum and bladder mucosa For detecting parametrial invasion: sensitivity, 17–100 % (average, 64 %); specificity, 50–100 % (average, 81 %) **Value of CT increased with higher stage disease** Detection of distant metastases and nodal assessment Based on the ACRIN trial results, sensitivity, specificity, and negative predictive value (NPV) for staging FIGO stage IIB or greater tumors: 42, 82, and 84 %, respectively **Nodal assessment** Low sensitivity as it relies on size criterion alone(>1 cm in short axis)for diagnosis of malignant adenopathy Cannot detect micrometastases Sensitivity, 31–65 %; positive predictive value (PPV), 51–65 %; and NPV, 86–95 %
Magnetic resonance imaging (MRI)	**Imaging modality of choice** for assessment of tumor location (exophytic or endocervical), its size, and presence of invasion into the parametria, pelvic sidewall or adjacent organs **Complimentary to clinical assessment in staging FIGO stage IB or higher tumors** Overall staging accuracy, 75–96 % Superior to clinical examination in assessing tumor size, especially its craniocaudal dimension Superior to CT in detecting parametrial invasion; sensitivity and specificity in evaluating parametrial invasion, 40–57 % and 77–80 %, respectively Neither CT nor MRI are accurate for evaluating cervical stroma MRI is mandatory in patients considered for fertility sparing radical trachelectomy **MRI performs similar to CT in nodal assessment** Also relies on size criteria for assessing lymph nodes Sensitivity, 30–73 % and specificity, 93–95 %, respectively

Table 3.6 (continued)

Positron emission tomography (PET) and PET/CT	**Imaging modality of choice** for assessment of pelvic and extrapelvic lymph nodes and distant organ involvement, particularly in patients with advanced cervical cancer (*i.e.*, FIGO stage IIB or higher) Sensitivity, 58–72 %; specificity, 93–95 %; accuracy, 85–99 % in detection of nodal metastases; these values are higher than those for MRI and CT Value of FDG PET in early stage disease (FIGO I to IIA) is questionable Low sensitivities for detection of nodal metastases, 25–73 % Does not replace the need for lymphadenectomy for nodal assessment **FDG activity** may be important in predicting outcome **Detection of persistent or recurrent disease** after chemoradiation Future studies may use the best of both techniques with MRI/PET fusion imaging

Imaging Techniques

Table 3.7 CT imaging techniques [15]

Patient position	Supine Prone Maybe use in CT-guided biopsy or drainage
Imaging	Oral contrast medium 750–1,000 mL diluted oral contrast 2 h prior to examination Intravenous contrast medium 100–150 mL iodinated contrast medium Injection rate: 2–3 mL/s 70–120 s delay after IV contrast administration 5 mm collimation (thinner for 3D or small lesion characterization)

Table 3.8 MRI techniques [15, 16]

Patient preparation	To limit artifacts due to small bowel peristalsis Fasting for 4–6 h before MRI examination Optional: use of antiperistaltic agents (hyoscine butyl bromide or glucagon) Optional: vaginal opacification with sonographic gel Helpful in cases of suspected cervical tumor extension into the vagina, especially posterior fornix Empty bladder
Coil selection	Image supine using pelvic surface array multichannel coil Improves signal-to-noise ratio, increases resolution, and decreases imaging time Endoluminal coils: rarely used Advantages High-resolution images of small tumors Aid in detection of early parametrial extension Disadvantages Extra cost Patient discomfort Small FOV which is inadequate for evaluation of large tumors and their extrauterine extent Not an issue if combined with the use of the pelvic surface array coil
Imaging sequences and planes	Transverse T1-WI using large FOV that includes entire pelvis Evaluation of lymph nodes and pelvic bones Small FOV T2-WI without fat suppression in **at least two** orthogonal planes such as sagittal and oblique: Sagittal plane Distance to the internal cervical os and tumor extension into the lower uterine segment (if fertility sparing surgery is desired) Evaluation of tumor invasion into the urinary bladder and vagina Oblique planes Transverse oblique (perpendicular to the long axis of the cervical canal) and/or coronal oblique (parallel to the long axis of the cervical canal) Crucial for accurate evaluation of parametria Preferred imaging parameters FOV 20–25 cm, slice thickness (3–4 mm/0.4 mm skip), matrix 512×512 mm Optional: Large FOV coronal T2-WI Assessment of kidneys and ureters in patients with advanced stage disease (FIGO stage III-IV) Dynamic contrast-enhanced sagittal 3D GRE T1-WI Can be useful in detection of small cervical tumors, assessment of tumor response, and distinguishing radiation-induced fibrosis from residual or recurrent tumor Precontrast and 4 postcontrast sequences at 1 min intervals DWI –MR (b values: 0, 500–1,000 s/mm^2) Potentially useful in tumor detection/ staging and assessment of tumor response

Normal Anatomy

Table 3.9 Normal zonal anatomy of the cervix on T2-WI [17]

Layer	Thickness	Signal intensity (SI) relative to muscle
Endocervix	<10 mm	High SI with plicae palmatae
Inner stroma	Variable	Low SI
Outer stroma	Variable	High SI

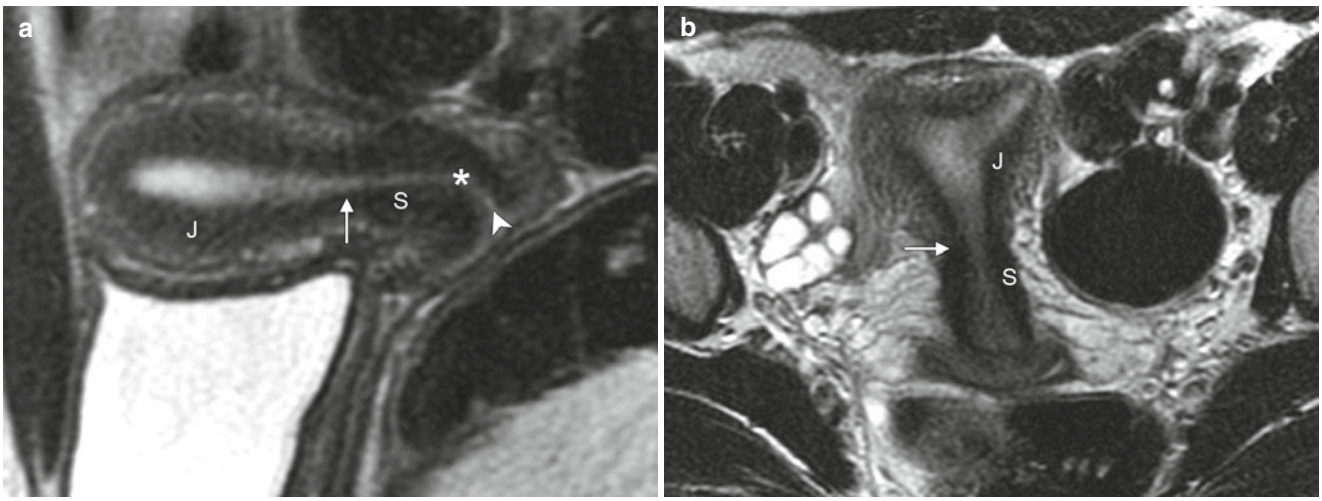

Fig. 3.1 Normal zonal anatomy of the cervix on a sagittal (**a**) and a coronal oblique (**b**) T2-WI. The cervix extends from the internal cervical os (*arrows*) to the external cervical os (*arrowhead*). The external cervical os protrudes into the vagina. The junctional zone of the uterus (*J*) is continuous with the fibrous inner cervical stroma (*S*) and the outer myometrium is continuous with the outer cervical stroma. Intermediate-to-high SI layer between anterior and posterior fibrous stroma represents cervical mucosa (*asterisk*)

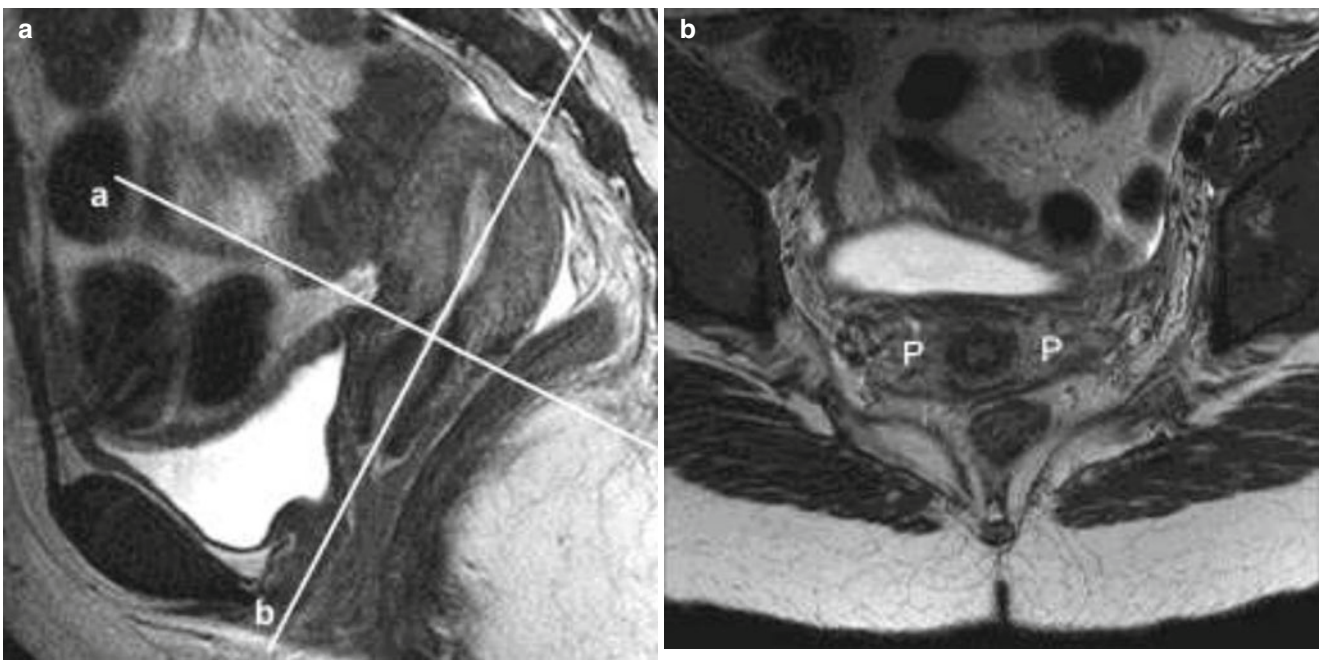

Fig. 3.2 Normal anatomy of the cervix and routine imaging planes. MRI of the cervix should include small FOV high resolution T2-WI without fat saturation in at least two orthogonal planes, typically sagittal, transverse oblique, and/or coronal oblique planes. (**a**) Sagittal plane images are acquired first and are used to plot oblique planes (*a* transverse oblique, *b* coronal oblique). (**b**) Transverse oblique images are acquired perpendicular to the long axis of the cervix (plane a). This plane provides optimal evaluation of the cervical stromal ring and parametria (*P*) (*i.e.*, paracervical soft tissues lateral to the cervix). (**c**) Coronal oblique images are acquired parallel to the long axis of the cervix (plane b) and nicely depict entire cervix including cervical stromal ring, internal cervical os (*arrowhead*) and external cervical os (*arrow*), and parametria (*P*)

Diagnosis

Benign Lesions

Fig. 3.2 (continued)

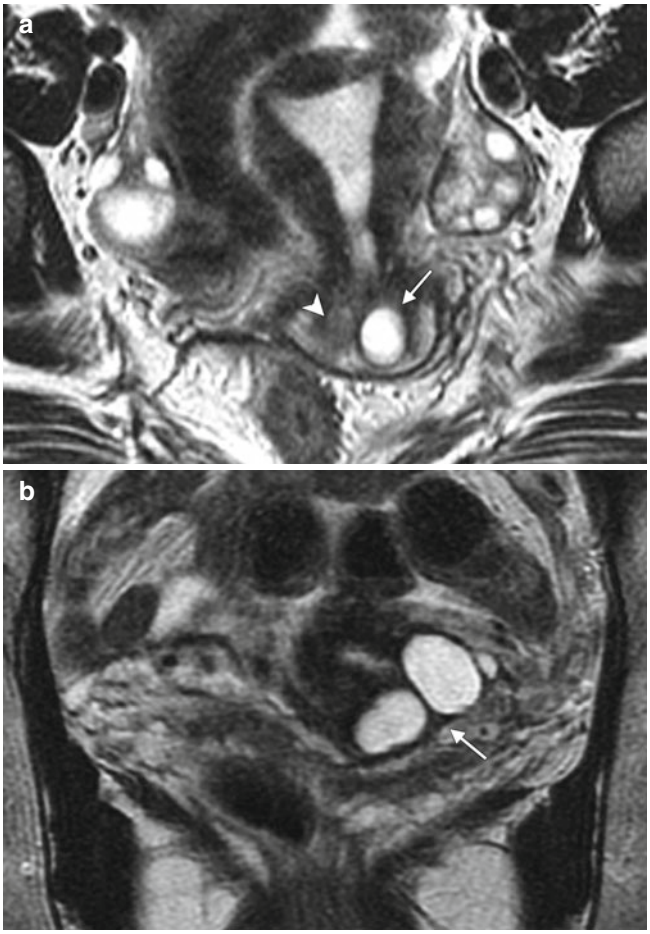

Fig. 3.3 Nabothian cyst(s). Nabothian cysts are a common incidental finding. They represent retention cysts that arise from the endocervical glands secondary chronic inflammation and scarring. Nabothian cysts appear as single or multiple round, unilocular, high T2 SI cyst(s)/cystic lesion(s) on the cervical surface or in the inner portion of the cervical stroma adjacent to the endocervical canal. They are typically hypo- to isointense to cervix on T1-WI although a minority is T1 hyperintense due to mucinous contents. (**a**) Coronal oblique T2-WI image demonstrates a well-defined cyst in the cervix, consistent with a nabothian cyst (*arrow*), next to a small intermediate SI cervical carcinoma (*arrowhead*). (**b**) Transverse oblique T2-WI image shows several nabothian cysts (*arrow*) in a different patient

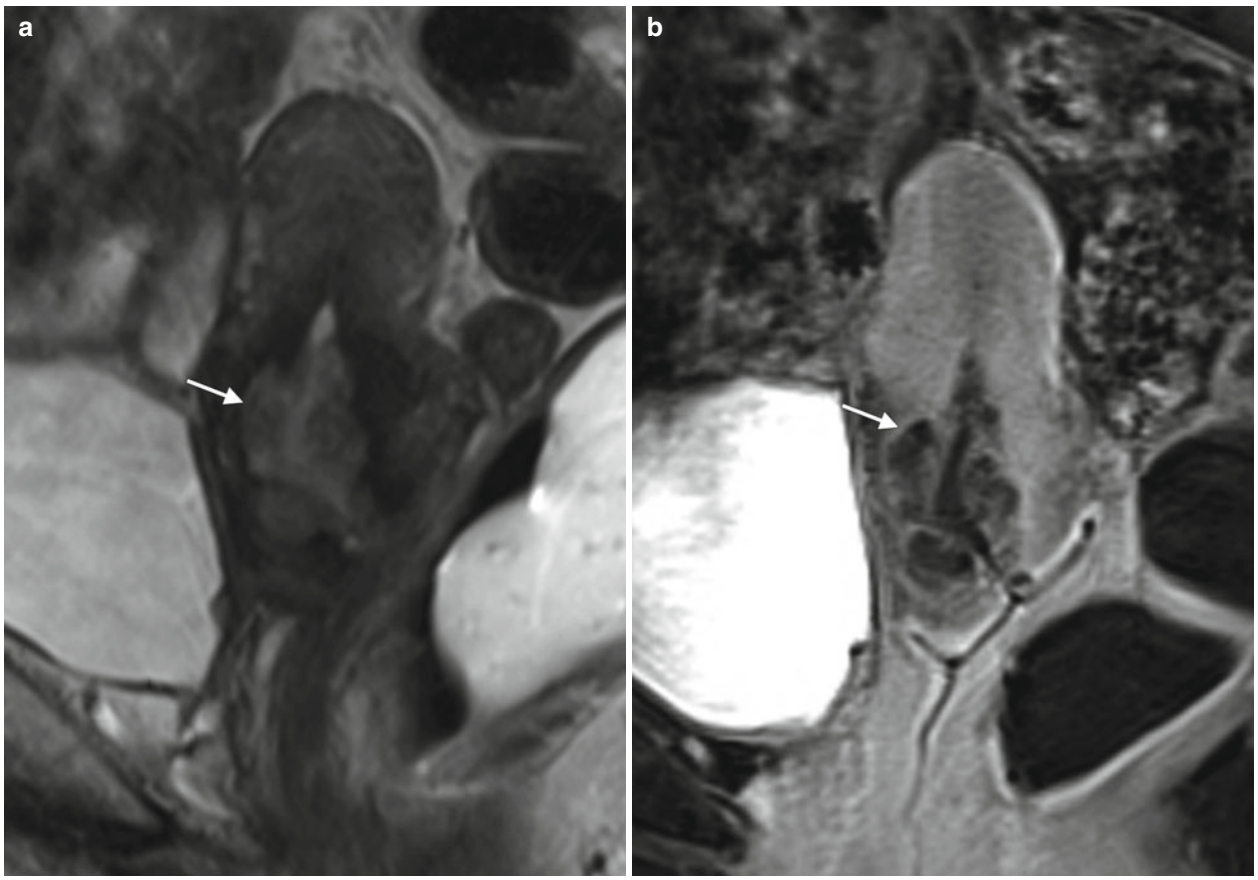

Fig. 3.4 Tunnel cluster is a specific type of nabothian cyst characterized by complex multicystic dilatation of the endocervical glands [18]. It is a benign pseudoneoplastic glandular lesion of the cervix occurring in multiparous women. They might develop during pregnancy due to hormonal stimulation and persist for variable period of time thereafter. Tunnel clusters are divided into type A (non-cystic) and type B (cystic) that frequently coexist. Type A tunnel clusters have mass-like appearance on imaging and may be hard to distinguish from cervical adenocarcinoma or adenoma malignum and have to be verified with histology. (**a**) Sagittal T2-WI image depicts multilobular intermediate T2 SI mass-like lesion in the enlarged cervix (*arrow*). (**b**) Fat-suppressed, contrast-enhanced, transverse T1-WI in the same patient better demonstrates that this lesion consists of multiple nabothian cysts surrounded by contrast-enhancing proliferated glands in the cervical stroma adjacent to a preserved endocervical canal (*arrow*)

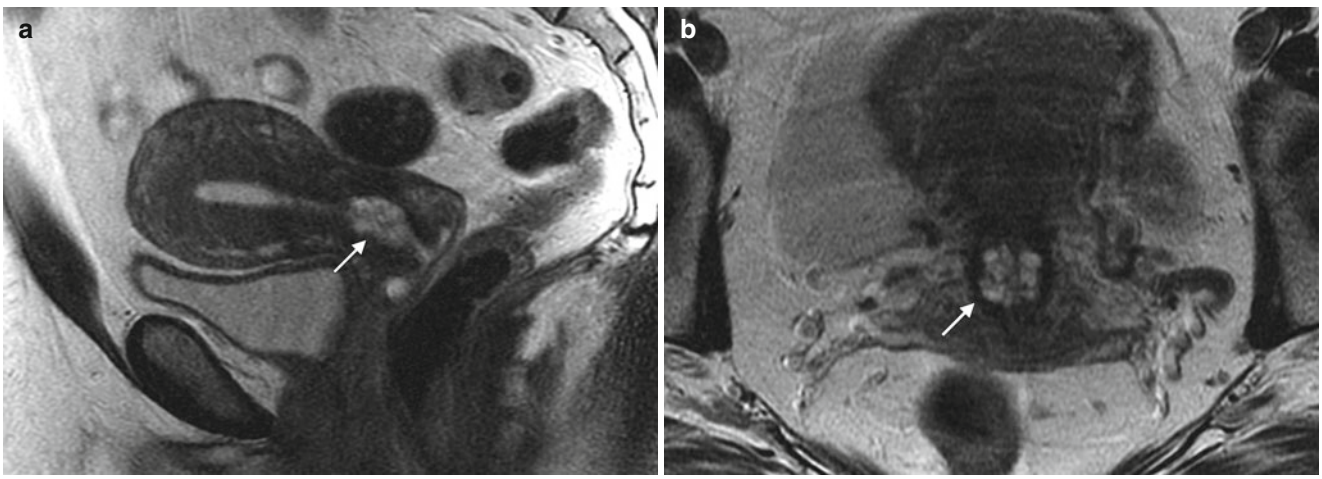

Fig. 3.5 Type B tunnel cluster. Sagittal (**a**) and (**b**) transverse T2-WI images show multilocular cystic lesions within enlarged cervix (*arrow*). Pathologic findings via deep cervical biopsy indicated a tunnel cluster

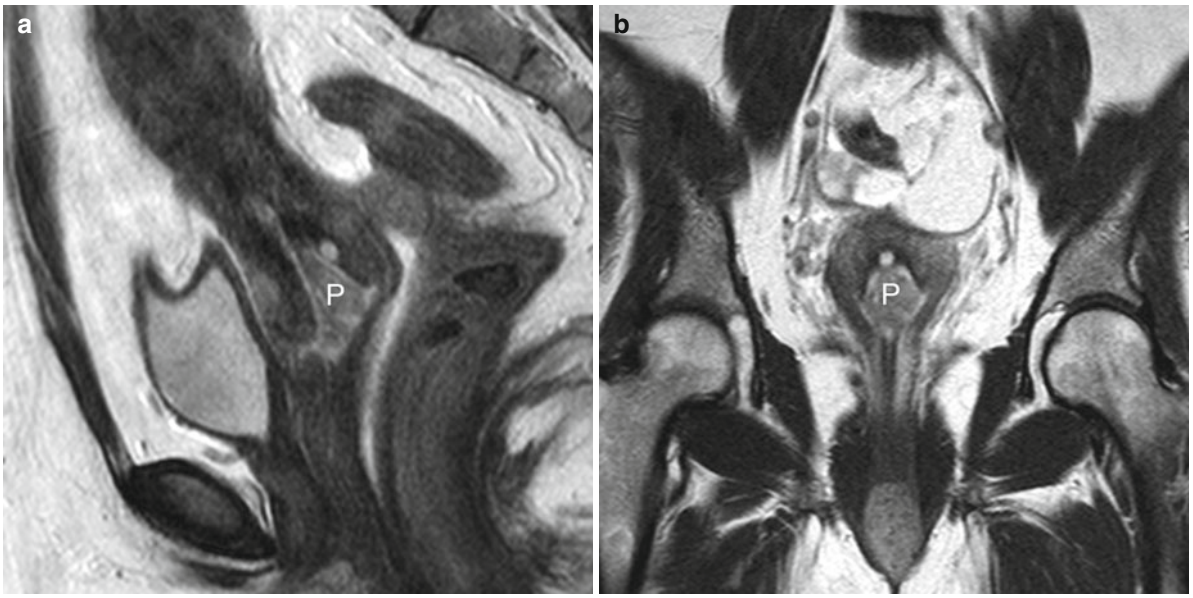

Fig. 3.6 Endocervical polyp. Endocervical polyps are focal, hyperplastic protrusions of endocervical folds. They constitute 4–10 % of all cervical lesions and less than 1 % harbor dysplasia and in situ or invasive carcinoma. Many patients are asymptomatic whereas some present with vaginal spotting. Possible etiologies include tamoxifen use, multiparity, chronic cervicitis, foreign bodies, and estrogen secretion. Hysteroscopy and curettage is a treatment of choice since imaging cannot distinguish between a purely benign polyp, a polyp harboring noninvasive cancer, and a polypoid adenocarcinoma. One must also consider endometrial polyp prolapsing through the cervix. Sagittal (**a**) and coronal (**b**) T2-WI images show intermediate T2SI endocervical mass (*P*) surrounded by high-signal intensity fluid

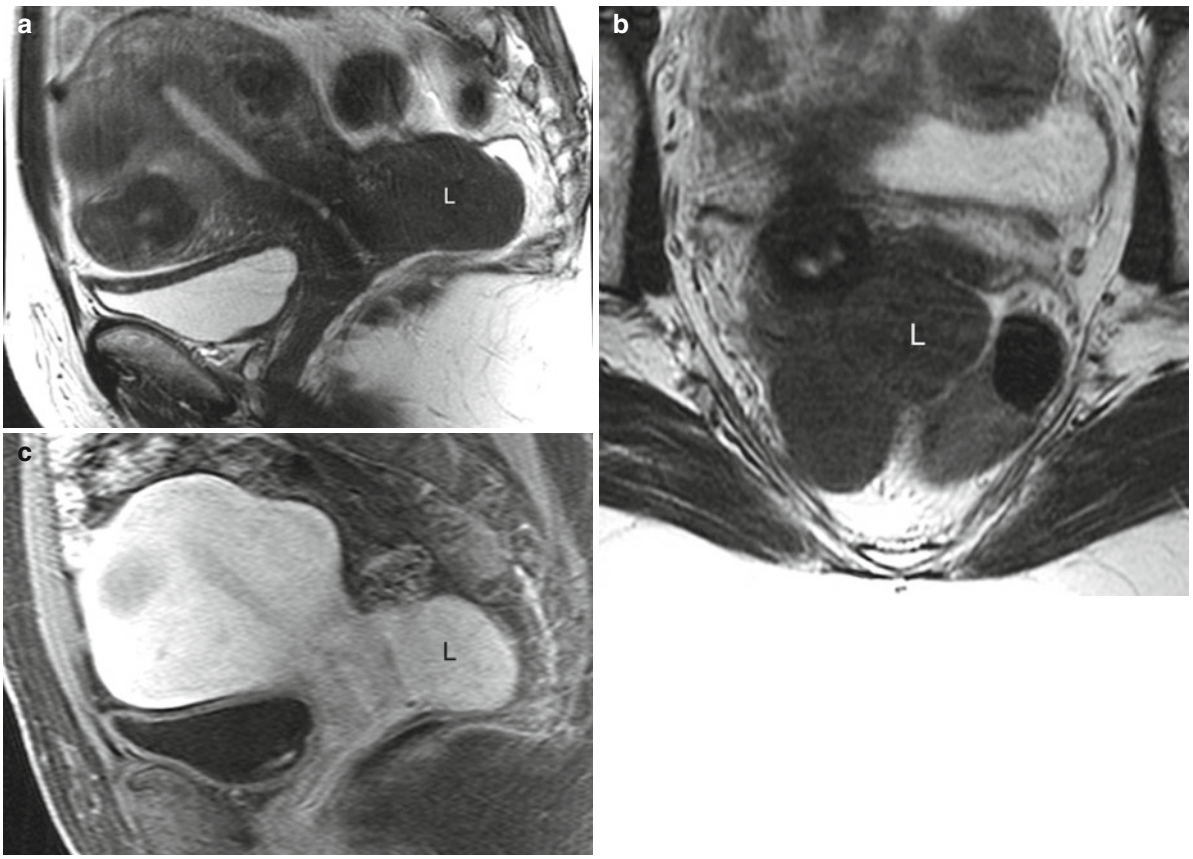

Fig. 3.7 Leiomyoma of the cervix. It is a benign smooth muscle tumor that is much more common in the uterus. Only 8–10 % of cases originate in the cervix. Similar to uterine fibroids, leiomyomas of the cervix are round well-defined homogeneous hypointense T2 SI enhancing masses. Degenerated leiomyomas (usually if >5–8 cm) are heterogenous with areas of high SI on T2-WI and heterogenous enhancement after contrast. Sagittal (**a**) and transverse (**b**) T2-WI show a well-defined homogeneous mass with low T2 SI arising from the posterior lip of the cervix (*L*). (**c**) Sagittal T1-WI after intravenous contrast enhancement confirms a homogeneous mass with marked contrast uptake (*L*)

Cervical Cancer

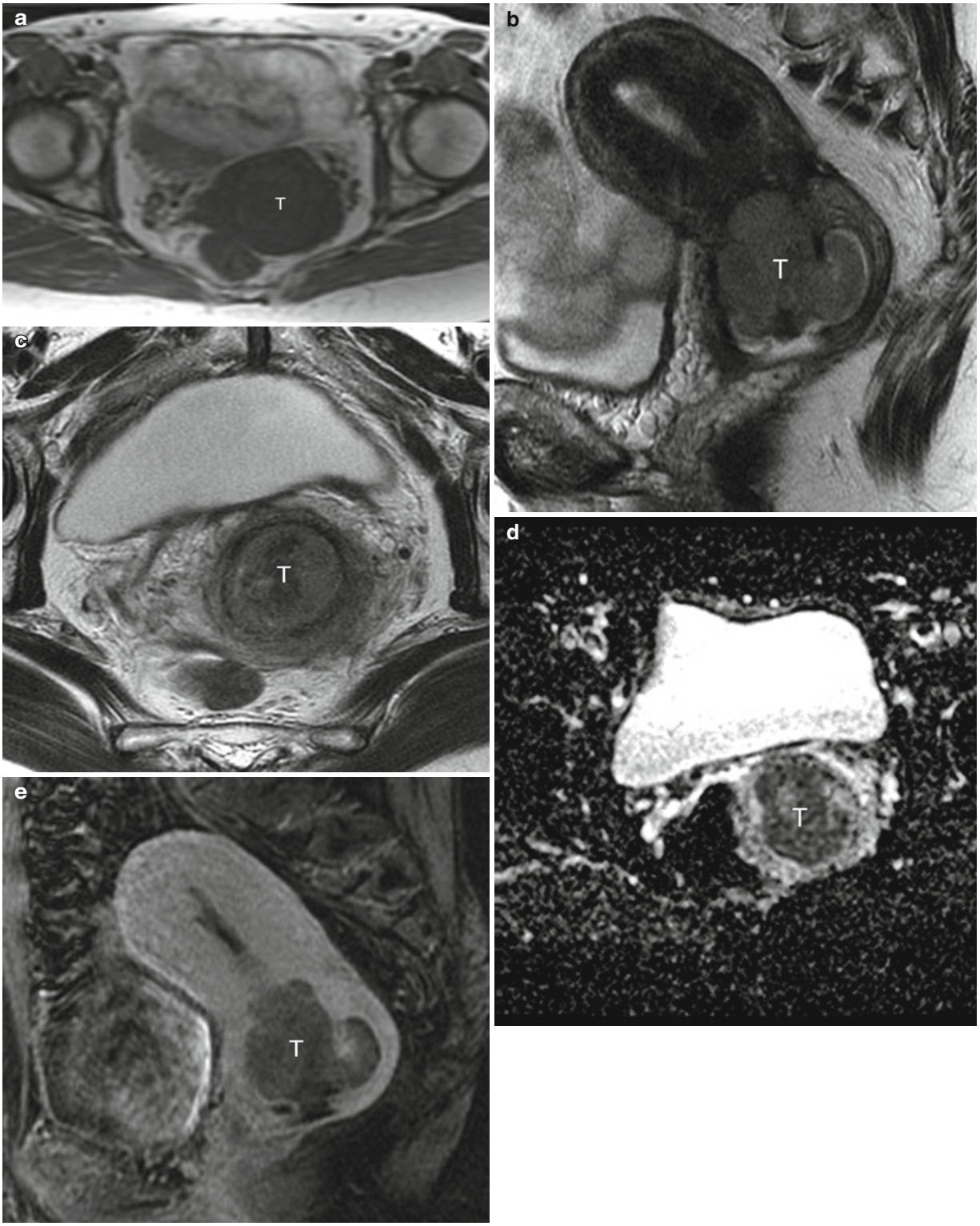

Fig. 3.8 Squamous cell carcinoma of the cervix. Cervical cancer presents as a solid mass in the uterine cervix. It originates from the squamocolumnar junction in the endocervical canal and demonstrates variable degree of cervical stromal invasion. (**a**) The tumor is isointense to cervical stromal on T1-WI (*T*). (**b**, **c**) T2-WI sequences are the most useful for tumor depiction and tumor staging because cervical cancer (*T*) is hyperintense relative to low SI cervical stroma. (**d**) ADC map of diffusion weighted images shows restricted diffusion in the primary tumor (*T*). (**e**) The tumor demonstrates variable contrast-enhancement. T1 C+ may be helpful in depicting small tumors because of their hypervascularity on early dynamic postcontrast sequences relative to the hypovascular cervical stroma (*T*)

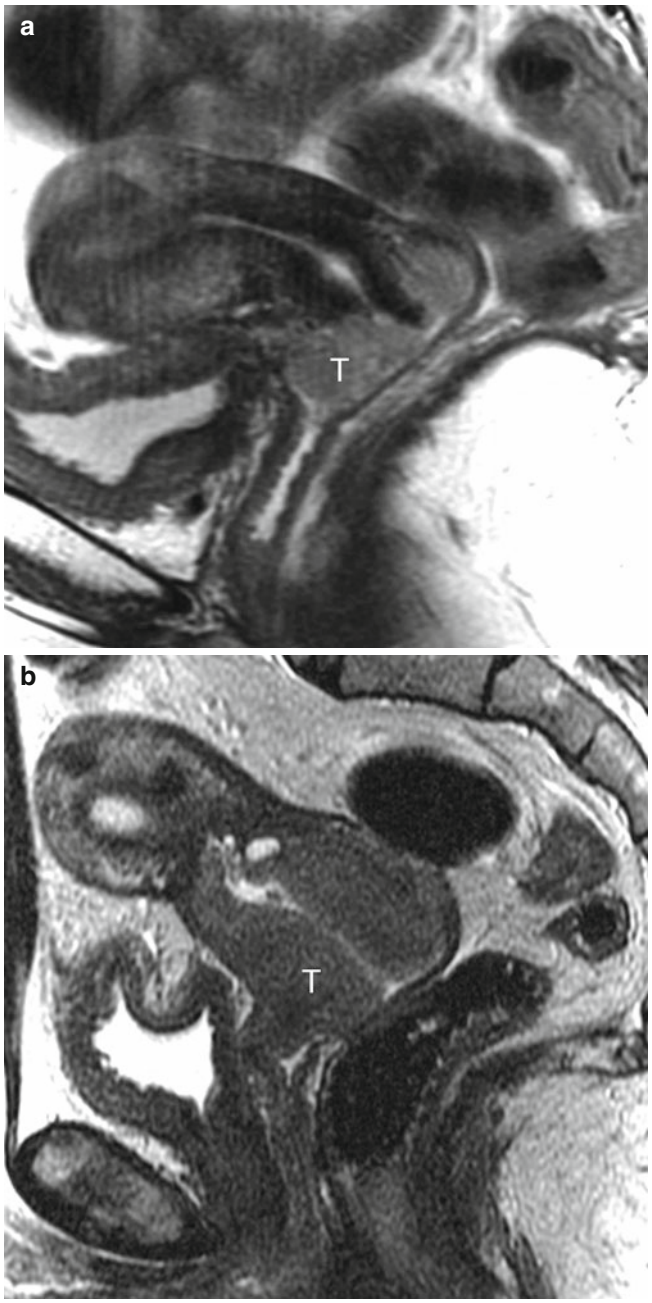

Fig. 3.9 Two different patients illustrating exophytic and endophytic growth patterns. Squamous cell carcinoma of the cervix originate from the squamocolumnar junction zone. This junction zone migrates into the cervical canal over the years. Therefore the exophytic growth pattern is more commonly seen in younger women. Sagittal T2-WI (**a**) with a large intermediate SI tumor (*T*) protruding into the upper vagina in a 32-year-old woman, versus sagittal T2-WI (**b**) with a bulky tumor (*T*) with an endophytic growth pattern in a 55-year-old woman

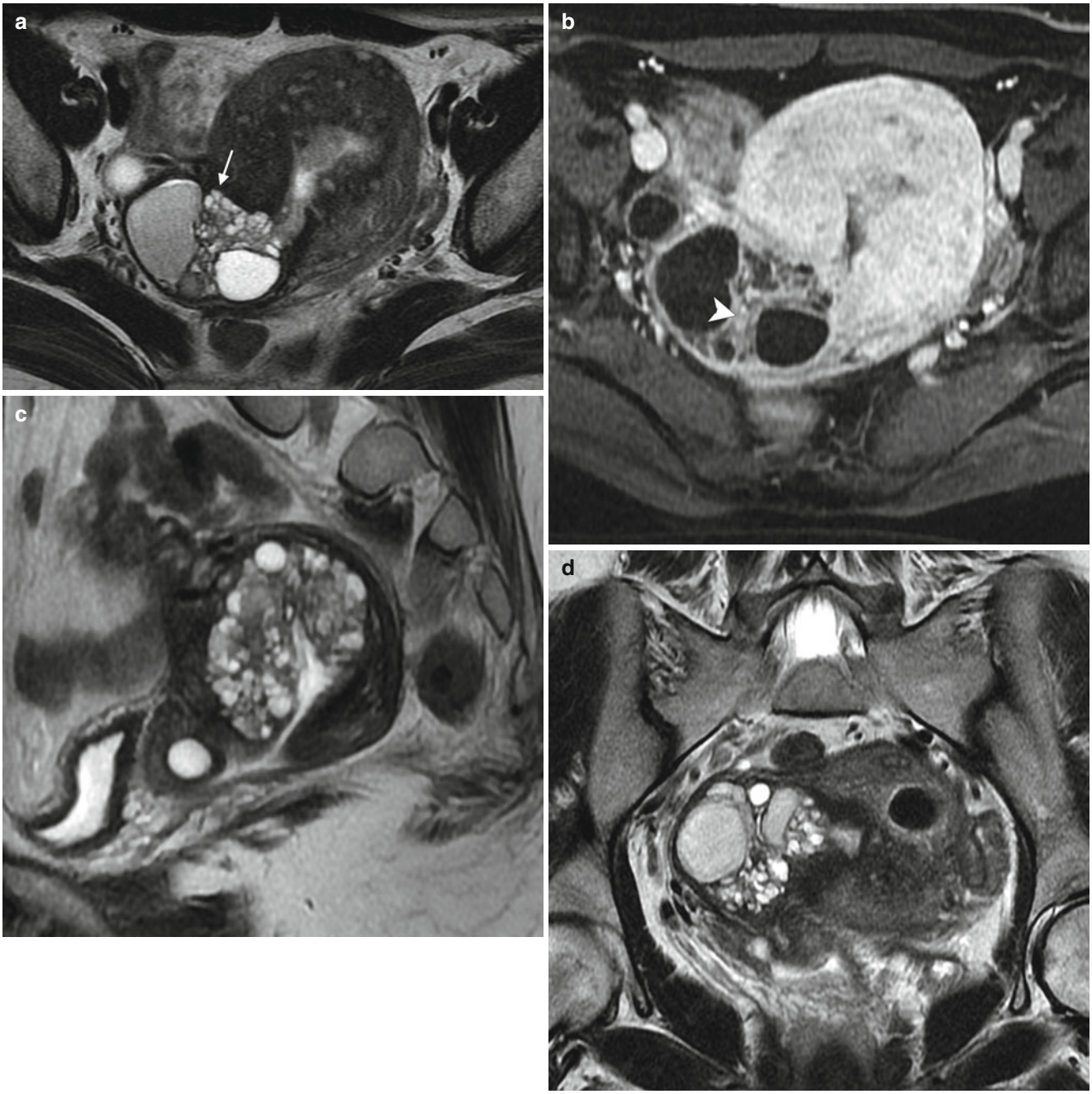

Fig. 3.10 Adenoma malignum (also known as mucinous minimal deviation adenocarcinoma). Adenoma malignum is a rare tumor accounting for 3 % of cervical adenocarcinomas. Peutz-Jeghers syndrome is a known risk factor. Watery discharge and vaginal bleeding are the most common presenting symptoms. Although it is more indolent than typical squamous cell carcinoma or adenocarcinoma of the cervix, adenoma malignum has unfavorable prognosis due to early dissemination into the peritoneal cavity. Its deceptive benign histologic appearance may leads to wrong diagnosis and deep cervical stromal biopsy is required to make the correct diagnosis. (**a**) Transverse T2-WI depicts multiple high SI cysts (*arrow*) within low SI cervical stroma. (**b**) Transverse C+ images demonstrate multiple low SI cysts embedded in enhancing stroma (*arrowhead*). Sagittal (**c**) and coronal oblique T2-WI (**d**) confirming a well-defined cystic lesion with variable T2 hyperintensity without invasion of adjacent structures. Adenoma malignum may be difficult to distinguish on imaging from deep-seated nabothian cysts

Staging

FIGO Stage IB. Clinically visible lesions confined to the cervix uteri or preclinical cancers greater than stage IA.

- IB1: clinically visible lesion ≤4 cm in greatest dimension
- IB2: clinically visible lesion >4 cm in greatest dimension

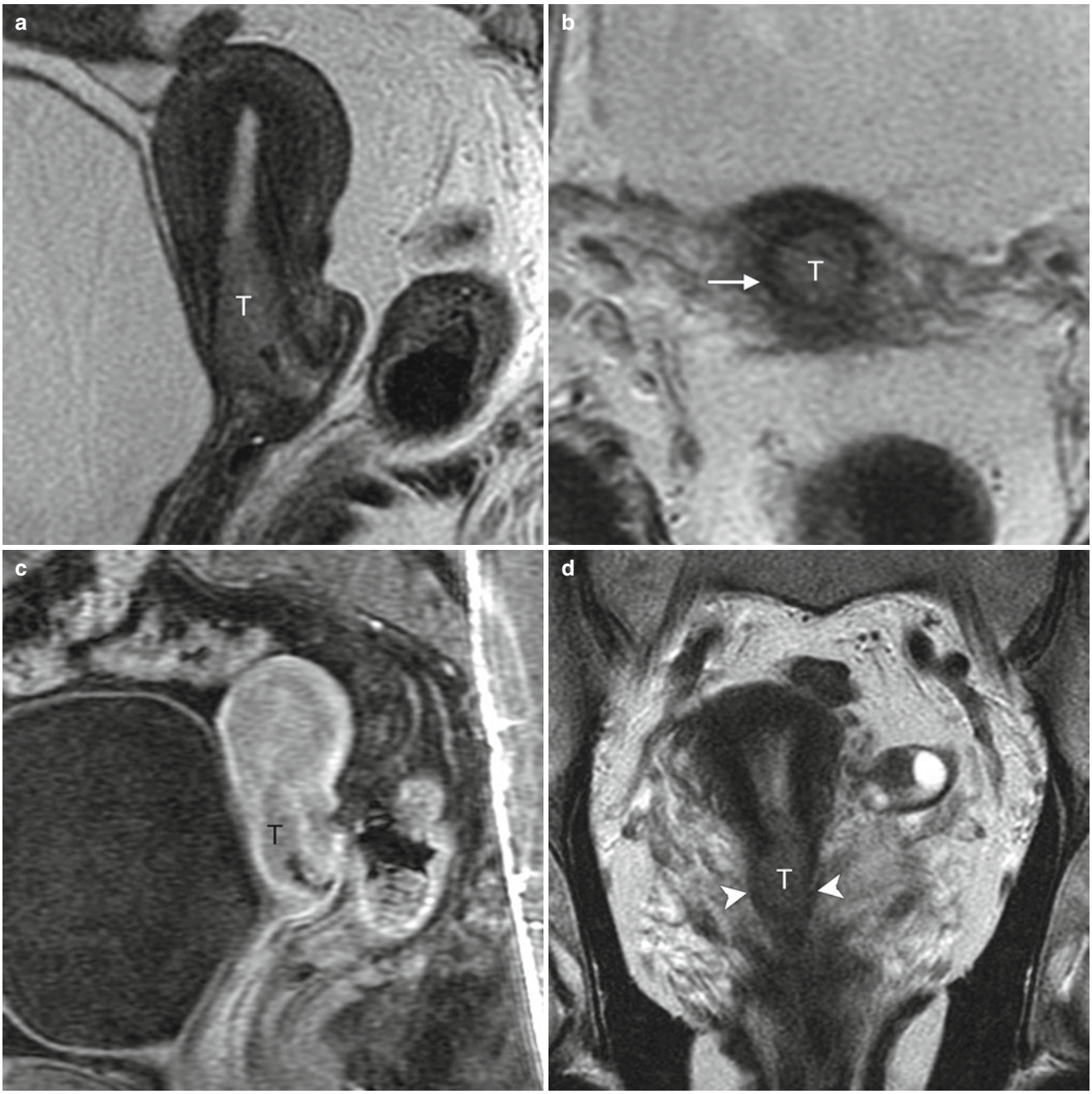

Fig. 3.11 Stage IB1 cervical cancer. Sagittal (**a**) and transverse oblique T2-WI (**b**) show intermediate SI cervical cancer (*T*) enlarging endocervical canal. The cervical cancer is confined to the cervical stroma, as indicated by the intact low SI cervical stromal ring surrounding high SI tumor. (**c**) Sagittal T1-WI C+ showing a slightly hypointense tumor (*T*) compared to the well-vascularized cervical stroma. (**d**) Coronal oblique T2-WI in cases of full thickness stromal invasion, the low SI stroma is entirely replaced by higher SI tumor, but the presence of a smooth tumor-parametrial interphase (*arrowhead*) excludes parametrial invasion

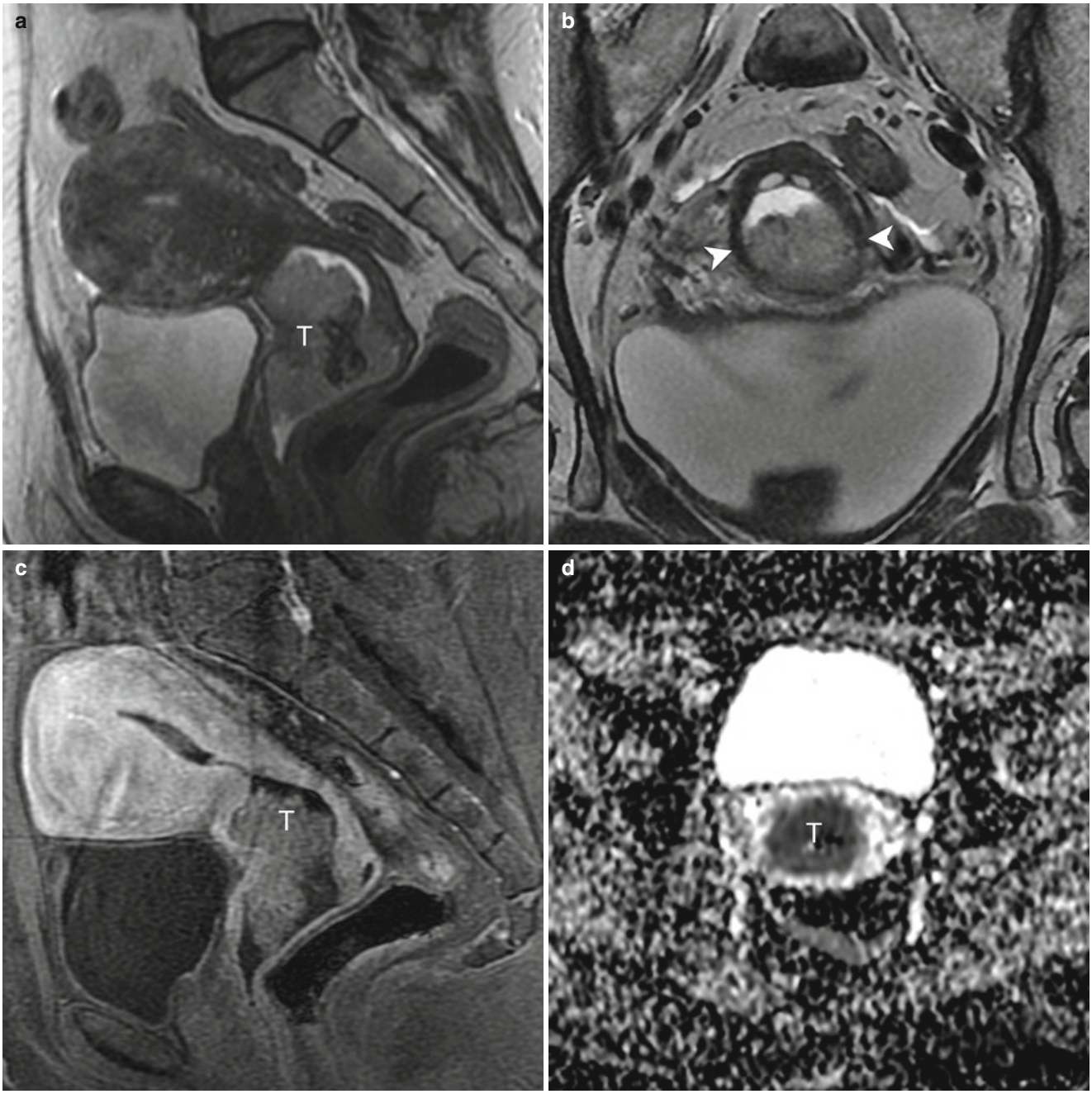

Fig. 3.12 Stage IB2 cervical cancer. Sagittal (**a**) and transverse T2-WI (**b**) depict a 5.1 cm intermediate SI cervical cancer (*T*) confined to the cervix. Low SI cervical stromal rim around the tumor is preserved (*arrowhead*). (**c**) Sagittal T1-WI C+ showing a slightly hypointense tumor (*T*). (**d**) ADC map of diffusion-weighted images shows restricted diffusion in the primary tumor (*T*)

FIGO Stage II. Cervical carcinoma invades beyond the uterus, but not to the pelvic wall or to the lower third of the vagina

- Stage IIA: **without** parametrial invasion
  - IIA1: clinically visible lesion ≤4 cm in greatest dimension
  - IIA2: clinically visible lesion >4 cm in greatest dimension
- Stage IIB: **with** parametrial invasion

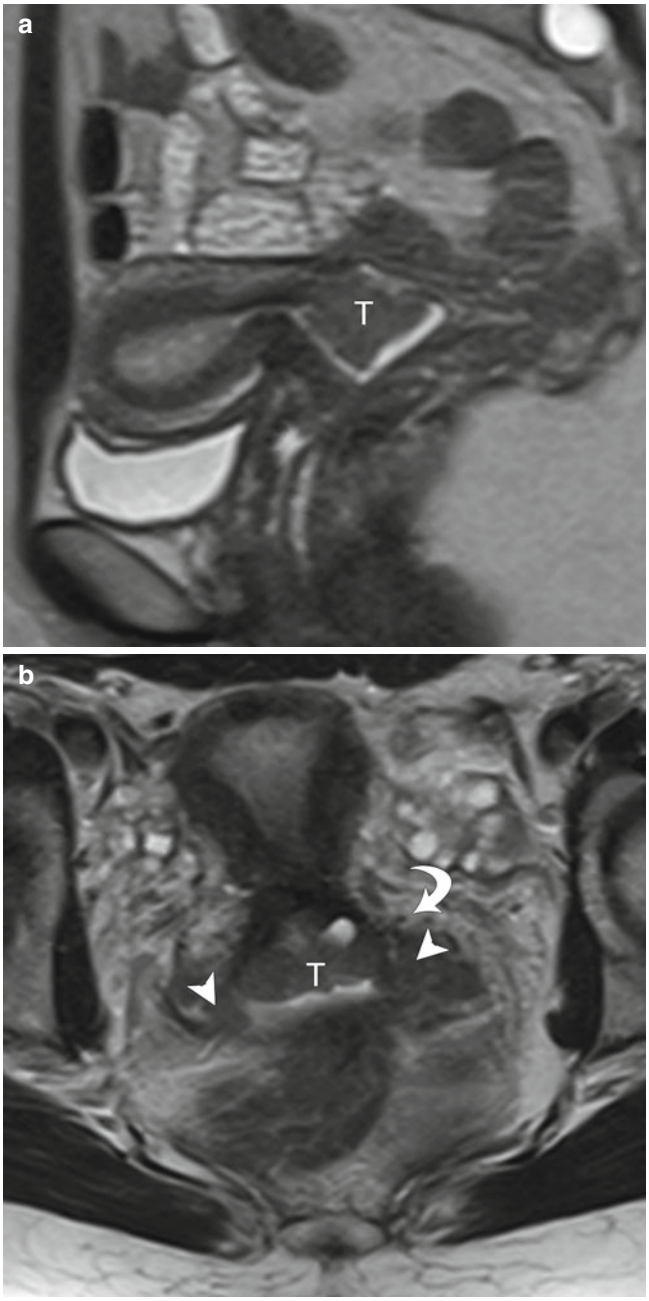

Fig. 3.13 Stage IIA cervical cancer. Sagittal (**a**) and coronal oblique T2-WI (**b**) demonstrate a cervical mass (*T*) invading the upper vagina and disrupting low SI of both vaginal fornices (*arrowhead*). Cervical stromal ring is thinned but no parametrial invasion is present (*curved arrows*)

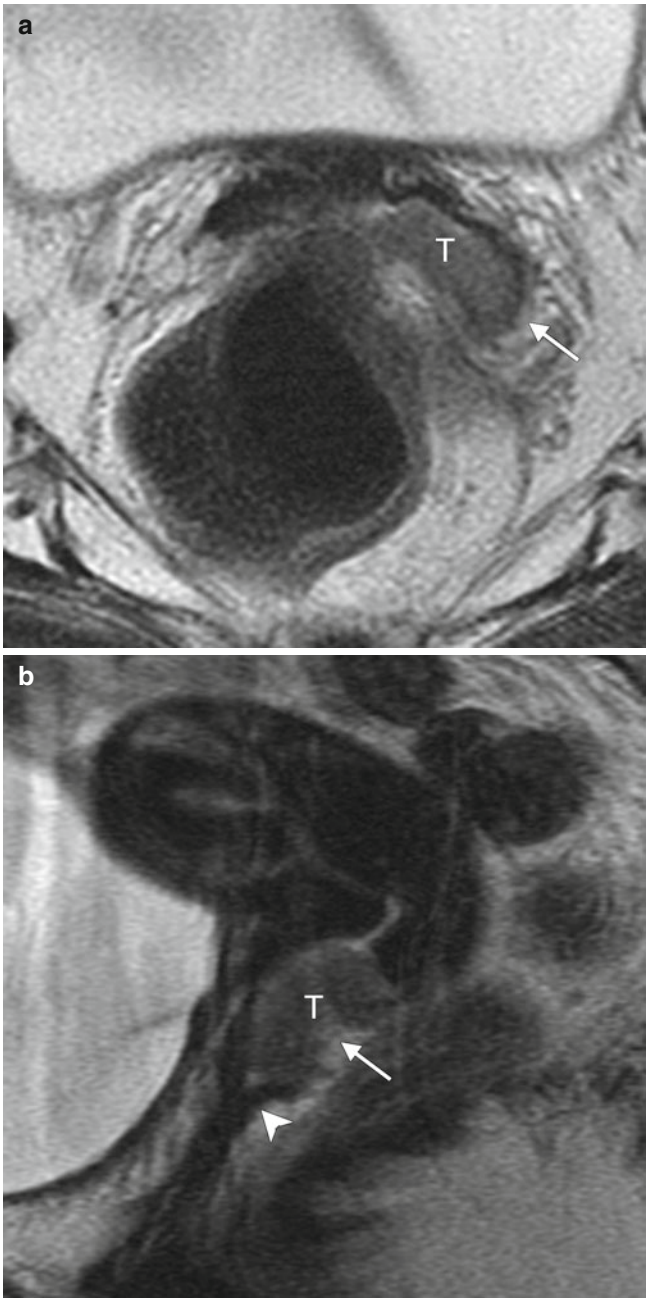

Fig. 3.14 Stage IIA cervical cancer in a different patient. Sagittal (**a**) and transverse (**b**) T2-WI demonstrate a cervical tumor (*T*) disrupting low SI vaginal wall (*arrowhead*) consistent with invasion of the upper third of the vagina (*arrow*), therefore not involving the lower third of the vagina

FIGO IIB cervical cancer is diagnosed if
- Full thickness stromal invasion **AND**
- Spiculated tumor–parametrium interface, soft-tissue extension into the parametria, or encasement of the periuterine vessels

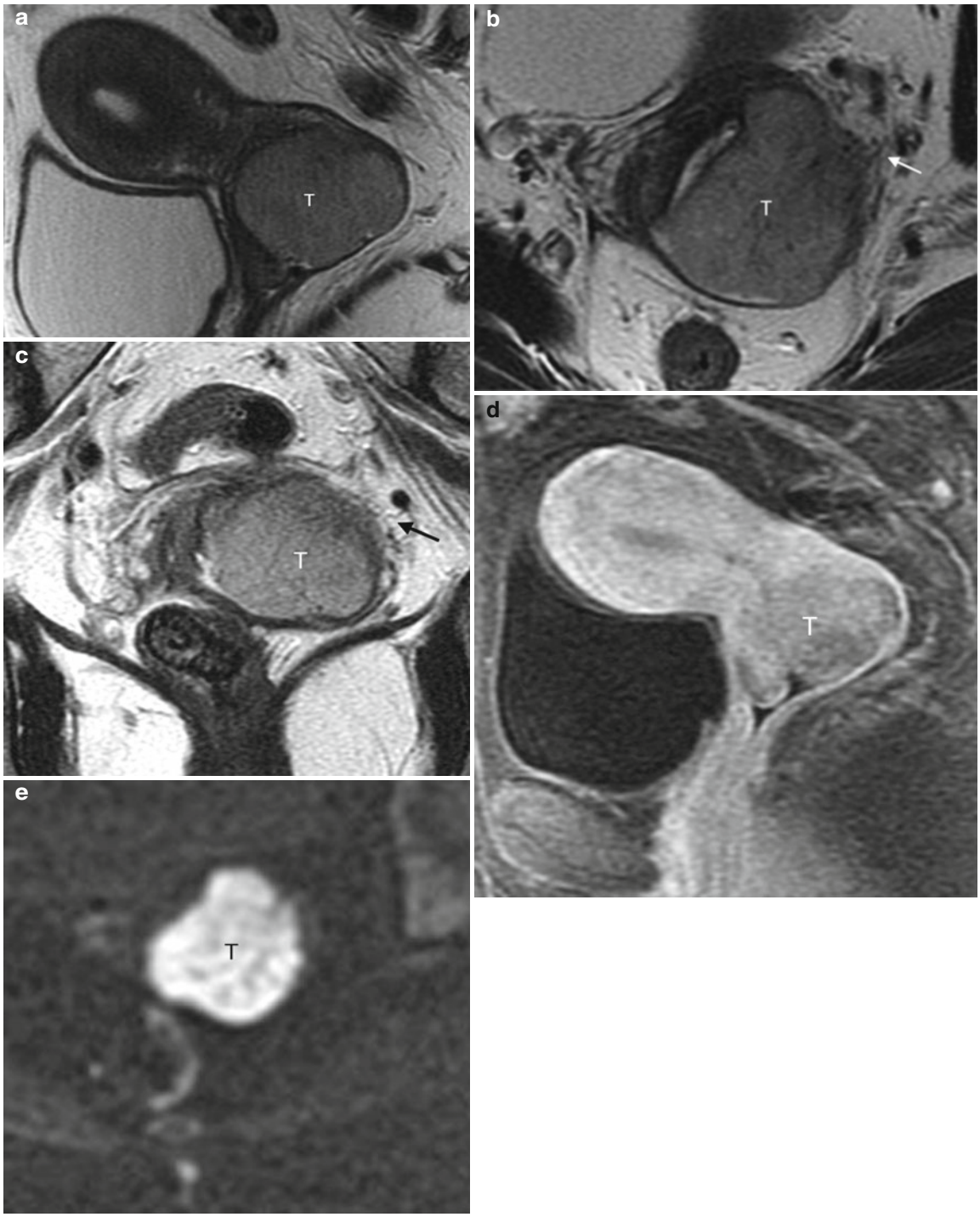

Fig. 3.15 Stage IIB cervical cancer. Sagittal (**a**), transverse oblique (**b**), and coronal oblique T2-WI (**c**) images show a bulky cervical tumor (*T*) disrupting the cervical stromal ring and demonstrating obvious parametrial invasion on the left side (*arrow*). The accuracy of MRI for indentifying parametrial invasion is influenced by the size of the primary tumor. T2-WI tend to overestimate parametrial invasion by large tumors (accuracy, 70 %) compared to smaller tumors (accuracy, 96 %) because large cervical cancers can cause stromal edema that can obscure tumor borders [19]. T1-WI C+ (**d**) or diffusion-weighted images (**e**) do not increase the accuracy for parametrial involvement

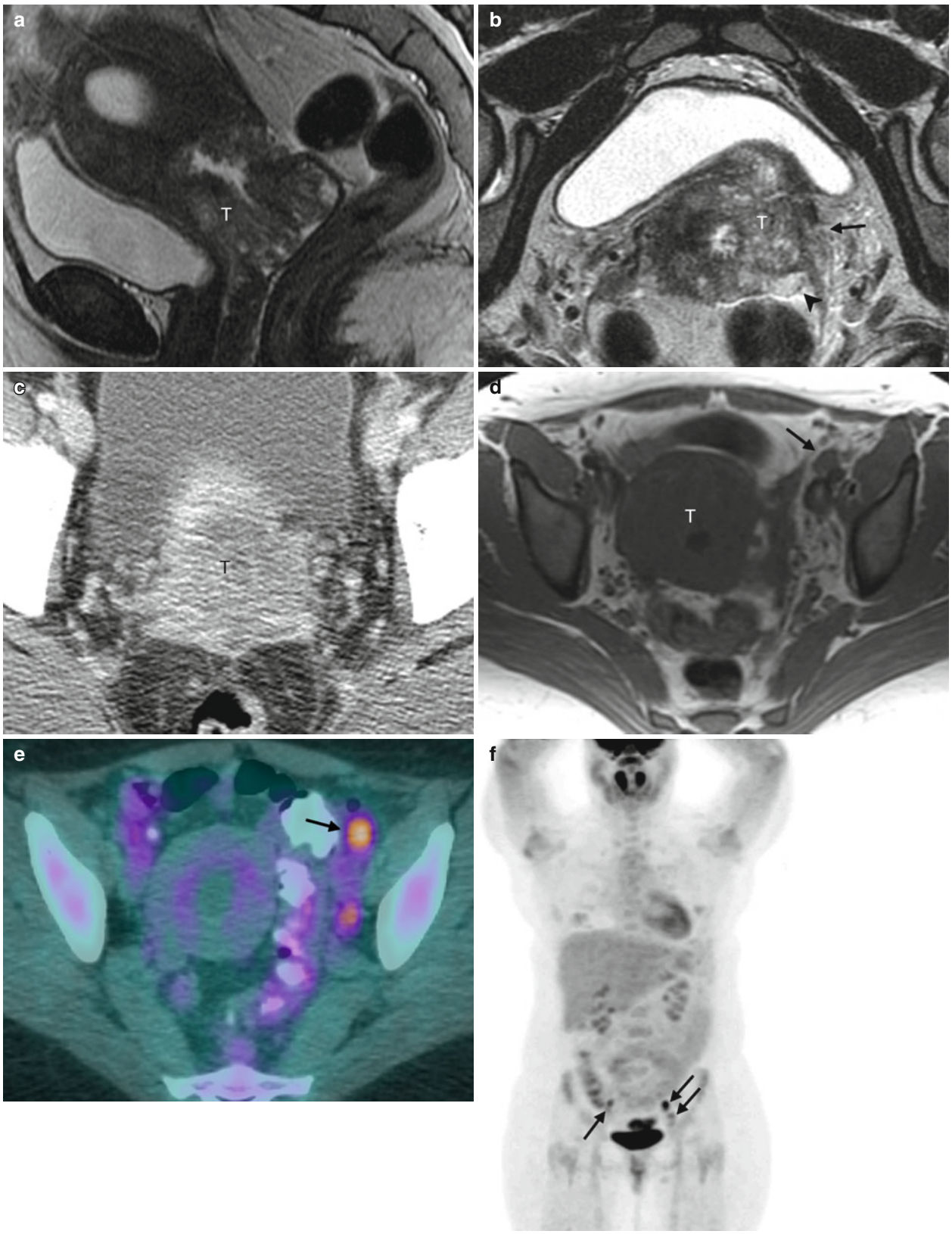

Fig. 3.16 Stage IIB cervical cancer in a different patient. Sagittal T2-WI (**a**) and transverse T2-WI (**b**) depict a large cervical mass (*T*) with full thickness cervical stromal invasion and obvious parametrial invasion on the left side (*arrow*), with infiltration of the mesorectal fascia and fat (*arrowhead*). No evidence for organ (bladder or rectal) infiltration. (**c**) The parametrial infiltration is also detectable on the contrast-enhanced CT scan, however local extend is better delineated on MRI. (**d**) T1-WI with a large field of view is helpful to detect lymphadenopathy. In this case, an enlarged external iliac lymph node is suspicious on MRI. (**e**) PET/CT confirmed increased FDG activity consistent with lymph node metastasis. (**f**) MIP FDG PET image with multiple pelvic lymph node metastases (*thin arrows*) and no evidence for distant metastasis

FIGO Stage III. The tumour extends to the pelvic wall and/or involves lower third of the vagina and/or causes hydronephrosis or non-functioning kidney

- Stage IIIA: tumor involves lower third of the vagina, with no extension to the pelvic wall
- Stage IIIB: extension to the pelvic wall and/or hydronephrosis or nonfunctioning kidney

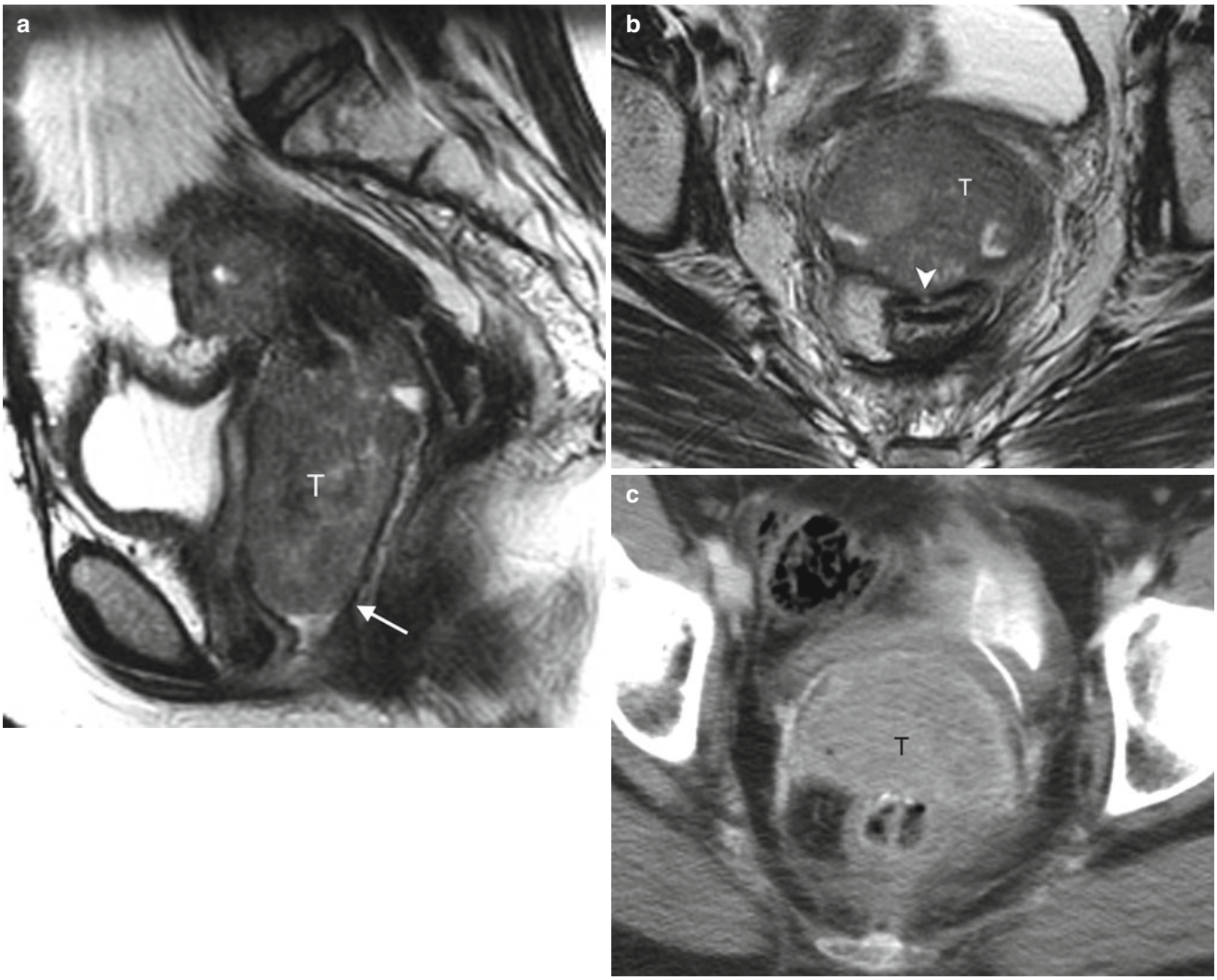

Fig. 3.17 Stage IIIA cervical cancer. Sagittal T2-WI (**a**) and transverse oblique T2-WI (**b**) demonstrate a bulky exophytic cervical tumor (*T*) distending and invading the lower vagina (*arrow*). Infiltration of the mesorectal fascia and rectal serosa without evidence of mucosal invasion (*arrowhead*). (**c**) Transverse contrast-enhanced CT well-depicting the tumor extension of the vagina, but less accurate in delineating depth of rectal invasion

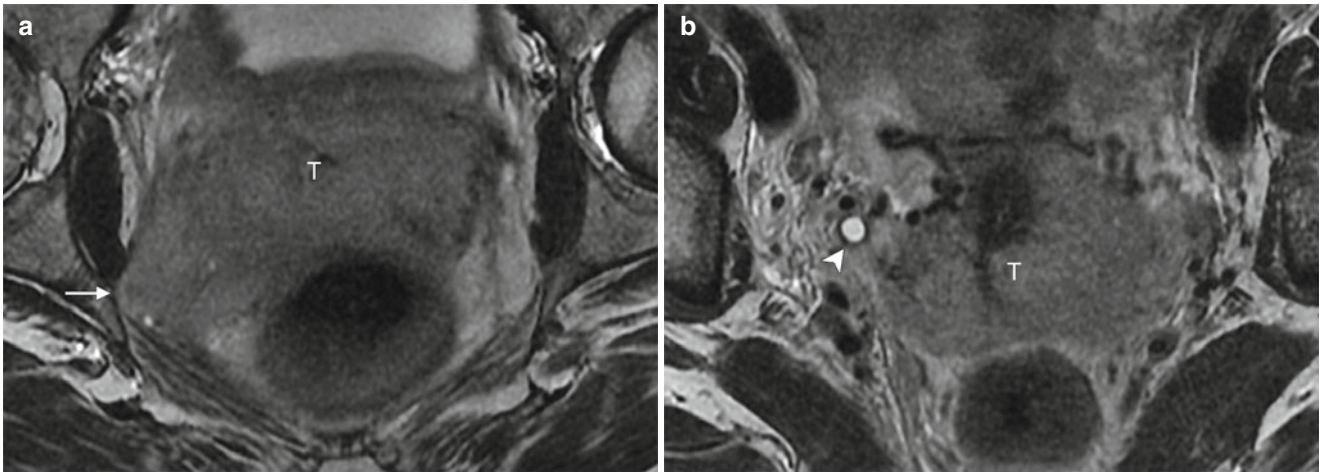

Fig. 3.18 Stage IIIB cervical carcinoma. Transverse (**a**) and coronal oblique T2-WI (**b**) show a large cervical mass (*T*) with bilateral gross parametrial invasion, right pelvic side-wall involvement (*arrow*), and right ureter invasion and dilatation (*arrowhead*)

Teaching points: pelvic wall involvement and hydronephrosis
- Pelvic side-wall invasion: tumor extends within 3 mm of pelvic side-wall
- Hydronephrosis: indication of ureteral invasion

FIGO Stage IV. The carcinoma has extended beyond the true pelvis or has involved (biopsy proven) the mucosa of the bladder or rectum.
- Stage IVA: spread of the growth to adjacent organs
- Stage IVB: spread to distant organs

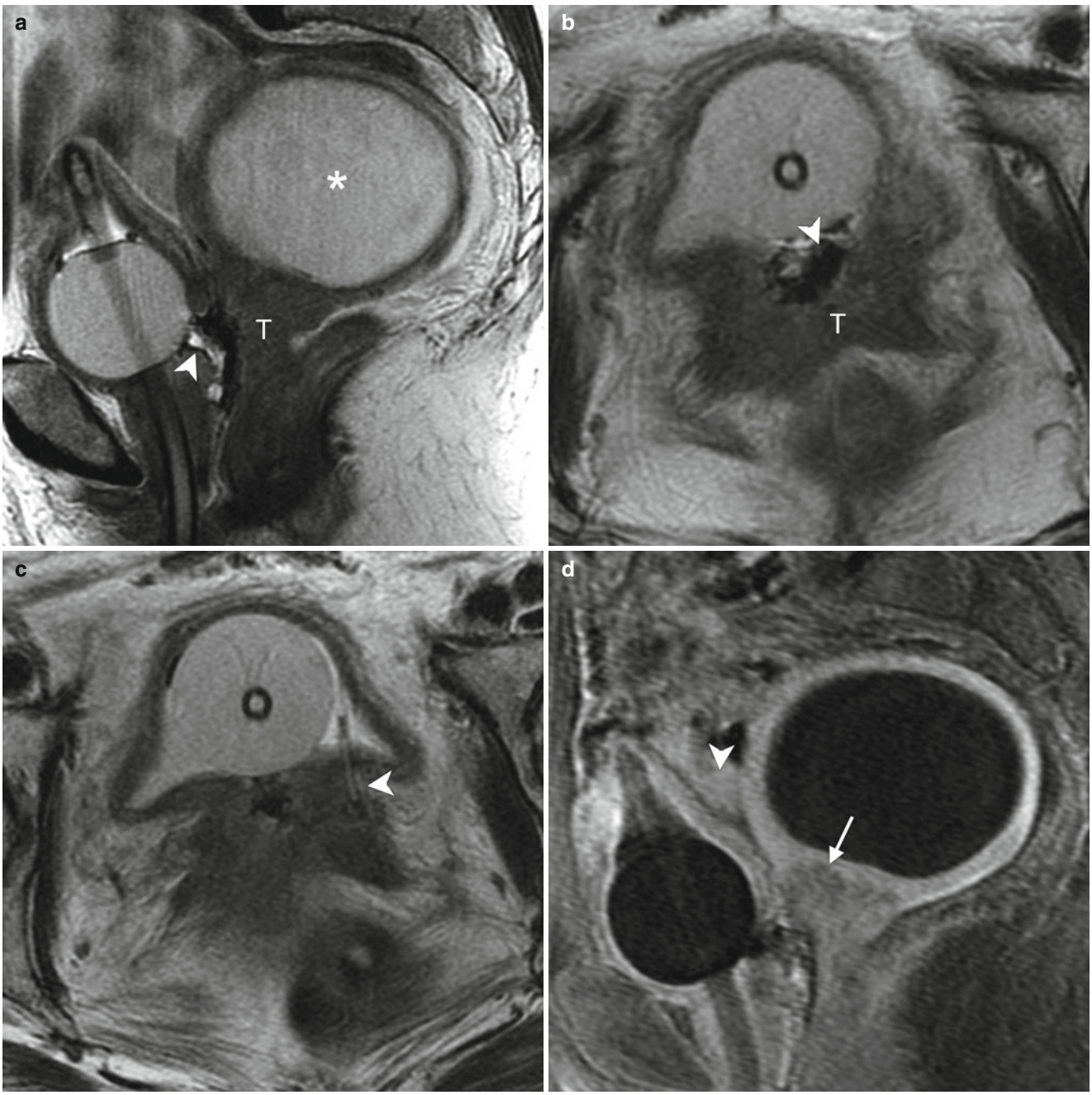

Fig. 3.19 Stage IVA cervical cancer. Sagittal (**a**) and transverse T2-WI (**b**) illustrating a cervical tumor (*T*) invading the upper and middle vagina and posterior wall of the urinary bladder with secondary vesico-vaginal fistula (*arrowhead*). The tumor also causes cervical stenosis and hematometra (*asterisk*). (**c**) Transverse T2-WI showing tumor invasion of both uretero-vesicular junctions, with urethral stent on the left side (*arrowhead*). (**d**) T1-WI C+ showing a hypointense tumor (*arrow*) compared to hypervascular uterine stroma or bladder wall. Diffuse increased contrast enhancement is also seen in adjacent fat tissue due to inflammatory changes (*arrowhead*)

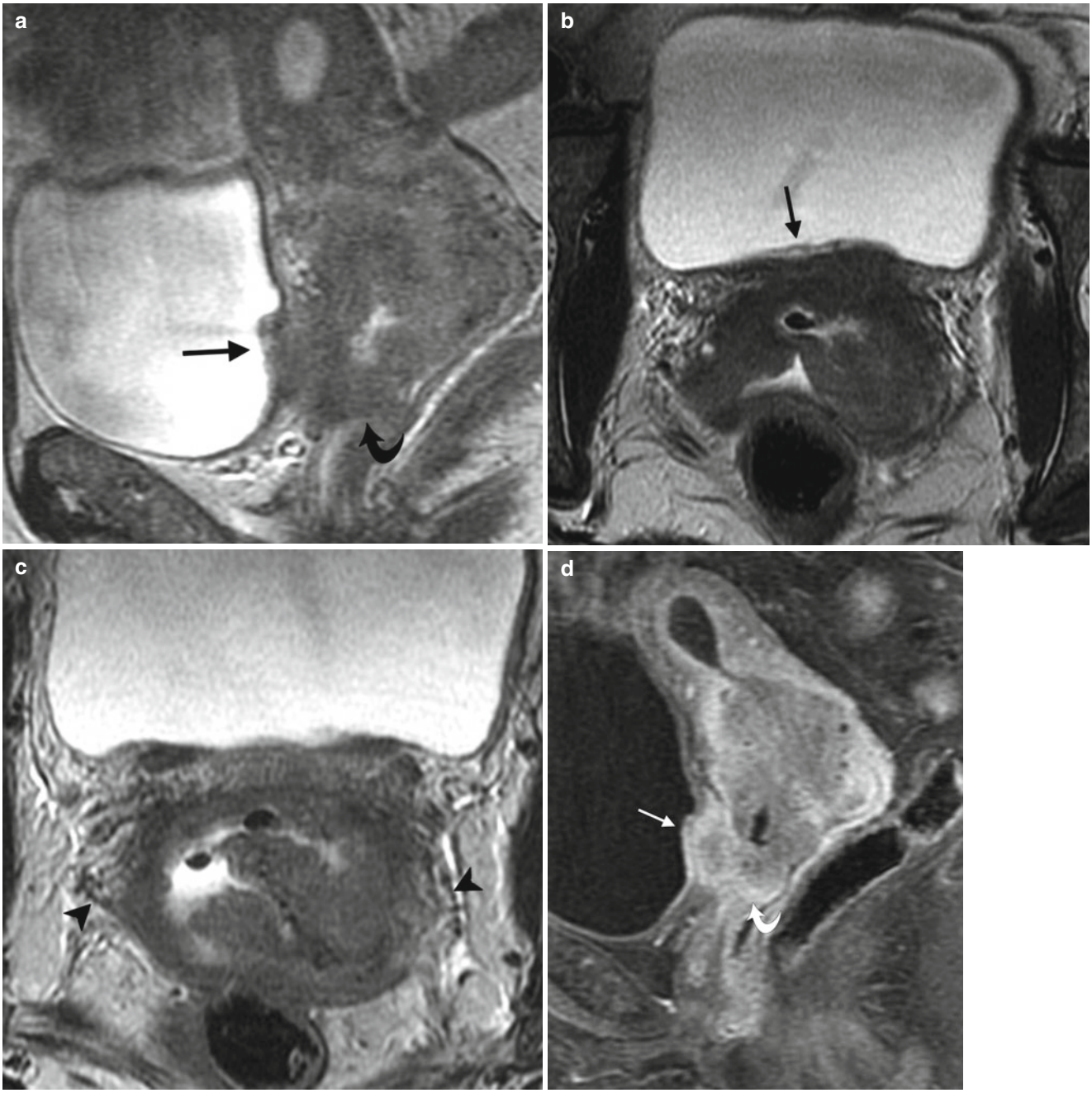

Fig. 3.20 Stage IVA cervical cancer. Sagittal (**a**) and transverse T2-WI (**b**) with a large, centrally necrotic cervical tumor invading the posterior wall of the urinary bladder (*arrow*), causing a bullous edema in the bladder wall. (**c**) Transverse T2-WI with obvious gross parametrial invasion on both sides (*arrowhead*). (**d**) T1-WI C+ the invasion of the posterior bladder wall causes increased contrast enhancement in the bladder wall adjacent to the cervical tumor (*arrow*). The tumor also invades the upper vagina (*curved arrow*)

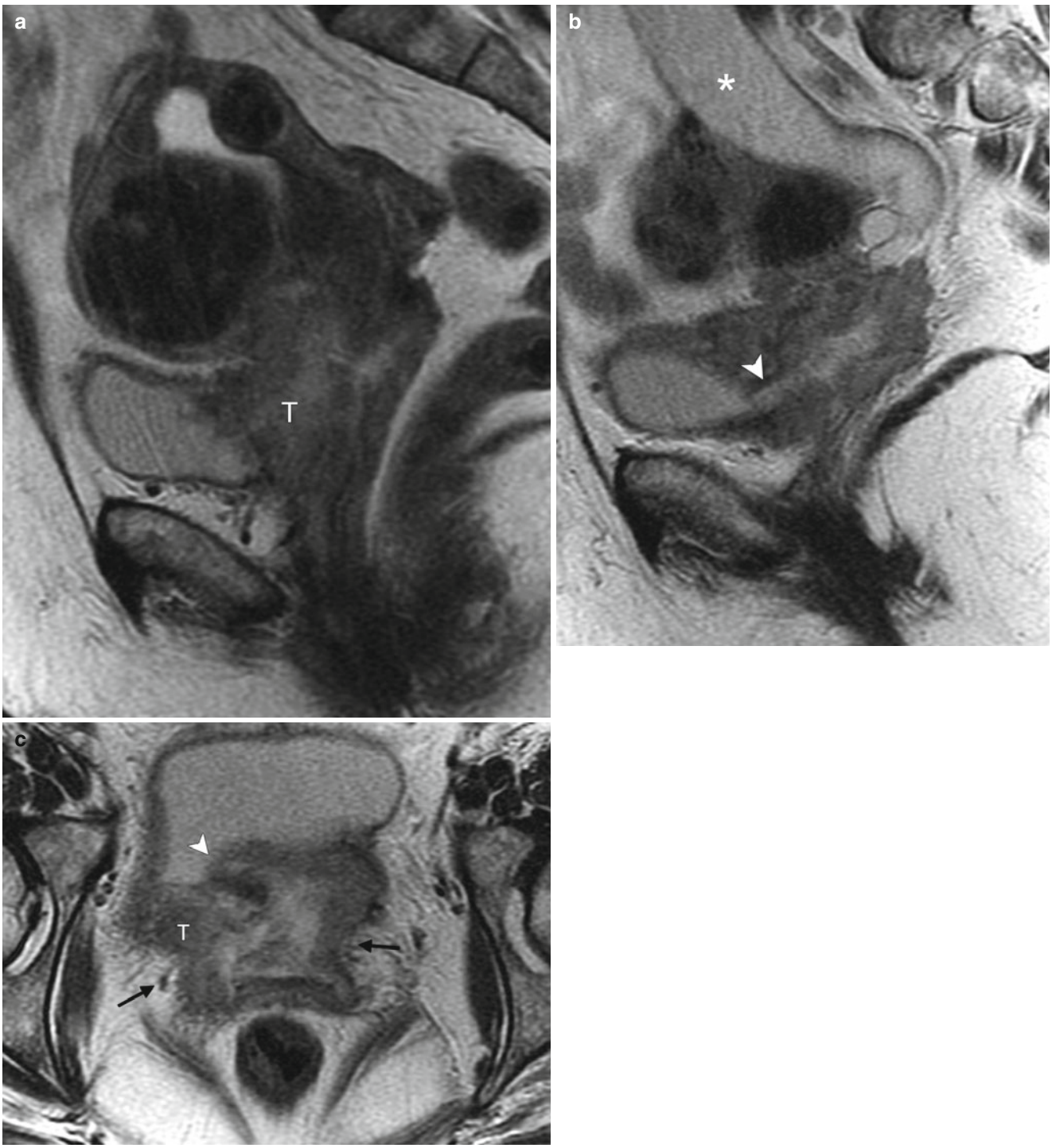

Fig. 3.21 Stage IVA cervical cancer in a different patient. (**a**, **b**) Two sagittal T2-WI with a centrally necrotic cervical mass (*T*) with gross urinary bladder wall invasion, causing a large vesicovaginal fistula (*arrowhead*). The tumor also obstructs the right ureter causing severe hydroureter (*asterisk*). (**c**) On transverse T2-WI, the tumor is very heterogeneous with parametrial invasion (*arrow*). (**d**) T1-WI C+ with heterogeneous enhancement of the uterus with multiple fibroids and a large vesicovaginal fistula (*arrowhead*). (**e**) Transverse T2-WI with a mildly enlarged external iliac lymph node on the left side, suspicious for metastasis (*thin arrow*) and a right hydroureter (*asterisk*). (**f**) Fused transverse FDG PET/CT image with increased FDG activity in the external iliac lymph nodes on both sides, consistent with lymph node metastasis

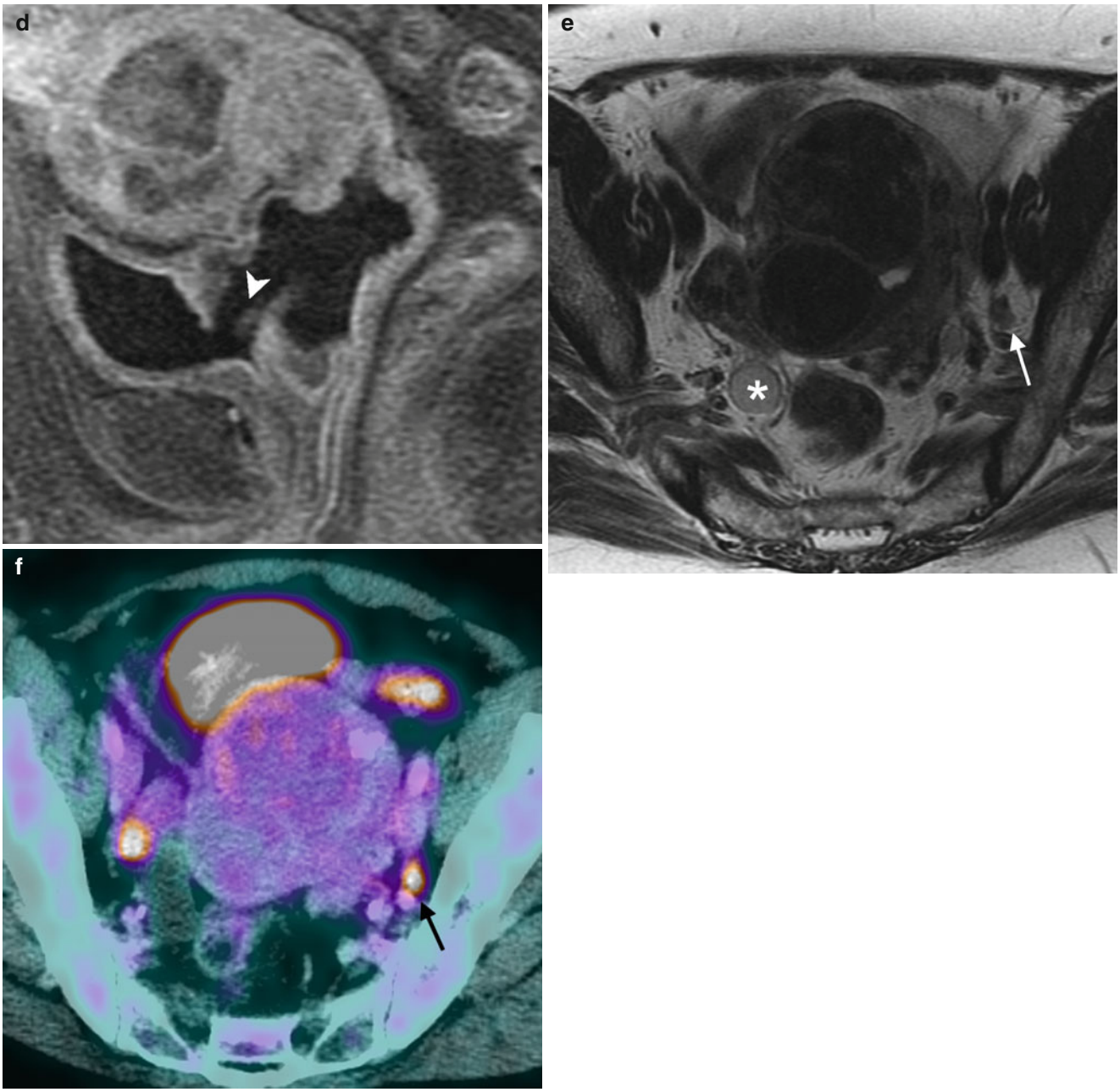

Fig. 3.21 (continued)

FIGO Stage IVB.

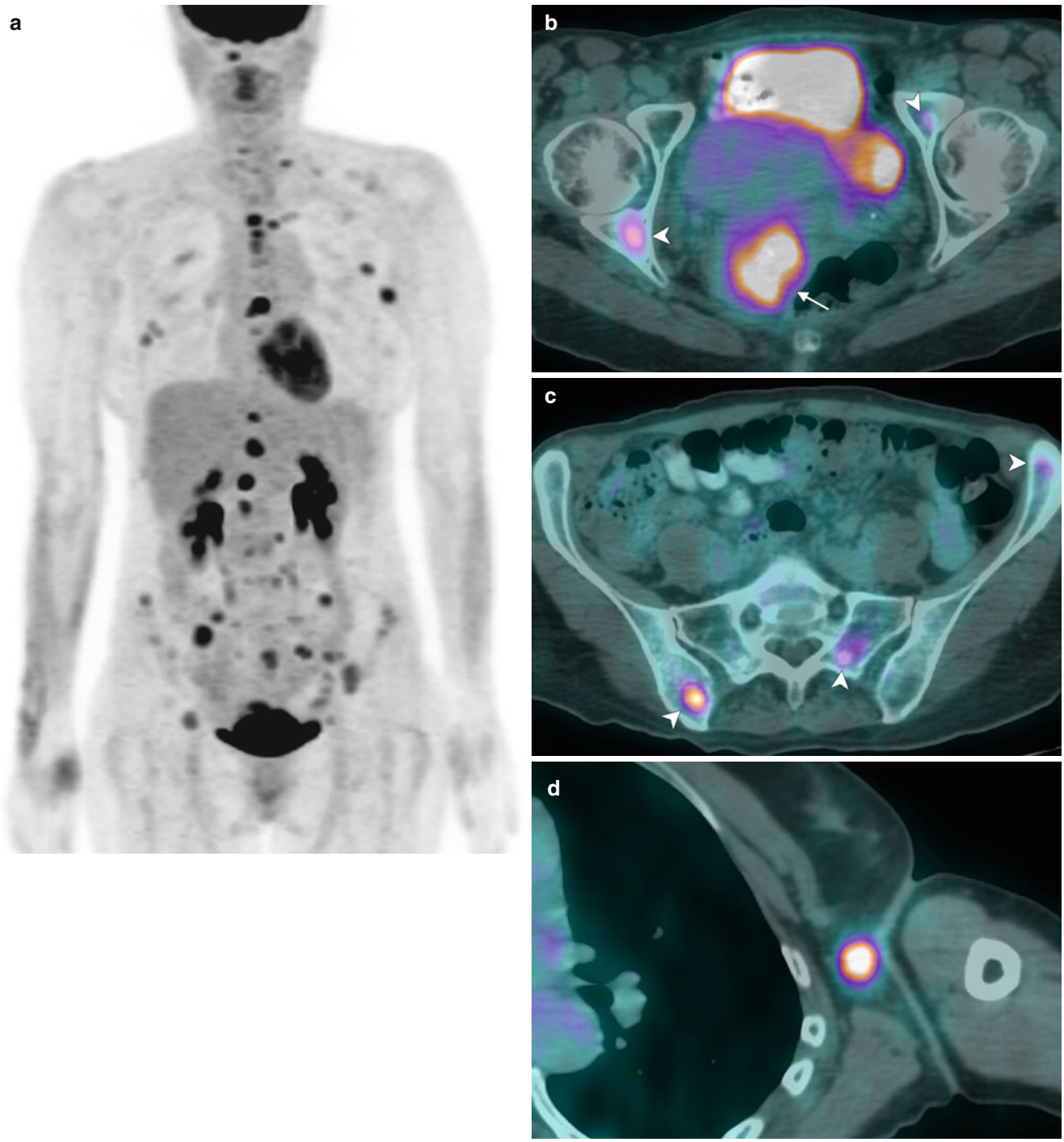

Fig. 3.22 Stage IVB cervical adenocarcinoma with neuroendocrine differentiation. (**a**) MIP FDG PET image showing extent of disease with multiple osseous metastases in the pelvis, vertebral column, rips and sternum as well as axillary lymph nodes. (**b**) Transverse fused FDG PET/CT images at the level of the cervix showing a highly avid primary (SUV 8, *arrow*) and two osseous metastasis (*arrowheads*). (**c**) Transverse fused FDG PET/CT images with multiple osseous metastases in the pelvis (*arrowheads*) with increased osseous sclerosis. (**d**) Pathological uptake in an axillary lymph node level III left side, consistent with lymph node metastasis

Imaging Evaluation Prior to Fertility-sparing Radical Trachelectomy [20]

Teaching points:

- Radical trachelectomy is a surgical procedure that includes removal of the cervix with parametrial tissue and pelvic lymphadenectomy
- Candidates: Women of child-bearing age with early stage cervical cancer (FIGO stage IA1 with lymphovascular invasion, IA2 and IB1) who desire to preserve their fertility
  - Tumor size ≤2 cm for most centers; some ≤2.0 cm for vaginal trachelectomy and <4 cm for abdominal trachelectomy
  - Distance between the tumor and internal cervical os at least 1 cm for most centers
  - Infiltration of less than one-half thickness of the cervical stroma

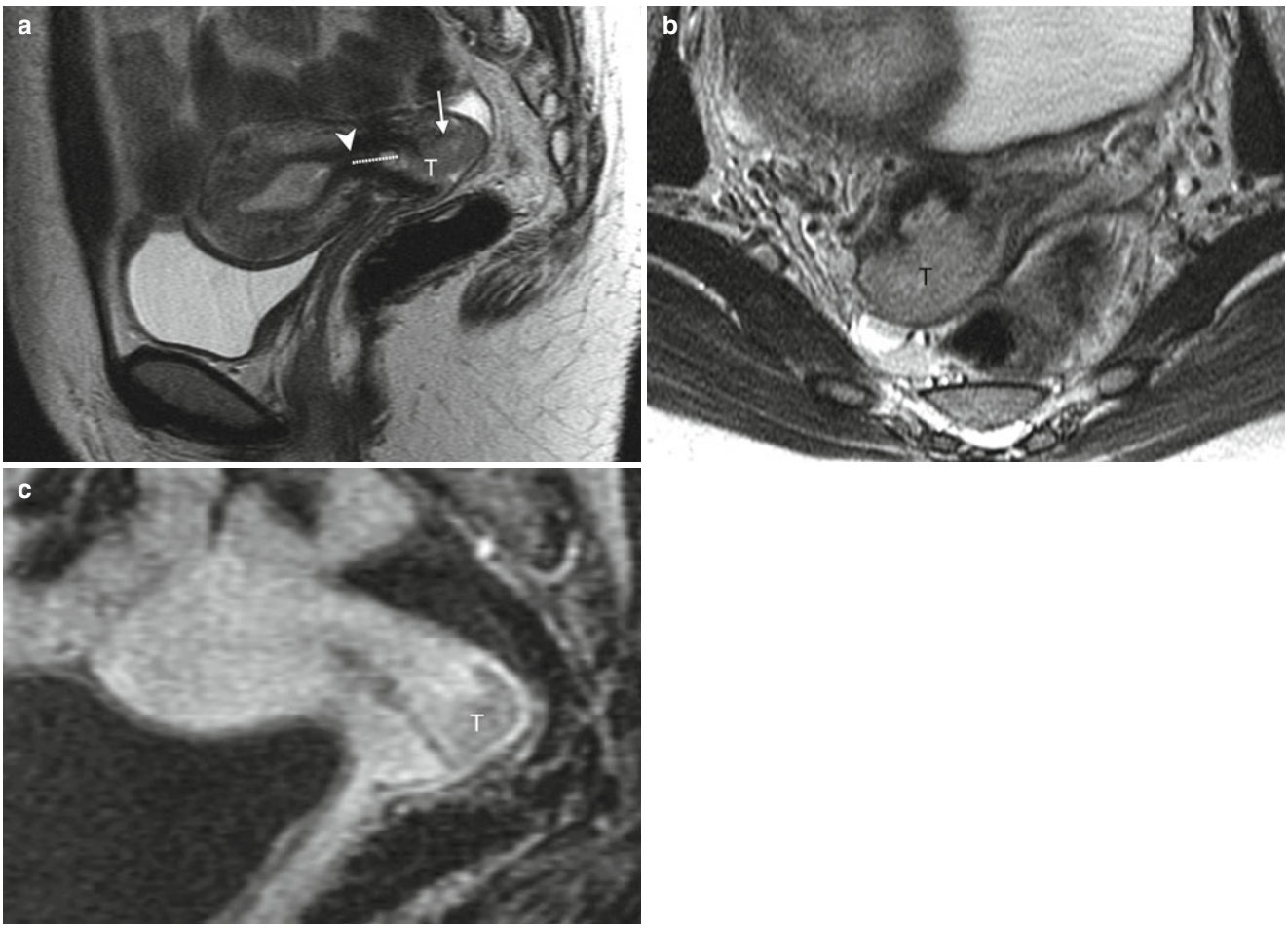

Fig. 3.23 Stage IB1 cervical cancer in a young patient who wants to preserve her fertility. Sagittal (**a**) and transverse oblique T2-WI (**b**) images show less than 2 cm exophytic cervical tumor (*T*) located 1.1 cm (*dashed line*) caudal to the internal cervical os (*arrowhead*) and infiltrating less than half of the cervical stroma (*arrow*). (**c**) T1-WI C+ with hypointense tumor (*T*) compared to cervical and uterine stroma

Postoperative/Post-treatment Findings and Tumor Recurrence

- Evaluate treatment response and treatment-related complications
- Examine the extent of local tumor recurrence and lymph node status
  - Recurrence is defined as local tumor re-growth or development of distance metastasis at least 6 months after successful prior treatment.
  - Recurrent tumor presents as a soft tissue mass with variable amount of central necrosis
  - Most common site of recurrence
- Local
  - Vaginal cuff
  - Cervix
  - Parametria
  - Pelvic side wall
  - Pelvic lymph nodes
- Distant
  - Extrapelvic lymph nodes
  - Peritoneum, lung, liver, and bone

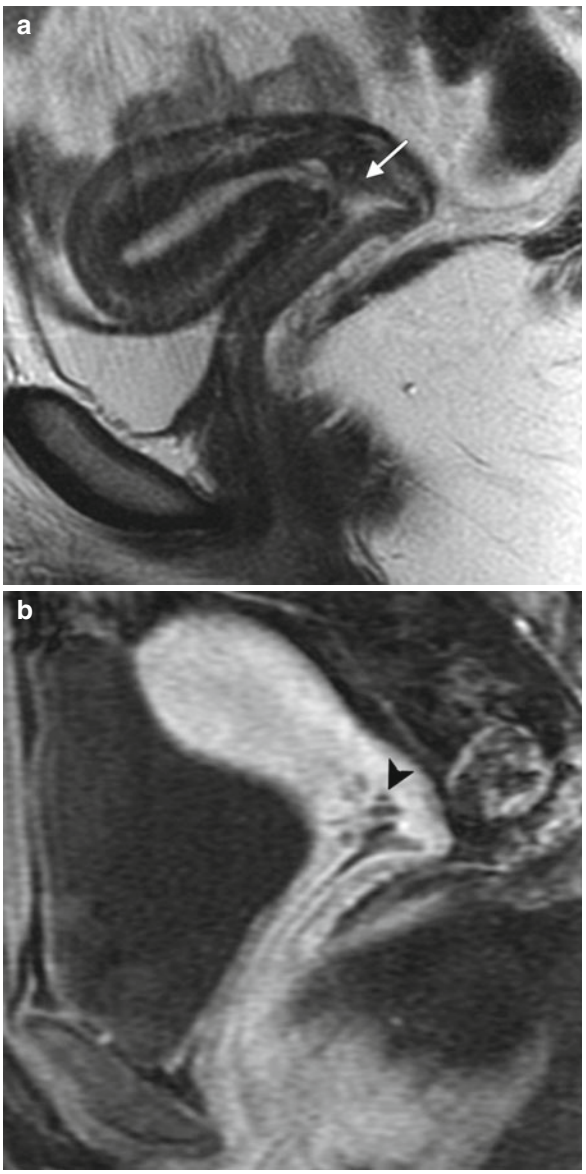

Fig. 3.24 Post-conization appearance of the cervix. Sagittal T2-WI (**a**) and sagittal T1 C+ (**b**) in the same patient depict cone-shaped defect (*arrow*) and metal susceptibility artifact (*arrowhead*) in the inferior aspect of the cervix consistent with prior procedure. No residual or recurrent tumor is seen

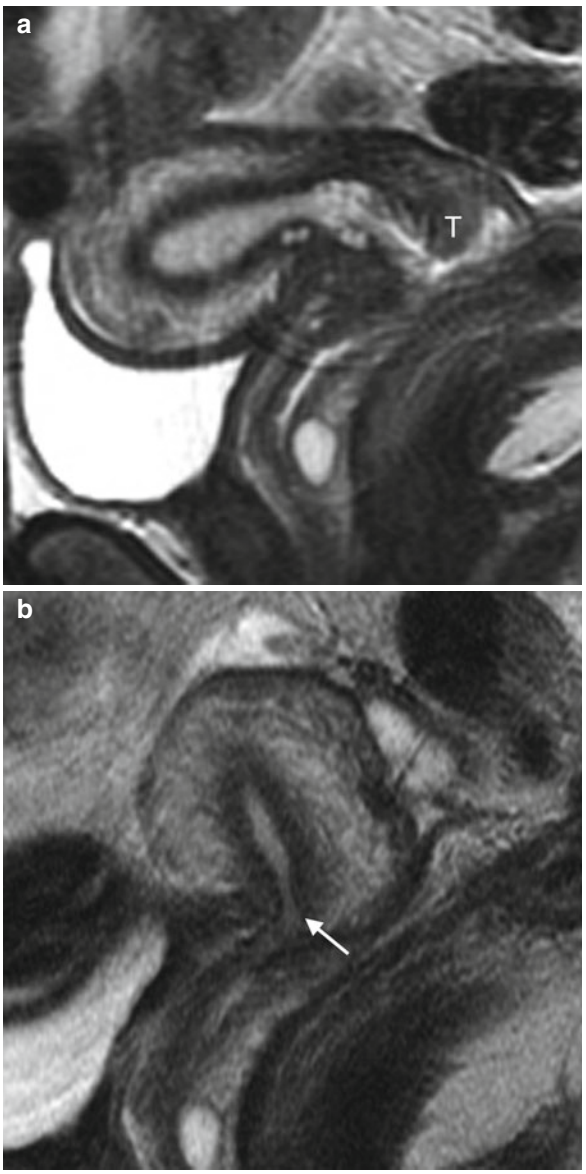

Fig. 3.25 Post-trachelectomy appearance. (**a**) Sagittal T2-WI demonstrates stage IB1 cervical cancer (*T*). (**b**) Sagittal T2-WI shows post-trachelectomy appearance with end-to-end anastomosis between the uterine remnant and the vagina (*arrow*)

Teaching points: postoperative complications after radical trachelectomy

- Isthmic stenosis (2 %)
- Vaginal wall hematoma (5 %)
- Lymphoceles (25 %)

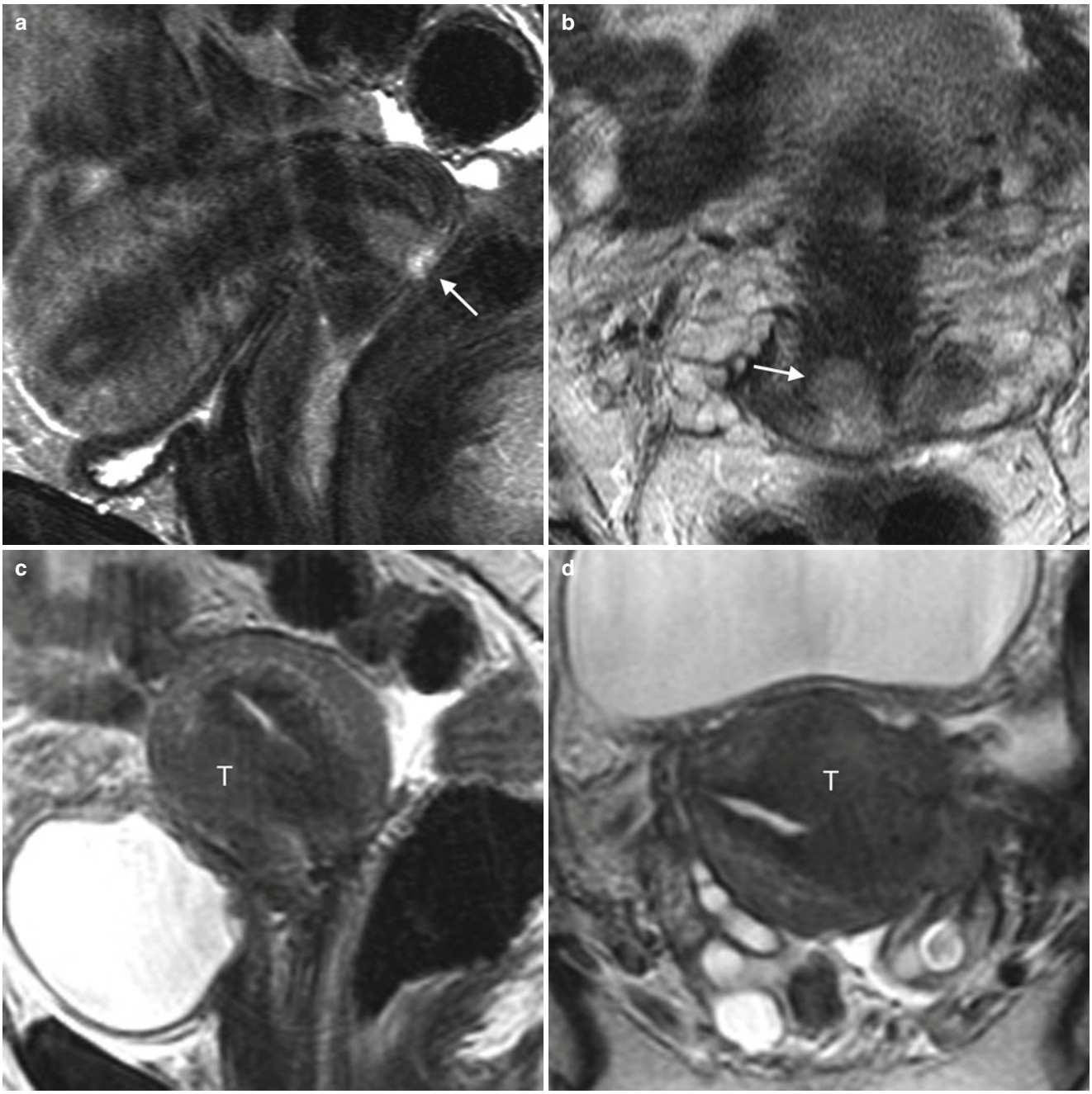

Fig. 3.26 Local recurrence after radical trachelectomy. Preoperative sagittal (**a**) and transverse T2-WI (**b**) images with a small intermediate T2 SI cervical cancer (*arrow*). (**c**–**e**) Postoperative images 2 years after total radical trachelectomy. Sagittal (**c**) and transverse (**d**) T2-WI, as well as sagittal (**e**) and transverse T1 C+ (**f**) images with a large intermediate T2 SI recurrent tumor (*T*) arising from the surgical anastomosis and extending superiorly into the uterine remnant. The recurrent tumor has a similar SI to the original tumor and enhances after intravenous contrast administration. Risk factors for tumor recurrence after radical trachelectomy include large original tumor size, deep cervical stromal invasion, lymphovascular invasion, and unfavorable histology

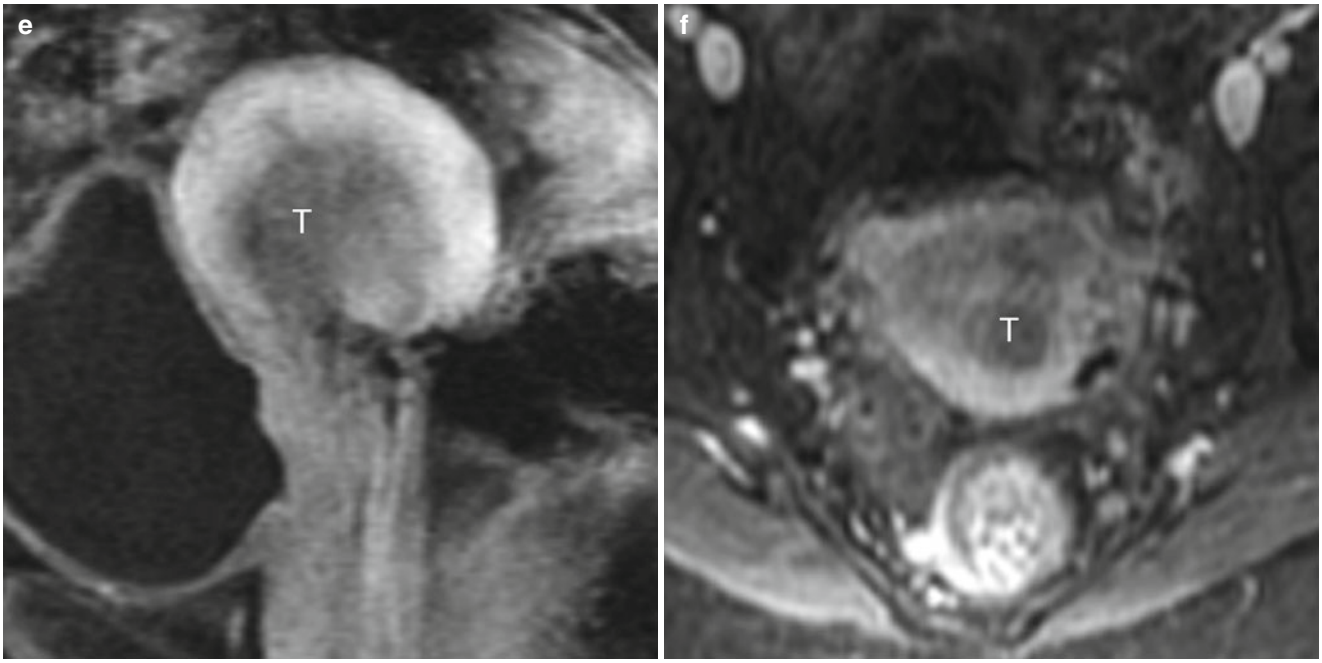

Fig. 3.26 (continued)

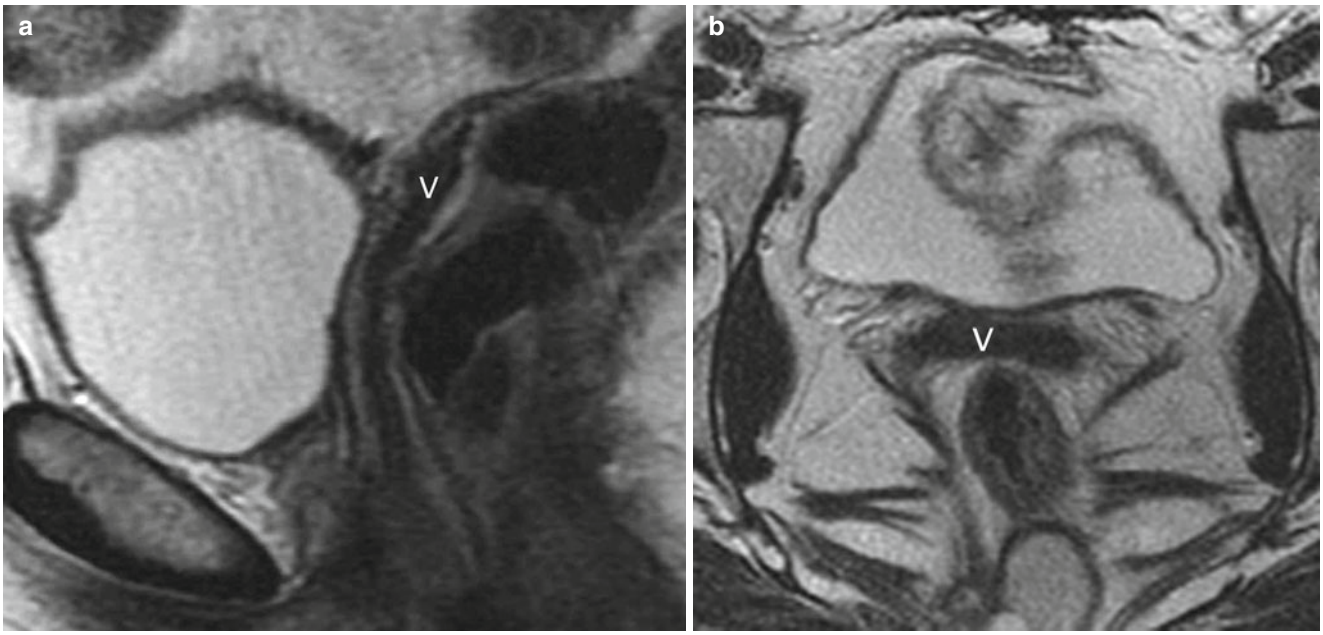

Fig. 3.27 Post-hysterectomy appearance. Sagittal (**a**) and transverse T2-WI (**b**) depict normal vagina (*v*) including vaginal cuff after simple hysterectomy without evidence of recurrence. Sagittal (**c**) and transverse T2-WI (**d**) in another patient after radical hysterectomy with resection of the upper two-thirds of the vagina with fat tissue in the rectovesical space (*asterisk*). Sagittal (**e**) and transverse T2-WI (**f**) images in a patient after simple hysterectomy with an intravaginal pessary in situ (*arrows*)

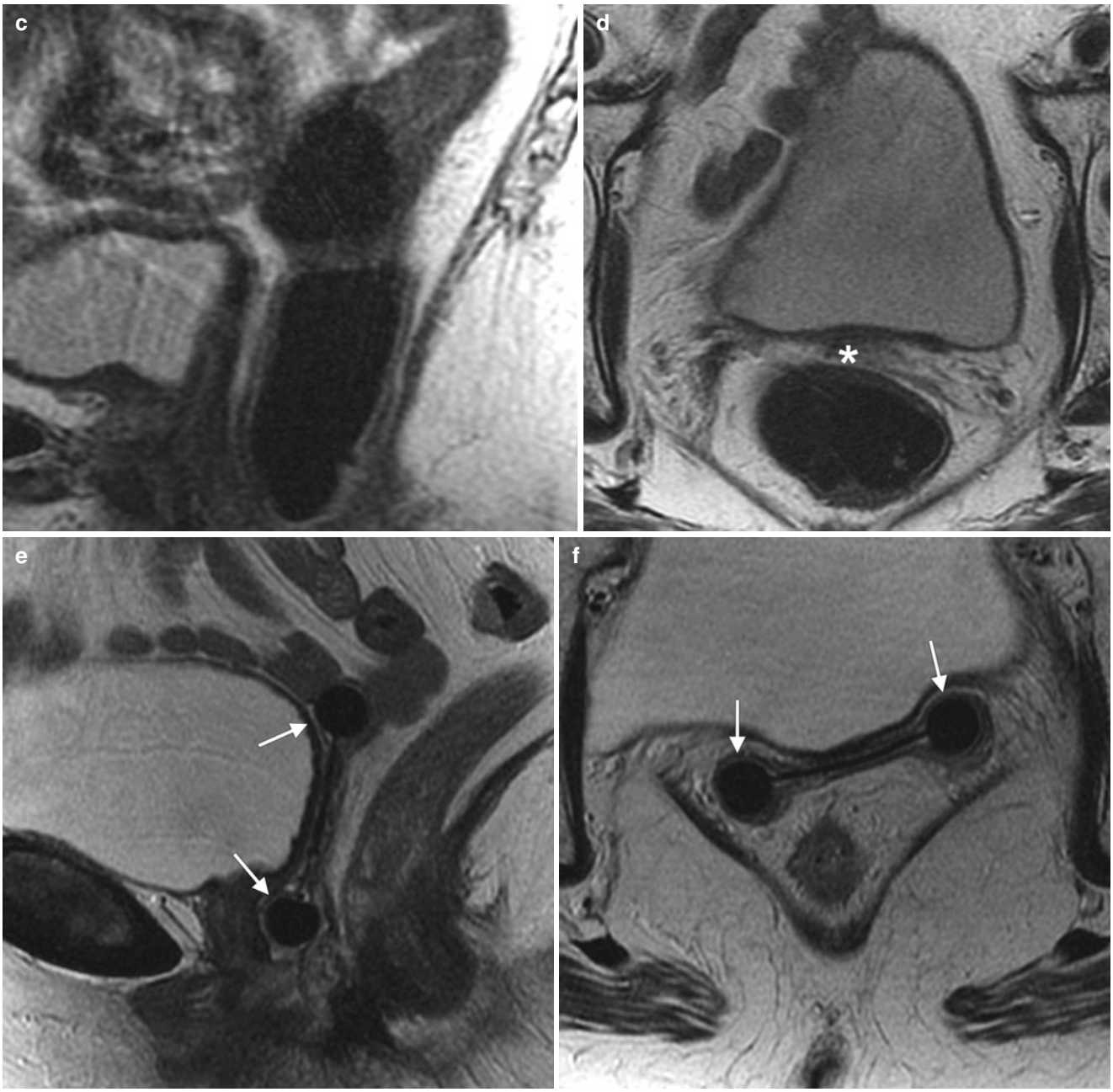

Fig. 3.27 (continued)

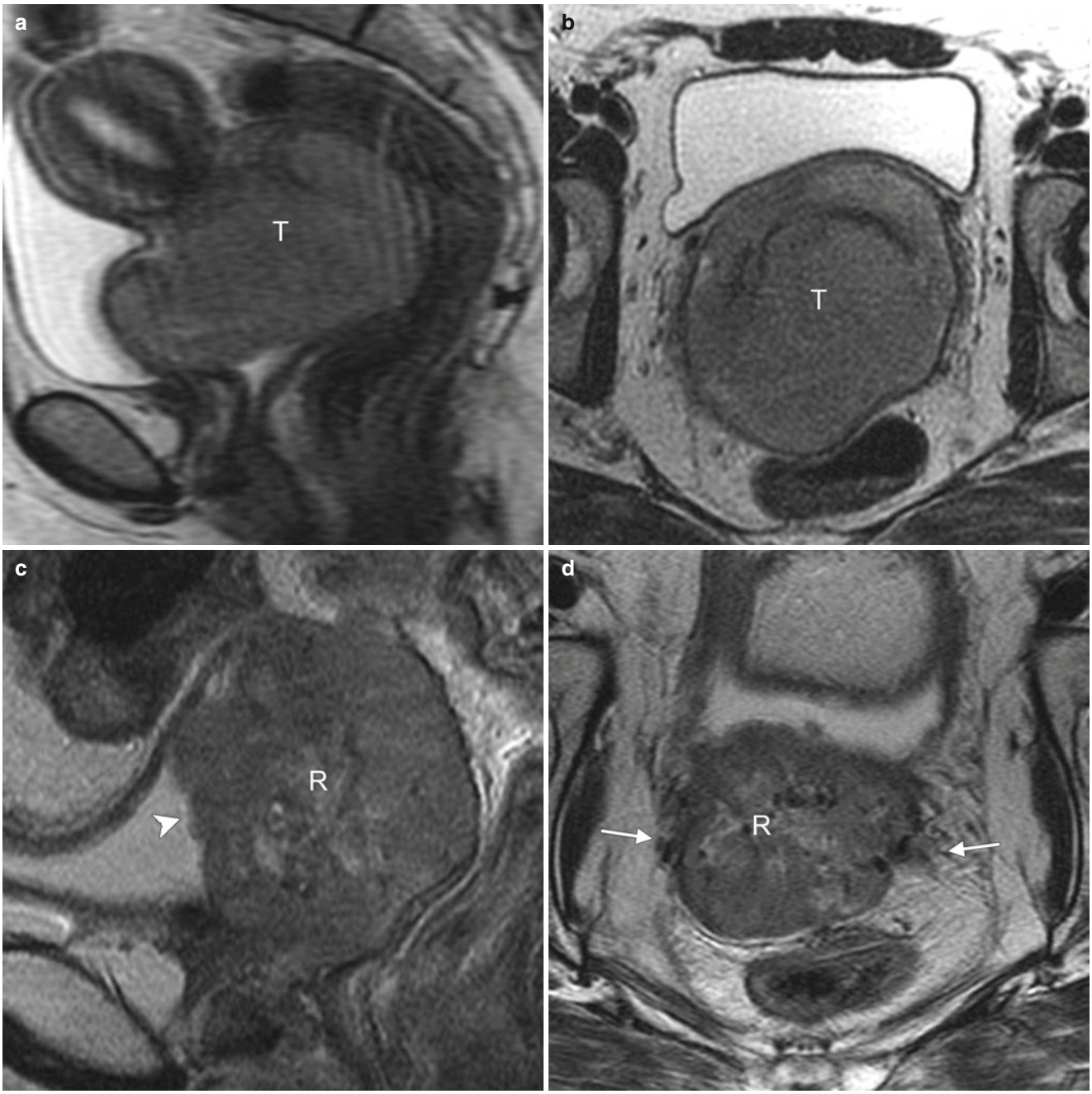

Fig. 3.28 Vaginal recurrence after hysterectomy. Vaginal cuff is the most common site of local recurrence after hysterectomy. Recurrent cervical cancer may present as either a well-defined or an ill-defined infiltrative mass. (**a**, **b**) Preoperative images of a cervical cancer FIGO stage IIA2. (**a**) Sagittal T2-WI with a large cervical tumor (*T*) distending the anterior and posterior vagina but on transverse T2-WI (**b**) without parametrial infiltration. (**c**, **d**) Follow-up images 2 years after radical hysterectomy and pelvic lymphadenectomy. (**c**) Sagittal T2-WI with a bulky heterogenous intermediate to high SI recurrent tumor (*R*) in the vagina, grossly invading the urinary bladder (*arrowhead*). (**d**) Transverse T2-WI with gross invasion of the parametria on both sides (*arrows*)

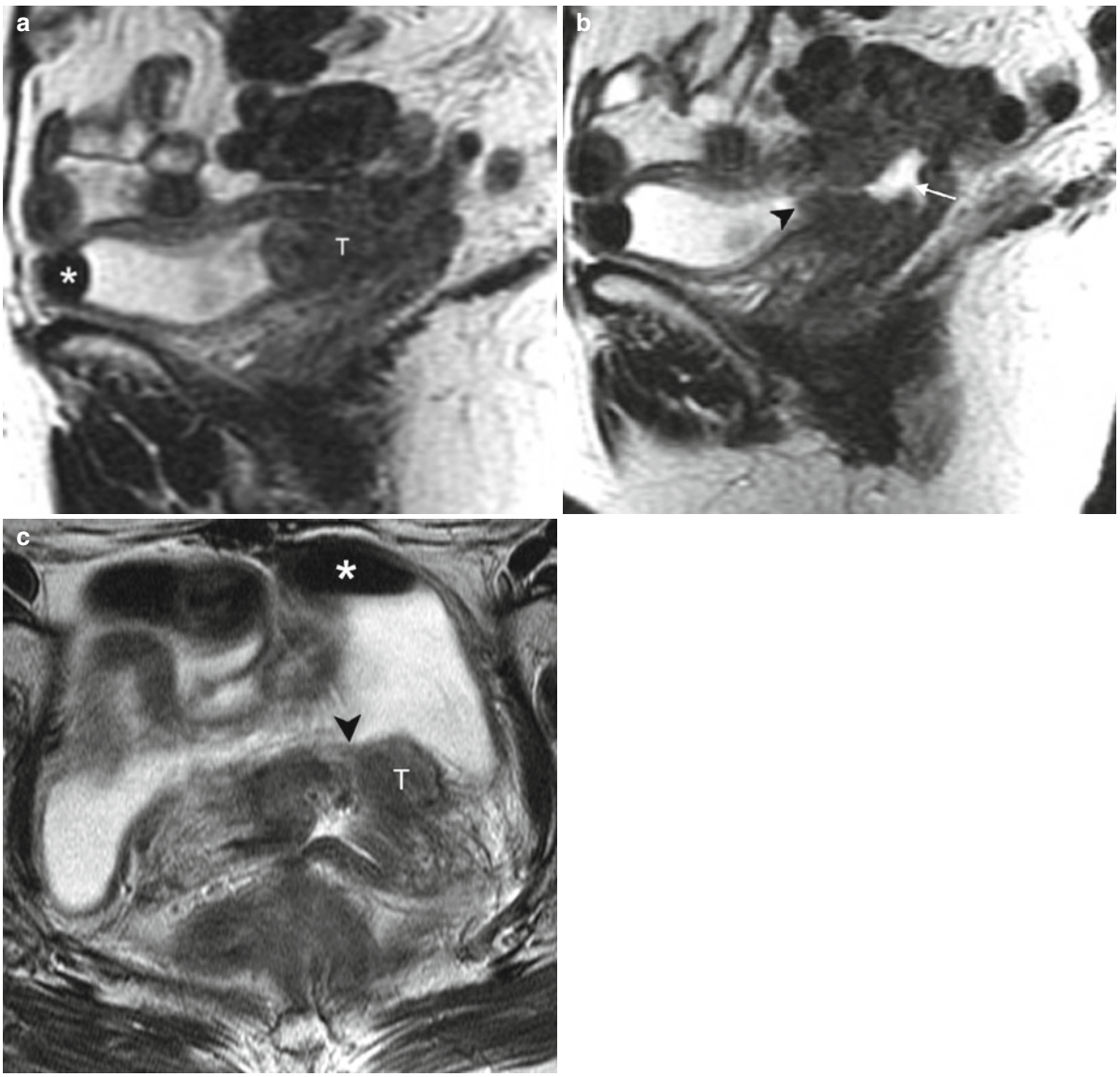

Fig. 3.29 Local recurrence after hysterectomy. Sagittal (**a**, **b**) and transverse T2-WI (**c**) show recurrent cervical cancer as an infiltrative intermediate T2 SI mass (*T*) invading the rectum (*arrow*) and the urinary bladder wall, causing a vesicovaginal fistula (*arrowhead*). Note air in the urinary bladder (*asterisk*)

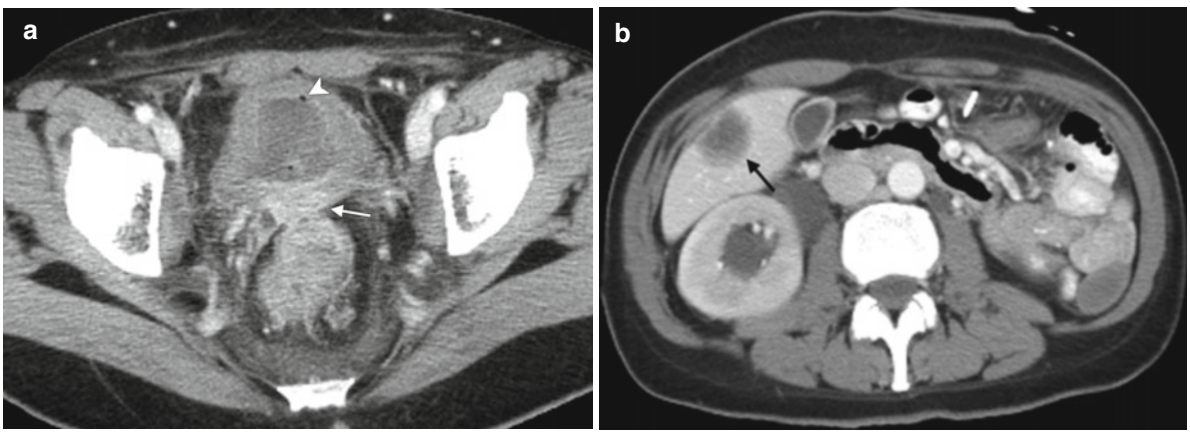

Fig. 3.30 Recurrent cervical cancer with liver metastasis. (**a**) Transverse CT scan with IV contrast with hyper-enhancing mass at the vaginal cuff (*arrow*), infiltrating the posterior bladder wall and leading to a vesicovaginal fistula, with air in the bladder and bladder wall thickening (*arrowhead*). (**b**) Transverse CT scan over the liver, with a heterogeneous liver metastasis in segment V/VI (*arrow*), with reduced perfusion compared to the normal liver parenchyma

Post-radiation Changes and Tumor Recurrence [21]

- Follow-up MRI helps to guide treatment decisions
  - Response to radiation therapy is evidenced by decrease in the size of the tumor as early as 2 months after treatment and is a predictor of good response
    - Imaging obtained too soon after radiotherapy can be misleading
    - Postradiation inflammation and radiation necrosis could mimic tumor
  - Following radiotherapy, tumor becomes more fibrotic and contracted, resulting in decreased SI on T2-WI
    - **Reconstitution of the normal low SI cervical stroma is the most reliable indicator of tumor-free postradiation cervix**
  - Recurrent tumor presents as soft tissue mass with higher T2 SI than the muscles in the adjacent pelvic sidewall

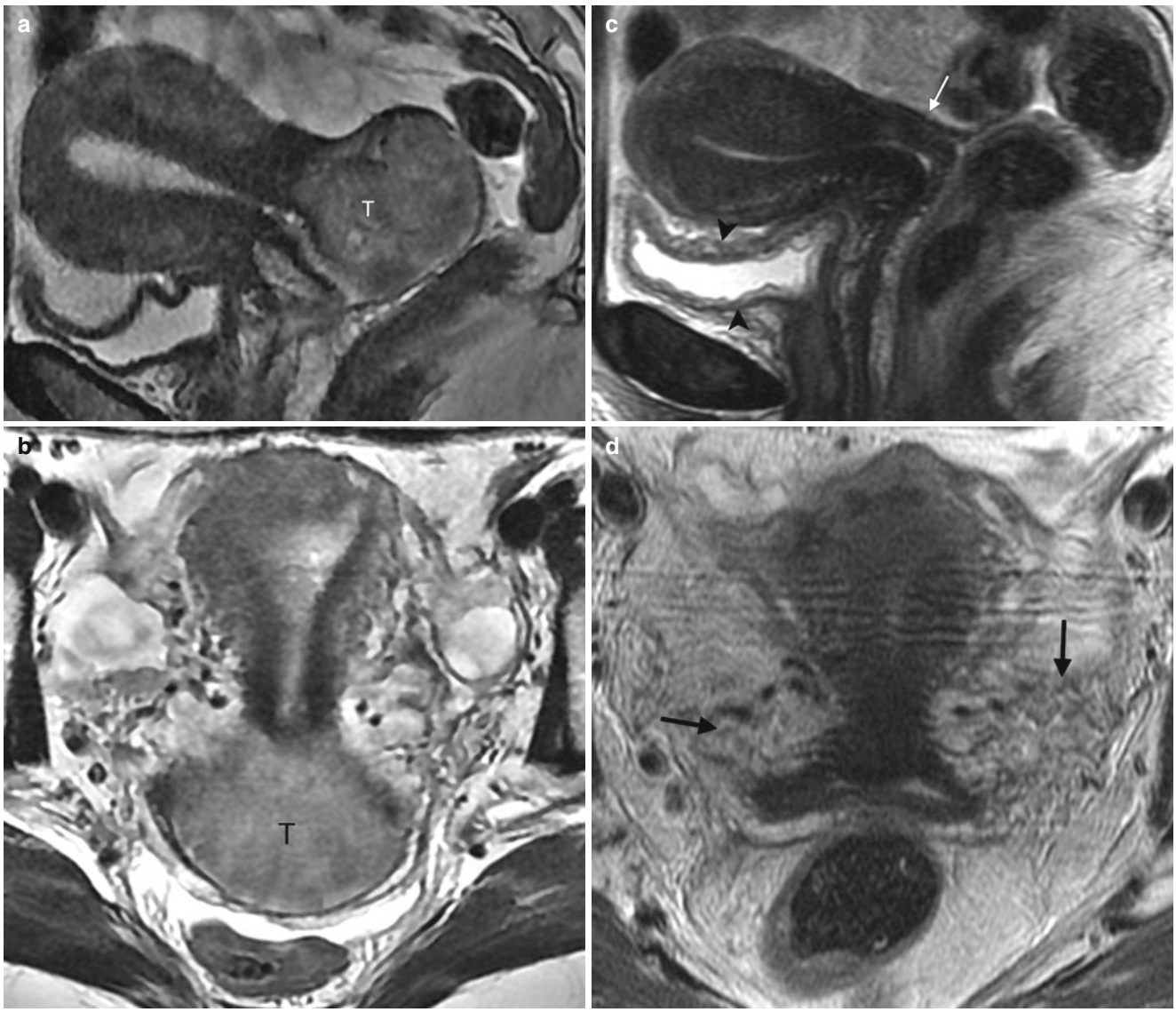

Fig. 3.31 Normal post-radiation cervix. Sagittal (**a**) and transverse T2-WI (**b**) of an untreated large stage IIB cervical cancer (*T*). Sagittal (**c**) and transverse T2-WI (**d**) 8 months after completion of chemoradiation demonstrates completely resolution of the previously seen tumor and reconstitution of the normal zone anatomy of the cervix (*arrow*). Note the postradiation changes in the bladder mucosa with extensive edema off the entire bladder (*arrowheads*) and slight scaring and decreased T2 SI in the parametrial fat (*black arrow*)

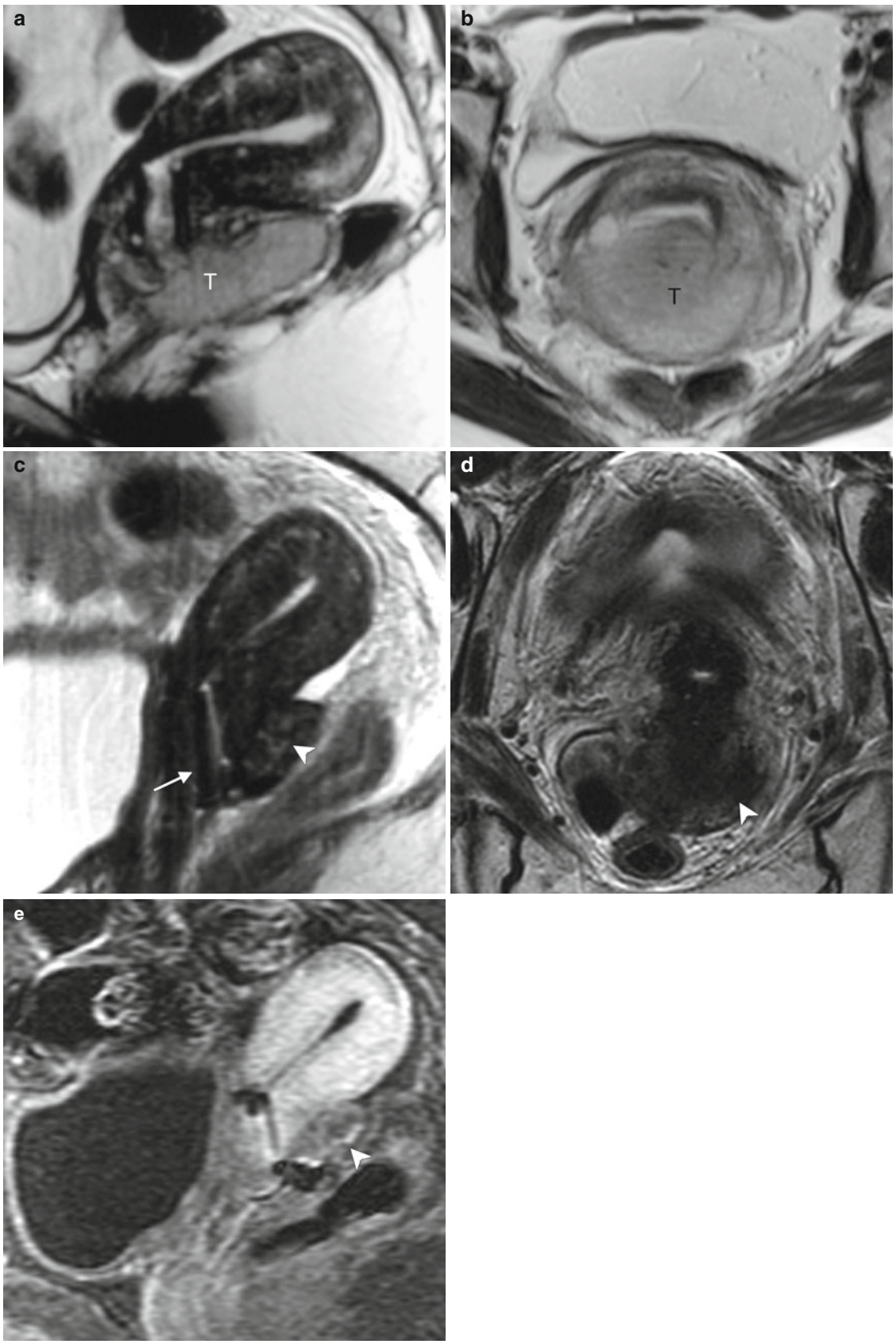

Fig. 3.32 Persistent cervical cancer after chemoradiation. Pretreatment sagittal (**a**) and transverse (**b**) T2-WI depicts a large stage IB2 cervical cancer (*T*). (**c**–**e**) Posttreatment evaluation 5 months after completion of chemoradiation. Sagittal (**c**) and transverse T2-WI (**d**) images depict a residual tumor (*arrowhead*) that has a slightly higher SI than the adjacent cervical stroma (*arrow*). (**e**) T1-WI C+ with slightly hypointense tumor in the posterior cervix (*arrowhead*)

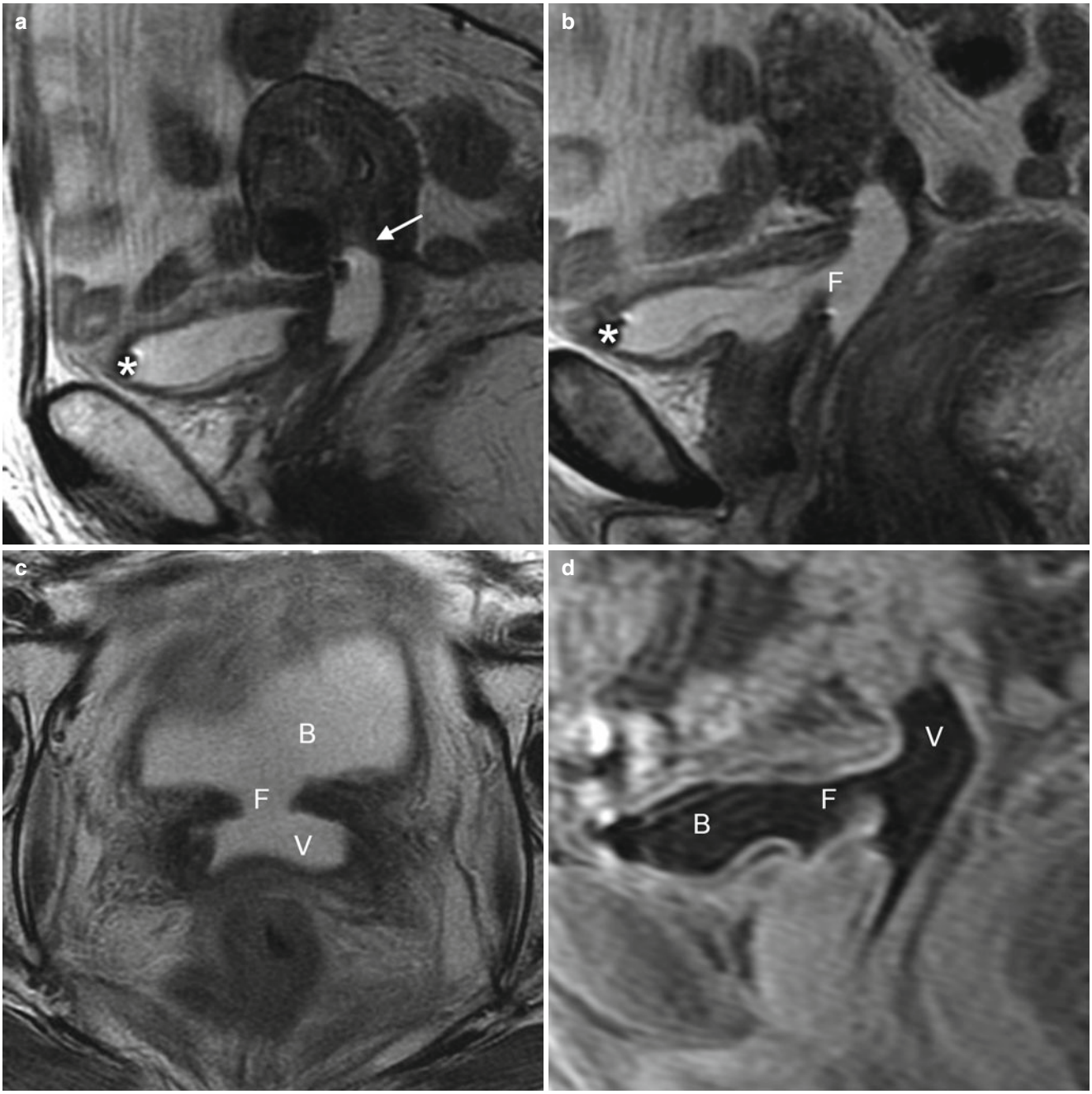

Fig. 3.33 Vesicovaginal fistula after radiotherapy. Radiation therapy causes fibrosis and sometimes necrosis, which can lead to fistula formation. Fistulas are a late complication of radiation and most commonly occur between vagina and urinary bladder or vagina and rectum. T2 WI and C+ sequences are optimal for detection of fistula with high T2 SI fluid-filled tracts on T2 WI and low SI rim-enhancing tracts on contrast-enhanced images. (**a**, **b**) Two sagittal T2-WI with a large vesicovaginal fistula (*F*) and air in the urinary bladder (*asterisk*) 2 years after chemoradiation and brachytherapy for a cervical cancer stage IIB. The remaining uterus is atrophic without evidence for recurrent diseases (*arrow*). Transverse T2-WI (**c**) and sagittal T1-WI C+ (**d**) images confirm the large vesicovaginal fistula (*F*) between bladder (*B*) and vagina (*V*) without evidence for tumor recurrence

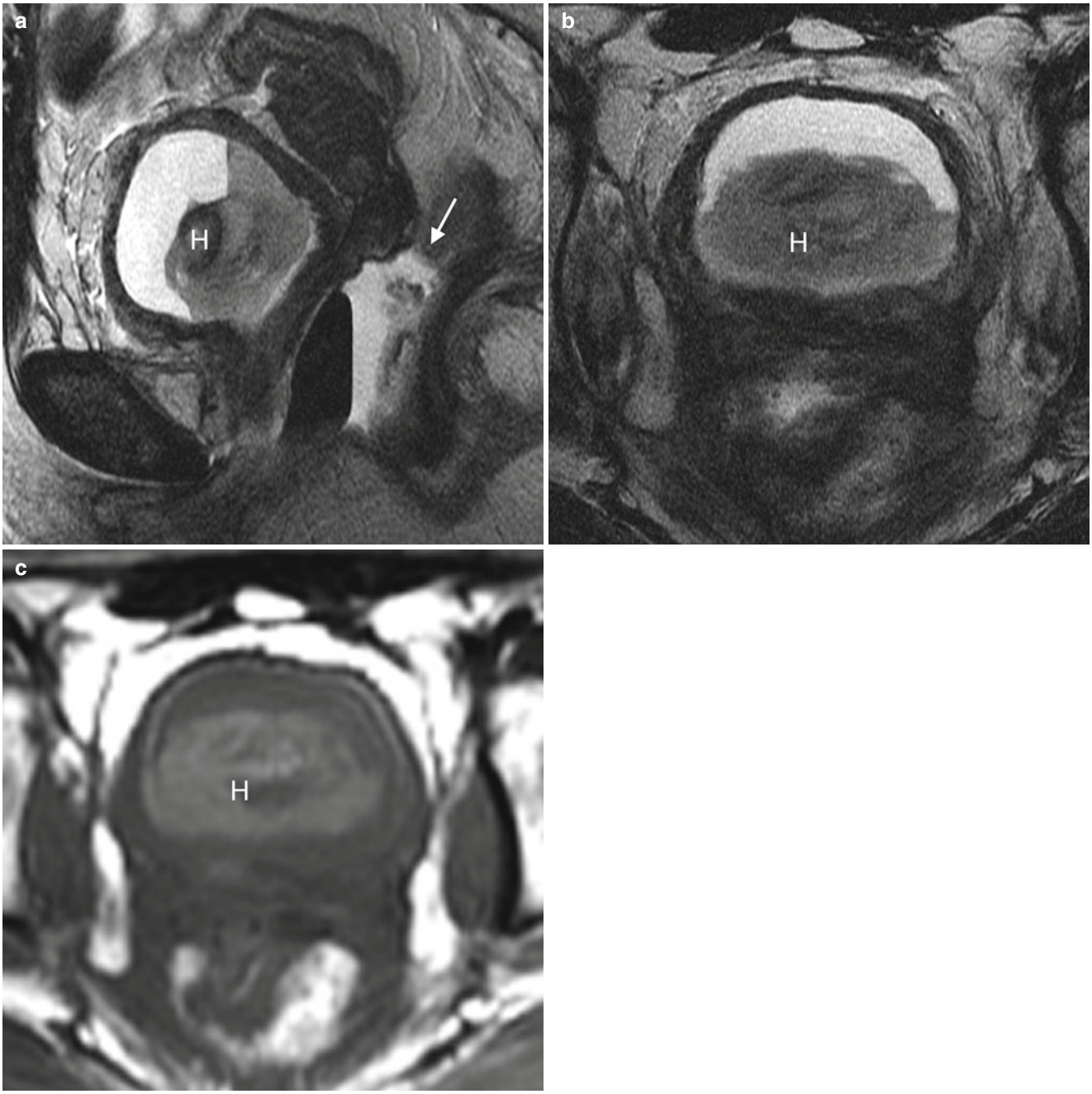

Fig. 3.34 Rectovaginal fistula and radiation-induced cystitis with blood clot in the urinary bladder. Radiation-induced cystitis occurs in approximately 12 % of cases with its incidence proportional to the radiation dose. In the acute-subacute phase, imaging findings include urinary bladder wall thickening and edema, mucosal hyperemia, and blood clots due to necrosis and hemorrhage. In the chronic phase, urinary bladder has small volume and cannot be distended due to extensive fibrosis. Post-treatment sagittal (**a**) and transverse T2-WI (**b**) obtained in a patient with hematuria with obvious wall thickening of a small volume urinary bladder. Large rectovaginal fistula is also present (*arrow*). (**c**) Transverse T1-WI with high SI within the intraluminal lesion, consistent with hemorrhage and intra vesical thrombus formation

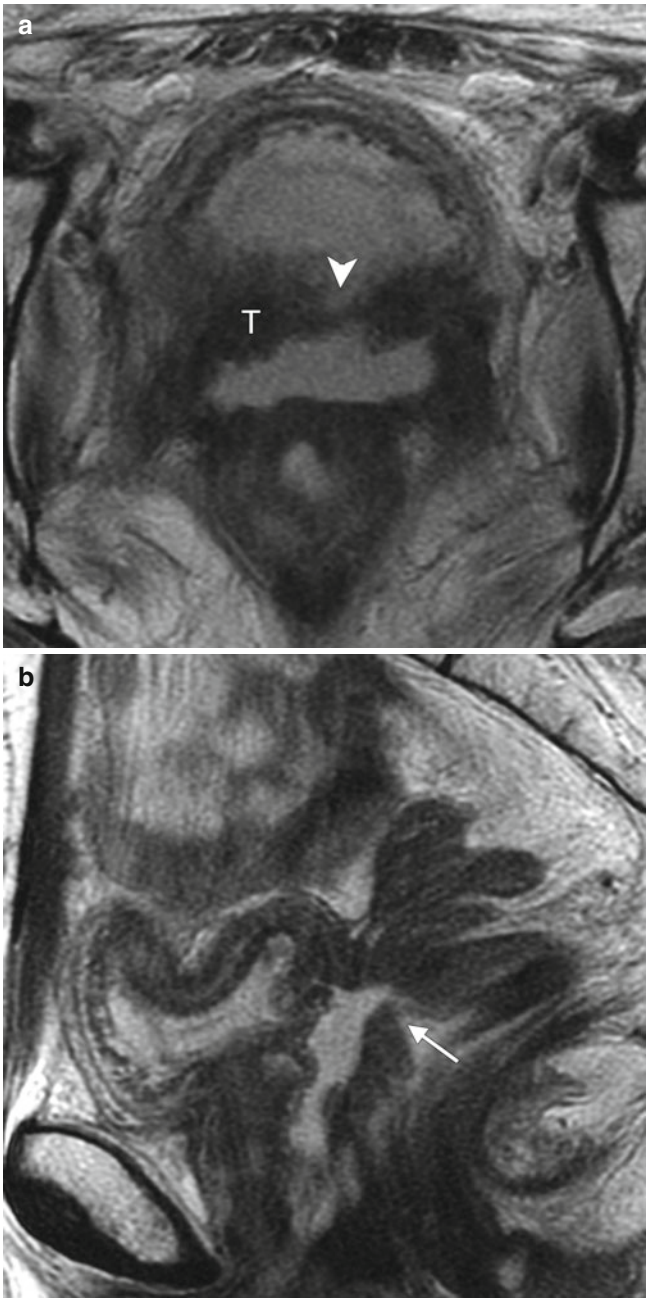

Fig. 3.35 Recurrent necrotic tumor after radiation with vesicovaginal and rectovaginal fistulas. Recurrent disease that invades adjacent organs can also cause a fistulous tract. Therefore, careful evaluation should be performed to exclude signs of malignancy such as a soft-tissue mass and/or adenopathy. Transverse (**a**) and sagittal T2-WI (**b**) images show a necrotic recurrent cervical tumor (*T*) invading the urinary bladder and the rectum with secondary formation of vesicovaginal (*arrowhead*) and rectovaginal (*arrow*) fistulas

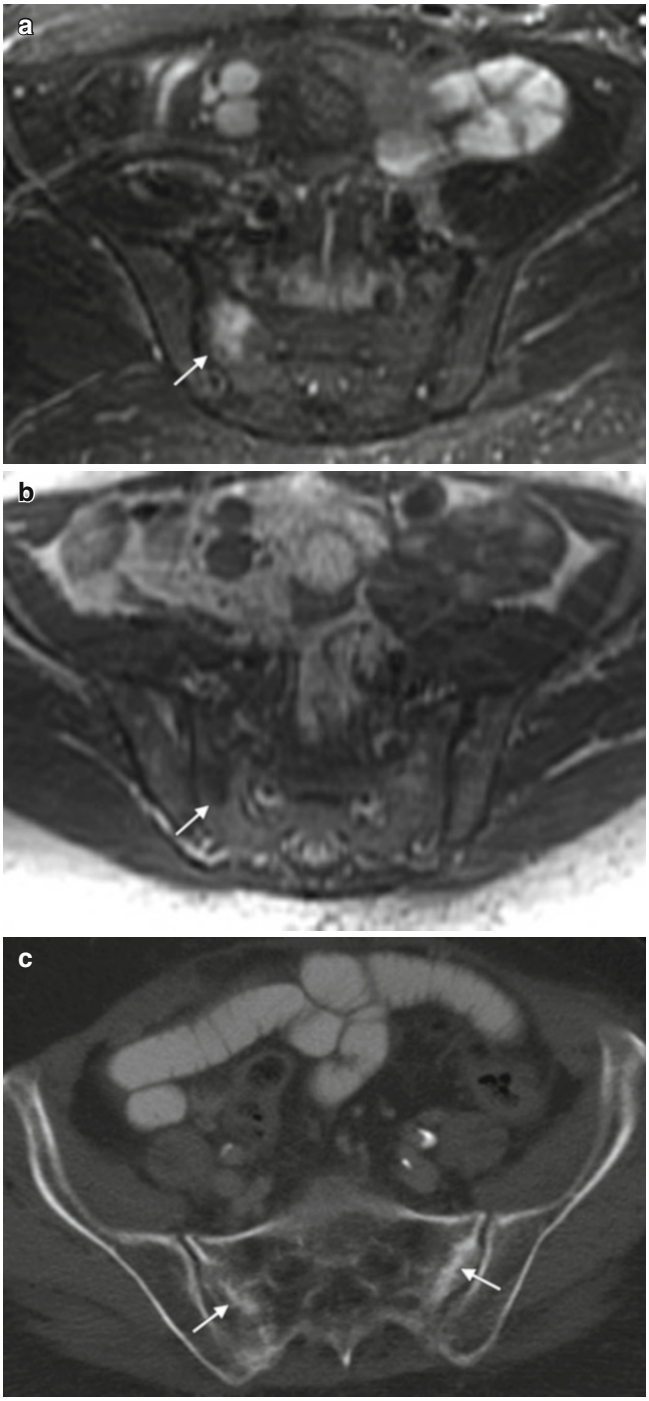

Fig. 3.36 Radiation-induced insufficiency fracture of the sacrum. T2 WI (**a**) with fat suppression in a patient with an unilateral insufficiency fracture in the right sacral wing, corresponding to the focal hypointensity on T1 image (**b**). (**c**) Bone window of a transverse CT of another patient, with increased sclerosis in the massa lateralis of the sacrum on both sides consistent with healing sacrum insufficiency fracture

3.8 Rare Histologies

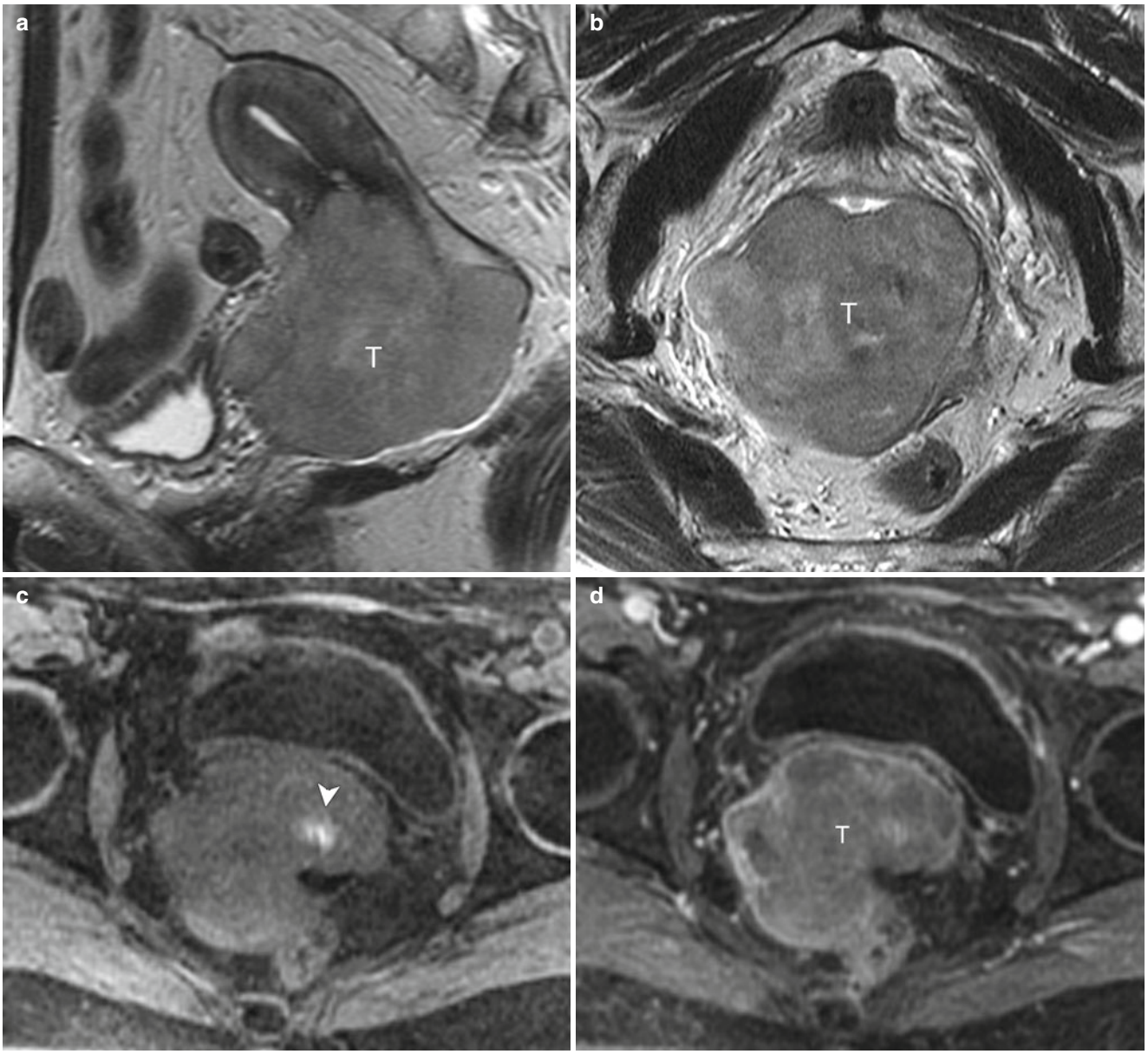

Fig. 3.37 Cervical melanoma. Sagittal (**a**) and transverse T2-WI (**b**) with a large heterogeneous lesion of high T2 SI in the anterior cervix with expansion of the vagina (*T*). (**c**) Transverse T1-WI FS with focal increased signal intensity (*arrowhead*) probably correlating with focal pigmentation on pathology. (**d**) Transverse T1-WI C+ with moderate heterogeneous enhancement. (**e**) Coronal FDG PET maximum intensity projection detecting the primary tumor (*arrow*) and focal activity right inguinal (*curved arrow*) and over the liver (*arrowhead*). (**f**) Fused transverse FDG PET/CT image confirming an inguinal lymph node metastasis (*thin arrow*). The primary tumor (*T*) in the cervix is highly FDG avid (SUV 31). (**g**) Nonenhanced, transverse CT scan with hardly detectable lesion in the liver. (**h**) Fused transverse FDG PET/CT detecting the liver metastasis (*arrowhead*)

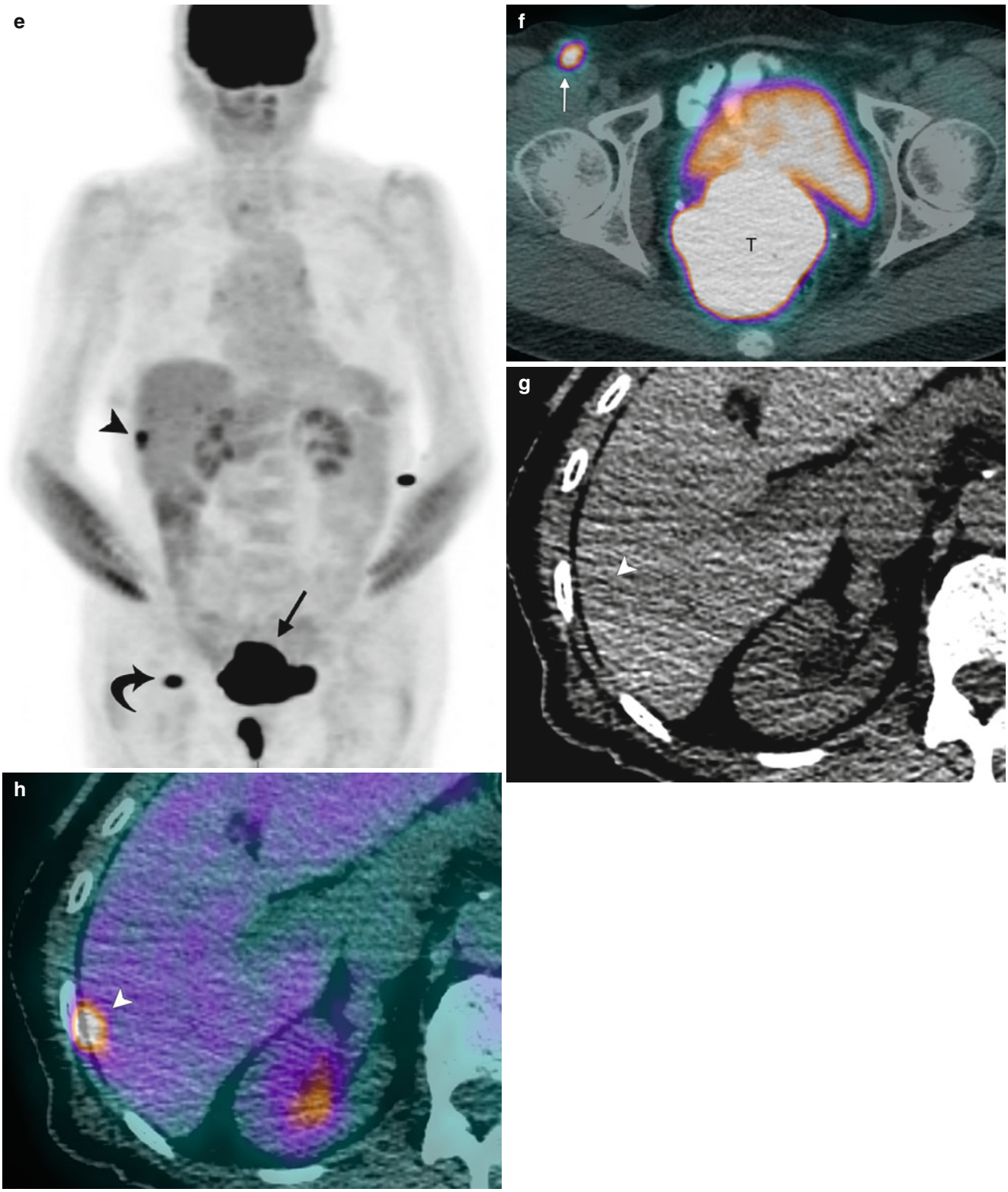

Fig. 3.37 (continued)

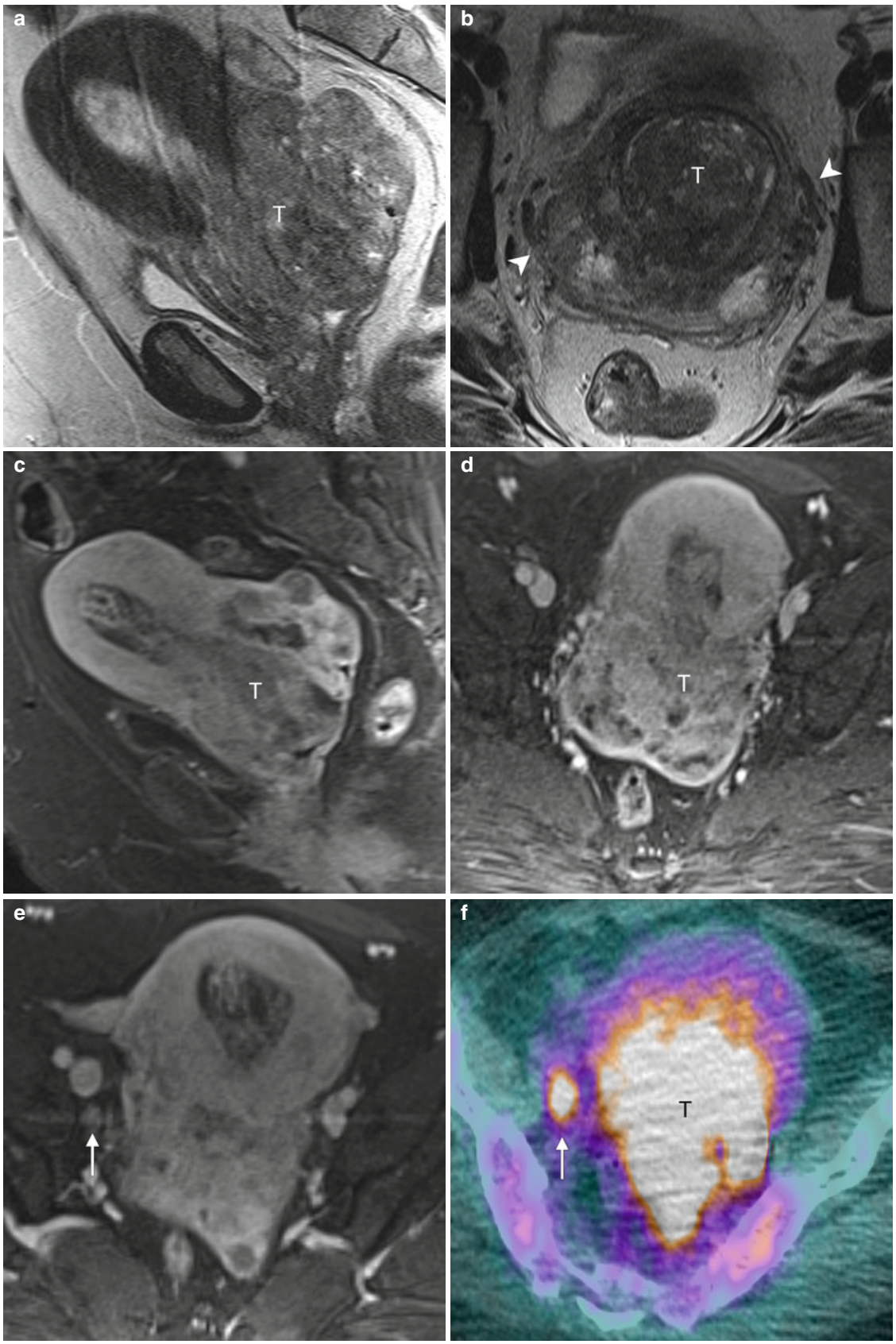

Fig. 3.38 Carcinosarcoma cervix. Sagittal (**a**) and transverse T2-WI (**b**) with a large very heterogeneous tumor of intermediate to high T2 SI in the cervix (*T*) with gross, bilateral parametrial infiltration (*arrowheads*). Sagittal (**c**) and transverse T1-WI FS C+ (**d**) with very heterogeneous enhancement pattern of the entire tumor (*T*). (**e**) Additional T1-WI FS C+ scan with mildly enlarged right iliacal lymph node (*arrow*). (**f**) Fused transverse FDG PET/CT with high FDG activity (SUV 7.5) in the right iliacal lymph node (*arrow*), consistent with lymph node metastasis. High FDG activity in the primary tumor (*T*) with SUV 13

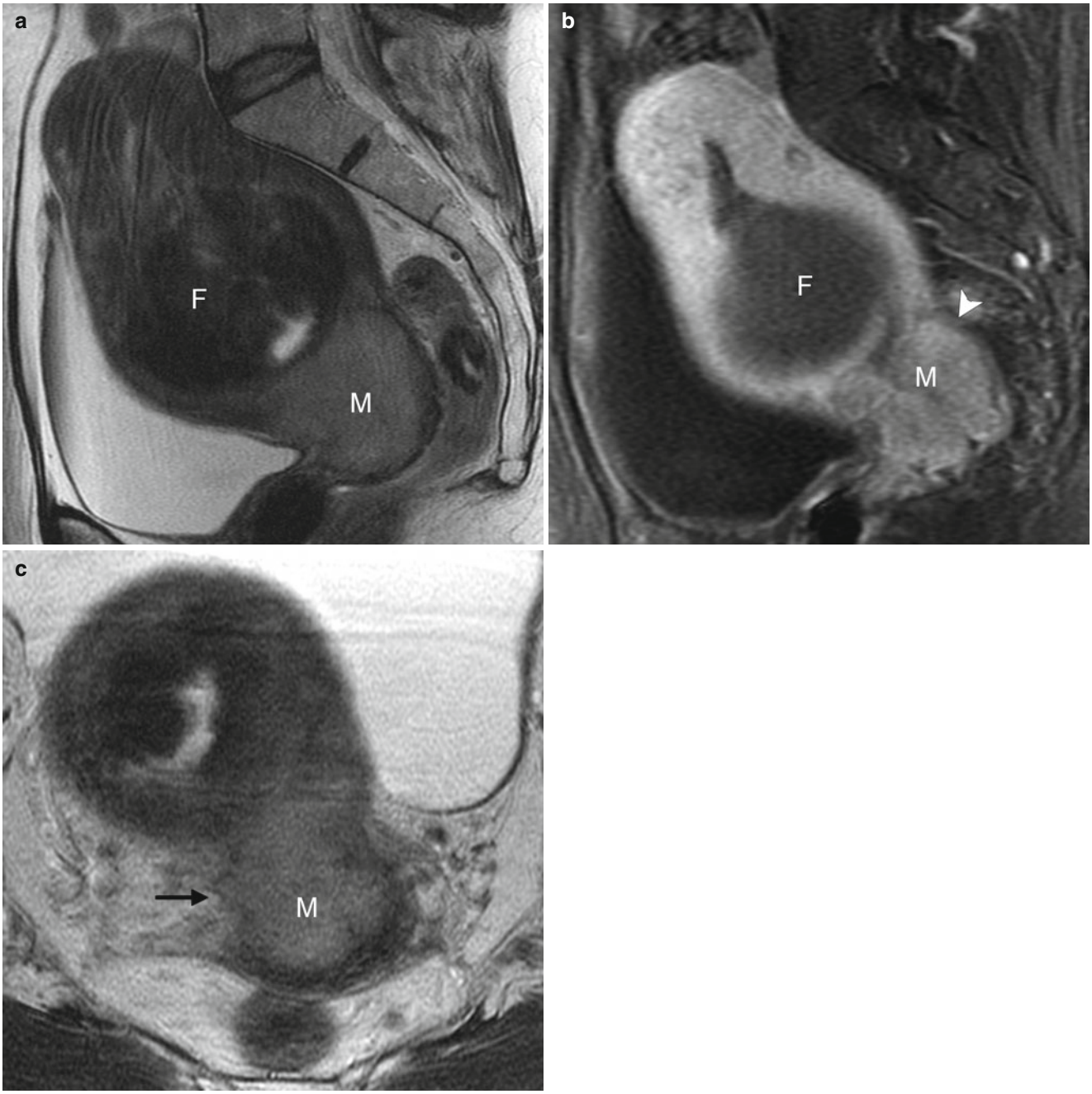

Fig. 3.39 Lung cancer metastasis. Metastasis of the cervix are very rare: breast cancer, ovarian carcinoma, colon cancer or non small cell lung cancer have been described to metastasize into the cervix. (**a**) Sagittal T2-WI with homogenous T2 hyperintense lesion (*T*), adjacent to a uterine fibroid (*F*). (**b**) T1-WI FS C+ with hyper-enhancing mass (*M*) compared to cervical stroma (*arrowhead*). (**c**) Transverse T2-WI with gross parametrial invasion on the right side (*arrow*)

3.9 Key Radiology Report Elements [22]

Table 3.10 Key Radiology Report Elements: Initial Staging

Primary tumor	Size
	Especially whether the tumor is larger than 2–4 cm
	Local extent
	Invasion of the vagina (more or less than two-thirds)
	Parametrial invasion
	Tumor reaching the pelvic wall
	Invasion of adjacent organs (bladder or rectum)
Lymph nodes	Location and dimensions of regional lymph nodes:
	Perivesicular, presacral, internal iliac, obturator, and external iliac nodes
Metastases	Peritoneal spread
	Distant lymph nodes: paraaortic, mediastinal or supraclavicular
	Lung
	Liver
	Bone

Table 3.11 Key Radiology Report Elements: Follow-up Examinations

General	Date of each comparison study used
	Without prior surgery (*see* Table 3.9)
	Metastatic tumor recurrence
	Acute or late complications
	Indicate change in previous and list new sites of disease since prior study
	If extensive measurable disease is present:
	Measure same lesions as on prior scans
	Give overall assessment of response
	Increase, decrease, or no change in size and number of lesions
	Incorporate Response Evaluation Criteria in Solid Tumors (RECIST) or WHO guidelines, if institution or clinical trial uses them
Specific	
After conization	Intact fibrous stromal ring
After trachelectomy	Intact surgical anastomosis with no mass
After hysterectomy	Local tumor recurrence: mass at the vaginal stump, pelvic mass, pelvic lymphadenopathy

References

1. Jemal A, Bray F, Center MM, Ferlay J, Ward E, Forman D. Global cancer statistics. CA Cancer J Clin. 2011;61:69–90.
2. American Cancer Society. What are the key statistics about cervical cancer? www.cancer.org/Cancer/CervicalCancer/DetailedGuide/cervical-cancer-key-statistics. Accessed 24 Sep 2012.
3. Waggoner SE. Cervical cancer. Lancet. 2003;361:2217–25.
4. Walboomers JM, Jacobs MV, Manos MM, et al. Human papillomavirus is a necessary cause of invasive cervical cancer worldwide. J Pathol. 1999;189:12–9.
5. Schiffman M, Castle PE, Jeronimo J, et al. Human papillomavirus and cervical cancer. Lancet. 2007;370:890–907.
6. Noller KL, Decker DG, Lanier AP, et al. Clear-cell adenocarcinoma of the cervix after maternal treatment with synthetic estrogens. Mayo Clin Proc. 1972;47:629–30.
7. Pecorelli S. Revised FIGO staging for carcinoma of the vulva, cervix, and endometrium. Int J Gynaecol Obstet. 2009;105:103–4.
8. Lagasse LD, Creasman WT, Shingleton HM, et al. Results and complications of operative staging in cervical cancer: experience of the Gynecologic Oncology Group. Gynecol Oncol. 1980;9:90–8.
9. Michell DG, Synder B, Coakley F, et al. Early invasive cervical cancer: tumor delineation by magnetic resonance imaging, computed tomography, and clinical examination, verified by pathologic results, in the ACRIN 6651/GOG 183 Intergroup Study. J Clin Oncol. 2006;24:5687–94.
10. Kidd EA, Siegel BA, Dehdashti F, et al. Lymph node staging by positron emission tomography in cervical cancer: relationship to prognosis. J Clin Oncol. 2010;28:2108–13.
11. NCCN Clinical Practice Guidelines in Oncology. http://www.nccn.org/professionals/physician_gls/f_guidelines.asp.
12. American College of Radiology. ACR Appropriateness Criteria: Pretreatment Planning of Invasive Cancer of the Cervix. http://www.acr.org/ac.
13. Hricak H, Gatsonis C, Chi DS, et al. Role of imaging in pretreatment evaluation of early invasive cervical cancer: results of the intergroup study American College of Radiology Imaging Network 6651-Gynecologic Oncology Group 183. J Clin Oncol. 2005;23:9329–37.
14. Mitchell DG, Snyder B, Coakley F, et al. Early invasive cervical cancer: tumor delineation by magnetic resonance imaging, computed tomography, and clinical examination, verified by pathologic results, in the ACRIN 6651/GOG 183 Intergroup Study. J Clin Oncol. 2006;24:5687–94.
15. Hricak H, Akin O, Sala E, et al., editors. Diagnostic imaging: gynecology. Salt Lake City: Amirsys; 2007.
16. Balleyguier C, Sala E, Cunha TD, et al. Staging of uterine cervical cancer with MRI: guidelines of the European Society of Urogenital Radiology. Eur Radiol. 2011;21:1102–10.
17. Siegelman ES. Body MRI. Philadelphia: Elsevier/Saunders; 2005.
18. Park SB, Lee JH, Lee YH, et al. Multilocular cystic lesions in the uterine cervix: broad spectrum of imaging features and pathologic correlation. AJR Am J Roentgenol. 2010;195:517–23.
19. Barakat RR. Principles and practice of gynecologic oncology. 5th ed. Philadelphia: Lippincott Williams & Wilkins; 2009.
20. Rob L, Skappa P, Robova H, et al. Fertility-sparing surgery in patients with cervical cancer. Lancet Oncol. 2011;12:192–200.
21. Addley HC, Vargas HA, Moyle PL, et al. Pelvic imaging following chemotherapy and radiation therapy for gynecologic malignancies. Radiographics. 2010;30:1843–56.
22. Hricak H, Husband J, Panicek D. Oncologic imaging: essentials of reporting common cancers. Philadelphia: Elsevier/Saunders; 2007.

Vaginal Cancer

4

Harpreet K. Pannu

Malignancy of the vagina is usually metastatic, and less commonly primary, in origin [1]. Metastases to the vagina usually originate from other sites in the genital tract such as the cervix, vulva, endometrium and ovary, and can also occur from non-gynecologic sites such as the rectum and breast [2]. Tumor spreads to the vagina by direct extension from adjacent viscera or by hematogenous route from distant malignancies.

Primary malignancies of the vagina account for less than 5 % of female genital tract cancers [1, 2]. Squamous cell cancer, the most common type, is seen in over 85 % of cases [1, 3]. The remaining tumors include melanoma, adenocarcinoma, sarcoma, and less common histologies such as undifferentiated and small cell tumors, and lymphoma. Squamous cell cancer and melanoma usually occur in postmenopausal women, whereas adenocarcinoma predominates in young women [2]. A subtype of adenocarcinoma, clear cell carcinoma, is associated with in utero exposure to diethylstilbestrol. Embryonal rhabdomyosarcoma is the most common type of sarcoma affecting infants and young girls.

Patients with vaginal malignancy can present with vaginal bleeding or discharge, or the tumor may be detected during screening for cervical cancer [2]. The tumor is often located in the posterior upper third of the vagina and tends to be multicentric [1, 2]. It can grow to directly involve surrounding soft tissues and adjacent viscera such as the paracolpos, cervix, urethra, bladder, rectum, and pelvic side wall. The lymphatic drainage follows the embryologic origins of the vagina: The upper two-thirds is derived from the müllerian tract, and the distal third arises from the urogenital sinus [3]. Lymphatic spread from the upper vagina is to the external and internal iliac nodes, followed by the common iliac and para-aortic nodes [4, 5]. The lower vagina drains to the superficial inguinal nodes, followed by the deep inguinal nodes and then superiorly to the external iliac nodes [4]. Hematogenous spread to lungs, liver, and bone is typically seen in advanced disease [2, 3].

Radiation therapy, via brachytherapy or external beam therapy, is the primary treatment modality used in most patients [2]. Surgery with radical vaginectomy and lymphadenectomy can be considered for patients with small, early-stage tumors, and pelvic exenteration for those with recurrent or advanced disease [2]. Complications of therapy include vesicovaginal and rectovaginal fistulas and vaginal stenosis. Patient prognosis depends on the stage of disease (Tables 4.1 and 4.2). Patients with high stage, tumors larger than 4 cm, or melanoma have a poorer prognosis [2, 3].

Vaginal lesions seen on physical examination can be assessed with ultrasound or MRI. Cysts and solid masses are differentiated with ultrasound, but MRI is better for characterizing lesions and assessing local extension of the tumor [6]. Gel can be used to distend the vagina on MRI to evaluate the wall thickness and for intraluminal masses [7, 8]. Imaging in the axial and sagittal planes demonstrates vaginal wall thickness, focal masses, and the relationship of a mass to adjacent anterior and posterior viscera. On MRI, the normal vagina has a T2 hyperintense inner mucosal layer followed by a T2 hypointense muscular layer with surrounding outer adventitial tissue, which has a prominent T2 hyperintense venous plexus [3, 9–12]. The posterior fornix is typically situated more cranially than the anterior fornix on sagittal images. On axial images, the normal vagina has an "H" configuration, with the lateral walls directed anteriorly towards the pubis.

H.K. Pannu, MD
Department of Radiology, Memorial Sloan-Kettering Cancer Center,
1275 York Avenue, New York,
NY 10065, USA

O. Akin (ed.), *Atlas of Gynecologic Oncology Imaging*, Atlas of Oncology Imaging,
DOI 10.1007/978-1-4614-7212-4_4, © Springer Science+Business Media New York 2014

Table 4.1 FIGO staging of vaginal carcinoma

FIGO category	Description
I	The carcinoma is limited to the vaginal wall
II	The carcinoma has involved the subvaginal tissue but has not extended to the pelvic wall
III	The carcinoma has extended to the pelvic wall
IV	The carcinoma has extended beyond the true pelvis or has involved the mucosa of the bladder or rectum; bullous edema as such does not permit a case to be allotted to Stage IV
IVa	Tumor invades bladder and/or rectal mucosa and/or direct extension beyond the true pelvis
IVb	Spread to distant organs

From FIGO Committee on Gynecologic Oncology [13], with permission
FIGO International Federation of Gynecology and Obstetrics

Table 4.2 TNM staging of vaginal carcinoma

TNM category	Characteristics
Primary tumor (T)	
TX	Primary tumor cannot be assessed
T0	No evidence of primary tumor
Tis	Carcinoma in situ (preinvasive carcinoma)
T1	Tumor confined to vagina
T2	Tumor invades paravaginal tissues but not to pelvic wall
T3	Tumor extends to pelvic wall
T4	Tumor invades mucosa of the bladder or rectum and/or extends beyond the true pelvis (bullous edema is not sufficient evidence to classify a tumor as T4)
Regional lymph nodes (N)	
NX	Regional lymph nodes cannot be assessed
N0	No regional lymph node metastasis
N1	Pelvic or inguinal lymph node metastasis
Distant metastasis (M)	
M0	No distant metastasis
M1	Distant metastasis
Anatomic stage/Prognostic groups	
0	Tis – N0 – M0
I	T1 – N0 – M0
II	T2 – N0 – M0
III	T1-T3 – N1 – M0 *or* T3 – N0 – M0
IVA	T4 – any N – M0
IVB	Any T – Any N – M1

Used with the permission of the American Joint Committee on Cancer (AJCC), Chicago, Illinois. The original source for this material is the Edge SB, Byrd DR, Compton CC, editors. AJCC Cancer Staging Manual, Seventh Edition (2010) published by Springer Science and Business Media LLC, www.springer.com

4.1 Normal Anatomy

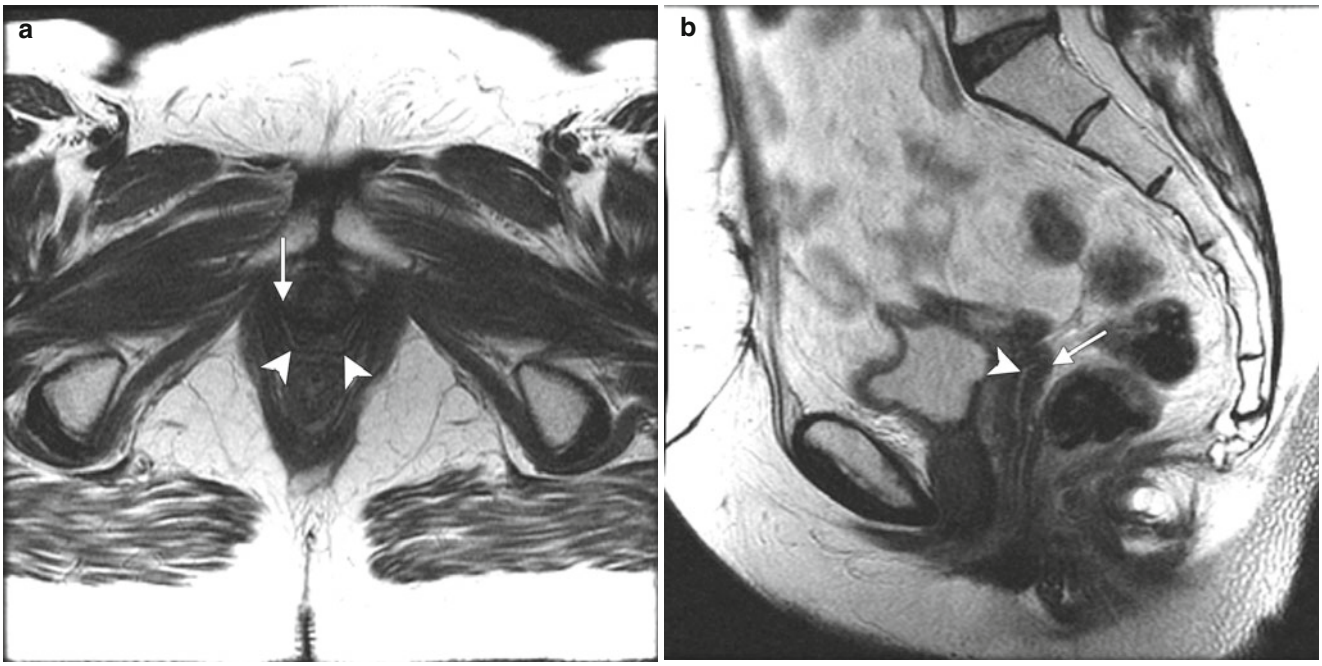

Fig. 4.1 Transverse (**a**) and sagittal (**b**) T2-weighted MR images of the pelvis without fat saturation show central hyperintense mucosa (*arrowheads*) and outer hypointense muscular layer (*arrows*), as well as "H"-shaped configuration of the vagina

4.2 Stages of Disease

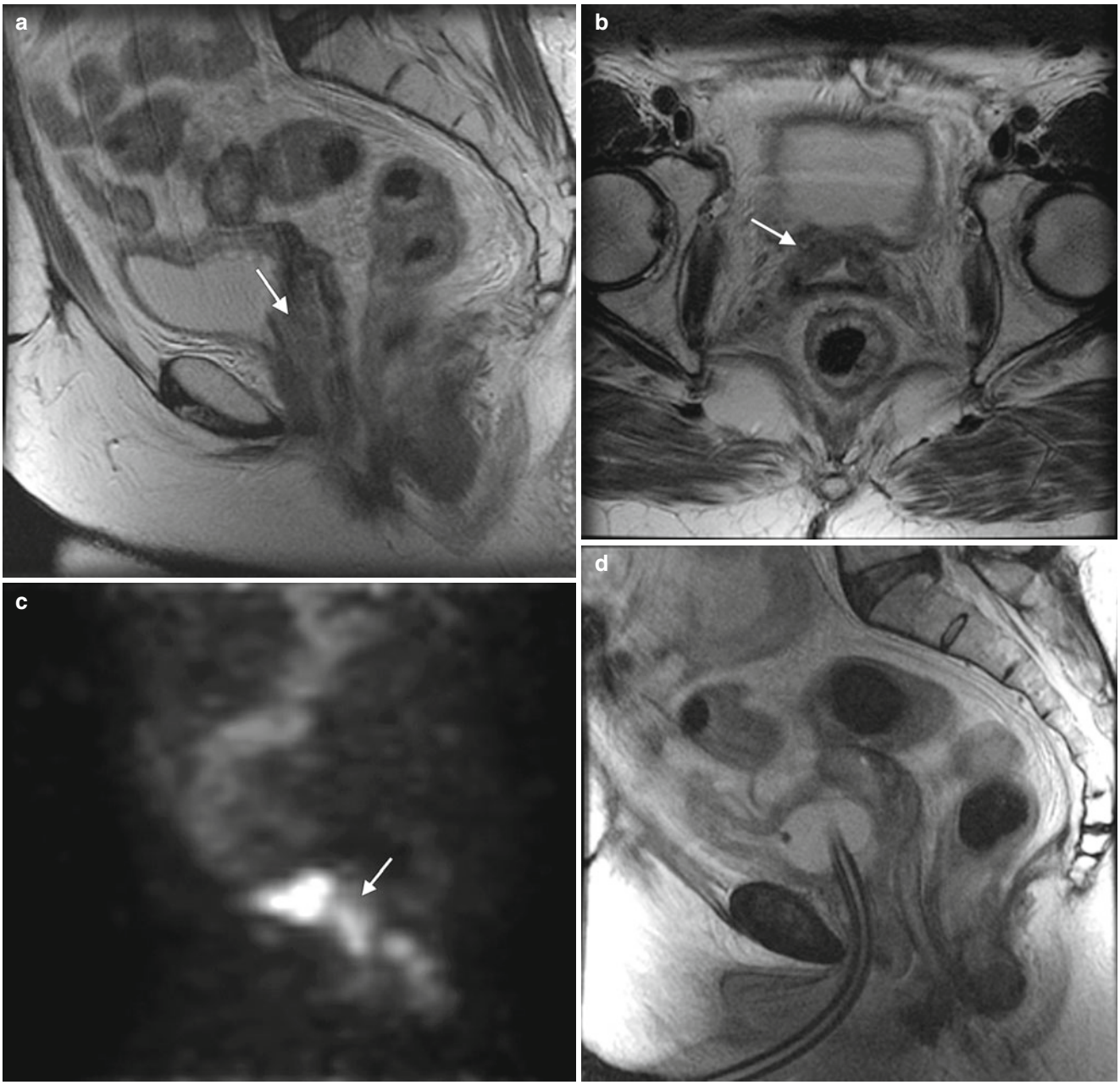

Fig. 4.2 Squamous cell carcinoma of the vagina, stage I at presentation. Perimenopausal patient with abnormal Pap smear and colposcopy. Sagittal (**a**) and axial (**b**) T2-weighted MR images of the pelvis show abnormal intermediate signal intensity and nodular thickening of the anterior vaginal wall (*arrow*) due to invasive squamous cell carcinoma. Increased activity was noted in the vagina (*arrow*) on fluorodeoxyglucose positron emission tomography (FDG-PET) (**c**). The patient was not felt to be a surgical candidate and was treated with radiation for stage I vaginal cancer. Followup MRI performed 7 months later showed diffuse thickening of the bladder and vagina, probably due to radiation. There was also new soft tissue in the left vesicovaginal space, inseparable from the bladder, that was suspicious for local extension of tumor (*arrow*): sagittal (**d**), axial (**e**), and coronal (**f**) T2-weighted images and a sagittal postcontrast T1-weighted image (**g**) with fat saturation. A Foley catheter is also noted in the bladder, as well as artifact at the vaginal cuff from a prior procedure. Followup CT images 14 months after the initial scan (**h**–**j**) show additional progression, with a necrotic central pelvic mass (*arrow*) involving the bladder and vagina, bilateral external iliac nodes (*arrows*), and a lung metastasis (*arrow*). Squamous cell carcinoma of the vagina is likely to be associated with infection with the human papillomavirus [1, 2]. Most patients are postmenopausal and have a mass in the proximal posterior vagina, which can be ulcerative or exophytic. A variant is verrucous carcinoma, which appears as a fungating mass with local spread [2]. On MRI, the mass tends to have intermediate signal intensity on T2-weighted images and to be homogeneous [1]. The lumen is expanded with exophytic tumors

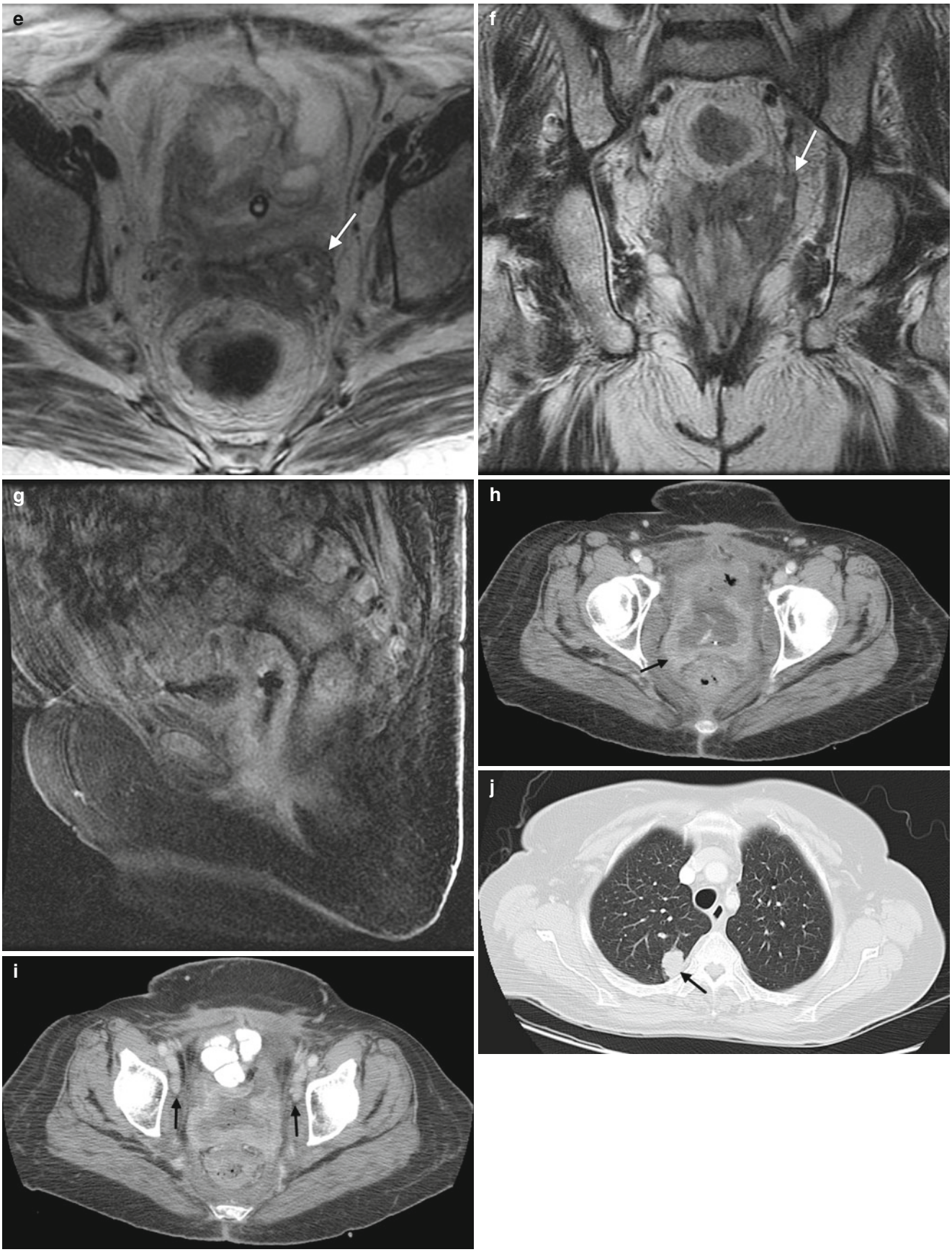

Fig. 4.2 (continued)

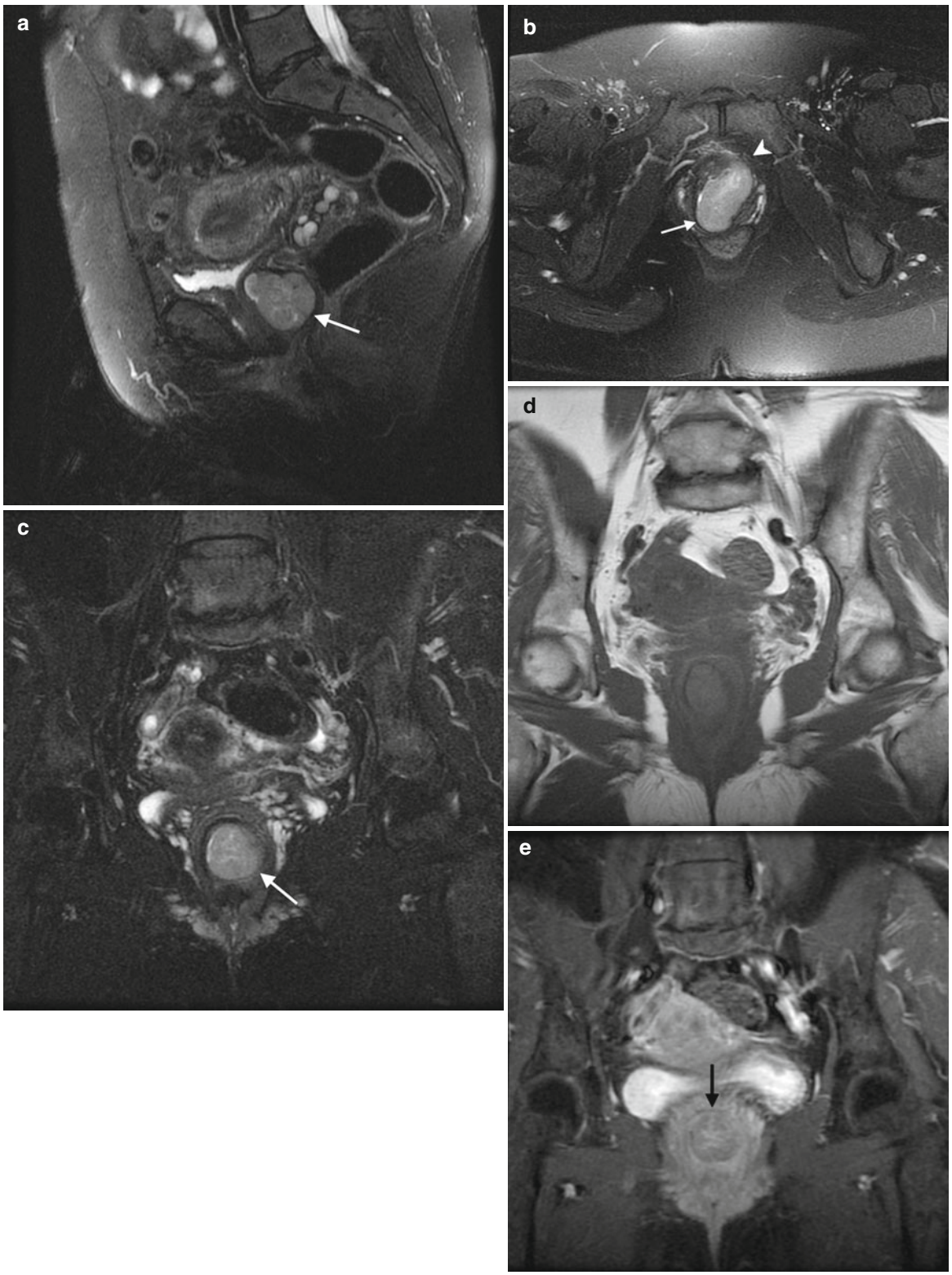

Fig. 4.3 Adenocarcinoma of the vagina, stage II at presentation. This postmenopausal patient presented with vaginal bleeding and a protruding vaginal mass. Sagittal (**a**), axial (**b**), and coronal (**c**) T2-weighted MR images with fat saturation show a mass within the vagina with intermediate signal intensity (*arrow*). The mass distends the vaginal cavity, with loss of definition of the left anterior vaginal wall. It abuts the urethra and extends anteriorly to the retropubic region (*arrowhead*). Coronal T1-weighted images before contrast (**d**) (without fat saturation) and after contrast (**e**) (with fat saturation) show enhancement (*arrow*). The vaginal mass and a short segment of urethra were excised, revealing a moderately differentiated adenocarcinoma. The patient was treated with radiation but recurrence occurred 2 years later, and she underwent a pelvic exenteration with no disease on subsequent followup. Adenocarcinoma represents the majority of vaginal carcinomas in young patients and typically occurs in the second decade of life [2]. Its possible origin is from adenosis, endometriosis, periurethral glands, or wolffian rests [1]. A variant is clear cell carcinoma, which is associated with in utero exposure to diethylstilbestrol. Adenocarcinoma tends to occur in the proximal anterior vagina and can be a polypoid mass or can appear as wall thickening [1]. On MRI, the mass has been described as hyperintense on T2-weighted images, with heterogeneous enhancement [14]. There is disruption of the normal low signal intensity of the vaginal wall with spread of the tumor to the paravaginal tissues [1]

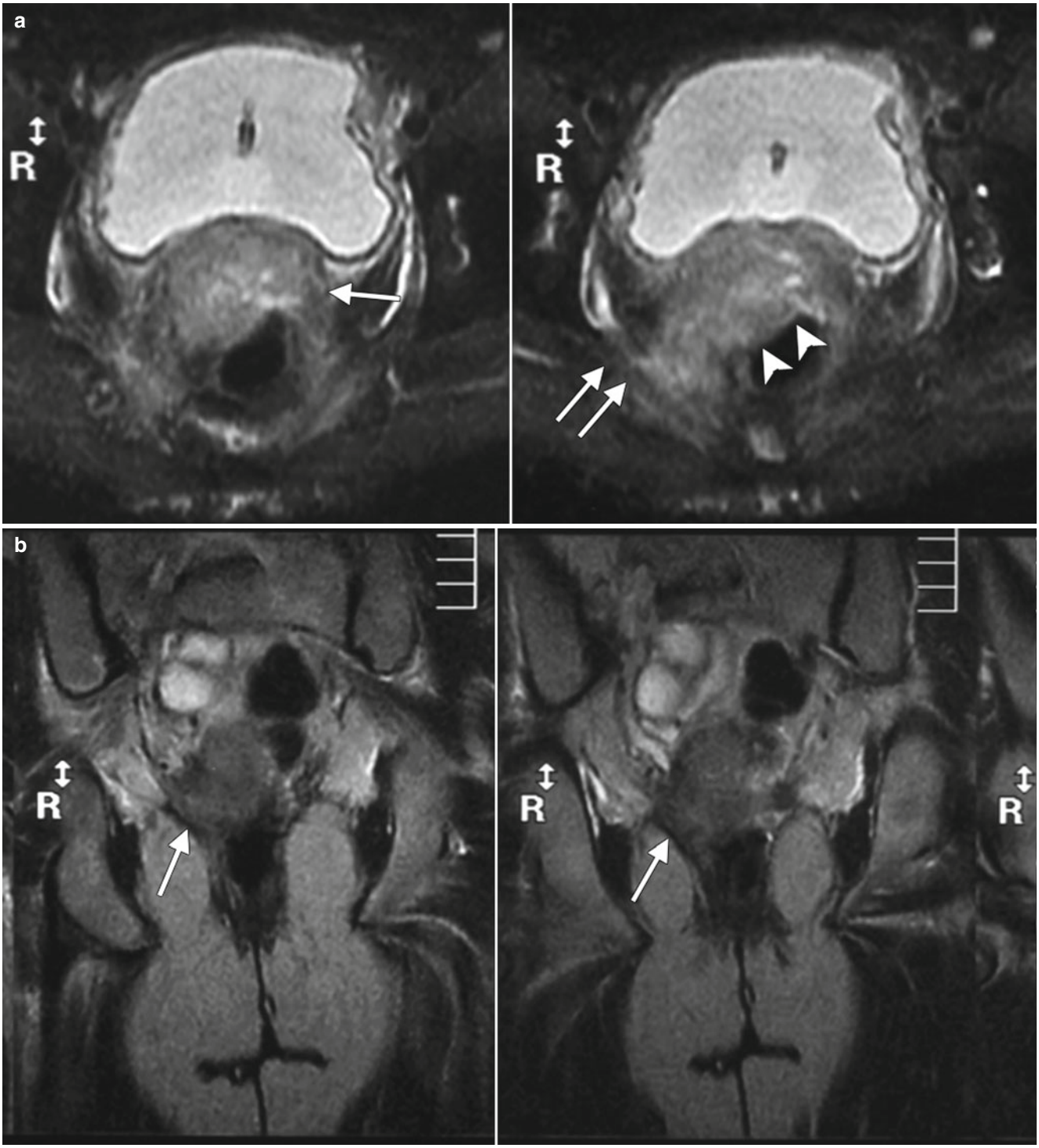

Fig. 4.4 Poorly differentiated carcinoma with sarcomatoid features of the vagina, stage III at presentation, in a perimenopausal patient. The patient had been treated with chemotherapy and radiation for colorectal carcinoma approximately 15 years previously and now presented with vaginal bleeding. (**a**) Axial T2-weighted MR images with fat saturation show a mass in the vagina (*arrow*), which extends into the perirectal fat and involves the right rectal wall (*arrowhead*) and pelvic musculature (*double arrows*). (**b**) Coronal T2-weighted images show right perirectal extension (*arrow*). (**c**, **d**), Precontrast and postcontrast T1-weighted images without fat saturation show enhancement of the mass (*arrow*). In summary, there is a vaginal mass with ill-defined margins and local extension to involve the right rectal wall and pelvic musculature. The patient underwent a total pelvic exenteration. At surgery, the vaginal tumor involved the cervix, bladder wall, rectal wall, and levator muscle. The bladder and rectal mucosa were benign. Local spread of tumor is best seen on MRI and on T2-weighted images in the axial and coronal planes or the oblique plane perpendicular to the long axis of the vagina [1]. The tumor tends to be higher in signal intensity than the bladder wall and rectal muscle, as well as the pelvic floor musculature. With erosion of the tumor into adjacent viscera, fistulas can be demonstrated as T2 hyperintense tracks with fluid as well as gas in the vagina

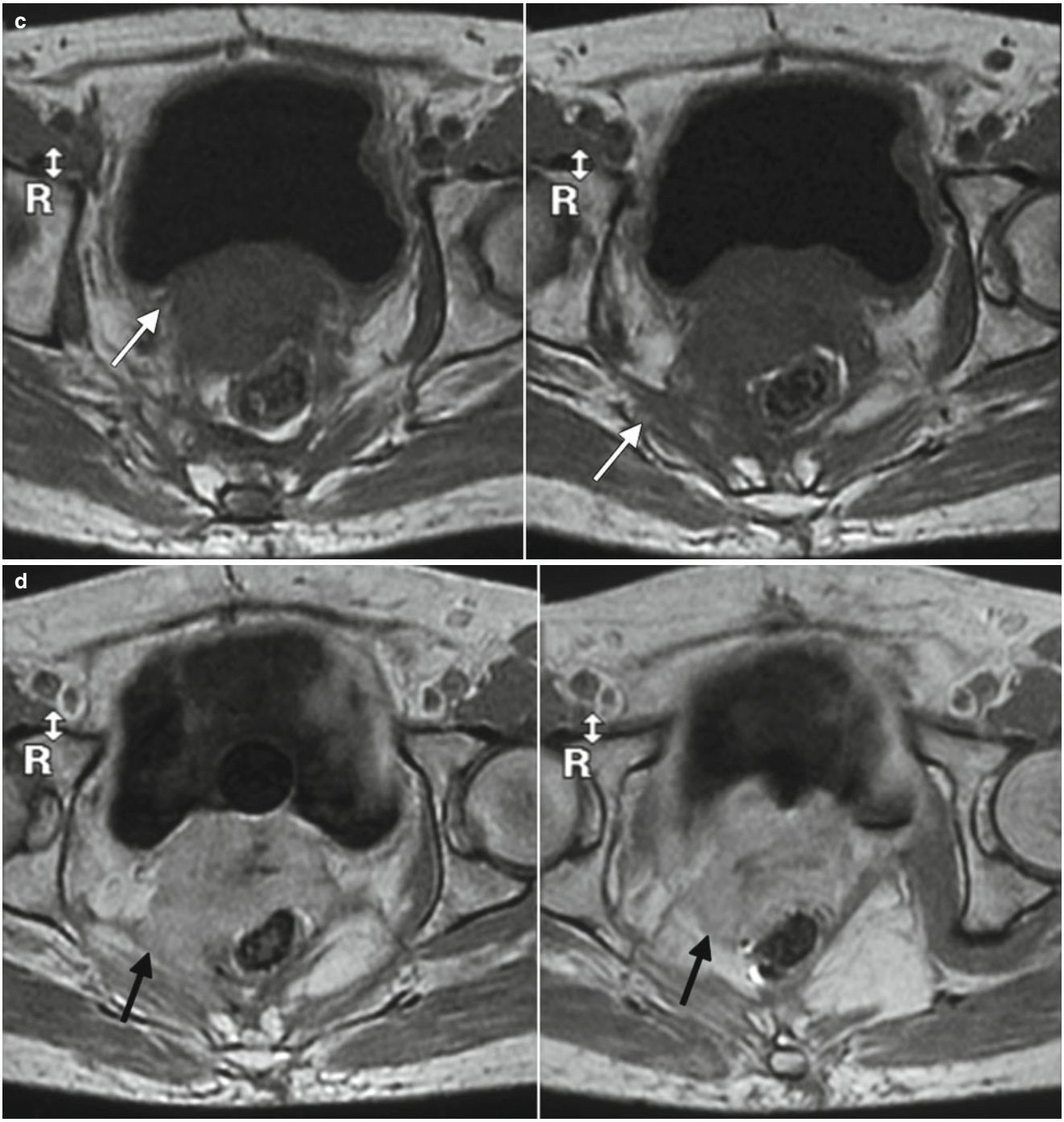

Fig. 4.4 (continued)

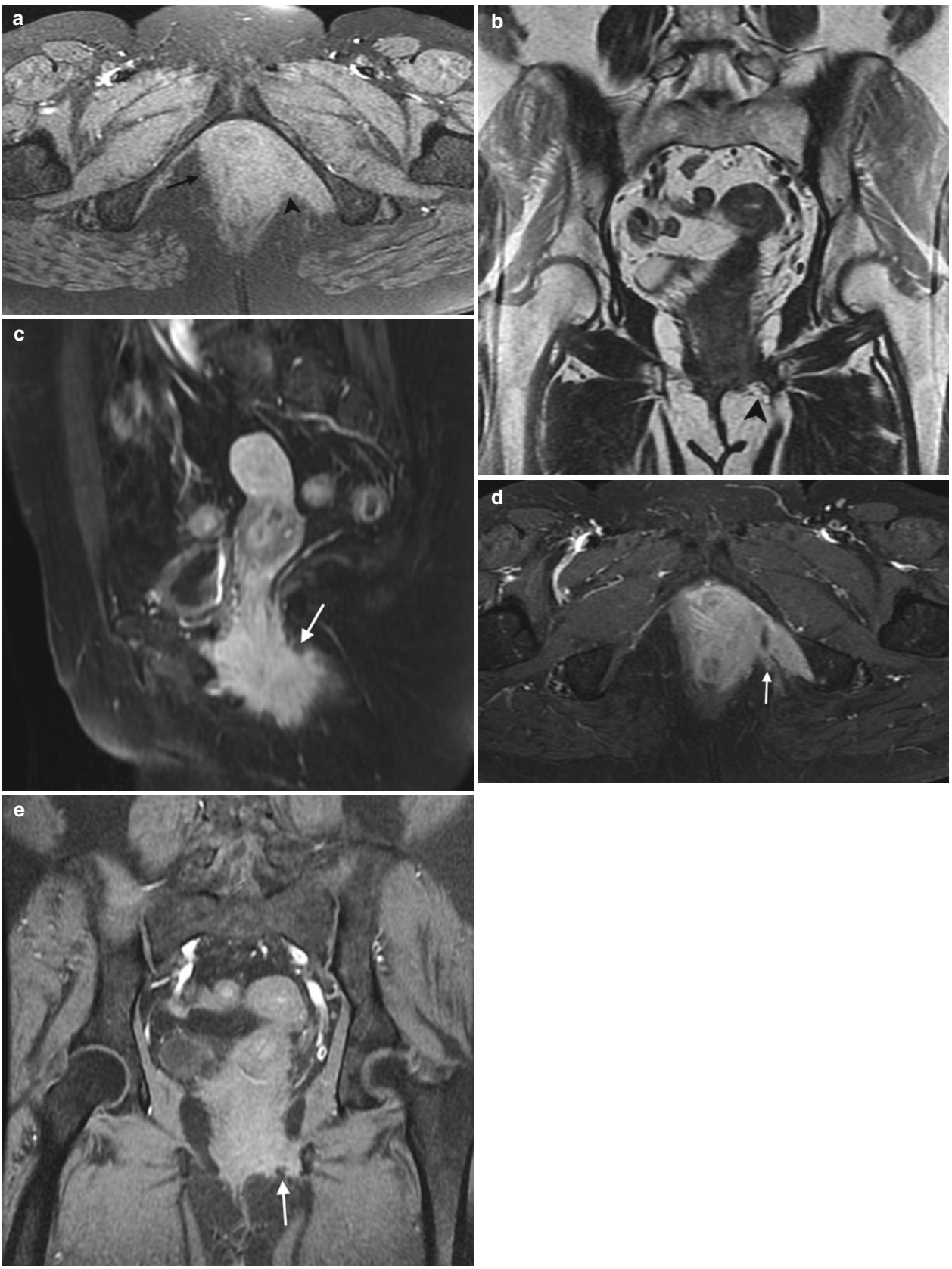

Fig. 4.5 Squamous cell carcinoma of the vagina, stage III at presentation. This postmenopausal woman presented with rectal and vaginal pain. A vaginal mass was seen on physical examination, and biopsy showed moderately differentiated invasive squamous cell carcinoma. An axial precontrast T1-weighted image with fat saturation (**a**) and coronal T2-weighted images (**b**) show an infiltrative vaginal mass (*arrow*) involving the urethra and rectum and extending to the ischioanal fossa (*arrowhead*) and pelvic musculature. T1-weighted MR images using contrast with fat saturation in the sagittal (**c**), axial (**d**), and coronal (**e**) planes show enhancing ill-defined tumor (*arrow*). The patient was treated with chemotherapy and radiation

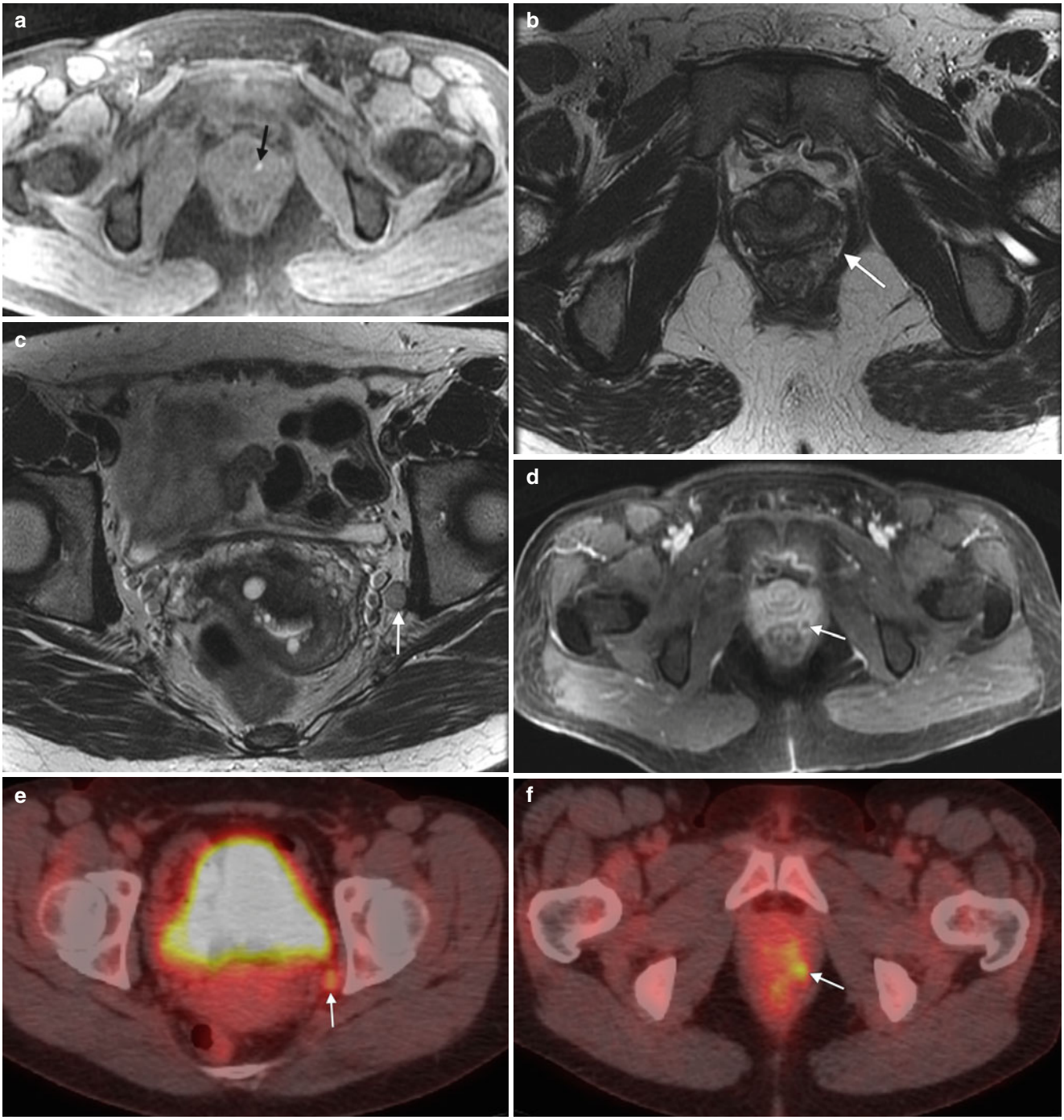

Fig. 4.6 Melanoma of the vagina with nodal metastasis. This perimenopausal woman presented with vaginal bleeding and several pigmented vaginal lesions. Biopsy showed left vaginal wall melanoma with invasion. (**a**) An axial T1-weighted MR image with fat saturation shows a T1-hyperintense focus in the left aspect of the vagina (*arrow*). (**b**, **c**), Axial T2-weighted images at different levels show soft tissue in the left rectovaginal space (*arrow*) and a left obturator node (*arrow*). (**d**) An axial postcontrast T1-weighted image with fat saturation shows enhancement of the rectovaginal nodule (*arrow*). (**e**, **f**) The obturator node (*arrow*) and perirectal nodule (*arrow*) were hypermetabolic on fused FDG-PET images. Biopsy of the pelvic node was positive for malignant melanoma, and the patient was treated with radiation as well as ipilimumab, a T-lymphocyte blocking antibody. Lymphatic spread from the upper vagina is to the obturator and external and internal iliac nodes, followed by the common iliac and para-aortic nodes [4]. The lower vagina drains to the superficial inguinal nodes, followed by the deep inguinal nodes and then superiorly to the external iliac nodes [4]. On MRI, nodes are evaluated by size and location. Nodes larger than 7–10 mm in short axis and in the expected drainage pathway may be due to metastatic disease. Evaluation with FDG-PET is helpful to identify malignant nodes. Malignant nodes may also appear heterogeneous and necrotic on CT scans

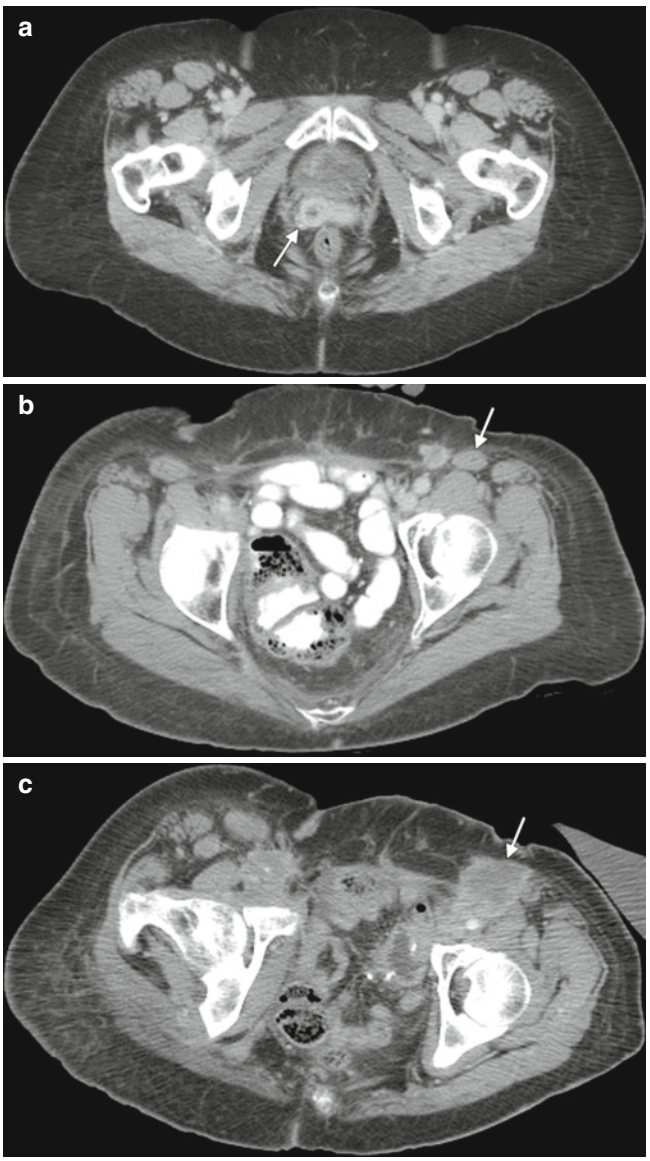

Fig. 4.7 Squamous cell carcinoma of the vagina with nodal metastasis. This perimenopausal patient has a history of multiple local excisions for squamous cell carcinoma. An axial CT scan (**a**) shows an enhancing right vaginal mass (*arrow*). The patient underwent a total pelvic exenteration, and pathology showed invasive squamous cell carcinoma. Followup CT scans with intravenous contrast after 6 months (**b**) and 9 months (**c**) show an enlarging, heterogeneous left inguinal node (*arrow*) due to metastatic disease, as well as an ill-defined soft-tissue nodal mass around the right femoral vessels

4.3 Other Types of Vaginal Tumors

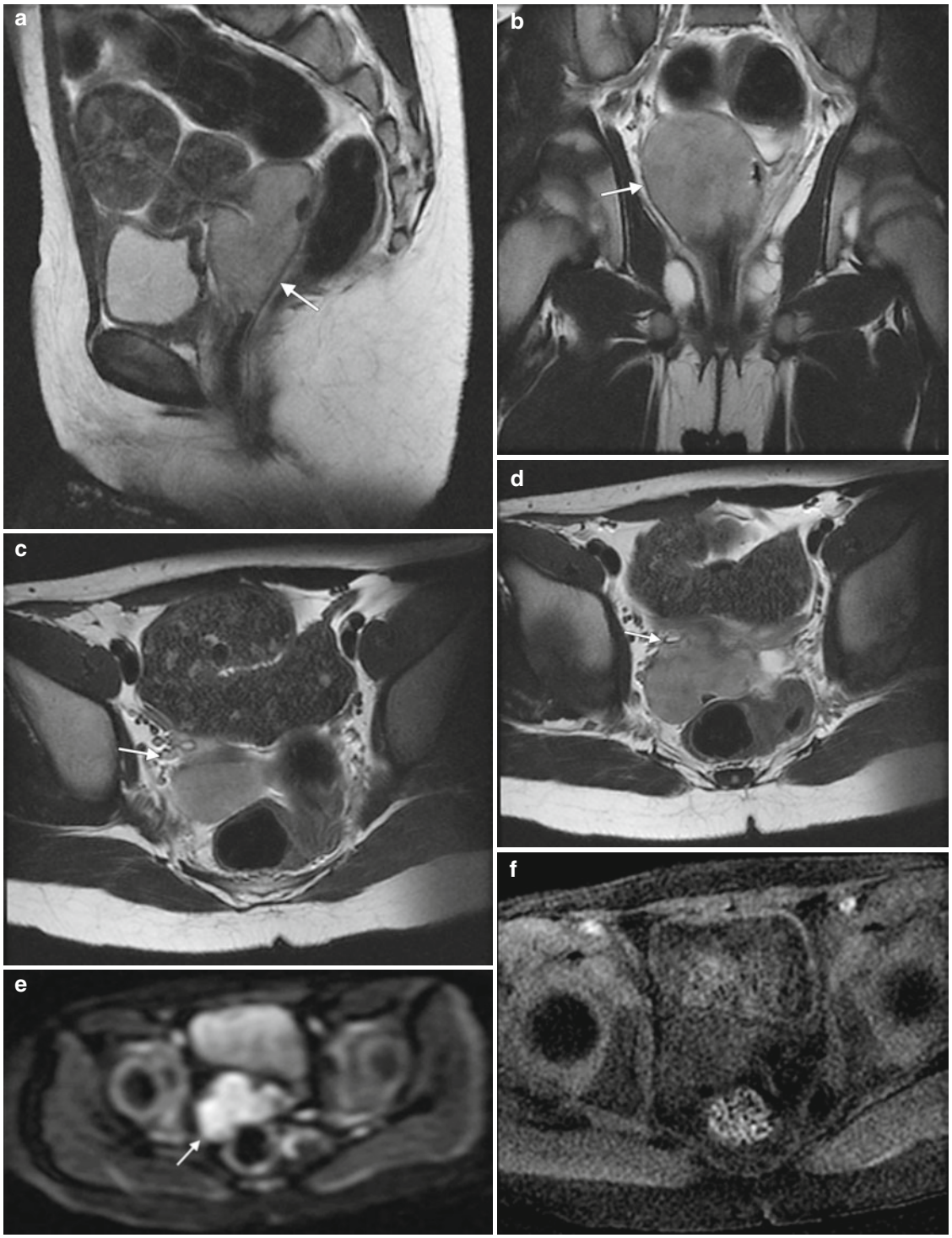

Fig. 4.8 Clear cell carcinoma of the vagina. This 8-year-old girl presented with vaginal bleeding and had no evidence of precocious puberty on evaluation by an endocrinologist. Examination under anesthesia revealed a vaginal mass, and biopsy showed clear cell carcinoma. (**a**, **b**) Sagittal and coronal T2-weighted MR images show a solid mass in the upper vagina (*arrow*). (**c**, **d**) Axial T2-weighted images show local extension of the lobulated vaginal mass with soft tissue surrounding the distal right ureter (*arrow*) and extension towards the rectosigmoid colon. (**e**) The mass has restricted diffusion (*arrow*) on diffusion-weighted imaging. (**f**–**h**) Precontrast (**f**) and postcontrast (**g**, **h**) T1-weighted MR images with fat saturation show enhancement of the mass (*arrow*). The patient received chemotherapy followed by upper vaginectomy and hysterectomy. Most patients with clear cell carcinoma have a polypoid tumor that is confined to the vagina or is stage I at diagnosis. The tumors tend to have a better outcome than adenocarcinoma that is not associated with diethylstilbestrol (DES) exposure [2]. In addition to clear cell carcinoma of the vagina, patients with DES exposure are also at risk for clear cell carcinoma of the cervix [2]. The median age of diagnosis for vaginal cancer in these patients is 19 years [2]. On MRI, clear cell carcinoma has been described as being hyperintense on T2-weighted images [15]

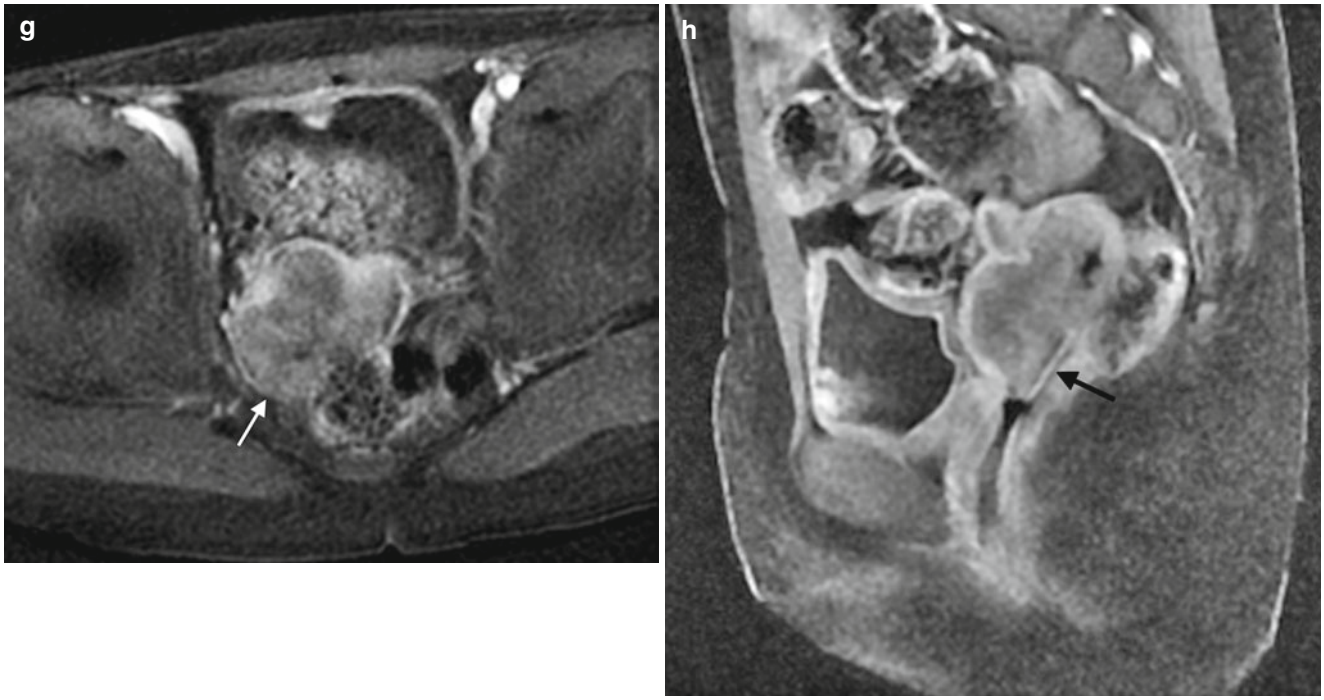

Fig. 4.8 (continued)

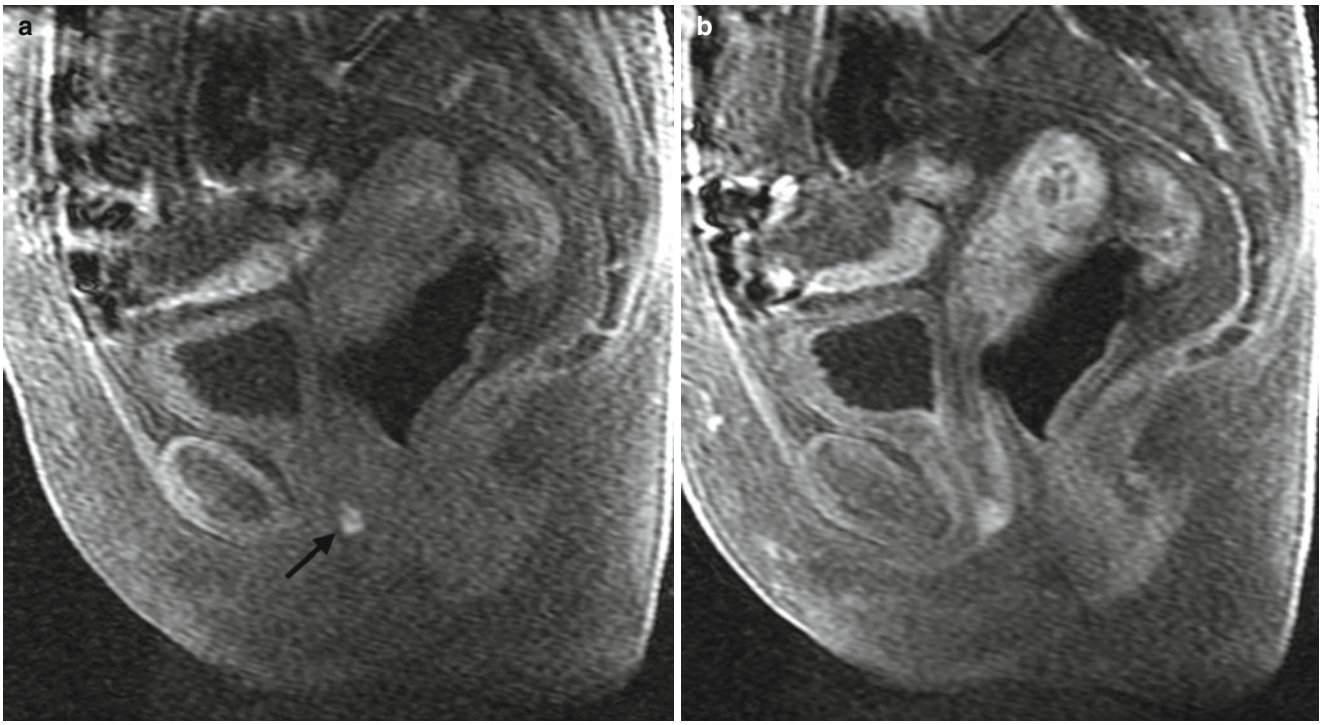

Fig. 4.9 Melanoma of the vagina. This postmenopausal woman presented with vaginal spotting and had pigmented vaginal and cervical lesions on physical examination. Biopsies showed malignant melanoma of the vaginal mucosa, and the patient was treated with radiation. Precontrast (**a**) and postcontrast (**b**) followup T1-weighted MR images with fat saturation show a T1-hyperintense lesion in the distal vagina (*arrow*). There was no distant disease on FDG-PET. Surgery was therefore performed, with radical hysterectomy, vaginectomy, and cystectomy with reconstruction. Surgical resection showed multifocal foci of melanoma in the urethra, vagina, cervix, and lower uterine segment. Eight months later, the patient presented with abdominal pain and bowel obstruction. Small bowel implants of metastatic melanoma (not conspicuous on imaging) were removed during laparotomy. Melanoma rarely occurs in the vagina and is usually seen in postmenopausal women of Caucasian descent [16]. Patients can present with vaginal bleeding and a discoloration of the mucosa, typically in the distal vagina. The tumors tend to be multicentric, with a propensity for local recurrence and poor 5-year survival [2]. On MRI, tumor foci can be hyperintense on T1-weighted images and can show moderate enhancement [16]. The increased signal intensity on T1-weighted images is more apparent when fat suppression is used, and endometriosis is in the differential diagnosis [17]. Less commonly, the tumor may be amelanotic [1]. The signal intensity on T2-weighted images can be low or intermediate to high [1, 17]. Enhancement is seen with contrast [17]

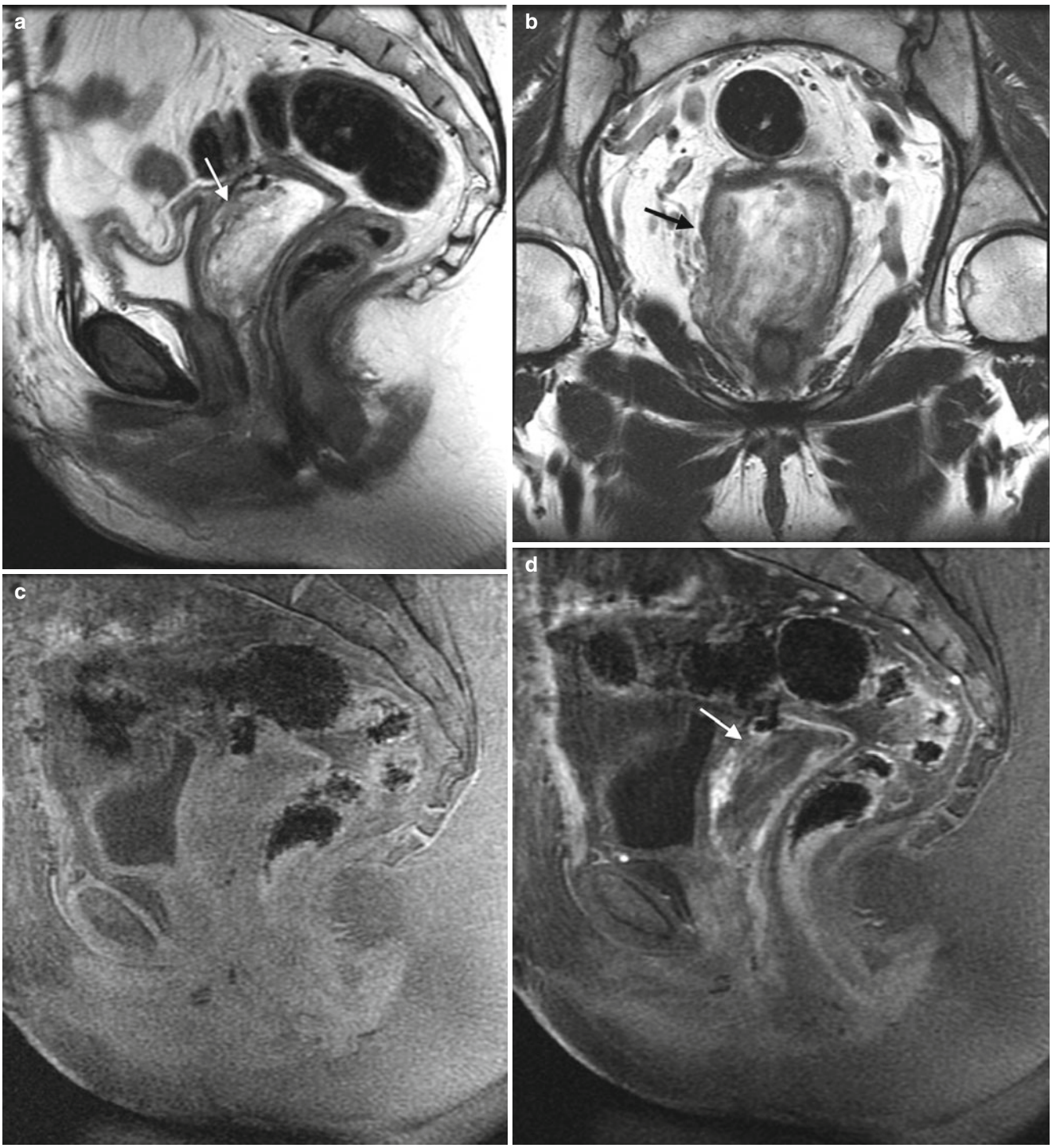

Fig. 4.10 Angiomyxoma of the vagina. This perimenopausal woman presented with lower-extremity edema and had a 8-cm cervical mass on pelvic ultrasound and MRI (*not shown*). A hysterectomy and vaginal resection was done and pathology showed angiomyxoma of the vagina. On followup 5 months later, the patient was found to have a nodular protuberance in the vagina. MRI at this time showed a bulky mass in the vagina. Sagittal (**a**) and coronal (**b**) T2-weighted MR images show a hyperintense, heterogeneous mass (*arrow*) in the upper vagina, with suggestion of a "swirled" internal architecture. Precontrast (**c**) and postcontrast (**d**, **e**) T1-weighted images with fat saturation show heterogeneous enhancement in the mass (*arrow*), with a suggestion of "swirled" appearance on the delayed postcontrast image (**e**). Resection of the recurrent mass again revealed angiomyxoma. The patient was treated with radiation and hormonal therapy, and the mass was stable on followup imaging 6 months later. Angiomyxoma is an infiltrative, locally aggressive pelvic tumor that tends to occur in women of reproductive age [18]. The tumors can present as large masses because of their asymptomatic nature and slow growth [18]. Imaging, particularly with MRI, is helpful for planning excision by defining the supra and infra levator extent of the mass and involvement of local structures. The tumor surrounds and displaces adjacent structures such as the vagina, urethra, and anorectum, rather than invading them [19]. It is difficult to excise the entire mass and the tumor has a tendency to recur. The mass is hyperintense on T2-weighted images, with a swirled internal architecture [20, 21]. A myxoid matrix and high water content contribute to a hypodense appearance on noncontrast CT images and a hyperintense appearance on T2-weighted MR images [19, 20]. A swirled pattern of enhancement can also be seen on postcontrast CT and MR images [20]. Moderate enhancement is seen because of prominent vascular stroma on CT and MRI, and the mass is hypervascular on angiography [18]

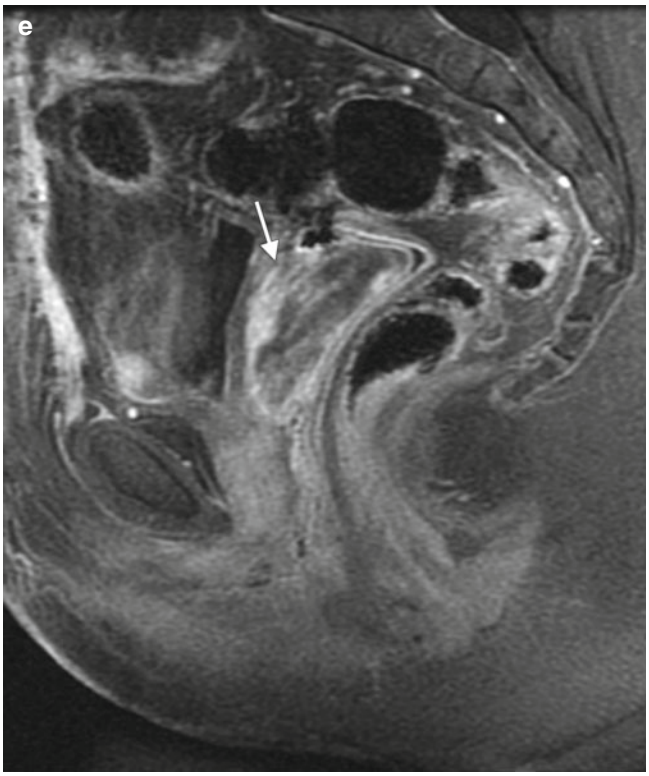

Fig. 4.10 (continued)

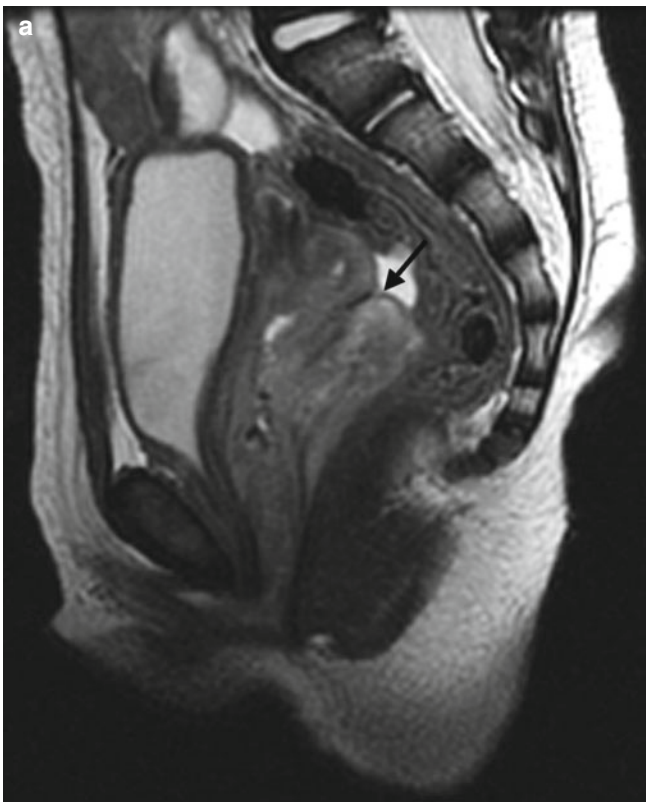

Fig. 4.11 Rhabdomyosarcoma of the vagina. This 2-year-old girl presented with vaginal bleeding and a protruding mass. The mass was partially excised, with pathology revealing rhabdomyosarcoma; the patient was treated with chemotherapy. Followup MRI shows diffuse vaginal wall thickening and a residual vaginal mass, which extends into the rectovaginal space (*arrow*) on T2-weighted images in the sagittal (**a**), coronal (**b**), and axial (**c**) planes. Precontrast (**d**) and postcontrast (**e**) sagittal T1-weighted MR images with fat saturation, as well as axial images (**f**), show moderate heterogeneous enhancement of the mass (*arrow*). Embryonal rhabdomyosarcoma of the vagina typically occurs in early childhood, with a mean age of 3 years [2]. The mass is usually large and heterogeneous and can mimic a cluster of grapes (sarcoma botryoides) [1]. Regions of hemorrhage and necrosis may be present, but calcification is rare [22]. Because of the large size of the mass, the site of origin may be difficult to determine. Patients may present with a mass bulging out of the vagina. Imaging can be used to assess for lung and bone metastases

Fig. 4.11 (continued)

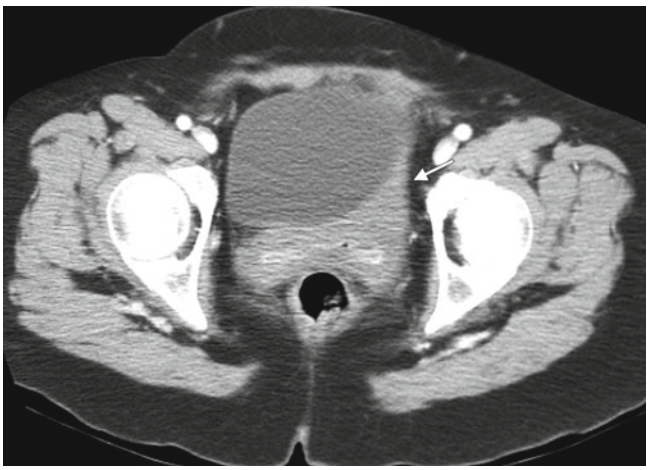

Fig. 4.12 Lymphoma of the vagina. In this perimenopausal patient, a left adnexal mass was palpated during a physical examination performed to evaluate a urinary tract infection. A CT scan (not shown) revealed a large pelvic mass in the left adnexa and left hydroureter. Biopsy of the vagina revealed diffuse large cell lymphoma. No lymphoma was identified in the bone marrow, and the patient was started on chemotherapy. A followup axial CT image of the pelvis after a few months shows residual moderate, circumferential, homogeneous soft-tissue thickening of the vagina due to treated disease with probable involvement of the posterior left bladder wall (*arrow*). Repeat vaginal biopsy showed fibrosis, scattered lymphocytes, and no lymphoma. Vaginal wall thickening gradually decreased but persisted on CT scans for several years. Involvement of the vagina by lymphoma is typically secondary to systemic lymphoma and usually of the non-Hodgkin type. The tumor is typically homogeneous and may appear as generalized wall thickening due to infiltrative disease or as a mass [14, 23–25]. There also may be other evidence of lymphoma on imaging, such as adenopathy or a history of lymphoma in the patient. On MRI, the mass is hypointense on T1-weighted images and has intermediate signal intensity on T2-weighted images; its submucosal location in the vaginal wall can be demonstrated [24, 26, 27]

4.4 Metastatic Disease to the Vagina

Fig. 4.13 Recurrent endometrial carcinoma in vagina. This postmenopausal woman had a history of vaginal bleeding treated with vaginal hysterectomy with morcellation of the uterus. Pathology of the uterus revealed well-differentiated endometrial cancer, and the patient received a short course of radiation. Four years later, the patient had an abnormal Pap smear, and biopsy of the vaginal apex revealed recurrent endometrial carcinoma. T2-weighted MR images of the pelvis in the sagittal plane (**a**) and the axial plane (**b**) show a mass in the vaginal cuff (*arrow*) with an intermediate signal intensity. A soft-tissue nodule is tethered to the vagina, abutting the sigmoid colon (*arrowhead*). T1-weighted images before contrast (**c**) and after contrast ((without fat saturation) **d** and with fat saturation **e**) show enhancement of the vaginal mass (*arrow*) and perisigmoid nodule (*arrowhead*), which were due to recurrent tumor. The patient was treated with radiation and chemotherapy. Of the gynecologic malignancies recurring at the vaginal cuff, cervical cancer is the most common, followed by endometrial cancer [9, 28, 29]. Focal thickening of the cuff on cross-sectional imaging and abnormal signal intensity or enhancement on MRI in conjunction with physical examination findings raise the suspicion of recurrent disease. The vagina can also be involved by direct extension of cervical cancer at initial presentation

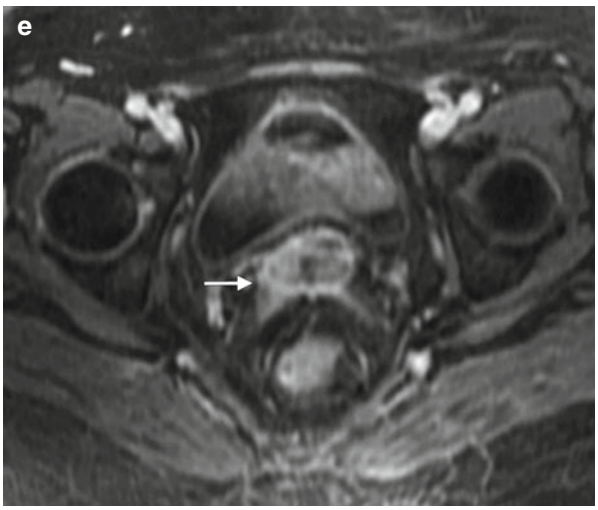

Fig. 4.13 (continued)

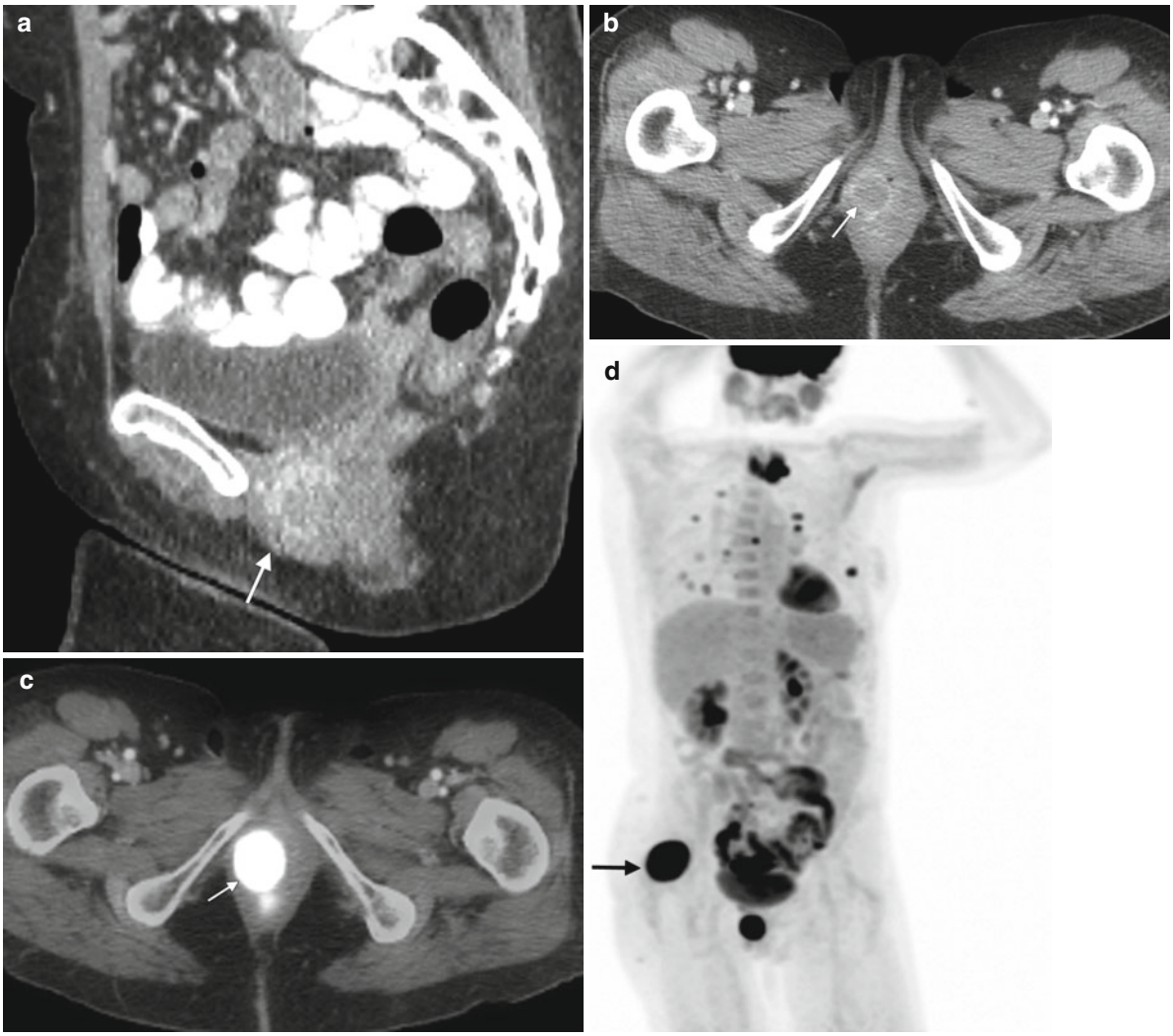

Fig. 4.14 Vaginal metastasis from uterine leiomyosarcoma. In this postmenopausal woman, an enlarging uterine mass on CT scans, which was FDG-avid on PET (*not shown*), proved to be a leiomyosarcoma at pathology. Followup CT scans showed a new mass (*arrow*) with peripheral enhancement in the distal vagina on sagittal (**a**) and axial (**b**) images. A fused axial PET-CT image (**c**) shows an FDG-avid vaginal mass (*arrow*). PET image (**d**) showed additional hypermetabolic lesions in the right gluteus muscle (*arrow*) and several lung nodules suspicious for metastases. Rarely, leiomyomas can occur in the vagina. They appear similar to uterine leiomyomas on MRI, with a circumscribed round margin, low signal intensity on T2-weighted images, and homogeneous enhancement [9, 30]. This appearance differs from the lobulated mass with heterogeneous, hyperintense appearance on T2-weighted images of leiomyosarcoma [1, 9, 27]. An enhancing, incidental vaginal metastasis in a patient presenting with a uterine leiomyosarcoma has been described in the literature [28]. High signal intensity of the mass on short inversion-time inversion recovery (STIR) images has also been reported with vaginal leiomyosarcoma [1]

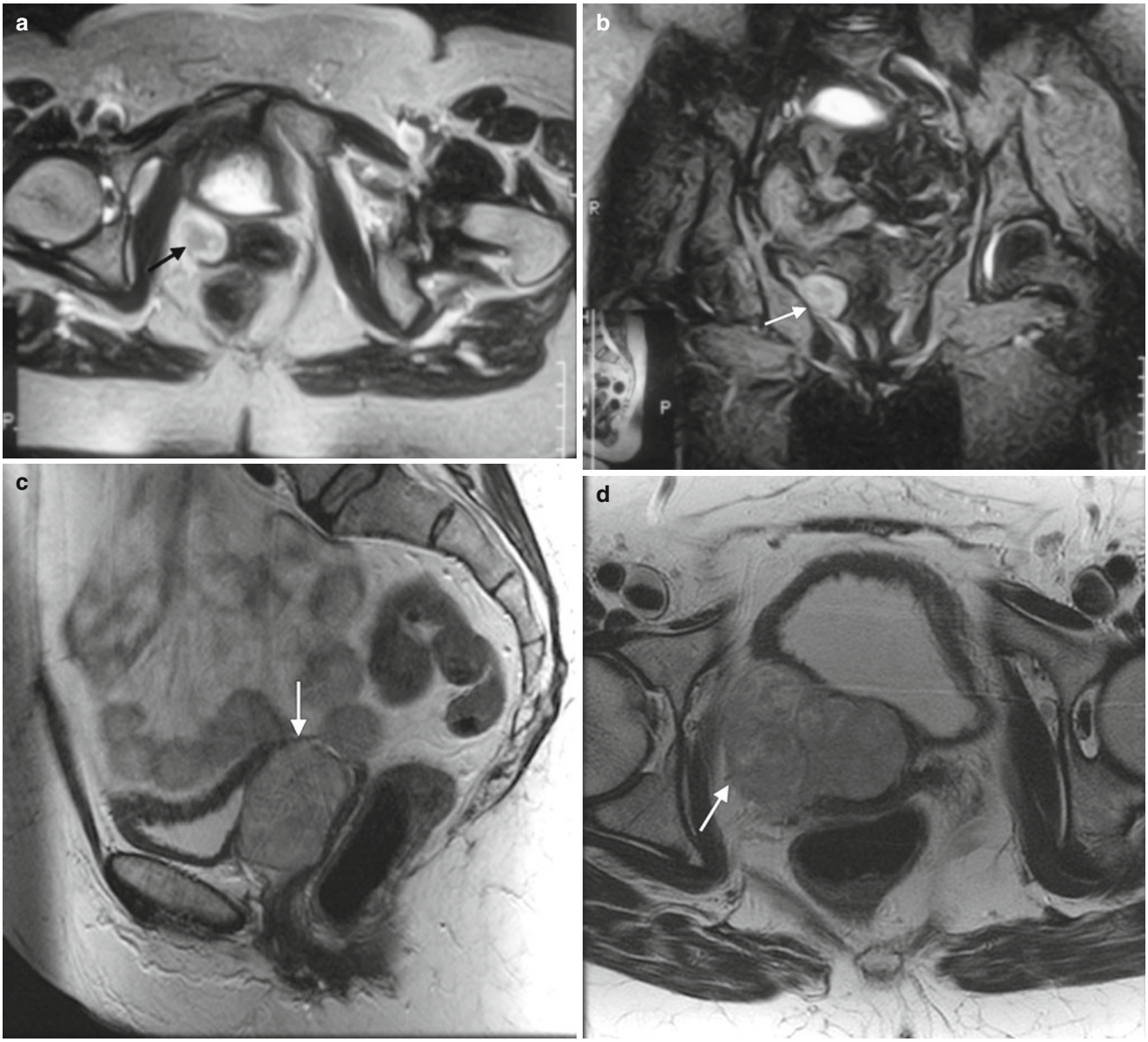

Fig. 4.15 Vaginal recurrence of leiomyosarcoma. This postmenopausal patient had a vaginal mass diagnosed on physical examination followed by MRI. T2-weighted MR images in the axial plane (**a**) and coronal plane (**b**) show a hyperintense mass (*arrow*) at the right cervicovaginal junction. The mass was primarily extrinsic to the vagina, and excision revealed leiomyosarcoma. A hysterectomy was performed without residual tumor in the vagina. A followup MRI 6 months later showed a recurrent mass at the vaginal cuff. T2-weighted MR images in the sagittal plane (**c**) and axial plane (**d**) show a mass with intermediate signal intensity (*arrow*) in the proximal vagina. T1-weighted axial MR images with fat saturation before contrast (**e**) and after contrast (**f**) show moderate, heterogeneous enhancement of the vaginal tumor recurrence (*arrow*). The patient subsequently developed bulky distant metastases as shown on CT scans of the lung (**g**) (*arrow*) and the liver (**h**) (*arrow*) and left adrenal

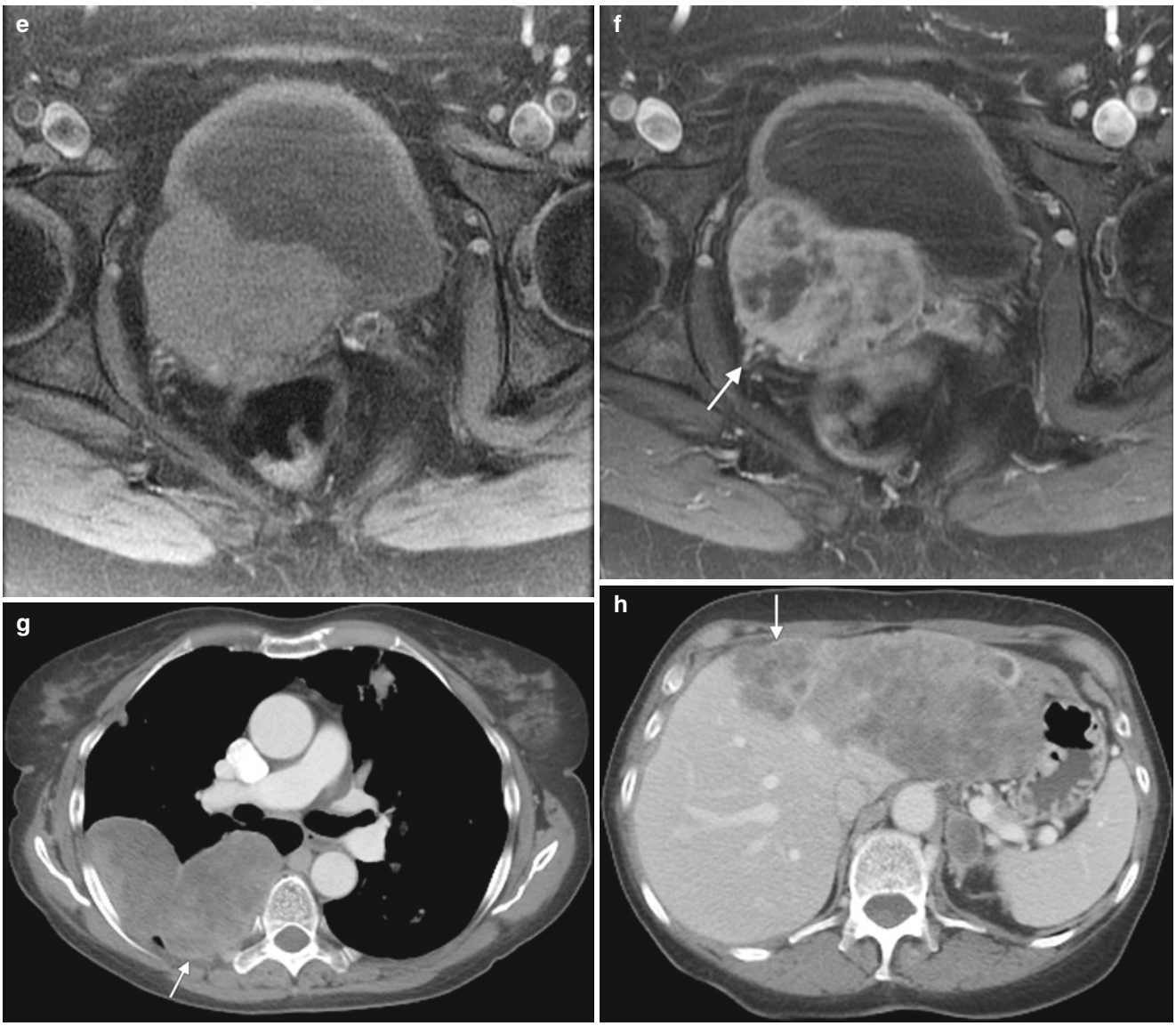

Fig. 4.15 (continued)

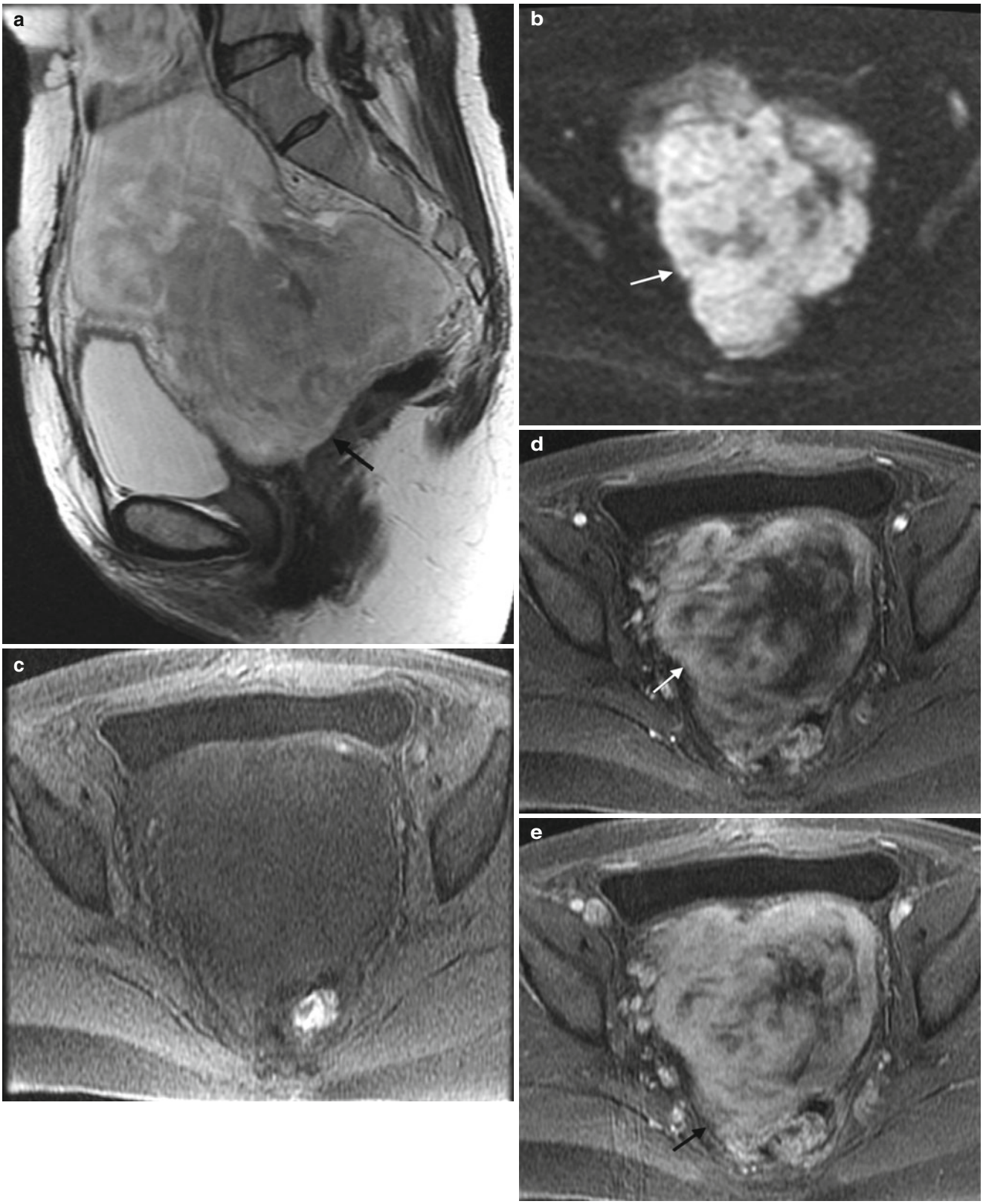

Fig. 4.16 Recurrent uterine leiomyosarcoma at the vaginal cuff. This perimenopausal woman presented with abdominal pain and a sensation of bladder pressure. Ultrasound and MRI revealed a uterine mass (*not shown*) measuring 15–20 cm, which was resected in its entirety; pathology showed leiomyosarcoma. The patient was treated with chemotherapy but had abdominal discomfort 6 months later, and imaging showed a large recurrent mass at the vaginal cuff. A sagittal T2-weighted MR image (**a**) shows a bulky mass (*arrow*) in the pelvis superior to the vagina. The mass had restricted diffusion (*arrow*) on a diffusion-weighted MR image (**b**). T1-weighted images with fat saturation before contrast (**c**) and after contrast (**d**, **e**) show heterogeneous, progressive enhancement of the tumor (*arrow*). The tumor was resected but recurred at the same site 3 months later, with additional sites of metastases

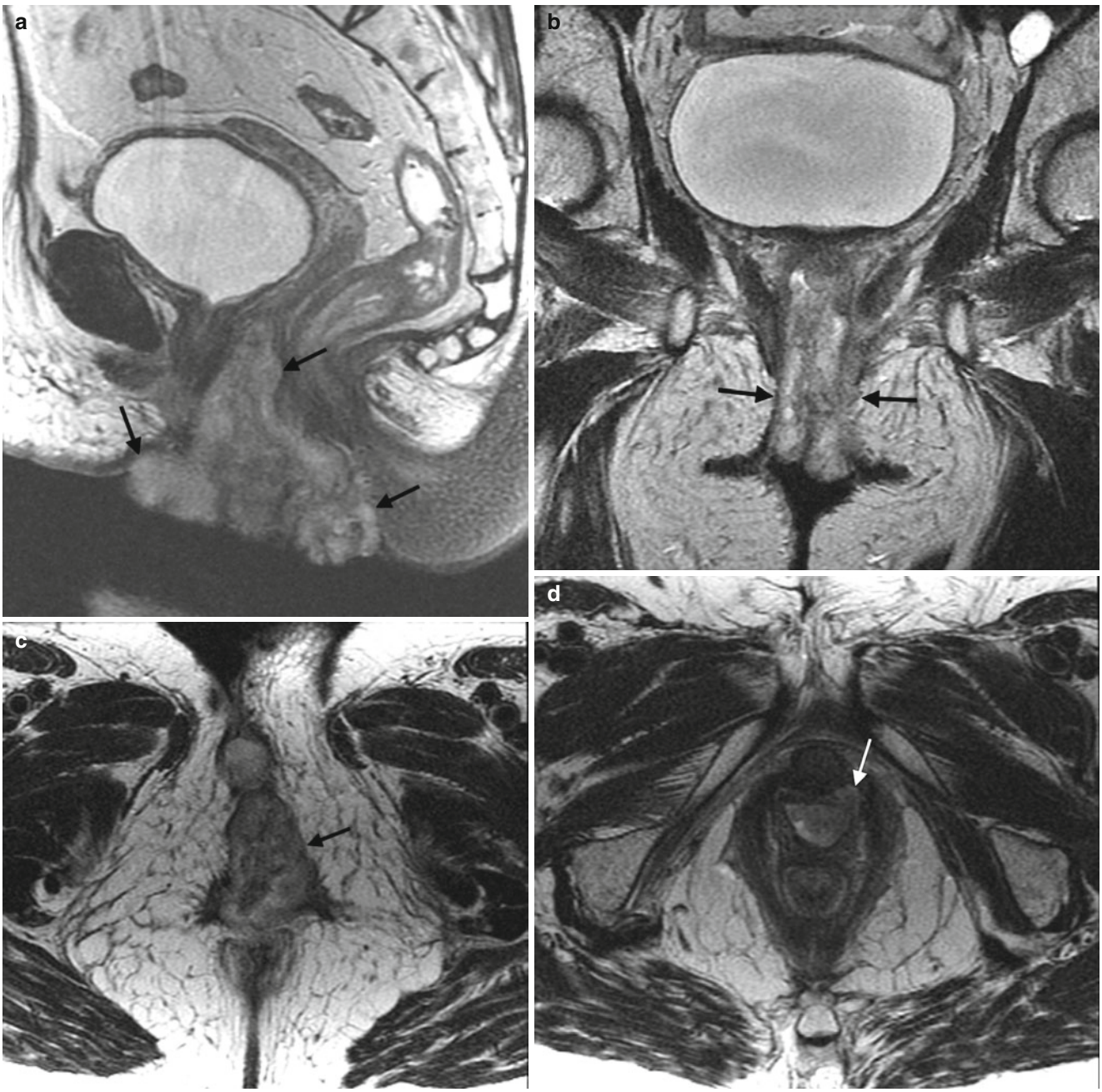

Fig. 4.17 Vulvar carcinoma invading the vagina. This postmenopausal woman had a history of squamous cell carcinoma of the vulva for several years. The patient had had several excisions of the local tumor as well as radiation therapy, and now presented with a fungating vulva mass. MRI showed a large, heterogeneous vulva mass extending into the vagina. T2-weighted MR images of the pelvis in the sagittal plane (**a**) and coronal plane (**b**) show a bulky vulva mass with intermediate signal intensity (*arrows*) distending the distal vagina. Transverse T2-weighted MR images of the vulva (**c**) and distal vagina (**d**) show the intraluminal vaginal mass (*arrow*). T1-weighted axial MR images with fat saturation before contrast (**e**) and after contrast (**f**, **g**) demonstrate peripheral enhancement in the mass (*arrow*). The mass (*arrow*) was avid on FDG-PET, as seen on an axial fused PET-CT image (**h**) and sagittal PET image (**i**). Resection revealed poorly differentiated, invasive squamous cell carcinoma

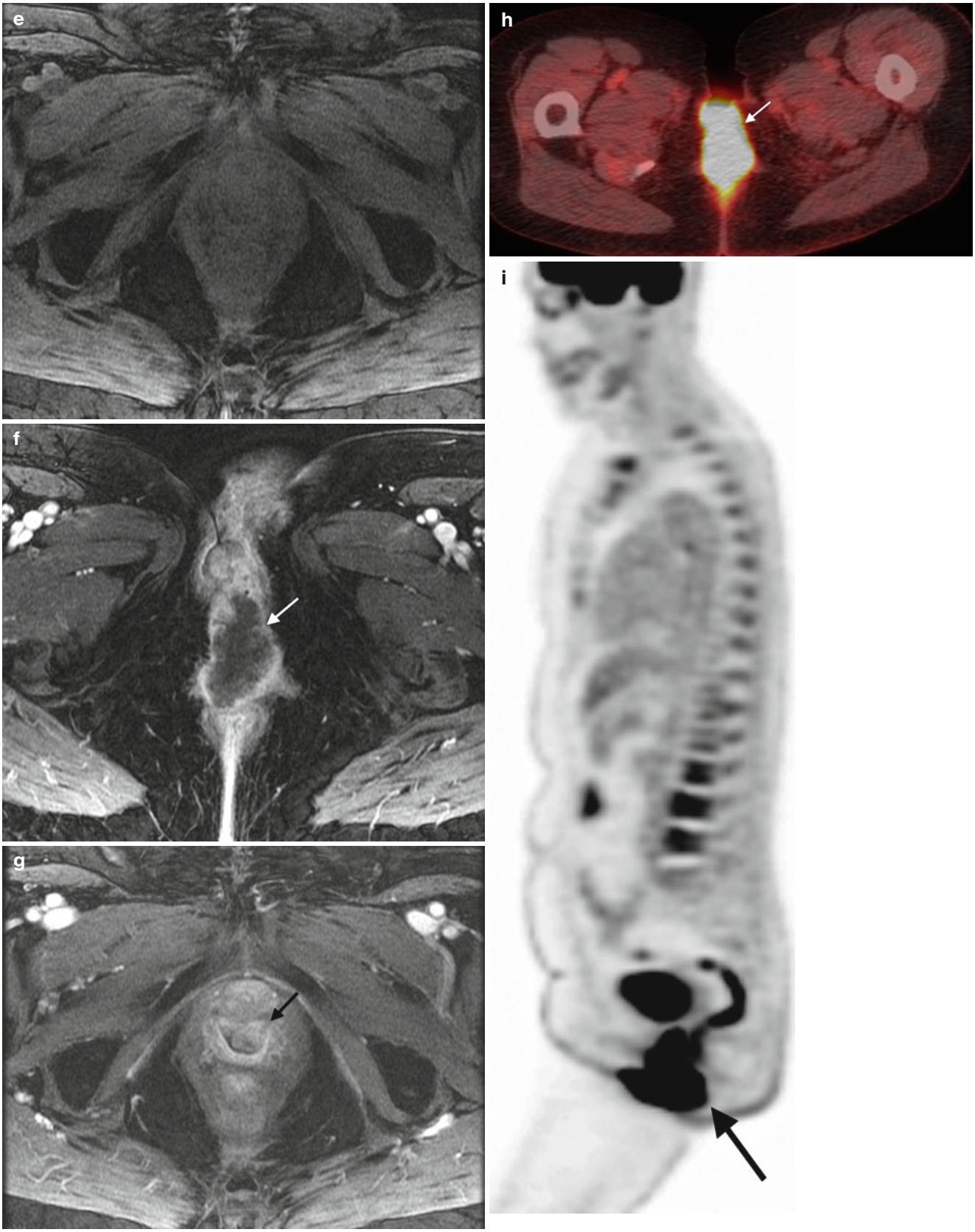

Fig. 4.17 (continued)

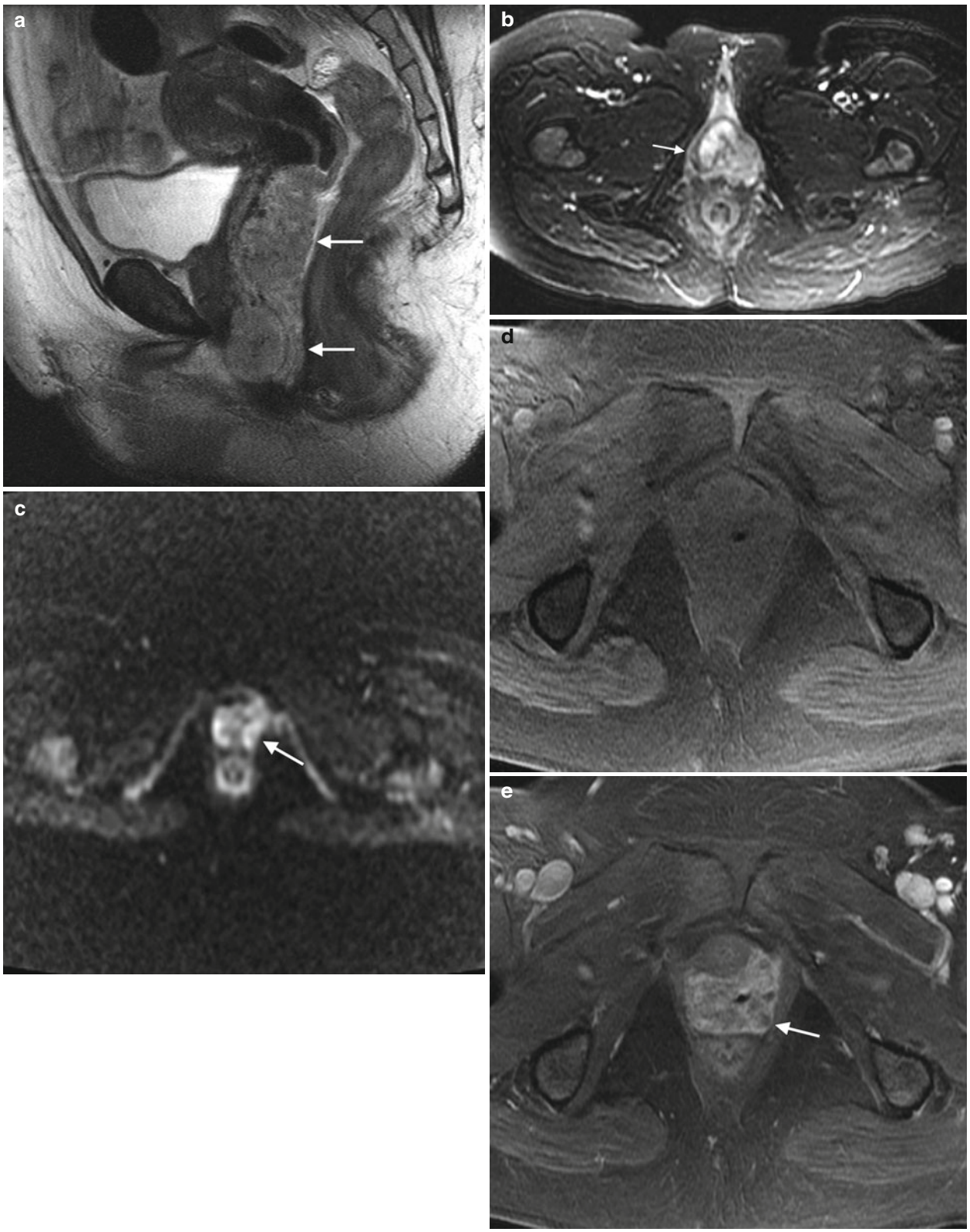

Fig. 4.18 Vaginal metastasis from renal cell carcinoma. This perimenopausal woman had an asymptomatic 12 cm renal cell carcinoma, which was discovered on imaging after an automobile accident. Two months after nephrectomy, the patient had heavy vaginal bleeding, which necessitated emergency surgery. Biopsy of the vaginal mass showed clear cell carcinoma, and the immunostaining profile was consistent with metastatic renal cell carcinoma. Initial MRI shows a vaginal mass (*arrows*) with intermediate signal intensity on sagittal (**a**) and axial (**b**) T2-weighted images. On an axial diffusion-weighted image (**c**), the mass had restricted diffusion (*arrow*). T1-weighted axial images with fat saturation before contrast (**d**) and after contrast (**e**) show enhancement of the vaginal mass. A followup sagittal T2-weighted image from MRI 1 month later (**f**) shows the vaginal tumor and a new myometrial mass (*arrow*). The patient was treated with pelvic radiation. The vaginal mass (*arrow*) persisted on sagittal reconstruction of a contrast-enhanced CT scan performed 6 months later (**g**)

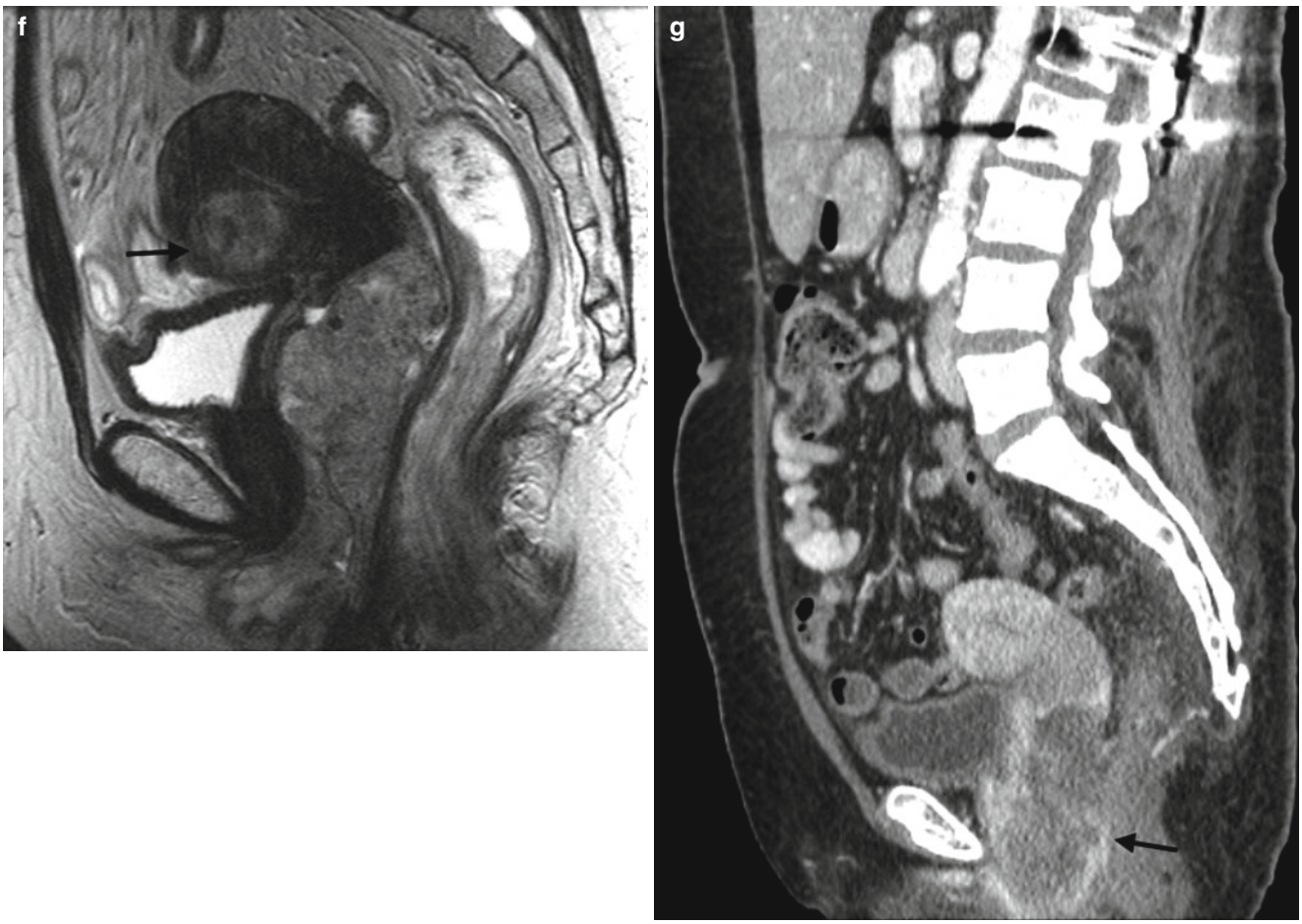

Fig. 4.18 (continued)

4.5 Complication of Vaginal Malignancy

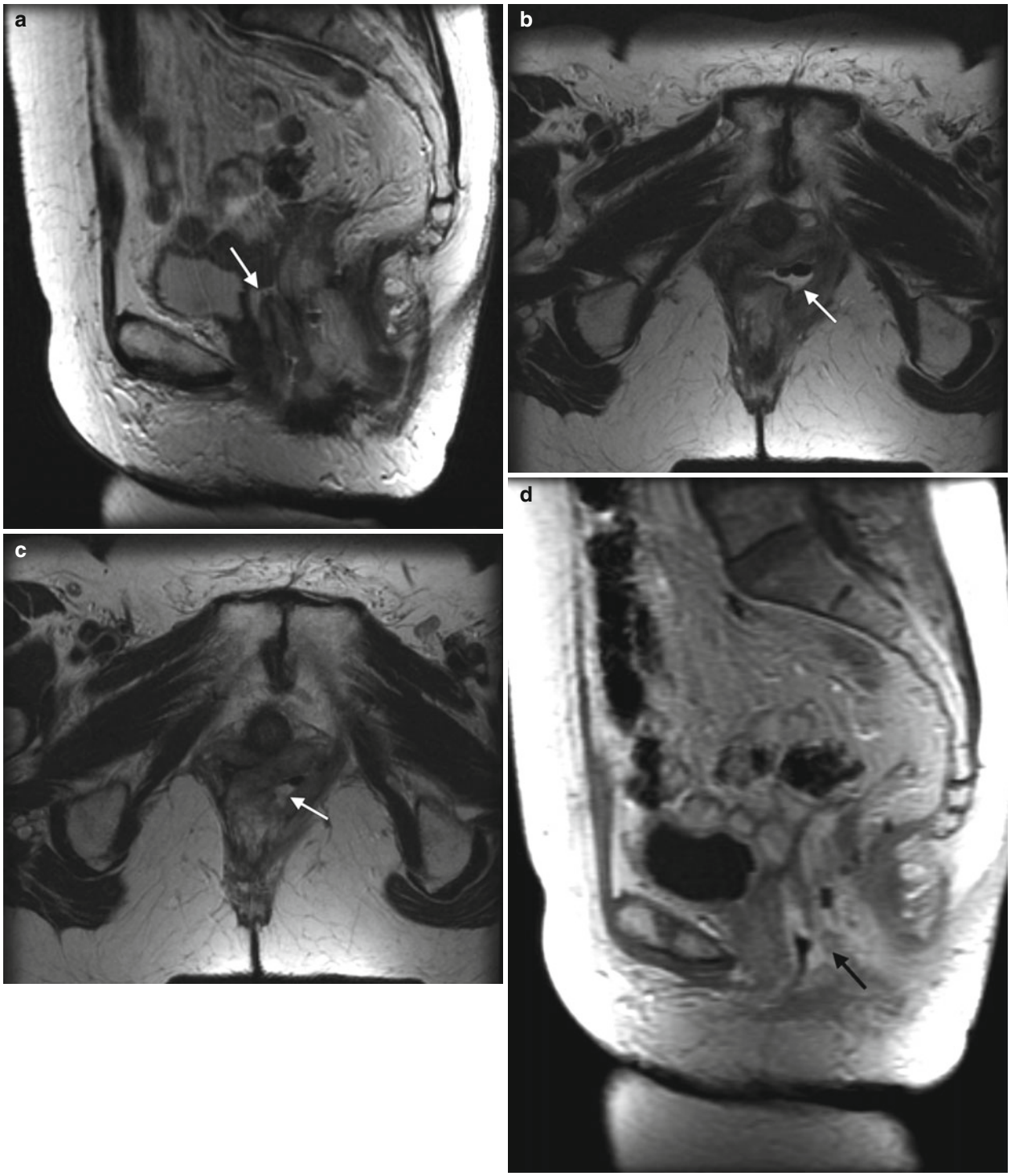

Fig. 4.19 Squamous cell carcinoma of the vagina with rectovaginal fistula. This postmenopausal patient had a history of endometrial cancer treated with vaginal brachytherapy 20 years ago. The patient now presented with vaginal discharge. Physical examination revealed nodularity of the vaginal mucosa most prominent along the posterior wall, as well as a rectal stricture. Biopsy of the vagina showed an invasive, moderately to poorly differentiated squamous cell carcinoma. A sagittal T2-weighted MR image (**a**) showed moderate diffuse thickening of the vagina (*arrow*), which was inseparable from the thickened rectum. Axial T2-weighted images (**b**, **c**) showed gas in the vagina (*arrow*) and a small fistulous tract with the rectum. A postcontrast sagittal T1-weighted image without fat saturation (**d**) shows diffuse enhancement of the vagina and rectum and a small fistulous tract (*arrow*). The patient was treated with chemoradiation and subsequently developed a vesicovaginal fistula, for which she was treated with urinary and colonic diversion with ileal conduit and colostomy. Vaginal fistulas to bowel or bladder can occur secondary to tumor, inflammation, radiation, and trauma [12, 31]. The fistulous tract and surrounding inflammation or mass are depicted with MRI and CT. Findings include obliteration of fat planes and adherence of the vagina to adjacent viscera, an enhancing fistulous tract, vaginal fluid or gas, and the transit of rectal or bladder contrast into the vagina

Acknowledgment The author wishes to thank Ms. Carolina Montalvo for her extensive help with preparing the images for publication.

References

1. Parikh JH, Barton DP, Ind TE, Sohaib SA. MR imaging features of vaginal malignancies. Radiographics. 2008;28:49–63.
2. Elkas JC, Berek JS. Vaginal cancer. UpToDate. www.uptodate.com. Accessed April 2012.
3. Chang SD. Imaging of the vagina and vulva. Radiol Clin North Am. 2002;40:637–58.
4. Park JM, Charnsangavej C, Yoshimitsu K, Herron DH, Robinson TJ, Wallace S. Pathways of nodal metastasis from pelvic tumors: CT demonstration. Radiographics. 1994;14:1309–21.
5. McMahon CJ, Rofsky NM, Pedrosa I. Lymphatic metastases from pelvic tumors: anatomic classification, characterization, and staging. Radiology. 2010;254:31–46.
6. Chang YC, Hricak H, Thurnher S, Lacey CG. Vagina: evaluation with MR imaging. Part II. Neoplasms. Radiology. 1988;169:175–9.
7. Brown MA, Mattrey RF, Stamato S, Sirlin CB. Pictorial essay: MRI of the female pelvis using vaginal gel. AJR Am J Roentgenol. 2005;185:1221–7.
8. Young P, Daniel B, Sommer G, Kim B, Herfkens R. Intravaginal gel for staging of female pelvic cancers—preliminary report of safety, distention, and gel-mucosal contrast during magnetic resonance examination. J Comput Assist Tomogr. 2012;36:253–6.
9. Walker DK, Salibian RA, Salibian AD, Belen KM, Palmer SL. Overlooked diseases of the vagina: a directed anatomic-pathologic approach for imaging assessment. Radiographics. 2011;31:1583–98.
10. Hricak H, Chang YC, Thurnher S. Vagina: evaluation with MR imaging. Part I. Normal anatomy and congenital anomalies. Radiology. 1988;169:169–74.
11. McCarthy S, Tauber C, Gore J. Female pelvic anatomy: MR assessment of variations during the menstrual cycle and with use of oral contraceptives. Radiology. 1986;160:119–23.
12. Siegelman ES, Outwater EK, Banner MP, Ramchandani P, Anderson TL, Schnall MD. High-resolution MR imaging of the vagina. Radiographics. 1997;17:1183–203.
13. FIGO Committee on Gynecologic Oncology. Current FIGO staging for cancer of the vagina, fallopian tube, ovary, and gestational trophoblastic neoplasia. Int J Gynecol Obstet. 2009;105:3–4.
14. Tsuda K, Murakami T, Kurachi H, Narumi Y, Kim T, Takahashi S, et al. MR imaging of non-squamous vaginal tumors. Eur Radiol. 1999;9:1214–8.
15. Gilles R, Michel G, Chancelier MD, Vanel D, Masselot J. Case report: clear cell adenocarcinoma of the vagina: MR features. Br J Radiol. 1993;66:168–70.
16. Fan SF, Gu WZ, Zhang JM. Case report: MR findings of malignant melanoma of the vagina. Br J Radiol. 2001;74:445–7.
17. Kim H, Jung SE, Lee EH, Kang SW. Case report: magnetic resonance imaging of vaginal malignant melanoma. J Comput Assist Tomogr. 2003;27:357–60.
18. Dahiya K, Jain S, Duhan N, Nanda S, Kundu P. Aggressive angiomyxoma of vulva and vagina: a series of three cases and review of literature. Arch Gynecol Obstet. 2011;283:1145–8.
19. Stewart ST, McCarthy SM. Case 77: aggressive angiomyxoma. Radiology. 2004;233:697–700.
20. Outwater EK, Marchetto BE, Wagner BJ, Siegelman ES. Aggressive angiomyxoma: findings on CT and MR imaging. AJR Am J Roentgenol. 1999;172:435–8.
21. Chien AJ, Freeby JA, Win TT, Gadwood KA. Aggressive angiomyxoma of the female pelvis: sonographic, CT, and MR findings. AJR Am J Roentgenol. 1998;171:530–1.
22. Agrons GA, Wagner BJ, Lonergan GJ, Dickey GE, Kaufman MS. From the archives of the AFIP. Genitourinary rhabdomyosarcoma in children: radiologic-pathologic correlation. Radiographics. 1997;17:919–37.
23. Kawakami S, Togashi K, Kojima N, Morikawa K, Mori T, Konishi J. MR appearance of malignant lymphoma of the uterus. J Comput Assist Tomogr. 1995;19:238–42.
24. Jenkins N, Husband J, Sellars N, Gore M. MRI in primary non-Hodgkin's lymphoma of the vagina associated with a uterine congenital anomaly. Br J Radiol. 1997;70:219–22.
25. McNicholas MM, Fennelly JJ, MacErlaine DP. Imaging of primary vaginal lymphoma. Clin Radiol. 1994;49:130–2.
26. Thyagarajan MS, Dobson MJ, Biswas A. Appearance of uterine cervical lymphoma on MRI: a case report and review of the literature. Br J Radiol. 2004;77:512–5.
27. Griffin N, Grant LA, Sala E. Magnetic resonance imaging of vaginal and vulval pathology. Eur Radiol. 2008;18:1269–80.
28. Cantisani V, Mortele KJ, Kalantari BN, Glickman JN, Tempany C, Silverman SG. Vaginal metastasis from uterine leiomyosarcoma. Magnetic resonance imaging features with pathological correlation. J Comput Assist Tomogr. 2003;27:805–9.
29. Fulcher AS, O'Sullivan SG, Segreti EM, Kavanagh BD. Recurrent cervical carcinoma: typical and atypical manifestations. Radiographics. 1999;19 Spec No:S103–16.
30. Shadbolt CL, Coakley FV, Qayyum A, Donat SM. MRI of vaginal leiomyomas. J Comput Assist Tomogr. 2001;25:355–7.
31. Kuhlman JE, Fishman EK. CT evaluation of enterovaginal and vesicovaginal fistulas. J Comput Assist Tomogr. 1990;14:390–4.

Vulvar Cancer

5

Weining Ma

Vulvar cancer is a rare malignancy, which accounts for about 4 % of female genital cancers. The average age of women diagnosed with invasive vulvar cancer is 70 years [1], but it is occurring with increasing frequency in younger women (<50 years of age), particularly those exposed to human papillomavirus (HPV).

About 85–90 % of vulvar cancers are squamous cell carcinoma (SCC), with two distinct pathways depending on whether the tumor is associated with HPV infection [2–5]. The HPV-negative vulvar SCC in older women (in the 7th and 8th decades) is assumed to be associated with vulvar inflammation or lichen sclerosis and typically is unifocal. HPV-positive vulvar cancer occurs in younger women and has a strong association with smoking and with vulvar intraepithelial neoplasm. Approximately 40 % of vulvar SCC can be linked to HPV [5]. These cancers tend to be early-stage disease with multifocal lesions and can occur with cervical cancer, vaginal cancer, or perianal cancer.

Melanoma is the second most common vulvar cancer (about 5–10 % of cases), followed by basal cell carcinomas, Bartholin gland cancers, sarcomas, adenocarcinomas, and Paget's disease [2, 6–11]. Aggressive angiomyxoma is a rare, locally aggressive myxoid mesenchymal neoplasm, preferentially arising in the pelvis and perineal region in women of reproductive age [12–14]. The tumors are generally regarded as benign and metastases are exceeding rare; overall, the prognosis is good [12–14]. However, local recurrence is cited in 30–40 % of cases, sometimes occurring as much as 15 years later [12]. Wide local excision is the treatment of choice. The tumor cells are characteristically positive for estrogen and progesterone receptors, suggesting a hormonal role in the development of the tumor.

The lymphatic drainage of vulvar cancers first occurs in superficial inguinal lymph nodes, followed by deep inguinal lymph nodes. Metastasis to deep pelvic lymph nodes such as the internal or external iliac lymph nodes is considered as a distant metastasis [2, 15–17]. Generally, lateralizing lesions (1 cm beyond the midline) drain to the ipsilateral superficial inguinal lymph nodes, whereas midline lesions can drain to either side.

Lymph node status is the single most important prognostic factor [18–20]. The 2009 revised FIGO staging system of vulvar cancers (Table 5.1) provides a better reflection of prognosis in patients with vulvar SCC [20]. Regardless of the diameter of the tumor, tumors with negative lymph nodes have a favorable prognosis [20]. The number of positive lymph nodes is a significant risk factor: For patients with one positive lymph node, 5-year disease-specific survival (DSS) is 77 % [20]. For patients with two or three node metastases, the DSS is similar, at about 62 % 5-year DDS [20]. The 5-year DSS is about 28 % for patients with four or more positive nodes [20]. Extranodal lymph node disease is an important risk factor, leading to a poor survival prognosis, compared with intranodal spread (Table 5.2) [20].

W. Ma, MD
Department of Radiology,
Memorial Sloan-Kettering Cancer Center,
1275 York Avenue, New York, NY 10065, USA

Department of Radiology, NewYork-Presbyterian Hospital/Weill
Cornell Medical Center Diagnostic Radiology,
520 East 70th Street, New York, NY 10021, USA
e-mail: maw@mskcc.org

O. Akin (ed.), *Atlas of Gynecologic Oncology Imaging*, Atlas of Oncology Imaging,
DOI 10.1007/978-1-4614-7212-4_5, © Springer Science+Business Media New York 2014

Table 5.1 2009 FIGO classification of vulvar squamous cell carcinomas

FIGO category	Description
Stage I	**Tumor confined to the vulva**
IA	Lesions ≤2 cm in size, confined to the vulva or perineum and with stromal invasion ≤1.0 mm, no nodal metastasis
IB	Lesions >2 cm in size or with stromal invasion >1.0 mm, confined to the vulva or perineum, with negative nodes
Stage II	Tumor of any size with extension to adjacent perineal structures (1/3 lower urethra, 1/3 lower vagina, and anus) with negative nodes
Stage III	Tumor of any size with or without extension to adjacent perineal structures (1/3 lower urethra, 1/3 lower vagina, and anus) with positive inguinofemoral lymph nodes
IIIA	With 1 lymph node metastasis (≥5 mm) or 1–2 lymph node metastases (<5 mm)
IIIB	With 2 or more lymph node metastases (≥5 mm) or 3 or more lymph node metastases (<5 mm)
IIIC	With positive nodes with extracapsular spread
Stage IV	Tumor invades other regions (2/3 upper urethra, 2/3 upper vagina) or distant structures
IVA	Tumor invades any of the following: Upper urethra and /or vaginal mucosa, bladder mucosa, rectal mucosa, or fixed to pelvic bone, or fixed or ulcerated inguinofemoral lymph nodes
IVB	Any distant metastasis including pelvic lymph nodes

From van der Steen [20], with permission
FIGO International Federation of Gynecology and Obstetrics

Table 5.2 Survival rates for squamous cell carcinoma of the vulva, by stage

	Relative survival rate (%)	
Stage	5 Years	10 Years
I	93	87
II	79	69
III	53	46
IV	29	16

5.1 Diagnosis and Treatment

Diagnosis of vulvar cancer and the assessment of superficial lymph node involvement are usually done clinically. Vulvar cancer is surgically staged. The early-stage vulvar cancers are treated surgically by radical wide excision of the primary lesion and inguinal lymphadenectomy [21–24]. Appropriate groin node dissection is the single most important factor in reducing mortality from vulvar cancer. Surgery is the treatment of choice even for locally advanced cancer, although neoadjuvant radiation and chemotherapy may be used either to enable surgery in a case initially deemed "inoperable" or to avoid exenteration in elderly patients.

5.2 Imaging

Imaging has a limited role in the evaluation of the primary site of disease in vulvar cancer, as this is readily assessed clinically. MRI may be helpful in evaluating the extent of disease in patients with advanced tumor involving the perineum, vagina, and anal canal. MRI is the best imaging modality to accurately assess the local extent of vulvar cancers for surgical planning, and to detect lymph node metastasis [25–32]. The size of the tumor and the involvement of the urethra, anus, and levator ani muscle can be defined with MRI. Clinically relevant information is whether the mass is less than or larger than 2 cm in size, as well as the depth of invasion. Nodes are evaluated by location, size, and morphology, with necrosis and large size having a high degree of specificity for metastatic disease. MRI can be highly specific in identifying abnormal lymph nodes by using size criteria and morphology, but sensitivity is low, ranging from 40 to 50 % [26]. Other criteria, including the ratio of the short axis to the long axis (S/L ratio), contour, presence of cystic changes/necrosis, loss of fatty hilum, and signal intensity, have been examined to improve sensitivity and accuracy [26]. The S/L ratio is a good quantitative maker for diagnosing lymph node metastasis, with 87 % sensitivity and 81 % specificity [26]. Protocols for MRI imaging of the pelvis use a torso coil with the patient in a supine position. Images include axial T1-weighted images, axial T2-weighted images with fat saturation, and axial, sagittal, and coronal T2-weighted precontrast and multiphase postcontrast images.

CT scans are useful to detect lymph nodes or other distant metastases. The use of positron emission tomography (PET) for patients with vulvar cancer is undefined [27, 28]. One prospective surgical study was performed, evaluating fluorodeoxyglucose (FDG)-PET before groin surgery for patients with vulvar cancer. PET/CT had a sensitivity of 67 %, a specificity of 95 %, a positive predictive value of 86 %, and a negative predictive value of 86 % [27, 28]. For detection of extranodal disease, FDG-PET demonstrated high specificity and accuracy [27, 28].

Ultrasound is used mainly to detect abnormal inguinal lymph nodes or for ultrasound-guided biopsy of suspicious lymph nodes. Focused ultrasound imaging is performed using a high-frequency transducer (linear 8–18 MHz).

5.3 Recurrence

Recurrence of vulvar cancer is most common in the vulvar region (43–50 %) [33–35]. The groin is the site of 6–30 % of recurrences. Groin recurrences develop earlier than vulvar recurrences, and the prognosis of these patients is much worse. Pelvic recurrences are rare, constituting about 5 % of all recurrences. Distant recurrences make up 8–23 % of all recurrences and are associated with a dismal prognosis.

5.4 Normal Anatomy

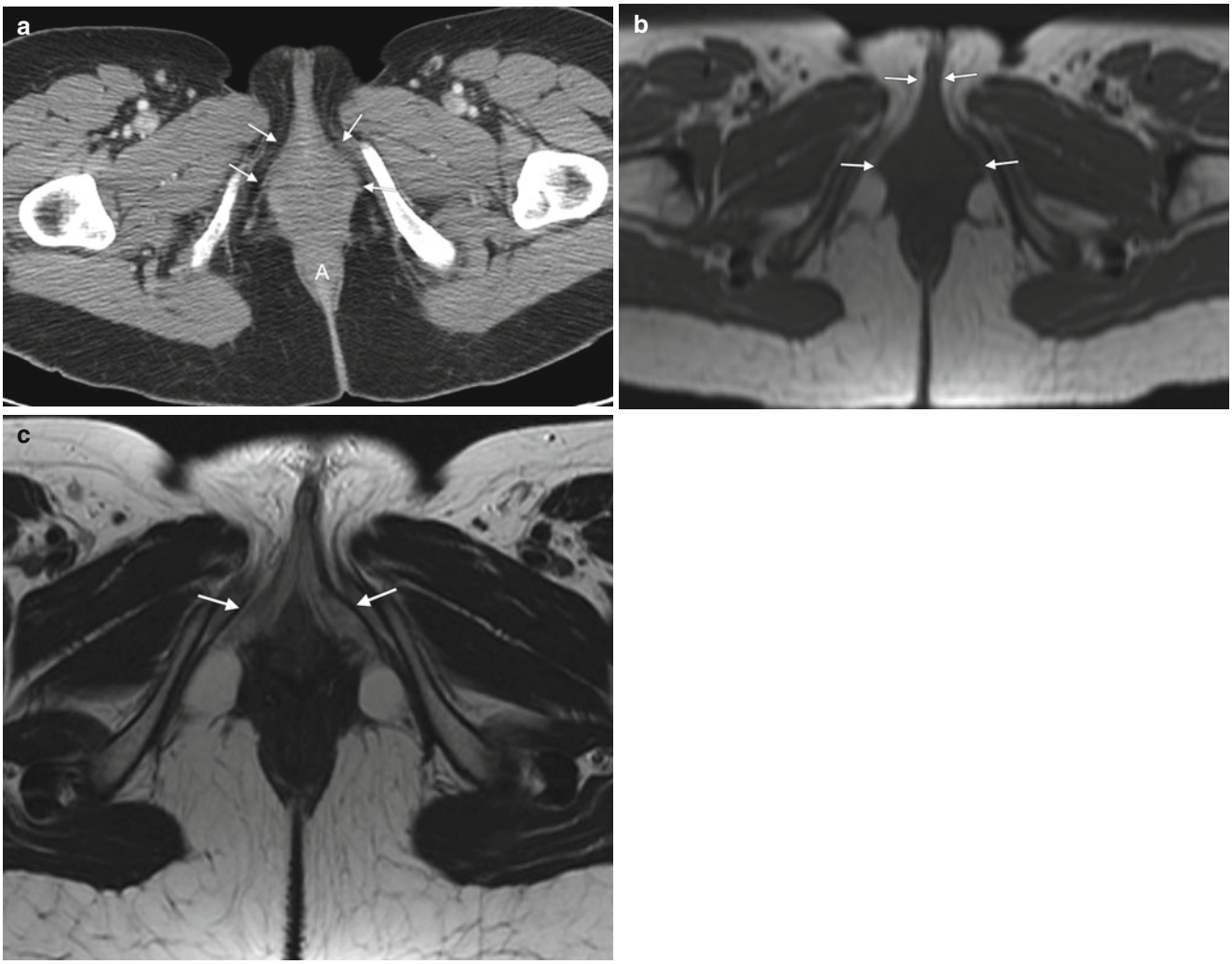

Fig. 5.1 The vulva refers to external female genitalia. It is comprised of the mons pubis, labia majora, labia minora, clitoris, vestibular bulb, vestibular glands, and the vestibule of the vagina. It appears as a triangular soft-tissue structure within the perineum, bounded by the symphysis pubis anteriorly, the anal sphincter posteriorly, and the ischial tuberosities laterally. (**a**) An axial contrast-enhanced CT scan shows the vulva (*arrows*) situated anterior to the anus (*A*). (**b**) Axial T1-weighted MR imaging demonstrates the vulva as intermediate in signal intensity (*arrows*). (**c**) Axial T2-weighted MR imaging shows the vulva as having intermediate to high signal intensity (*arrows*)

5.5 Vulvar Squamous Cell Carcinoma

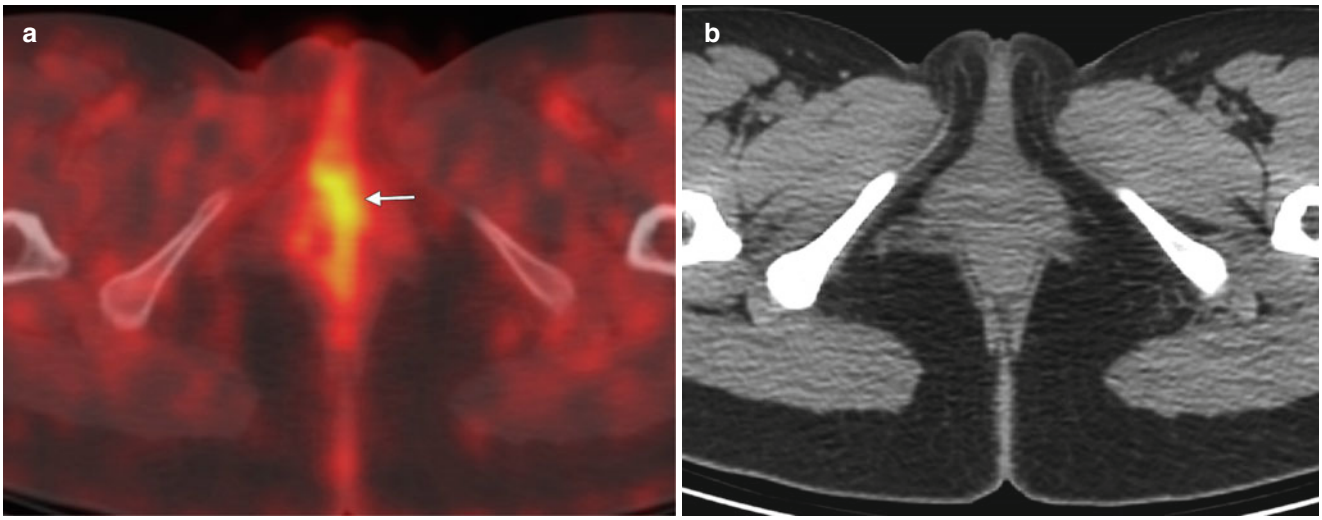

Fig. 5.2 Stage I vulvar squamous cell carcinoma (SCC). Currently, the standard treatment for vulvar cancers includes radical wide excision of the primary lesion with at least 1 cm of clear surgical margin [21–24], with unilateral or bilateral lymphadenectomy. Appropriate groin node dissection is the single most important factor in reducing mortality from vulvar cancer. However, the morbidity associated with lymphadenectomy is considerable. Sentinel lymph node excision is now being recommended in selected patients with early-stage SCC as a means to avoid the operative morbidity associated with inguinofemoral lymphadenectomy [15–17]. The optimal candidates for sentinel lymph node mapping are patients who have a lesion less than 4 cm in diameter with nonpalpable groin lymph nodes. The combination of radiotracer and blue dye is the most accurate technique for sentinel node detection. Patients with a positive sentinel node should undergo a full inguinofemoral lymphadenectomy followed by postoperative radiation therapy to the involved groin and pelvis. However, if sentinel lymph nodes are negative, no further treatment is indicated. The false negative rate of sentinel node biopsy is extremely low, 2–5 %. This 28-year-old woman presented with approximately 1 year of clitoral irritation. A right vulvar biopsy showed invasive SCC. The lesion was 0.8 cm in size, with depth of invasion of 1 mm or less (stage I disease). (**a**) An axial fused fluorodeoxyglucose positron emission tomography (FDG-PET)/CT scan showed mild focal tracer uptake in the vulvar region (*arrow*), without evidence of nodal involvement or distant metastatic disease. (**b**) The CT component of the PET/CT scan without contrast enhancement did not show any obvious vulvar lesion. CT has poor contrast resolution, however, so it does not delineate this mass. The patient underwent radical vulvectomy, including clitorectomy with bilateral sentinel lymph node dissection

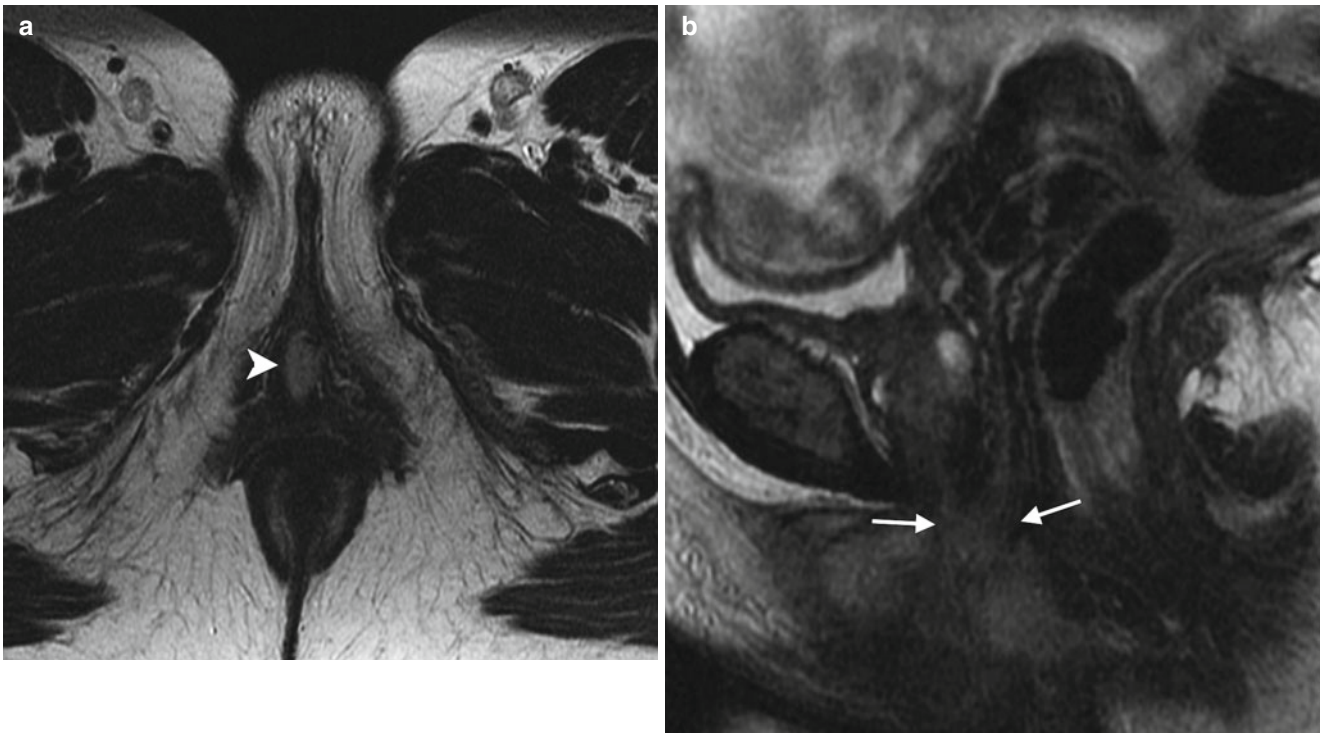

Fig. 5.3 Stage II vulvar squamous cell carcinoma (SCC), positive for human papillomavirus (HPV). In the vulva, about 40 % of malignancies can be linked to HPV [5]. Most cases of HPV-associated vulvar SCC occur in association with the HPV types known to be oncogenic: HPV 16, 18, or 33. HPV-positive vulvar SCC occurs in younger women and has strong association with smoking and with vulvar intraepithelial neoplasm (VIN). These cancers tend to be early-stage disease with multifocal lesions and can be combined with cervical cancer, vaginal cancer, or perianal cancer. A vulvar lesion was recently diagnosed in this 47-year-old woman, a long-time smoker. The lesion showed moderately differentiated SCC and was suggested to be HPV-positive on biopsy. Axial T2-weighted MR image (**a**) and a sagittal T2-weighted image (**b**) showed a midline vulvar mass with high signal intensity (*arrowhead*), extending to and abutting the posterior aspect of the urethral meatus and the most distal part of the vagina (*arrows*). Another axial T2-weighted image (**c**) showed a borderline-enlarged left external iliac lymph node (*curved arrow*). An axial T1-weighted image with gadolinium (**d**) demonstrated avid enhancement of the vulvar mass (*arrowhead*). Axial fused FDG-PET/CT scans (**e**, **f**) showed tracer uptake of the vulvar mass (*arrowhead*) and only low-grade uptake in the left external iliac lymph node (*curved arrow*), which was likely a reactive lymph node (stage II disease). Sentinel lymph node mapping using Tc-99m sulfur colloid and blue dye showed two hot and blue left superficial inguinal lymph nodes. Both left superficial inguinal lymph nodes were removed during the surgery and were proven to be benign lymph nodes by pathology. Lymph flow passes from the primary tumor to the sentinel lymph node and afterwards to other nonsentinel lymph nodes. Thus, the sentinel lymph node is the first lymph node that received lymphatic drainage from a lesion on the vulva [15–17]. If the sentinel lymph node is free of metastatic disease, the rest of the nodes in the lymphatic chain theoretically should also be free of tumor

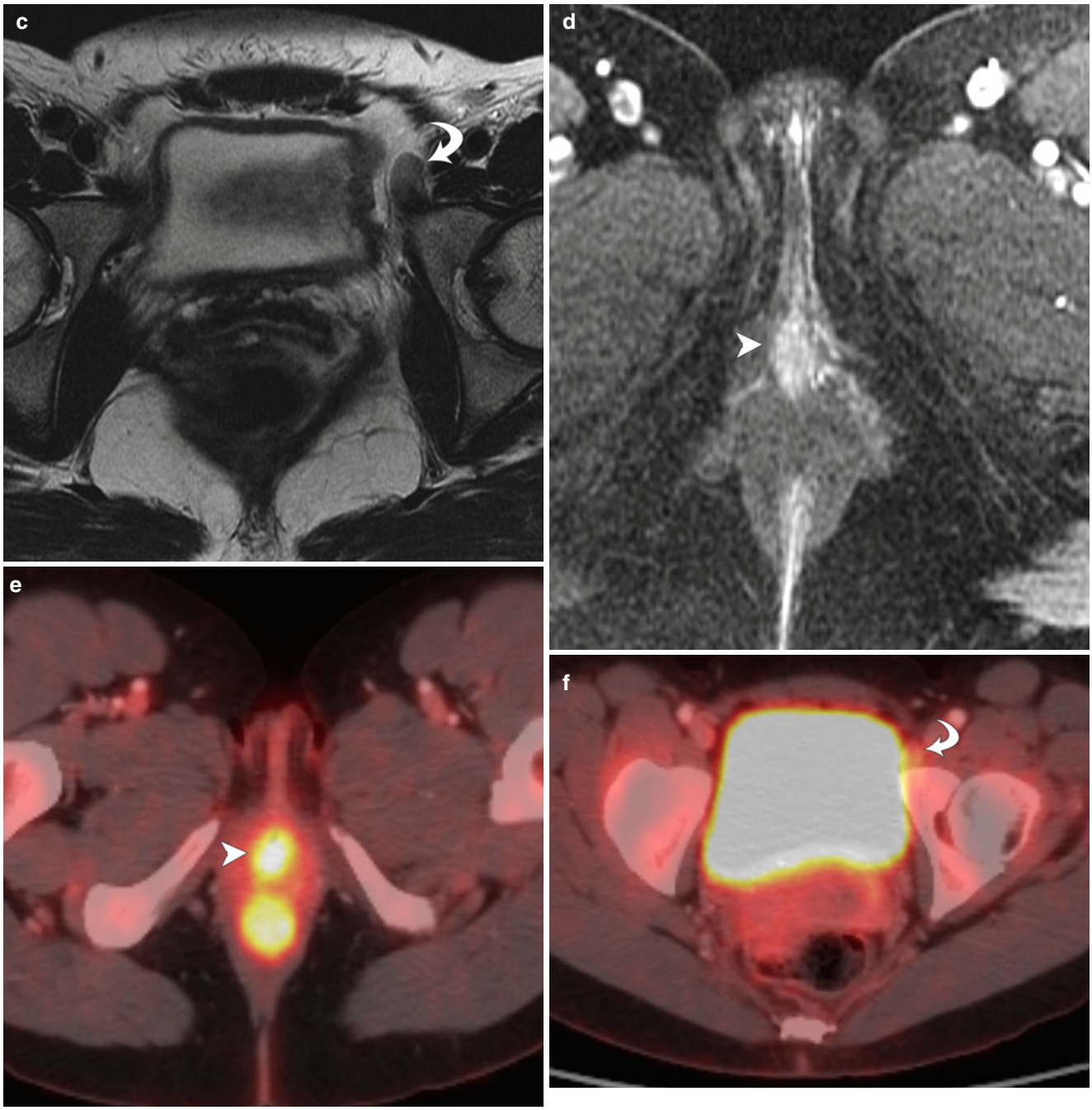

Fig. 5.3 (continued)

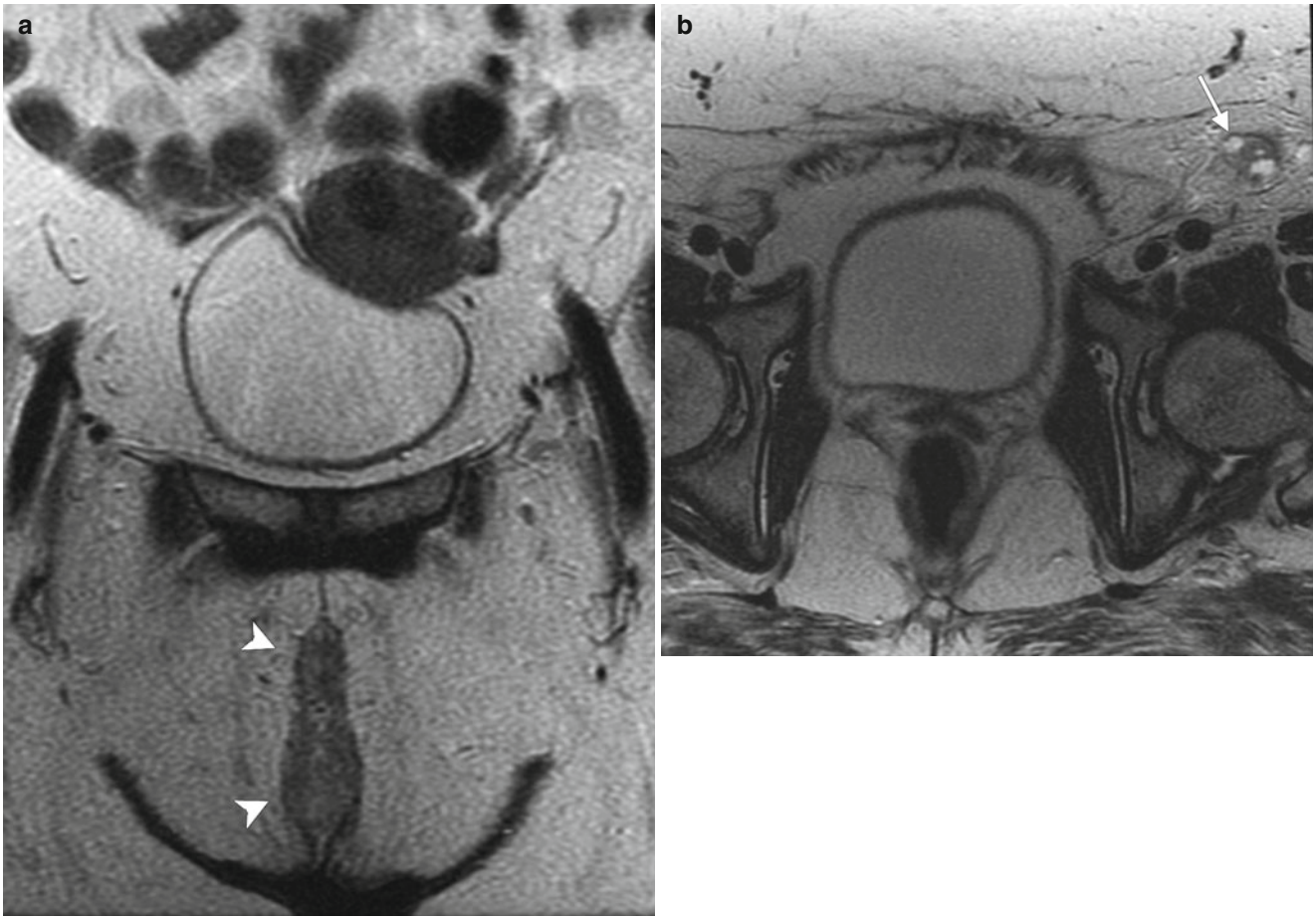

Fig. 5.4 Stage III vulvar squamous cell carcinoma (SCC). The lymphatic drainage of the vulva has been studied extensively. Typically, vulvar carcinoma metastasis is through nodal spread, which occurs first in superficial inguinal lymph nodes, followed by deep inguinal lymph nodes (below the cribriform fascia). Metastasis to deep pelvic lymph nodes, such as the internal or external iliac lymph nodes, is considered to be a distant metastasis [2, 12]. Generally, lateralizing lesions (1 cm beyond the midline) drain to the ipsilateral superficial inguinal lymph nodes, whereas midline lesions can drain to either side. It is extremely rare for lateralizing vulvar cancers to spread to the contralateral inguinal lymph nodes if there is no evidence of ipsilateral lymph node metastases. Likewise, it is unusual for the deep inguinal lymph nodes to be involved in the absence of superficial inguinal lymph node spread [15]. This 56-year-old woman complained of pruritus and tenderness in the vulvar region for more than 1 year. Recently, right vulvar biopsy showed invasive SCC. (**a**, **b**) Coronal and axial T2-weighted MR imaging showed a midline vulvar mass with high signal intensity (*arrowheads*) and an enlarged left superficial inguinal lymph node with cystic change (*arrow*). (**c**, **d**) Axial T1-weighted imaging with gadolinium demonstrated avid enhancement in the vulvar mass (*arrowheads*) and a left superficial inguinal lymph node containing cystic change (*arrow*). (**e**) Axial fused FDG-PET/CT imaging demonstrated tracer uptake in the left superficial inguinal lymph node (*arrow*) (stage III disease). The patient underwent neoadjuvant chemoradiation followed by partial vulvectomy and left inguinal lymph node dissection

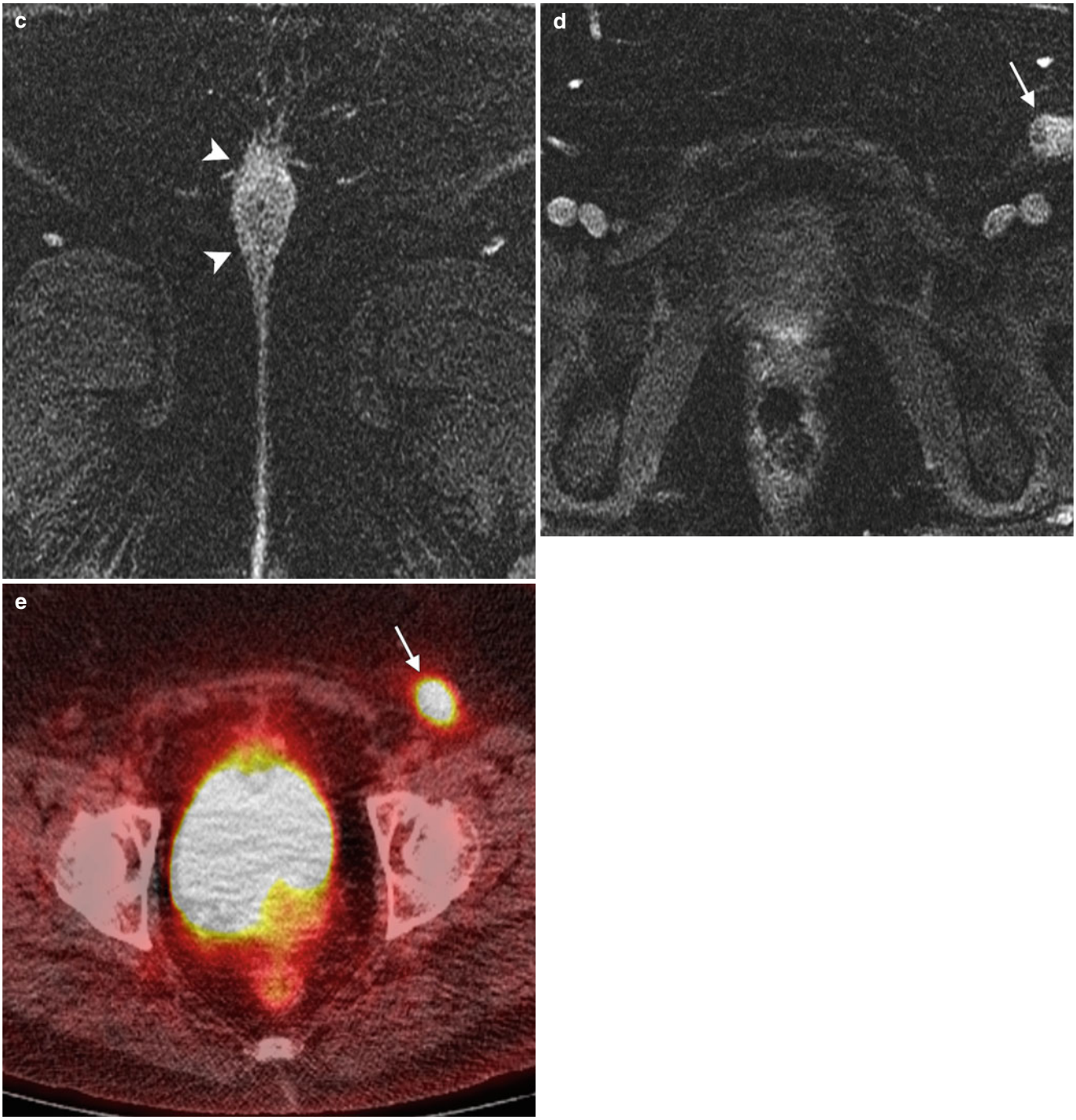

Fig. 5.4 (continued)

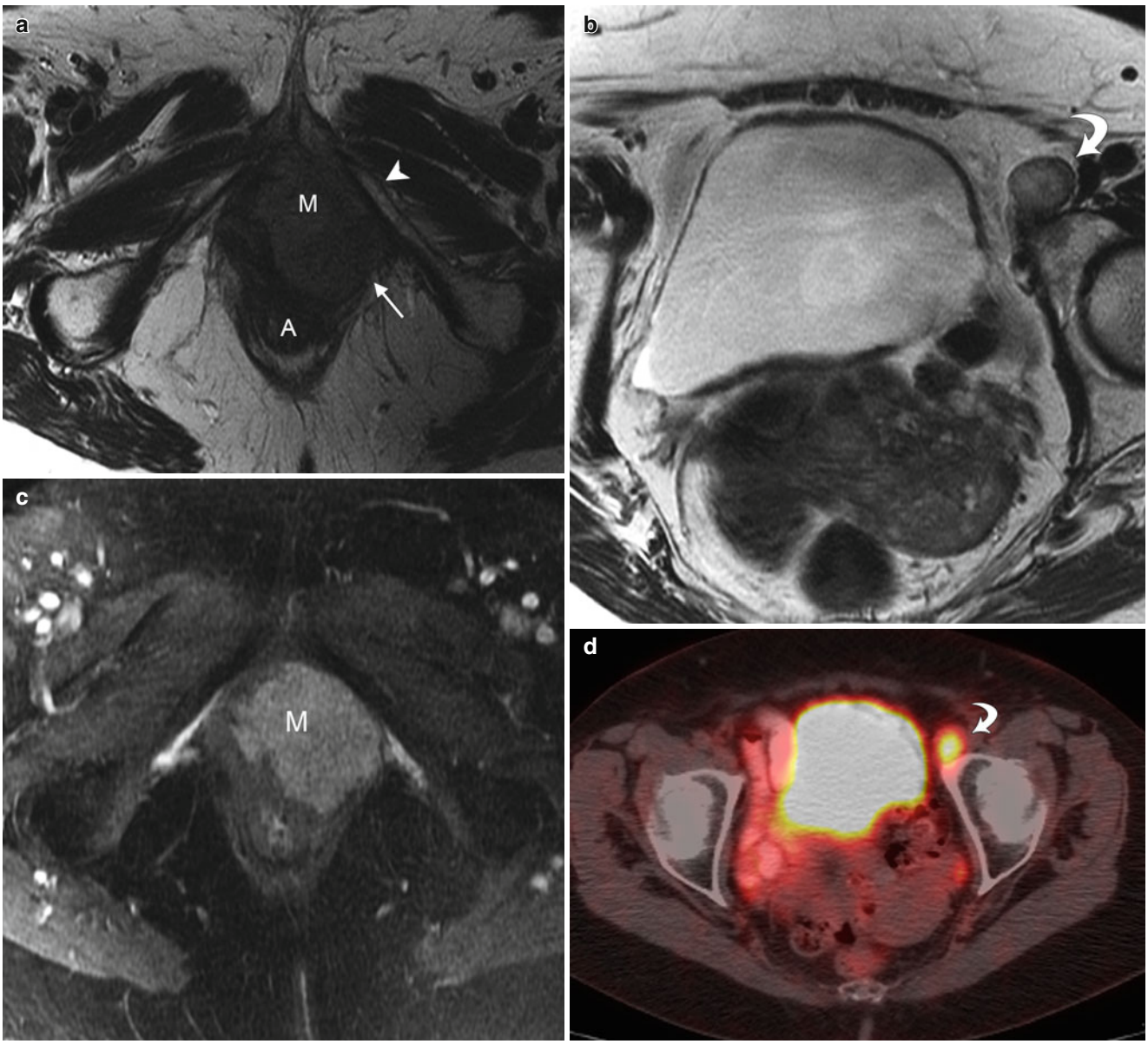

Fig. 5.5 Stage IV vulvar squamous cell carcinoma (SCC). This 80-year-old woman complained of irritation and enlargement of the left labia for several months. Left labial biopsy showed invasive SCC. (**a**, **b**) Axial T2-weighted MR imaging showed a high signal intensity mass in the left labia (*M*) and an enlarged left external iliac lymph node (*curved arrow*). The left labial mass invades through the pelvic floor, with involvement of the posterolateral urethra, lower vagina, and anal wall (*A*). The mass invaded the left levator ani muscle (*arrow*), and fixed to the left inferior pubic ramus (*arrowhead*). (**c**) Axial T1-weighted imaging with gadolinium showed avid enhancement of the left labial mass (*M*). (**d**, **e**) Axial and coronal fused FDG-PET/CT scans demonstrated tracer uptake of left labial mass (*arrow*) and left external iliac lymph node (*curved arrow*). Left external iliac lymph node metastasis is considered to be distant metastasis. Therefore, this is stage IVB disease

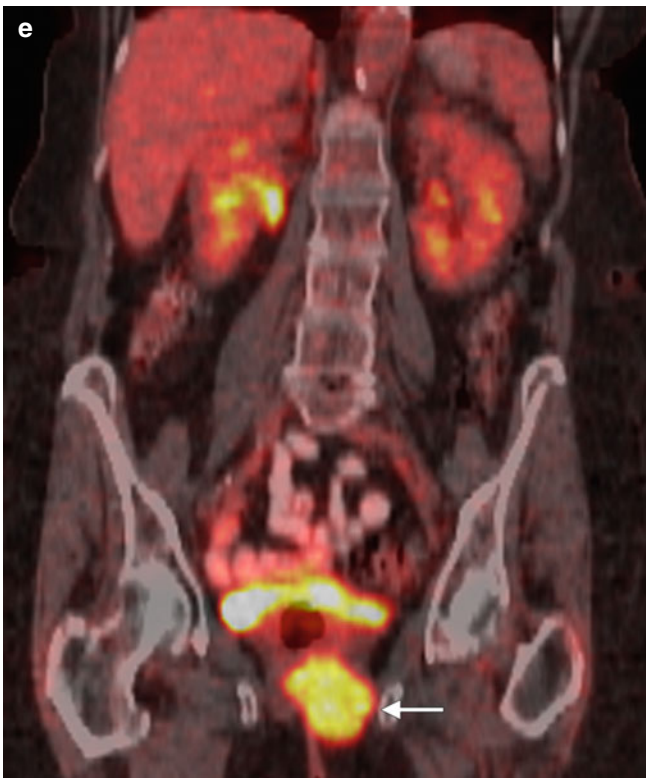

Fig. 5.5 (continued)

5.6 Local Recurrence of Vulvar Squamous Cell Carcinoma

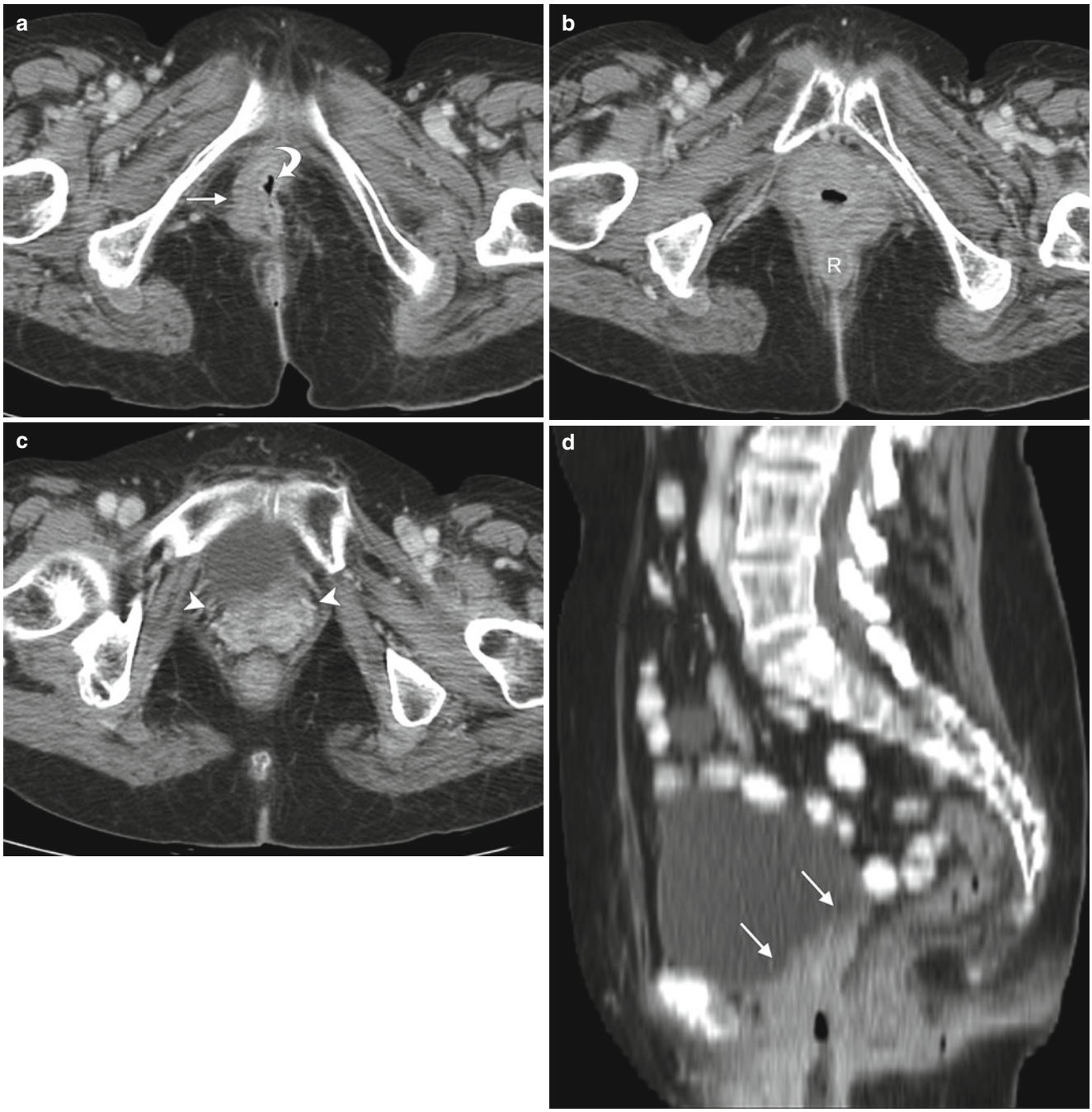

Fig. 5.6 Local recurrence of vulvar squamous cell carcinoma (SCC). The most common site of recurrence for vulvar cancer is the vulvar region (43–54 %) [34]. The groin is the site of 6–30 % of recurrences. Groin recurrences usually develop earlier than vulvar recurrences, and prognosis is much worse compared with patients with a recurrence on the vulva. Though local recurrences may be controlled with a new, wide local excision, radiotherapy, or both, groin recurrences are usually fatal [34, 35]. Pelvic recurrences are rare, accounting for about 5 % of all recurrences. Distant recurrences comprise 8–23 % of all recurrences and are associated with a dismal prognosis. This 75-year-old woman had a long history of squamous urothelial cancer, which was being treated by urologists. She developed vulvar SCC years ago and was treated with radiation at another institution. Now she presents with a right vulvar recurrent mass. Axial contrast-enhanced CT images (**a**–**c**) and a sagittal reformatted CT scan (**d**) showed a right vulvar mass (*arrow*), which involved the urethra (*curved arrow*), rectum (*R*), and lower vagina (*arrowheads*). There was no evidence of lymph node or distant metastases

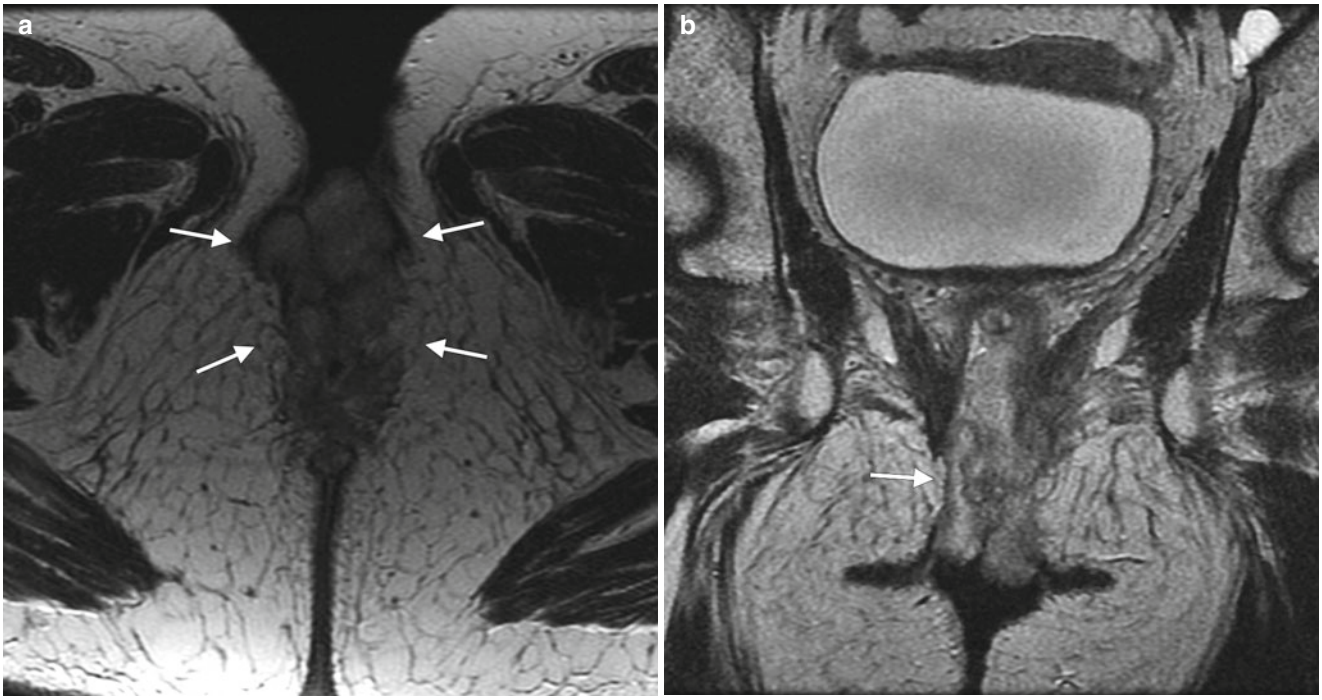

Fig. 5.7 Local recurrence of vulvar squamous cell carcinoma (SCC). Pelvic exenteration has progressively evolved into a potentially curative salvage therapy for locally advanced disease, and for central pelvic recurrence after prior radiation [36–38]. However, it comes with significant risks, associated morbidity, and impact on quality of life. The procedure-related mortality is approximately 3–5 %, and morbidity is also high, with complication rates approaching 60 % [37]. Imaging studies such as PET/CT and ultrasound-guided fine needle aspiration, as well as laparoscopic evaluation, have enabled physicians to more accurately assess the extent of disease preoperatively, refining the choice for candidates for exenteration [36–38]. This 78-year-old woman underwent radical vulvectomy and bilateral inguinal lymph node dissection for vulvar SCC 7 years ago. There was no evidence of inguinal or distant metastases at that time, but 3 years later she developed local recurrent disease, which was treated with wide excision and chemoradiation therapy. Recently, she presented with locally advanced current disease. (**a**–**c**) Axial, coronal, and sagittal T2-weighted MR imaging showed a vulvar mass with high signal intensity (*arrows*), which invades the urethra and anus. (**d**) Axial T1-weighted imaging with gadolinium showed avid enhancement of the vulvar mass (*arrow*). (**e**) Coronal fused FDG-PET/CT imaging showed tracer uptake of the mass (*arrow*), determined to be locally advanced disease without evidence of distant metastases on PET/CT. The patient underwent total pelvic exenteration with reconstruction. Unfortunately, she had postoperative complication (abdominal sepsis) and was admitted to the intensive care unit. Three months later, she developed extensive distant metastases, including pleural, lung, and liver metastases

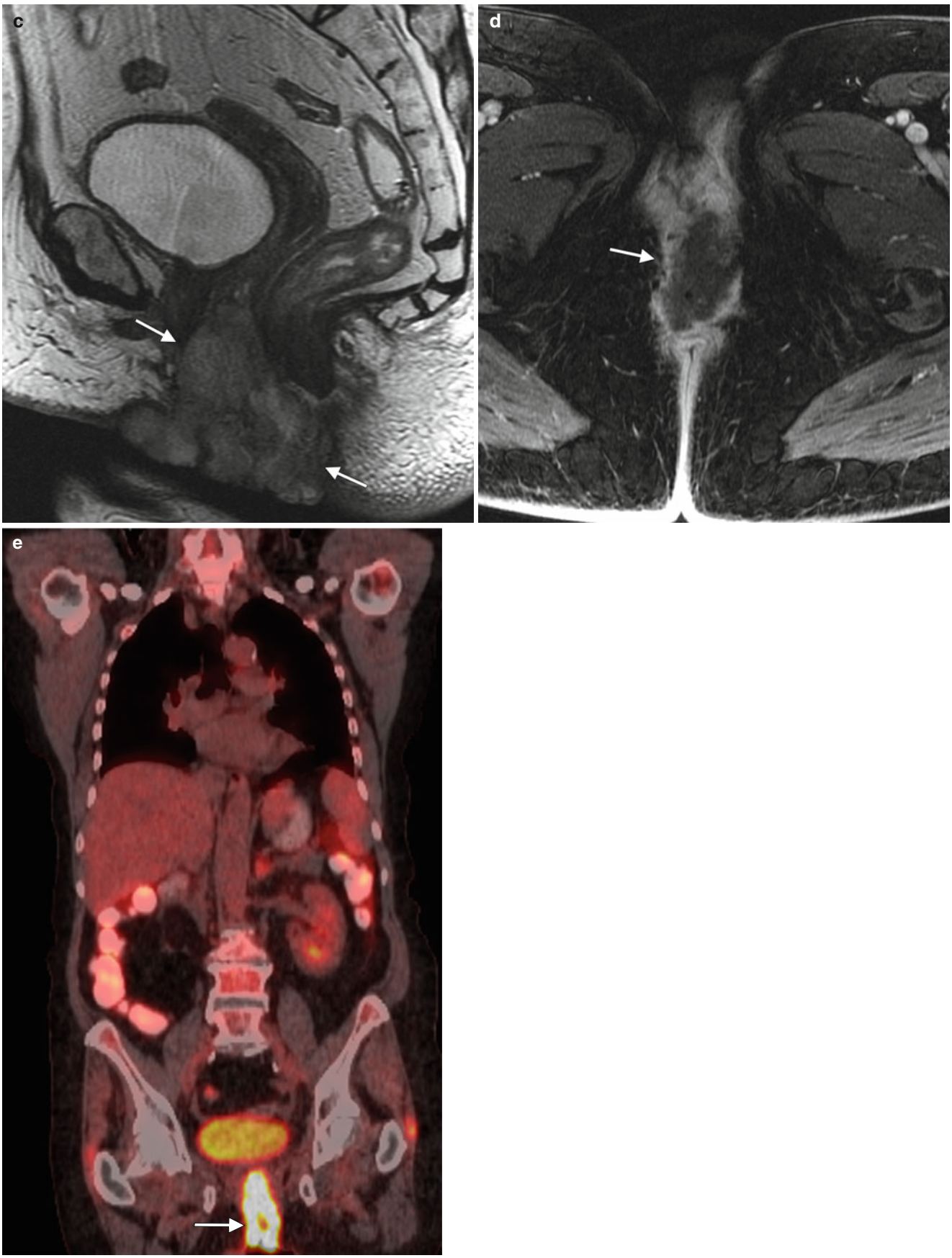

Fig. 5.7 (continued)

5.7 Other Vulvar Malignancies

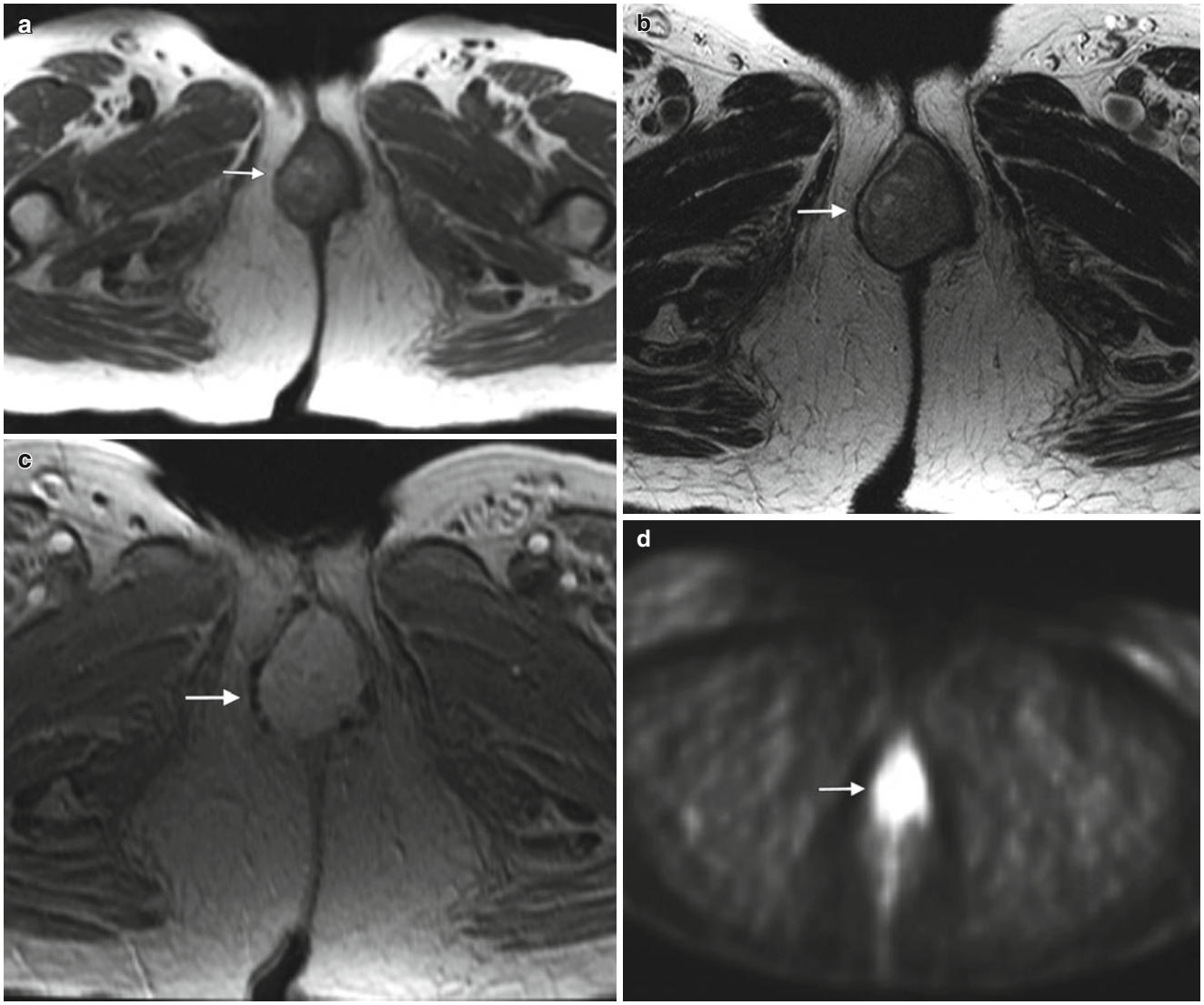

Fig. 5.8 Vulvar melanoma. Melanoma is the second-most-common vulvar cancer histology, accounting for about 5–10 % of primary vulvar cancers. It represents a subtype of cutaneous melanoma, with similar prognostic and staging factors. The most recent American Joint Committee on Cancer (AJCC) 2009 staging system for cutaneous melanoma (Tables 5.3, 5.4, 5.5, and 5.6) is applicable to vulvar melanoma [7, 8]. Vulvar melanoma is an aggressive disease, carries a poor prognosis (Table 5.7), and tends to recur locally as well as to develop distant metastases through hematogenous dissemination [6–9]. Surgical excision represents the single best definitive therapy for this neoplasm, which has a limited response to both chemotherapy and radiotherapy [8]. This 68-year-old woman had a history of vulvar melanoma and underwent vulvectomy 9 years ago. She developed local recurrence 7 years ago, which was treated with surgical excision. Recently, she noted some bright red blood in the perineal area. On physical examination, a periurethral mass in the vulvar region was noted and biopsy revealed recurrent melanoma. An axial T1-weighted MR image (**a**) and an axial T2-weighted image (**b**) showed a periurethral mass (*arrow*) in the vulvar region, which had high signal intensity on both the T1- and T2-weighted images. A vulvar melanoma typically shows high signal intensity on T1-weighted images because of the paramagnetic effect of the melanin content. Occasionally, the signal on a T1-weighted image may be low or intermediate in cases with low melanin content within the lesion (amelanotic melanoma). An axial T1-weighted image with gadolinium (**c**) showed avid enhancement of the mass (*arrow*). An axial FDG-PET scan (**d**) demonstrated tracer uptake of the mass (*arrow*), and an axial contrast-enhanced CT scan (**e**) showed multiple pulmonary metastases

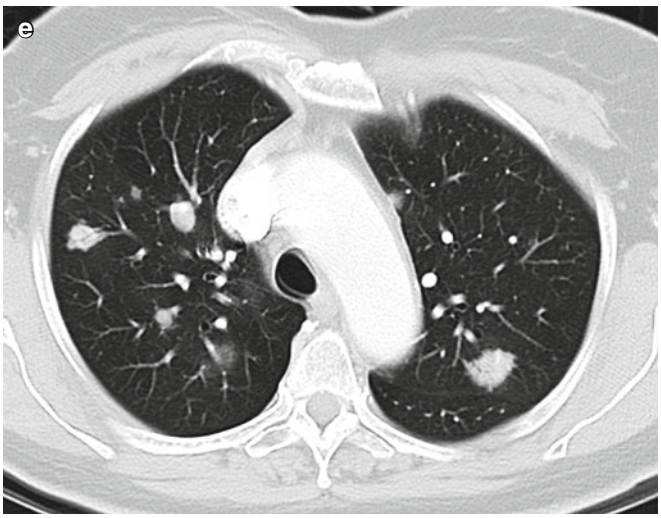

Fig. 5.8 (continued)

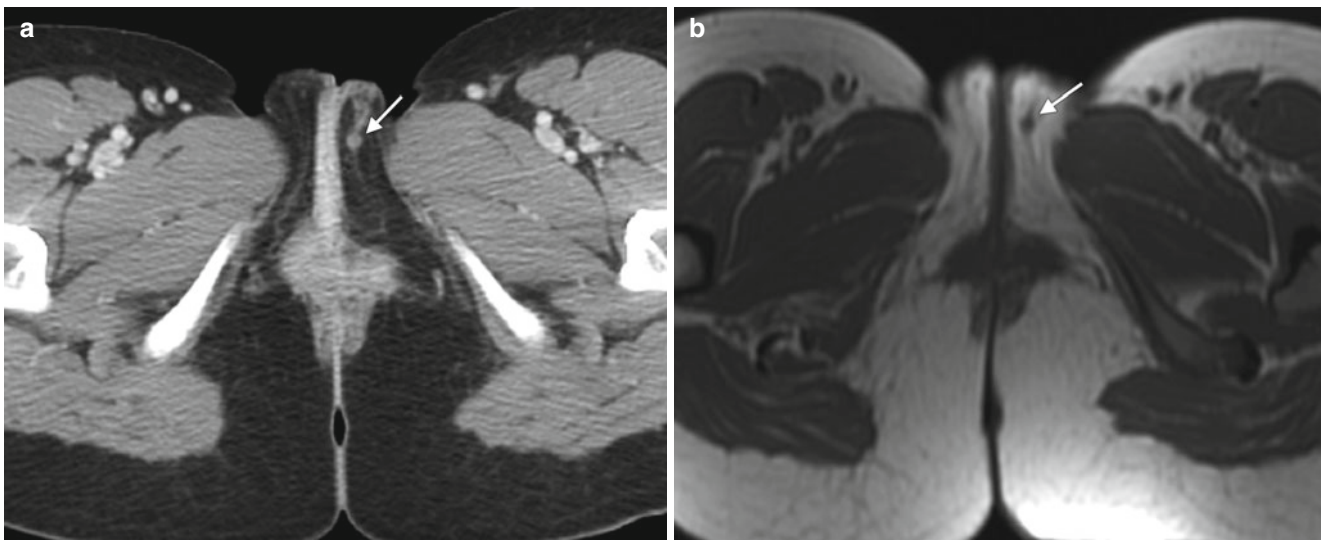

Fig. 5.9 Recurrent vulvar epithelioid sarcoma. Primary vulvar sarcomas are rare, constituting less than 3 % of all vulvar malignancies. The multiple histology types of vulvar sarcomas include leiomyosarcoma, fibrosarcoma, dermatofibrosarcoma, malignant fibrohistosarcoma, angiosarcoma, Ewing's sarcoma, angiomyxoma, rhabdosarcoma, and others. Epithelioid sarcoma is especially rare, with fewer than 20 cases reported in the literature. The clinical behavior of vulvar epithelioid sarcomas is not well understood, but there are some suggestions that their biologic behavior is more aggressive than the behavior of those occurring at other distal anatomic sites. Most of these sarcomas occur in younger patients in distal extremities, but proximal locations, vascular invasion, mitotic activity, and necrosis are associated with more aggressive behavior and worse prognosis [9–11]. Metastasis occurs primarily by lymphatics and later hematologically to distant sites. Regional lymph node involvement and pulmonary metastasis would be most common, but liver and scalp metastases also have been reported. There has been no real improvement in survival with either adjuvant chemotherapy or radiation. This 24-year-old woman presented with a recurrent mass in the left labia. Her original mass was noticed about a year ago; at that time she underwent left radical partial vulvectomy and left inguinal lymphadenectomy. Her pathology slides were reviewed at our hospital and confirmed epithelioid sarcoma, proximal type. (**a**) An axial contrast-enhanced CT scan showed a tiny enhancing mass in the left labia (*arrow*). An axial T1-weighted MR image (**b**), an axial T2-weighted image with fat saturation (**c**), and a T1-weighted image with fat saturation and gadolinium (**d**) demonstrated a mass in the left labia (*arrow*), which had low signal intensity on T1-weighted imaging, high signal intensity on T2-weighted images, and avid enhancement with the use of contrast

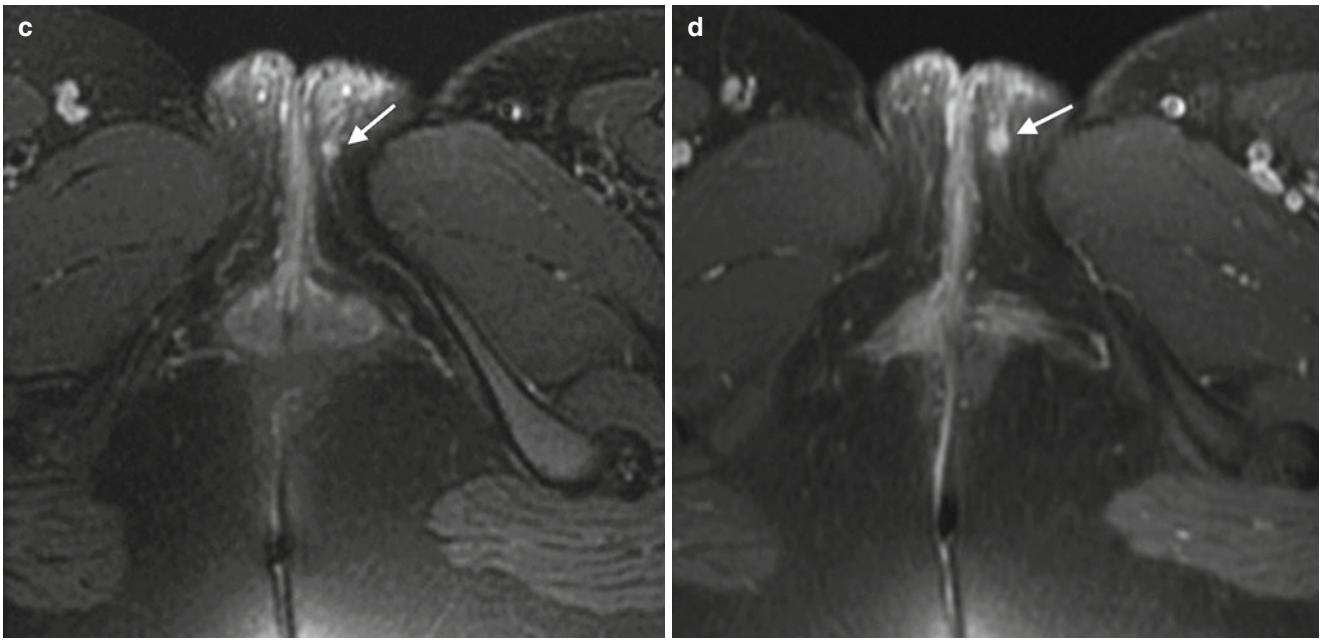

Fig. 5.9 (continued)

Fig. 5.10 Bartholin's gland carcinoma. Primary carcinoma of the Bartholin's gland is a rare malignancy accounting for about 2–3 % of vulvar malignancy [39, 40]. Bartholin's neoplasm may arise from the gland or from its duct. Adenocarcinoma and squamous cell carcinoma occur with approximately equal frequency, with a variety of less frequent histology types also being observed [39]. An enlargement of the Bartholin's gland in a postmenopausal woman is a concern for malignancy [9]. Survival is closely related to the status of inguinal and femoral lymph nodes and stage. Therapeutic principles in the management of vulvar cancer at other sites appear to be appropriate for the management of Bartholin's gland carcinoma [40]. This 48-year-old woman initially presented with a left vulvar mass. An axial T1-weighted MR image (**a**) and axial and sagittal T2-weighted images (**b**, **c**) showed a mass (*arrow*) posterolateral to the vulvar introitus within the left labia majora, in the typical location of a Bartholin's gland cyst. The mass had low signal intensity on T1-weighted images and intermediate signal intensity on T2-weighted images. An axial T1-weighted image with gadolinium (**d**) demonstrated enhancement of the mass (*arrow*). Typically, a Bartholin's gland cyst should not have any enhancement on images using gadolinium contrast. The patient underwent wide local excision of a left vulvar mass at another institution. Review of her pathology slides confirmed low-grade adenocarcinoma that was at least locally invasive

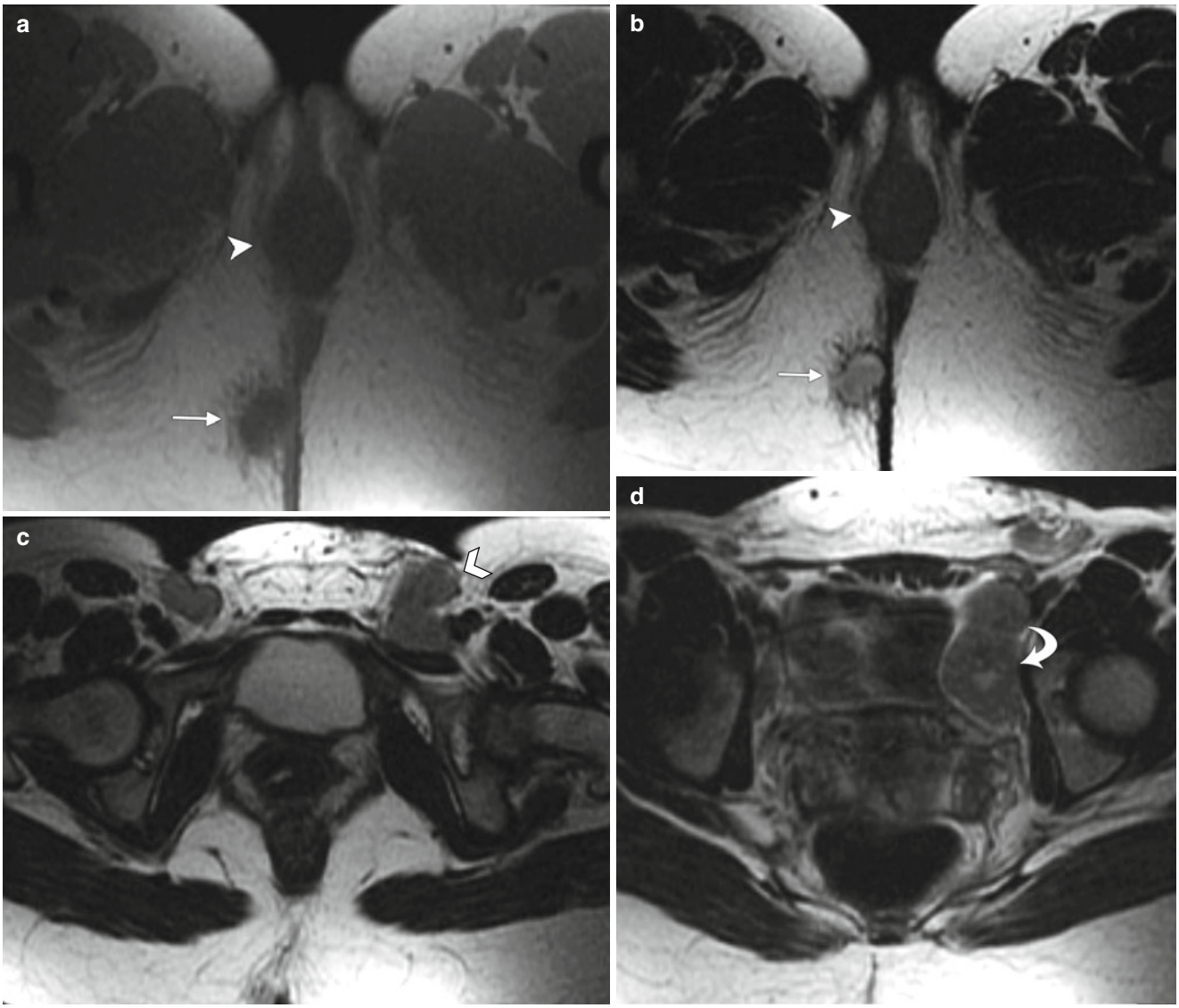

Fig. 5.11 Vulvar Merkel cell tumor. Vulvar Merkel cell tumor is a rare malignant cutaneous neuroendocrine neoplasm with a grave prognosis. Most commonly originating from the labia majora, it has more aggressive clinical behavior than Merkel cell tumors at other locations. Local recurrence and widespread metastases to lymph nodes, lungs, liver, or bone are common. The tumor has very limited response to chemoradiation therapy [41, 42]. This 26-year-old woman developed a mass in the left labia majora for several months. A biopsy at another institution revealed small-cell undifferentiated carcinoma, Merkel cell type, with lymphovascular invasion. (**a**) Axial T1-weighted MR imaging showed low-signal-intensity masses in the left labia majora (*arrowhead*) and right gluteal region (*arrow*). (**b–d**) Axial T2-weighted images showed masses with high signal intensity in the left labia majora (*arrowhead*) and right ischioanal region (*arrow*), left superficial inguinal adenopathy (*open arrowhead*), and left external iliac adenopathy (*curved arrow*). (**e**) Axial T1-weighted imaging with gadolinium demonstrated avidly enhancing masses in the left labia majora (*arrowhead*) and right ischioanal region (*arrow*). The patient was treated with radiation therapy for local symptom control, as well as chemotherapy. Because there is no standard chemotherapy regimen for vulvar Merkel cell tumor, her chemotherapy regimen was extrapolated from small-cell cancer of the lung. (**f–h**) Axial contrast-enhanced CT scans performed 10 months after the MRI imaging of the pelvis showed extensive distant metastases to the liver (*arrows*), lung (*arrowhead*), and bone (*curved arrow*)

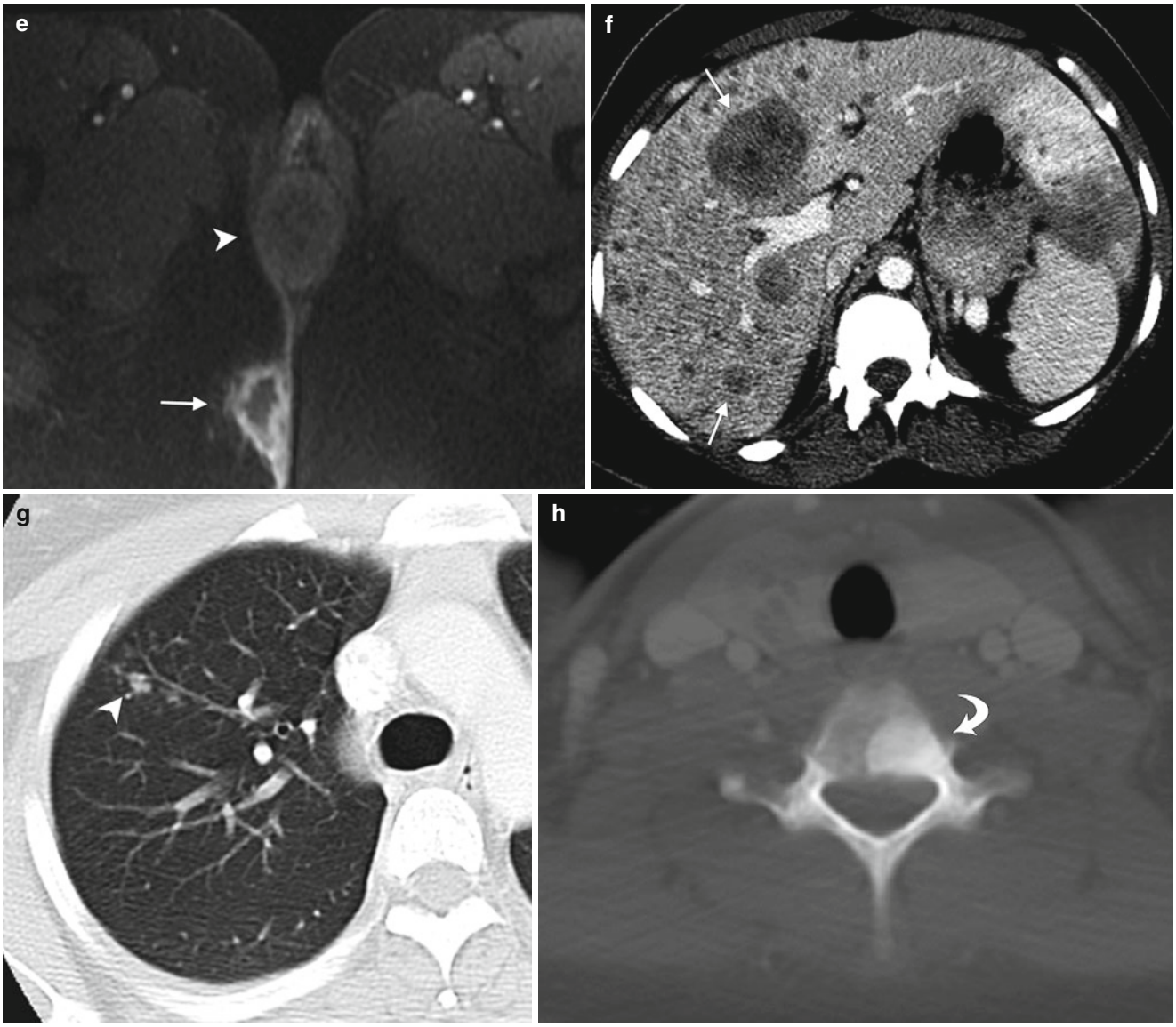

Fig. 5.11 (continued)

Table 5.3 Staging of melanoma of the skin: tumor definitions

Primary tumor (T)		
TX	Primary tumor cannot be assessed (*e.g.*, curettage or severely regressed melanoma)	
T0	No evidence of primary tumor	
Tis	Melanoma in situ	
T1	Melanomas ≤1 mm in thickness	
T2	Melanomas 1.01–2.0 mm	
T3	Melanomas 2.01–4.0 mm	
T4	Melanomas >4.0 mm	
T classification	**Thickness (mm)**	**Ulceration status/ mitoses**
T1	≤ 1.0	a: w/o ulceration and mitosis <1/mm^2
		b: with ulceration or mitoses ≥1/mm^2
T2	1.01–2.0	a: w/o ulceration
		b: with ulceration
T3	2.01–4.0	a: w/o ulceration
		b: with ulceration
T4	> 4.0	a: w/o ulceration
		b: with ulceration

Used with the permission of the American Joint Committee on Cancer (AJCC), Chicago, Illinois. The original source for this material is the AJCC Cancer Staging Manual, Seventh Edition (2010) published by Springer Science and Business Media LLC, www.springer.com

Table 5.4 Staging of melanoma of the skin: nodes

Regional lymph node (N)		
NX	Patients in whom the regional nodes cannot be assessed (*e.g.*, previously removed for another reason)	
N0	No regional metastases detected	
N1–N3	Regional metastases based upon the number of metastatic nodes and presence or absence of intralymphatic metastases (in transit or satellite metastases)	
N classification	**Number of metastatic nodes**	**Nodal metastatic mass**
N1	1 node	a: micrometastasis
		b: macrometastasis
N2	2–3 nodes	a: micrometastasis
		b: macrometastasis
		c: in transit metastasis or satellite *without* metastatic nodes
N3	4 or more metastatic nodes, or matted nodes, or in transit metastases or satellites with metastatic node(s)	

Used with the permission of the American Joint Committee on Cancer (AJCC), Chicago, Illinois. The original source for this material is the AJCC Cancer Staging Manual, Seventh Edition (2010) published by Springer Science and Business Media LLC, www.springer.com

Table 5.5 Staging of melanoma of the skin: metastases

Distant metastasis (M)		
M0	No detectable evidence of distant metastases	
M1a	Metastases to skin, subcutaneous, or distant lymph nodes	
M1b	Metastases to lung	
M1c	Metastases to all other visceral sites or distant metastases to any site combined with elevated serum LDH	
M classification	**Site**	**Serum LDH**
M1a	Distant skin, subcutaneous, or nodal metastases	Normal
M1b	Lung metastases	Normal
M1c	Any other visceral metastases	Normal
	Any distant metastasis	Elevated

Used with the permission of the American Joint Committee on Cancer (AJCC), Chicago, Illinois. The original source for this material is the AJCC Cancer Staging Manual, Seventh Edition (2010) published by Springer Science and Business Media LLC, www.springer.com

LDH lactate dehydrogenase

Table 5.6 Anatomic staging/prognostic groups

Clinical staging				Pathologic staging			
Stage 0	Tis	N0	M0	0	Tis	N0	M0
Stage IA	T1a	N0	M0	IA	T1a	N0	M0
Stage IB	T1b	N0	M0	IB	T1b	N0	M0
	T2a	N0	M0		T2a	N0	M0
Stage IIA	T2b	N0	M0	IIA	T2b	N0	M0
	T3a	N0	M0		T3a	N0	M0
Stage IIB	T3b	N0	M0	IIB	T3b	N0	M0
	T4a	N0	M0		T4a	N0	M0
Stage IIC	T4b	N0	M0	IIC	T4b	N0	M0
Stage III	Any T	≥ N1	M0	IIIA	T1–4a	N1a	M0
					T1–4a	N2a	M0
				IIIB	T1–4b	N1a	M0
					T1–4b	N2a	M0
					T1–4a	N1b	M0
					T1–4a	N2b	M0
					T1–4a	N2c	M0
				IIIC	T1–4b	N1b	M0
					T1–4b	N2b	M0
					T1–4b	N2c	M0
					Any T	N3	M0
Stage IV	Any T	Any N	M1	IV	Any T	Any N	M1

Used with the permission of the American Joint Committee on Cancer (AJCC), Chicago, Illinois. The original source for this material is the AJCC Cancer Staging Manual, Seventh Edition (2010) published by Springer Science and Business Media LLC, www.springer.com

Table 5.7 Survival rates for vulvar melanoma, by stage

	Relative survival rate (%)	
Stage	5 Years	10 Years
I	83	71
II	64	57
III	35	21
IV	Not available	Not available

Reprinted by the permission of the American Cancer Society, Inc. from www.cancer.org [1]. All rights reserved

References

1. American Cancer Society. Cancer facts & figures 2011. Atlanta: American Cancer Society; 2011.
2. Chang SD. Imaging of the vagina and vulva. Radiol Clin North Am. 2002;40:637–58.
3. van Beurden M, ten Kate FW, Tjong-A-Hung SP, et al. Human papillomavirus DNA in multicentric vulvar intraepithelial neoplasia. Int J Gynecol Pathol. 1998;17:12–6.
4. Kokka F, Singh N, Faruqi A, Gibbon K, et al. Is differentiated vulval intraepithelial neoplasia the precursor lesion of human papillomavirus-negative vulval squamous cell carcinoma? Int J Gynecol Cancer. 2011;21:1297–305.
5. Pinto AP, Miron A, Yassin Y, et al. Differentiated vulvar intraepithelial neoplasia contains Tp53 mutations and is genetically linked to vulvar squamous cell carcinoma. Mod Pathol. 2010; 23:404–12.
6. Irvin Jr WP, Legallo RL, Stoler MH, et al. Vulvar melanoma: a retrospective analysis and literature review. Gynecol Oncol. 2001;83:457–65.
7. Wechter ME, Reynolds RK, Haefner HK, et al. Vulvar melanoma: review of diagnosis, staging, and therapy. J Low Genit Tract Dis. 2004;8:58–69.
8. Moxley KM, Fader AN, Rose PG, et al. Malignant melanoma of the vulva: an extension of cutaneous melanoma? Gynecol Oncol. 2011;122:612–7.
9. Fuh KC, Berek JS. Current management of vulvar cancer. Hematol Oncol Clin North Am. 2012;26:45–62.
10. Nielsen GP, Rosenberg AE, Koerner FC, et al. Smooth-muscle tumors of the vulva. A clinicopathological study of 25 cases and review of the literature. Am J Surg Pathol. 1996;20:779–93.
11. Ulutin HC, Zellars RC, Frassica D. Soft tissue sarcoma of the vulva: a clinical study. Int J Gynecol Cancer. 2003;13:528–31.
12. Bigby SM, Symmans PJ, Miller MV, et al. Aggressive angiomyxoma of the female genital tract and pelvis—clinicopathologic features with immunohistochemical analysis. Int J Gynecol Pathol. 2011;30:505–13.
13. Haldar K, Martinek IE, Kehoe S. Aggressive angiomyxoma: a case series and literature review. Eur J Surg Oncol. 2010;36:335–9.
14. Sutton BJ, Laudadio J. Aggressive angiomyxoma. Arch Pathol Lab Med. 2012;136:217–21.
15. Desimone CP, Elder J, van Nagell Jr JR. Selective inguinal lymphadenectomy in the treatment of invasive squamous cell carcinoma of the vulva. Int J Surg Oncol. 2011;2011:284374.
16. de Hullu JA, Oonk MHM, Ansink AC, et al. Pitfalls in the sentinel lymph node procedure in vulvar cancer. Gynecol Oncol. 2004;94:10–5.
17. Zivanovic O, Khoury-Collado F, Abu-Rustum NR, et al. Sentinel lymph node biopsy in the management of vulvar carcinoma, cervical cancer and endometrial cancer. Oncologist. 2009;14:695–705.
18. Pecorelli S. Revised FIGO staging for carcinoma of the vulva, cervix and endometrium. Int J Gynaecol Obstet. 2009;105:103–4.
19. Hacker NF. Revised FIGO staging for carcinoma of the vulva. Int J Gynaecol Obstet. 2009;105:105–6.

20. van der Steen S, de Nieuwenhof HP, Massuger L, et al. New FIGO staging system of vulvar cancer indeed provides a better reflection of prognosis. Gynecol Oncol. 2010;119:520–5.
21. Dittmer C, Fischer D, Diedrich K, Thill M. Diagnosis and treatment options of vulvar cancer: a review. Arch Gynecol Obstet. 2012;285:183–93.
22. McMahon CJ, Rofsky NM, Pedrosa I. Lymphatic metastases from pelvic tumors: anatomic classification, characterization, and staging. Radiology. 2010;254:31–46.
23. Oonk MH, de Hullu JA, van der Zee AG. Current controversies in the management of patients with early-stage vulvar cancer. Curr Opin Oncol. 2010;22:481–6.
24. Whitcomb BP. Gynecologic malignancies. Surg Clin North Am. 2008;88:301–17.
25. Sohaib SA, Richards PS, Ind T, et al. MR imaging of carcinoma of the vulva. AJR Am J Roentgenol. 2002;178:373–7.
26. Kataoka MY, Sala E, Baldwin P, et al. The accuracy of magnetic resonance imaging in staging of vulvar cancer: A retrospective multi-centre study. Gynecol Oncol. 2010;117:82–7.
27. Basu S, Li G, Alavi A. PET and PET-CT imaging of gynecological malignancies: present role and future promise. Expert Rev Anticancer Ther. 2009;9:75–96.
28. Grigsby P. Role of PET in gynecologic malignancy. Curr Opin Oncol. 2009;21:420–4.
29. Tappouni RF, Sarwani NI, Tice JG, et al. Imaging of unusual perineal masses. AJR Am J Roentgenol. 2011;196:W412–20.
30. Lee SI, Oliva E, Hahn PF, Russell AH. Malignant tumors of the female pelvic floor: self-assessment module. AJR Am J Roentgenol. 2011;196(3 Suppl):S24–7.
31. Griffin N, Grant LA, Sala E. Magnetic resonance imaging of vaginal and vulval pathology. Eur Radiol. 2008;18:1269–80.
32. Takehara M, Saito T, Mizumoto H, Baba T, et al. Imaging studies in patients with malignant melanoma in the female genital tract. Int J Gynecol Cancer. 2002;12:506–9.
33. Crosbie EJ, Slade RJ, Ahmed AS, et al. The management of vulval cancer. Cancer Treat Rev. 2009;35:533–9.
34. Stehman FB, Look KY. Carcinoma of the vulva. Obstet Gynecol. 2006;107:719–33.
35. Woolderink JM, de Bock GH, de Hullu JA, et al. Patterns and frequency of recurrence of squamous cell carcinoma of the vulva. Gynecol Oncol. 2006;103:293–9.
36. Mclean KA, Zhang W, Dunsmoor-Su RF, et al. Pelvic exenteration in the age of modern chemoradiation. Gynecol Oncol. 2011;121:131–4.
37. Benn T, Brooks RA, Zhang Q, et al. Pelvic exenteration in gynecologic oncology: a single institution study over 20 years. Gynecol Oncol. 2011;122:14–8.
38. Forner DM, Lampe B. Exenteration in the treatment of Stage III/IV vulvar cancer. Gynecol Oncol. 2012;124:87–91.
39. Khoury-Collado F, Elliott KS, Lee YC, et al. Merkel cell carcinoma of the Bartholin's gland. Gynecol Oncol. 2005;97:928–31.
40. Kraemer B, Guengoer E, Solomayer EF, et al. Stage I carcinoma of the Bartholin's gland managed with detection of inguinal and pelvic sentinel lymph node. Gynecol Oncol. 2009;114:373–4.
41. Loret de Mola JR, Hudock PA, Steinetz C, et al. Merkel cell carcinoma of the vulva. Gynecol Oncol. 1993;51:272–6.
42. Husseinzadeh N, Wesseler T, Newman N, et al. Neuroendocrine (Merkel cell) carcinoma of the vulva. Gynecol Oncol. 1988;29:105–12.

PET-CT Imaging in Gynecologic Malignancies

6

Neeta Pandit-Taskar and Irene A. Burger

The primary tools used for diagnosis, staging, and followup surveillance of gynecologic malignancies include ultrasound, CT, and MRI; imaging with Positron imaging tomography (PET) with the tracer 2-[18] F fluoro 2 deoxy-D- glucose (FDG) has been increasingly used for selected indications. In recent years, encouraging data have emerged to support the use of [18]F-FDG, and imaging using both PET and CT has an established role in the management of ovarian and cervical cancer.

PET-CT imaging with FDG as the tracer is based upon the physiologic affinity of tumor cells to utilize glucose, given the high metabolic activity of growing cells. FDG, a glucose analogue, is incorporated into the glycolysis pathway, where (following the initial phosphorylation) it remains trapped without any further metabolism. This analogue is tagged with a positron-emitting radioisotope, [18]F, which has a half-life of 110 min. The radiation (511 KeV coincidence gamma) is detected using a PET scanner. Most malignant cells concentrate FDG more than normal tissue does, so they appear as areas of intense activity or "hot" foci. The scan area generally ranges from the skull base to the upper thighs, allowing the detection of disease throughout the body.

Guidelines for optimal imaging (Table 6.1) should be followed. The patient generally should fast before scanning to enable and enhance uptake by the tumor cells. High blood sugar decreases the sensitivity of the scan by competing for tumor uptake. Glucose higher than 200 mg/dL can be lowered with insulin, but doing so may lead to higher muscle uptake, making it more difficult to detect small and low-grade lesions, thereby lowering sensitivity. Because much of the disease may be in the pelvis, voiding immediately before scanning is helpful, to enhance the imaging of organs and lesions close to the bladder. The need for bladder catheterization is best judged on a case-by-case basis. The fusion of PET images with CT improves anatomic localization.

Table 6.1 Imaging guidelines for PET-CT imaging

Fast for 4–6 h prior to scan
Screen for diabetes, insulin injection
Finger stick to check fasting glucose level prior to injection (should be <200 mg/dL)
Inject intravenous tracer (10–20 mCi, generally 10–12 mCi[a])
Image 45–60 min after injection
Void bladder prior to imaging
Image from skull base to mid-thigh
CT (either low-dose or diagnostic) done first
Emission scan 5–6 fields, 3 min per field of view

From Society of Nuclear Medicine and Molecular Imaging (SNM) guidelines, www.snm.org/guidelines
mCi millicurie, *PET* positron emission tomography
[a]Adult dose

N. Pandit-Taskar, MD (✉)
Department of Radiology,
Memorial Sloan-Kettering Cancer Center,
1275 York Avenue, New York,
NY 10065, USA
e-mail: pandit-n@mskcc.org

I.A. Burger, MD
Department of Radiology,
University Hospital Zurich, Ramistrasse 100,
Zurich 8091, Switzerland
e-mail: irene.burger@usz.ch

O. Akin (ed.), *Atlas of Gynecologic Oncology Imaging*, Atlas of Oncology Imaging,
DOI 10.1007/978-1-4614-7212-4_6,

6.1 Physiologic Distribution and Variants

FDG uptake also occurs in nonmalignant tissues, most prominently the brain and heart. Lesser activity is seen in liver, spleen, and bone marrow. FDG is excreted by the kidneys, so prominent uptake is seen in the kidneys, ureters, and bladder. In females, certain physiological conditions of the reproductive system and benign lesions may be associated with increased uptake of FDG. Functional uptake in endometrium related to cyclic changes (Fig. 6.1) and menstruation (Fig. 6.2) is the most common cause of intense activity seen in the uterus in women without known malignancy of the reproductive tract [1, 2].

Uptake may be seen in the ovaries related to maturing or growing follicles (Fig. 6.3), especially in younger or premenopausal women [3]. Increased ovarian uptake of FDG in postmenopausal patients would raise the suspicion for malignancy (Fig. 6.4). Though high uptake suggests malignant disease, there is significant overlap in uptake for benign versus malignant lesions. In a reported study, a standardized uptake value (SUV) of 7.9 in ovary separated benign from malignant uptake with 57 % sensitivity and 95 % specificity [4]; an average SUV of 9.1 ± 4 was seen in malignant lesions versus 5.7 ± 1.5 in nonmalignant conditions. It is recommended that uptake in uterus or ovaries be correlated with history and corresponding CT scans. Other benign causes of uptake may be related to functional cyst, corpus luteum, adenoma, dermoid cyst, endometriosis, inflammation, and teratoma, reported to show variable uptake of FDG (Figs. 6.5 and 6.6) [3–6]. Uterine uptake can vary during the various phases of the menstrual cycle. Uterine fibroids are also a common benign cause of uptake of FDG in the uterus, generally appearing as low-grade, heterogeneous uptake (Fig. 6.7) but sometimes appearing as prominent activity; correlation with CT findings can help delineate the fibroids (Fig. 6.8) [6, 7]. Contamination may cause false focal uptake and should be ruled out (Fig. 6.9) [8].

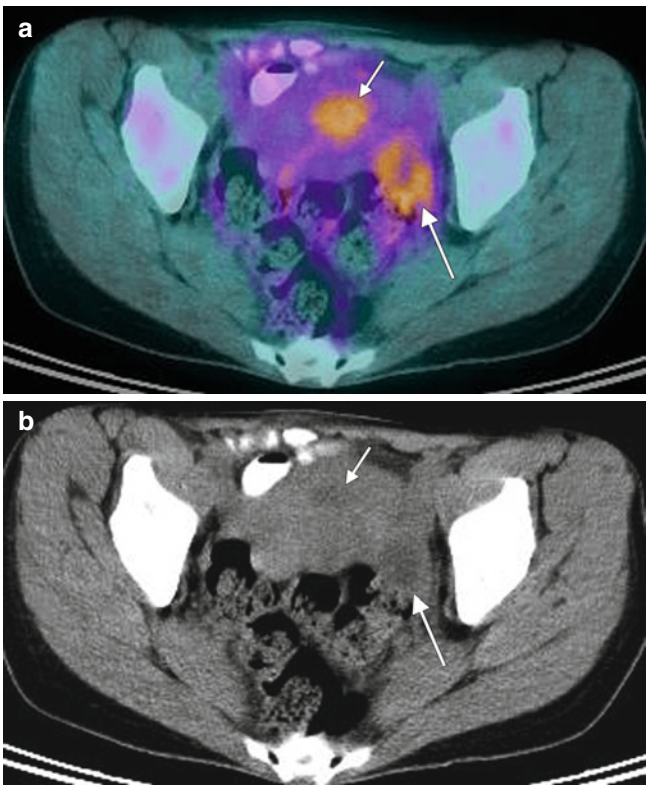

Fig. 6.1 Physiologic uptake in the endometrium related to cyclic changes. A 44-year-old premenopausal woman had an FDG PET-CT scan, performed to evaluate lung nodules. Transaxial fused images (**a**) show mild uptake in the region of the uterus (*short arrow*) and left adnexa (*long arrow*) with standardized uptake values (SUVs) of 3.6 and 3.2 respectively. Details on menstrual history revealed that this imaging was performed 17 days after the last menstrual cycle. There was no evidence of malignancy in the uterus or adnexa on CT (**b**). The activity reflects physiologic endometrial activity and uptake in the follicle in the left adnexa (**b**). The uterus had fibroids that did not show FDG uptake

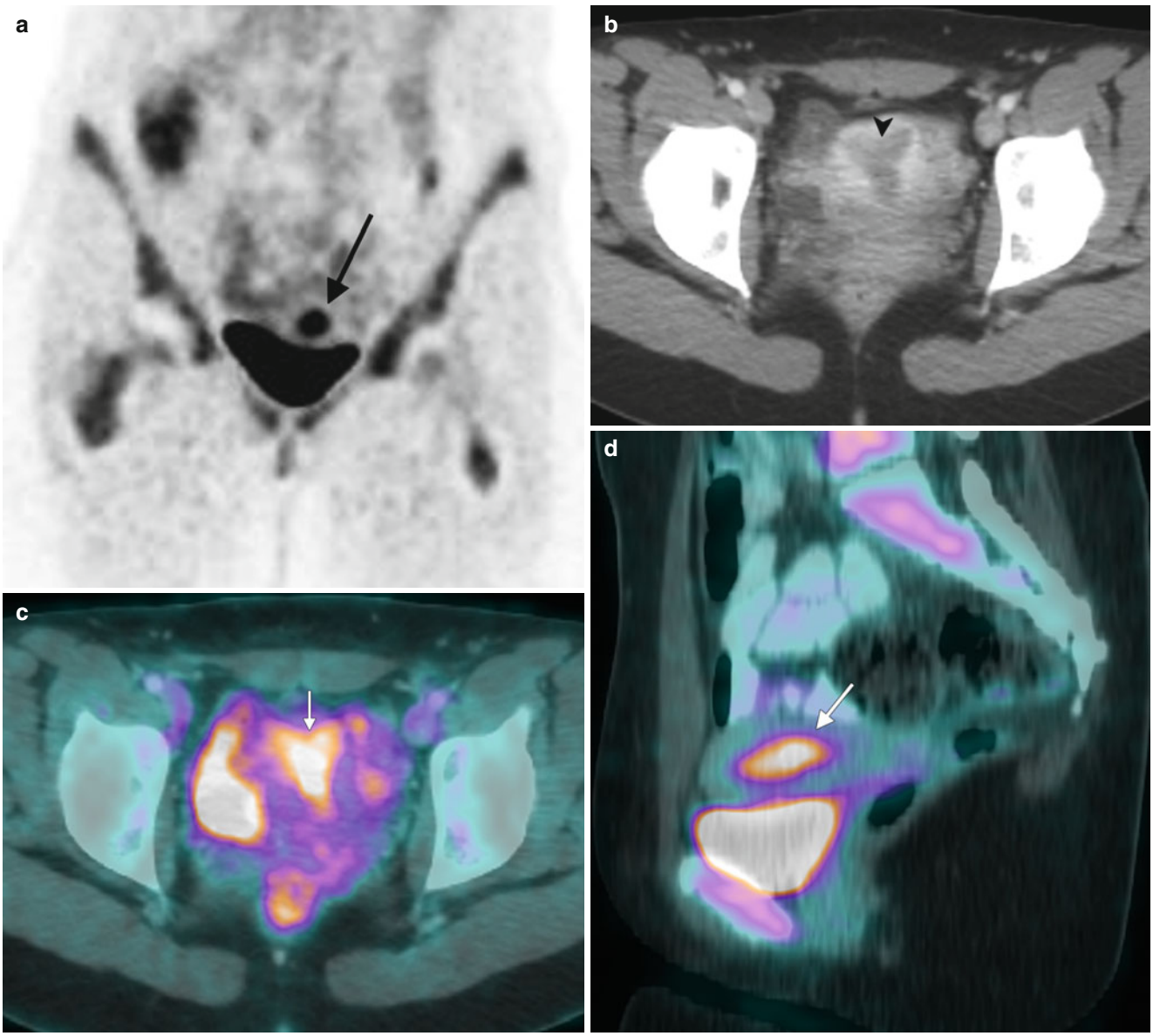

Fig. 6.2 Physiologic FDG uptake in the uterus with active menstruation. This FDG PET/CT scan of an 18-year-old woman was obtained for restaging of nongynecologic malignancy. Coronal images (**a**) show increased activity in the pelvis, superior to the bladder (*long black arrow*), which localized to the uterine cavity on a CT image (**b**) that showed a hypoenhancing central area of endometrium (*arrowhead*). On the axial (**c**) and sagittal (**d**) fused FDG PET-CT images, intense FDG uptake is seen in the uterine cavity (*short white arrows*), with a standardized uptake value (SUV) of 6.6. The patient was actively menstruating at the time of the scan, which was likely the cause of increased activity. There was no known malignancy of the uterus at this time or in followup. Uptake in the uterus secondary to menstruation is generally high-intensity within the central uterus and diffuse along the endometrium. It can be distinguished from other causes of uptake such as uterine fibroids, which may produce activity that is eccentric in location and of variable intensity; often FDG activity in patients with fibroids is heterogeneous and of low grade or nonexistent

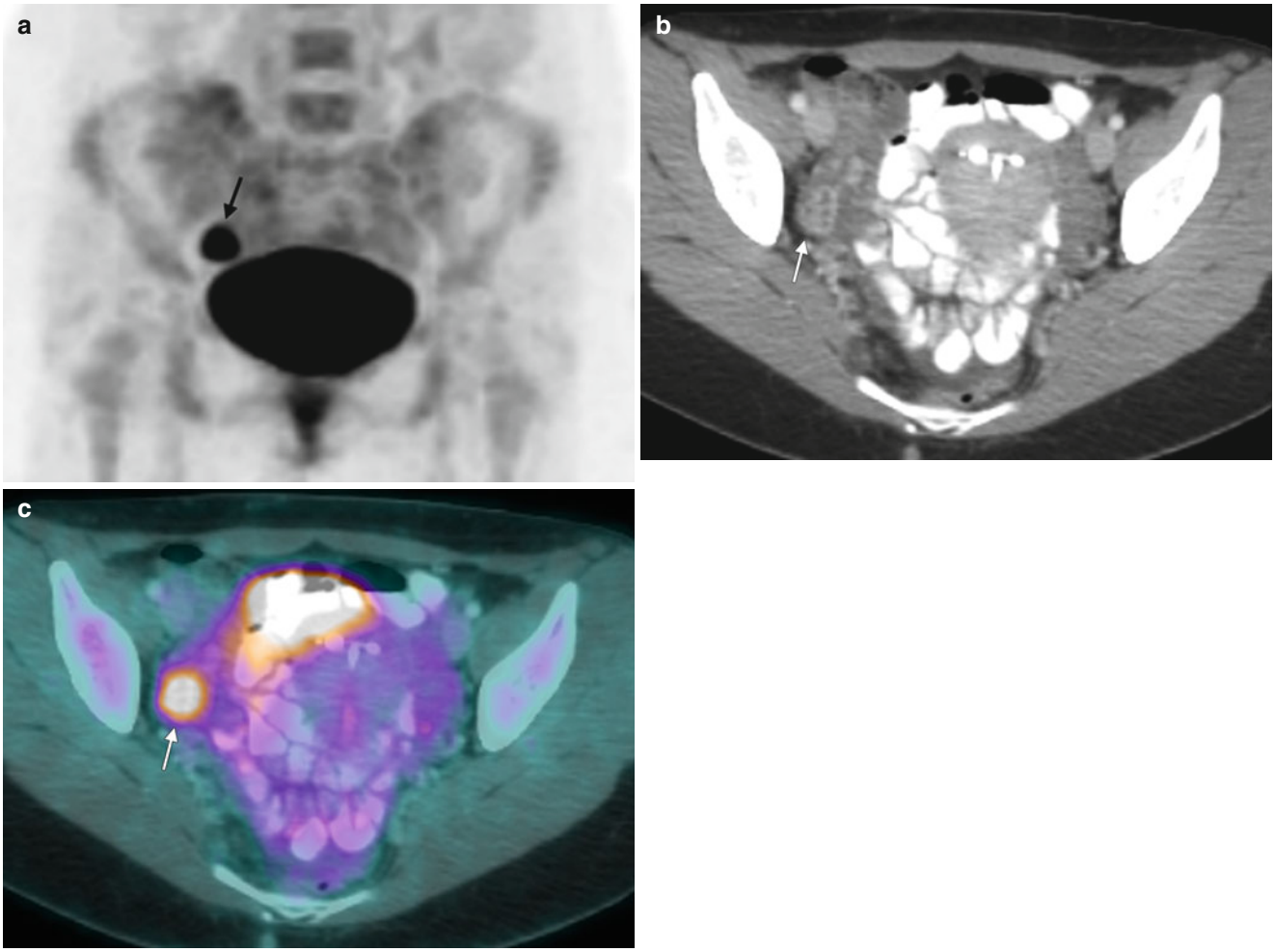

Fig. 6.3 Physiologic ovarian uptake in a young, premenopausal woman. This FDG PET-CT scan of a 27-year-old woman was obtained for restaging of a nongynecologic malignancy. The maximum intensity projection (MIP) PET image (**a**) shows an area of focal FDG uptake in the right pelvis just above the bladder (*arrow*). A contrast-enhanced axial CT image (**b**) delineates rimlike enhancement within the right adnexa. The fused FDG PET-CT image (**c**) confirms that the prominent focal activity is within the right adnexa along the enhancement in the right ovary, consistent with a corpus luteum. The patient was imaged on day 21 of her menstrual cycle. Corpus luteum can show prominent FDG uptake, in this case with a standardized uptake value (SUV) of 8.0

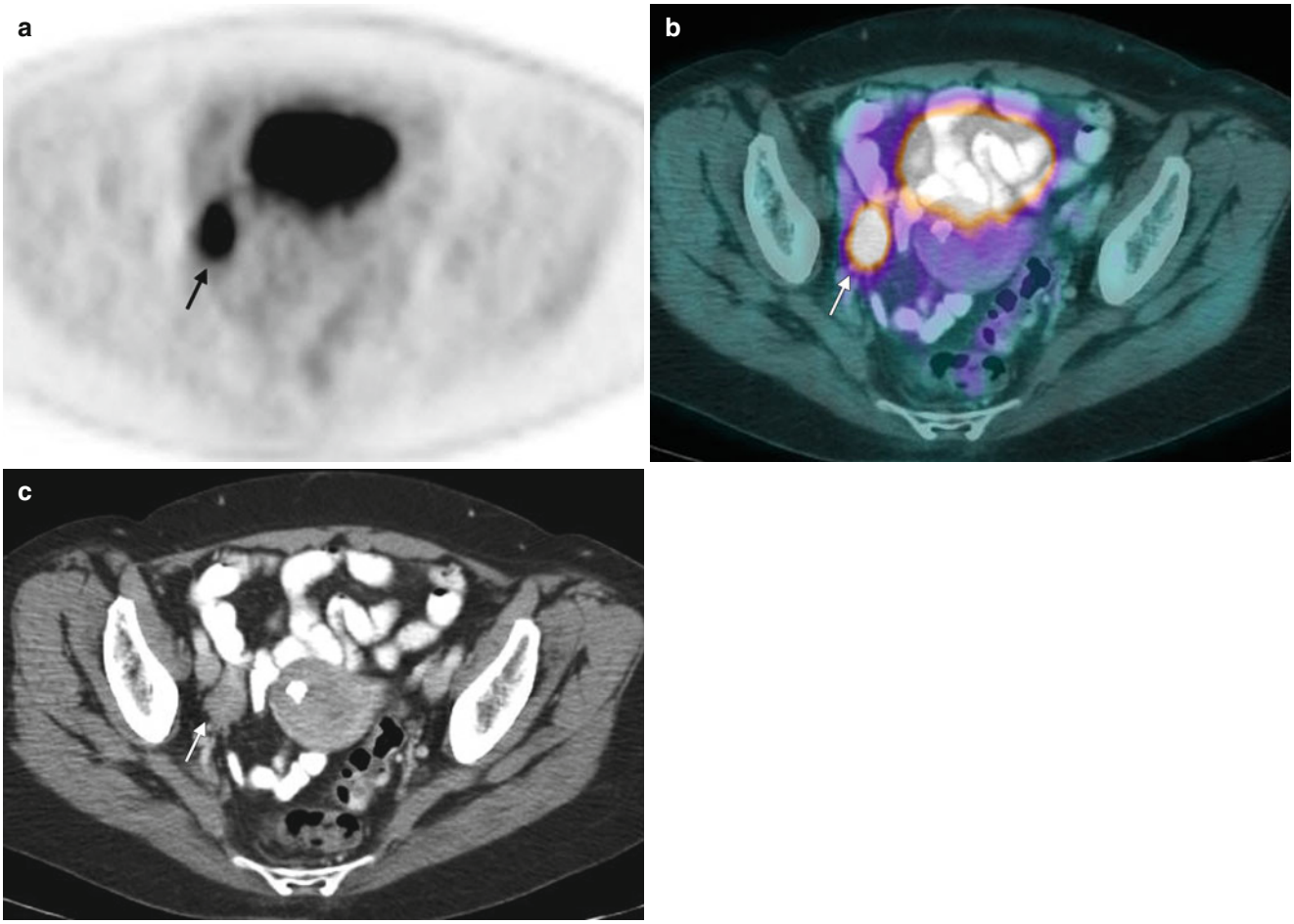

Fig. 6.4 Ovarian uptake in a postmenopausal woman. PET-CT imaging of this 61-year-old woman was obtained for nongynecologic malignancy. A transaxial PET image (**a**) shows increased activity in the right pelvis (*arrow*). Transaxial fusion PET-CT (**b**) and CT (**c**) images show uptake localizing to the right ovary (*arrows*). The SUV was 8.9. Such uptake is considered unusual and nonphysiologic in a postmenopausal woman. Further evaluation revealed malignant involvement of the right ovary. Increased uptake in postmenopausal women should always be investigated to exclude malignancy

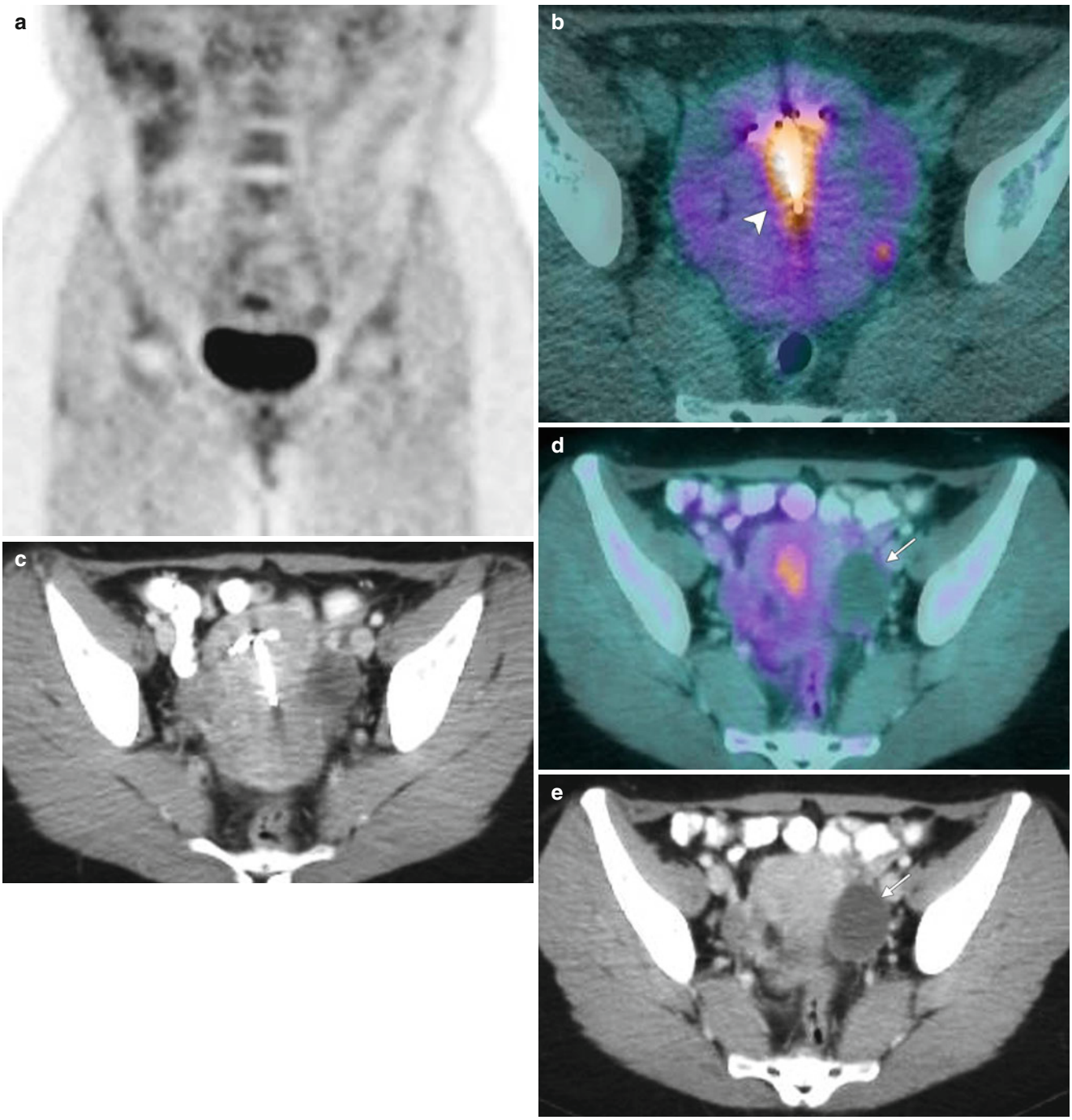

Fig. 6.5 Physiologic uptake in the uterus and a non–FDG-avid functional ovarian cyst. These images show a 34-year-old woman with nongynecologic malignancy. The coronal MIP PET image (**a**) shows focal FDG uptake in the pelvis just above the bladder. The fused axial FDG PET-CT image (**b**) and CT image (**c**) show uptake corresponding to the uterine cavity (*arrowhead*) with an IUD in situ. Uptake in the uterus may be related to physiologic endometrial changes or reactive changes to an IUD. No increased uptake is seen in left ovary cyst (*arrows*) consistent with a physiologic functional cyst (**d**, **e**).

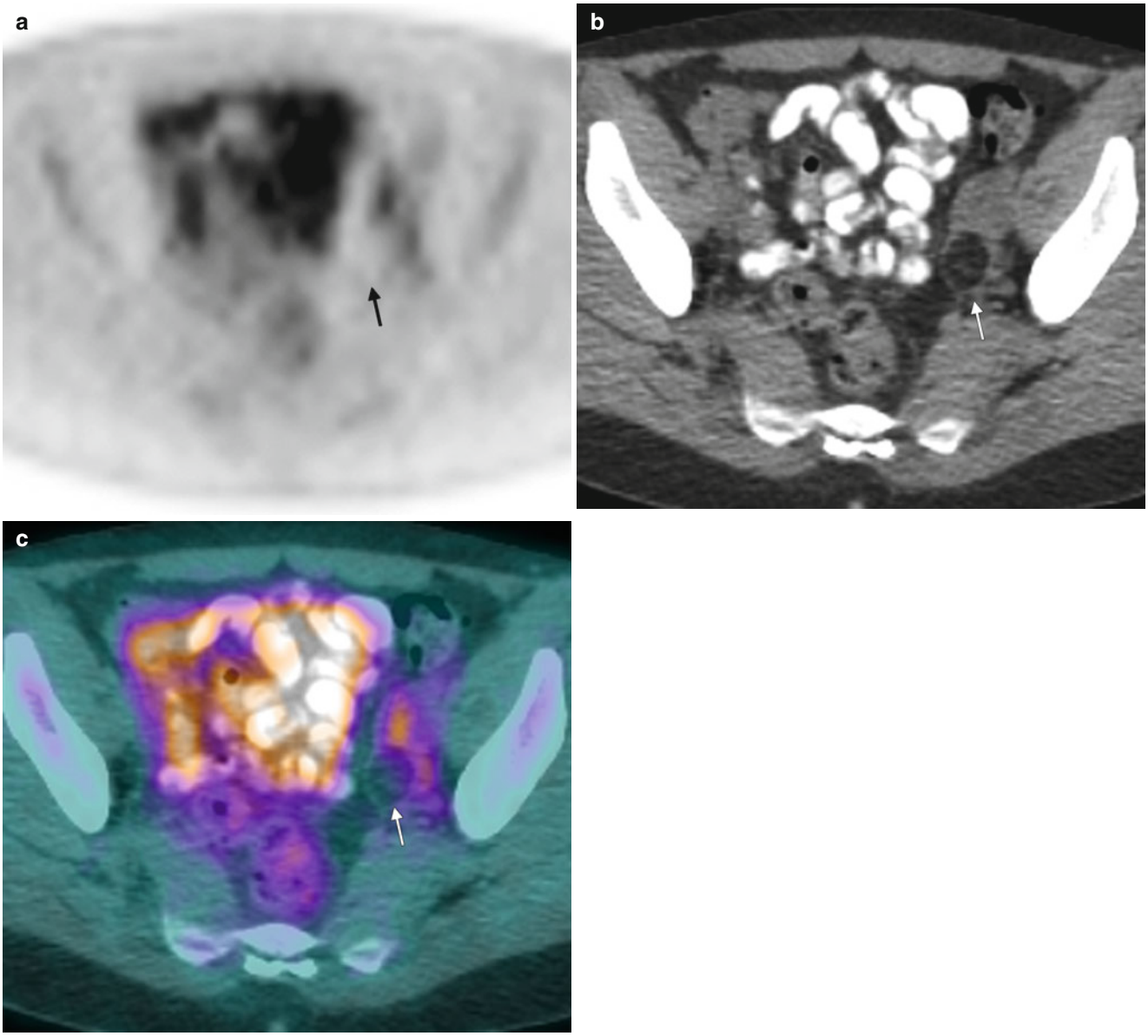

Fig. 6.6 FDG PET and benign lesions of the adnexa. In this 35-year-old woman, the axial PET image (**a**) shows no increased FDG uptake in the region of the left adnexa. On the contrast-enhanced axial CT image (**b**), there is a small, hypoattenuating mass within the left ovary (*arrow*). On the fused FDG PET-CT image (**c**), there is no increased FDG activity within this lesion in the left ovary. Fat-containing lesions within the ovaries are most commonly ripe teratomas, which typically do not take up FDG. Rare cases of uptake in mature teratomas and malignant transformation have been reported

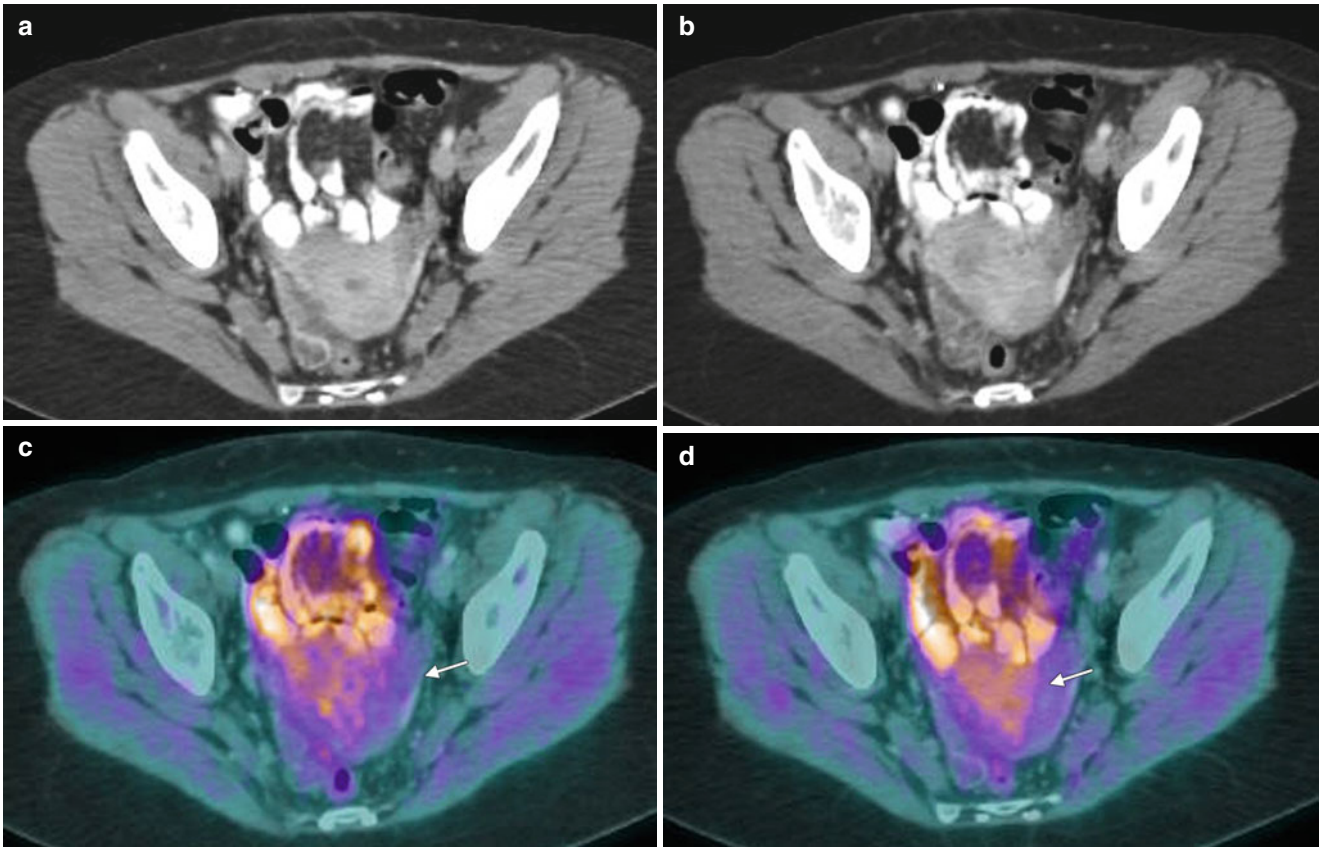

Fig. 6.7 FDG uptake in uterine fibroids: mild heterogeneous activity. A 35-year-old woman with breast cancer was imaged for evaluation of recurrent disease. CT images (**a**, **b**) of the pelvis showed uterine fibroids that show only minimal, heterogeneous activity of FDG (SUV 2.7), as seen on fused PET-CT images (**c**, **d**) (*arrow*)

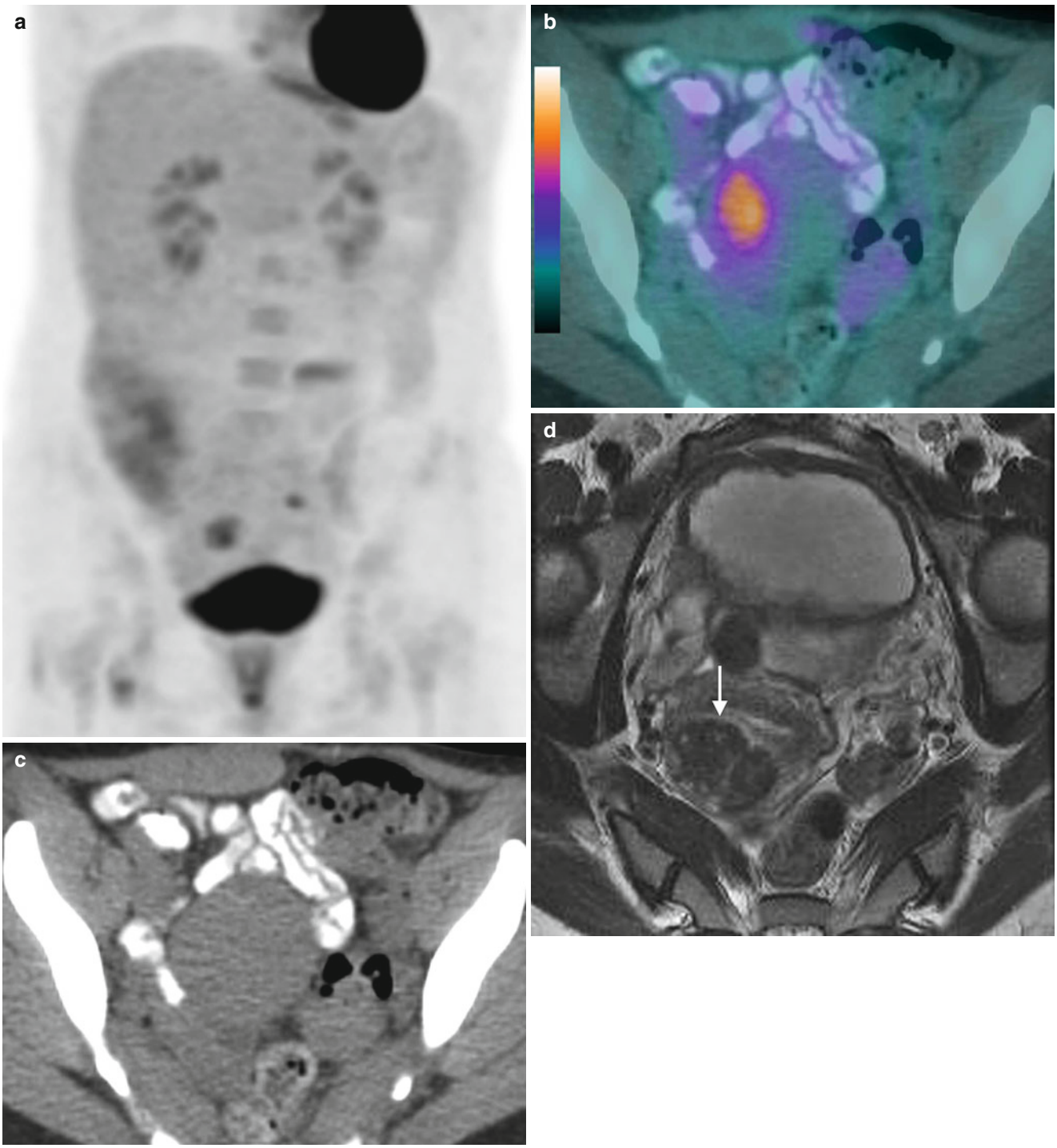

Fig. 6.8 Uptake in uterine fibroids: intense activity. A MIP PET image (**a**) of a 45-year-old woman observed for breast cancer with FDG PET-CT shows uptake in the pelvis. A fused PET-CT image (**b**) shows increased focal FDG activity in the uterus, corresponding to the fibroid (SUV 6.5) (**c**, **d**). Uterine fibroids have a higher incidence of increased FDG activity in premenopausal women (10.4 %) than in postmenopausal women (1.2 %). The FDG activity can be highly variable, with reported maximum standardized uptake values (SUV_{max}) up to 16. The predominance of uptake in premenopausal women suggests hormonal dependency. Vascularity, cellularity, and proliferation rate also have been reported to influence the FDG uptake of leiomyomas [6, 7]

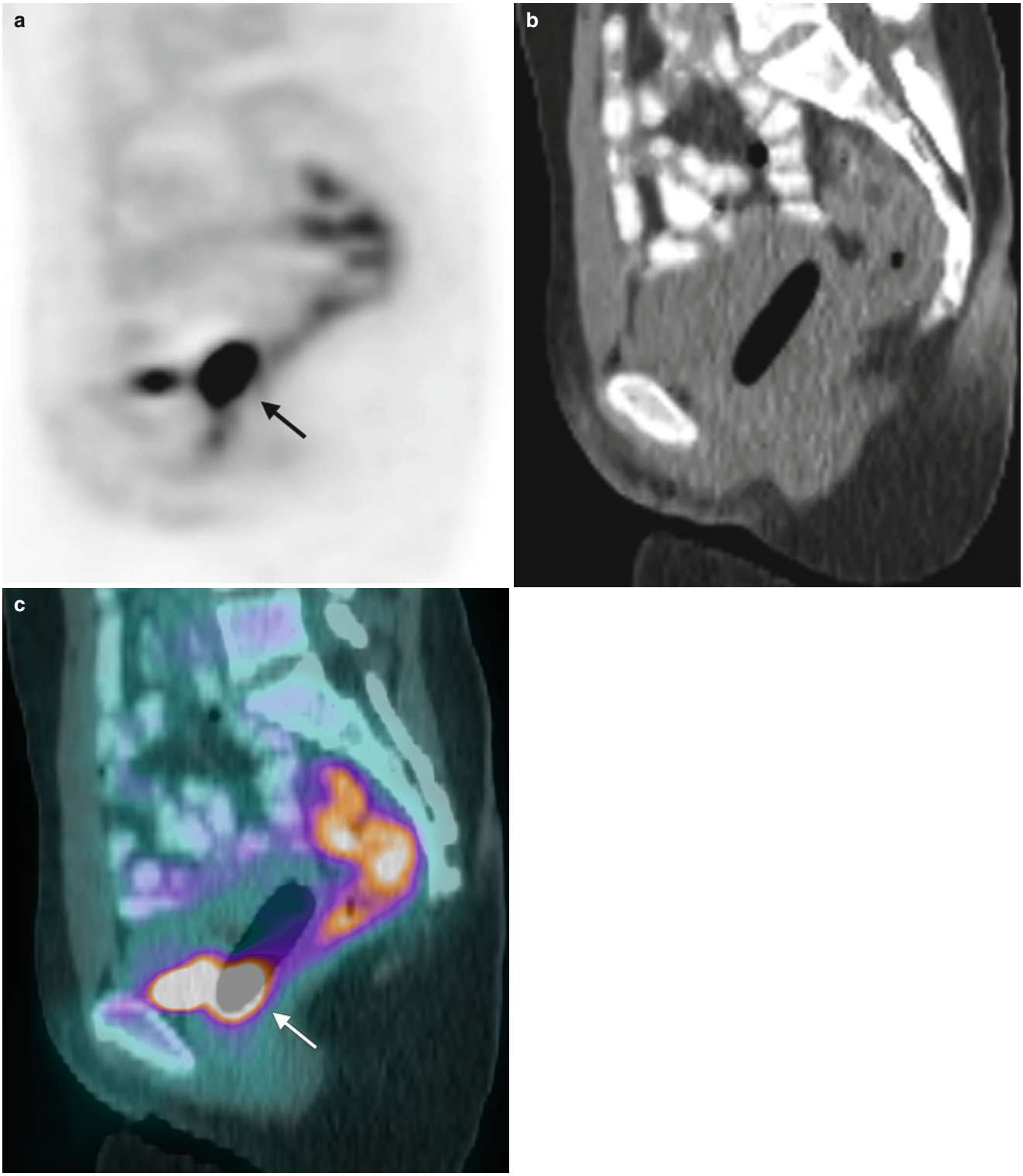

Fig. 6.9 Uptake in vagina secondary to tampon contamination. A 26-year-old woman was examined on day 5 of her menstrual cycle. The sagittal PET image (**a**) shows a focal FDG uptake behind the bladder (*arrow*) localizing to the vagina (SUV 21). The sagittal CT scan (**b**) illustrates an intravaginal tampon. The fused sagittal FDG PET-CT image (**c**) shows concentration of the FDG activity in the base of the tampon, most likely due to urine contamination [8]. The uptake is generally concentrated predominantly in the inferior portions and is similar to the uptake in the urine in the bladder

6.2 Cervical Cancer

Most primary cervical cancers concentrate FDG, especially those with poorly differentiated and squamous histology (Figs. 6.10 and 6.11). For staging, FDG PET-CT is useful in assessing pelvic or extrapelvic nodal involvement and detecting distant metastases (Figs. 6.12 and 6.13). This information is useful in planning the primary treatment of the patient, including surgery, radiation therapy, or both. Sensitivity and accuracy in detecting lesions are higher for advanced disease

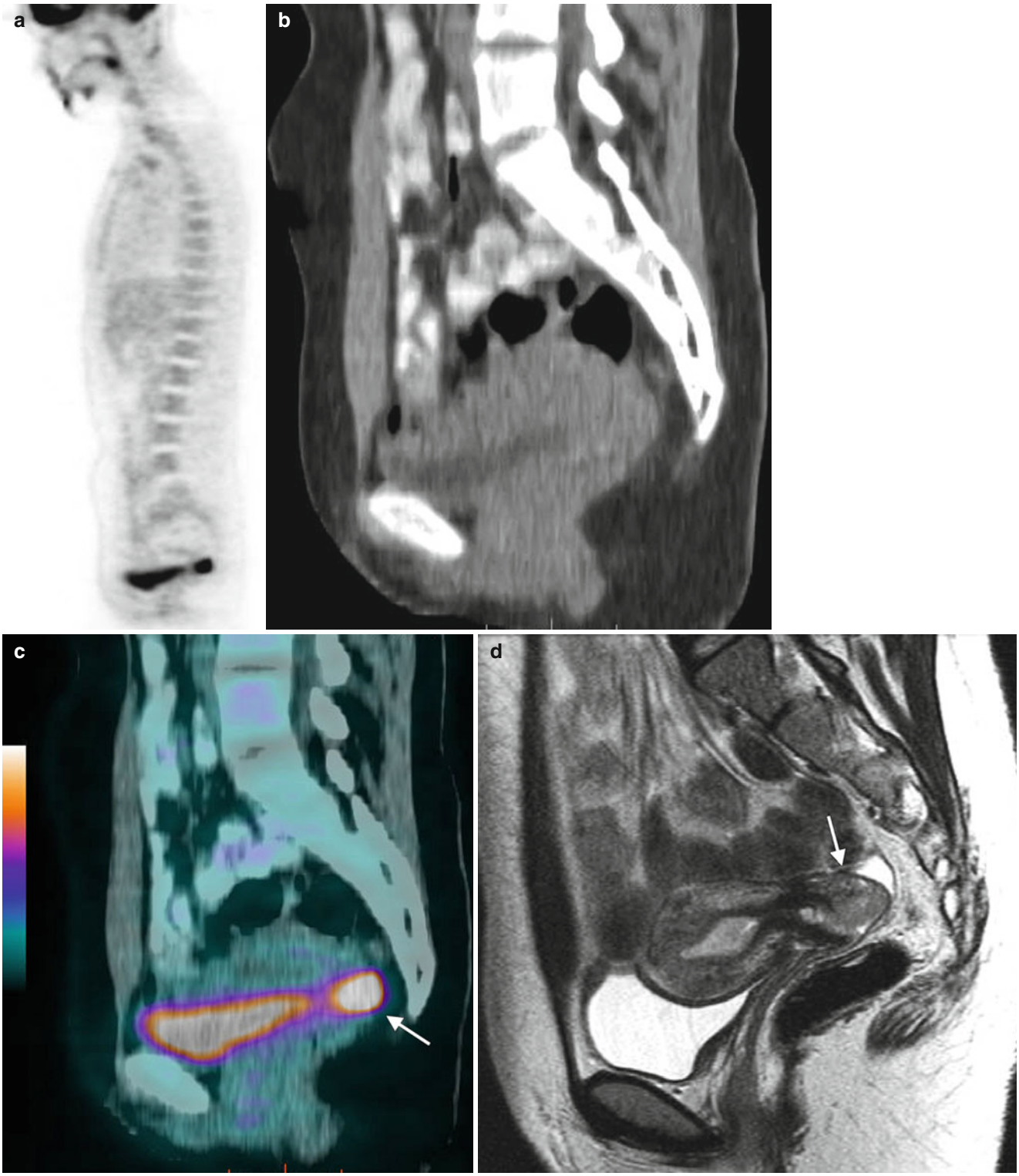

Fig. 6.10 High FDG uptake in primary adenocarcinoma of the cervix. This 23-year-old woman reported postcoital bleeding and metrorrhagia. A Pap smear was positive for human papillomavirus (HPV). MIP images (**a**, **b**) show increased FDG uptake just superior to the bladder (*arrow*) with a standardized uptake value (SUV) of 11.8. Sagittal CT, fused, and MRI images (**c**–**e** respectively) show focal uptake posterior to the bladder localizing to the cervical lesion. Fused axial CT and fused images (**f**, **g**) show localization of the activity in the cervix corresponding to the MRI images (**h**). Cervical biopsy revealed adenocarcinoma

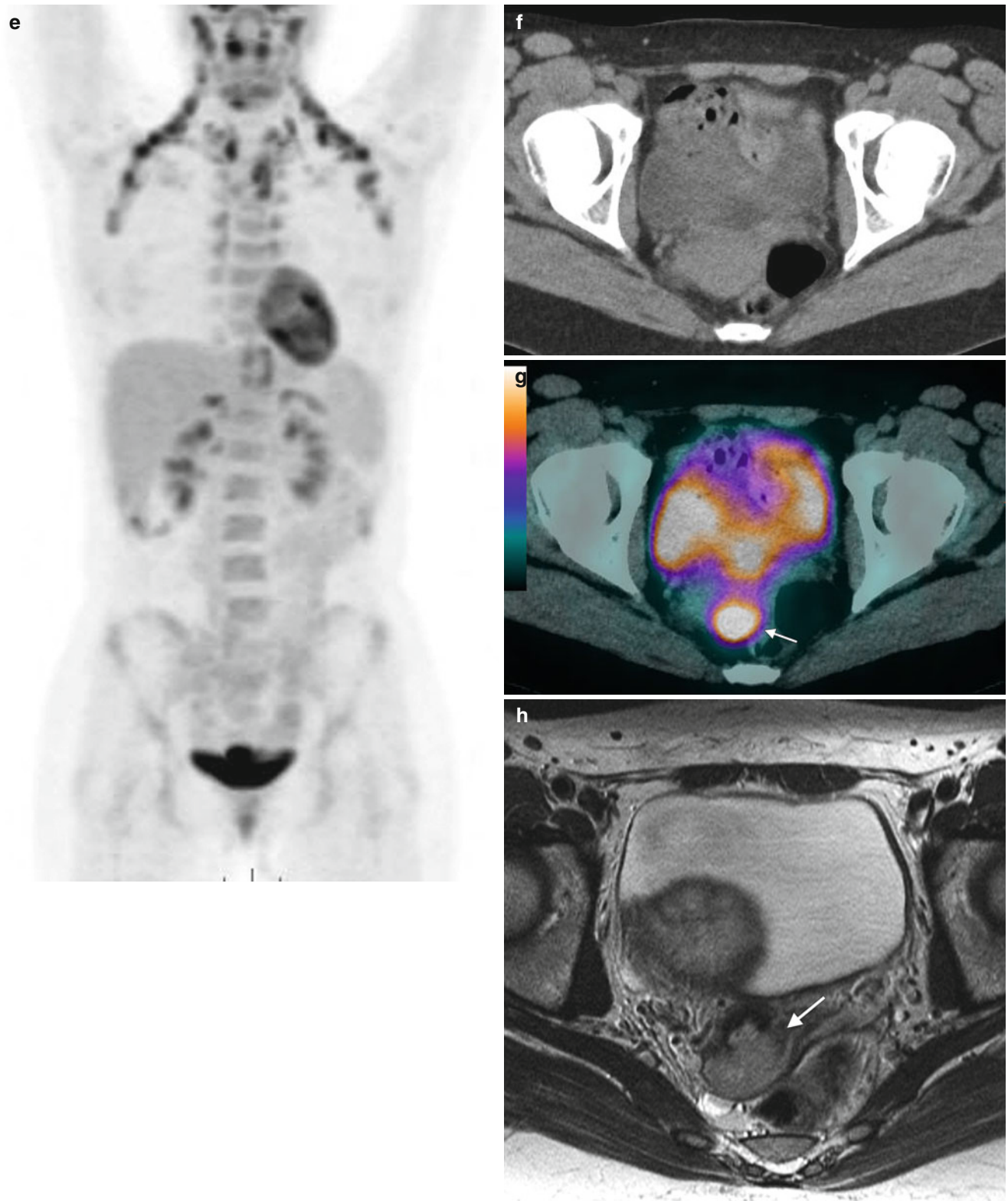

Fig. 6.10 (continued)

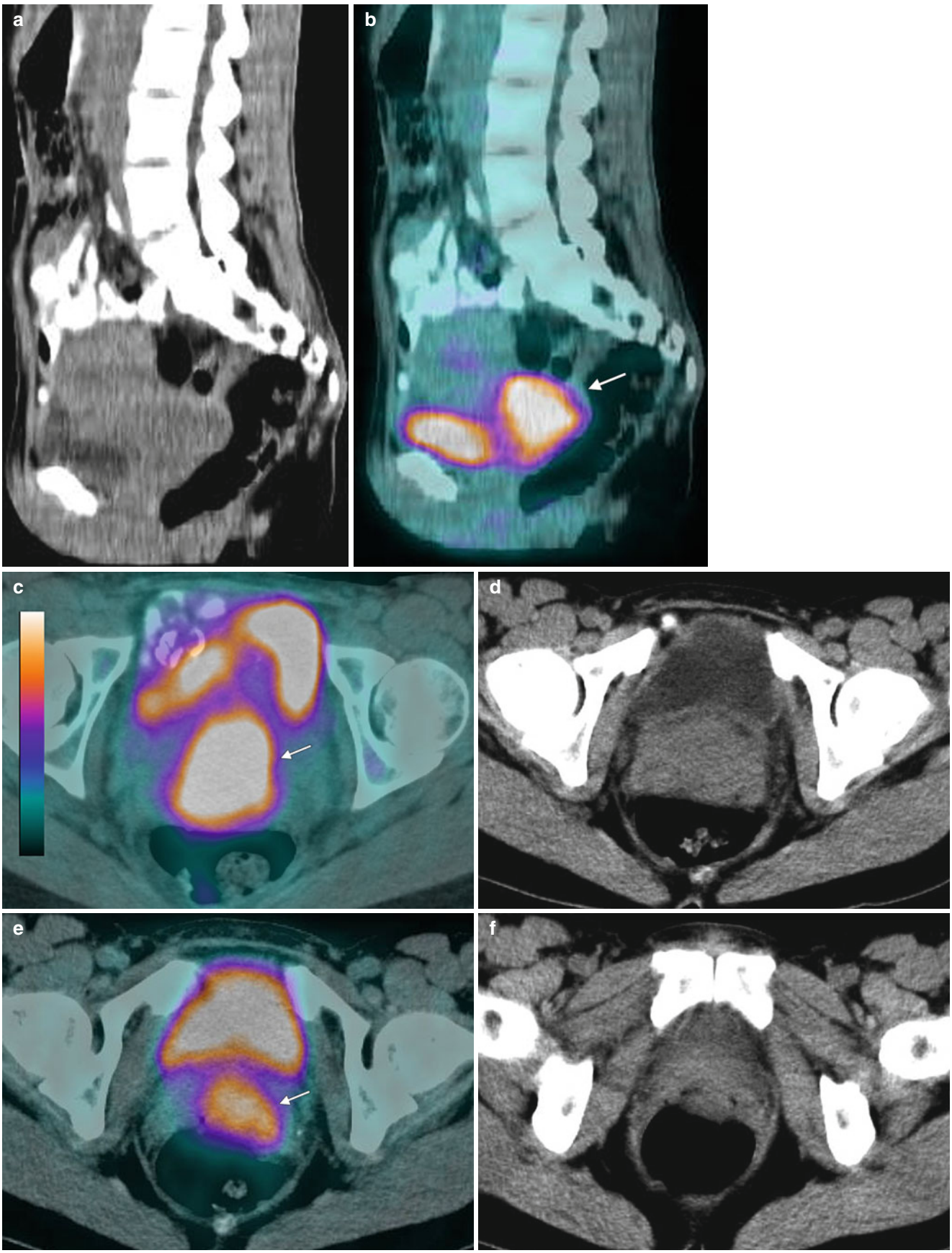

Fig. 6.11 High FDG uptake in primary squamous cell carcinoma of the cervix. This 45-year-old woman presented with abnormal bleeding. A Pap smear was positive for a high-grade lesion. Colposcopy was performed, and cervical biopsy revealed high-grade squamous cell carcinoma of the cervix. FDG PET was performed for staging. Intense uptake (SUV 9.2) was seen in the region of a cervical mass (*arrow*) seen on sagittal CT and fused PET/CT images (**a**, **b**) and axial image (**c**) that measured 4.9 × 4.4 × 3.7 cm, extending inferiorly up to the vaginal fornices seen on axial CT and fused PET/CT images (**d**–**g**). No FDG-avid nodal disease was seen

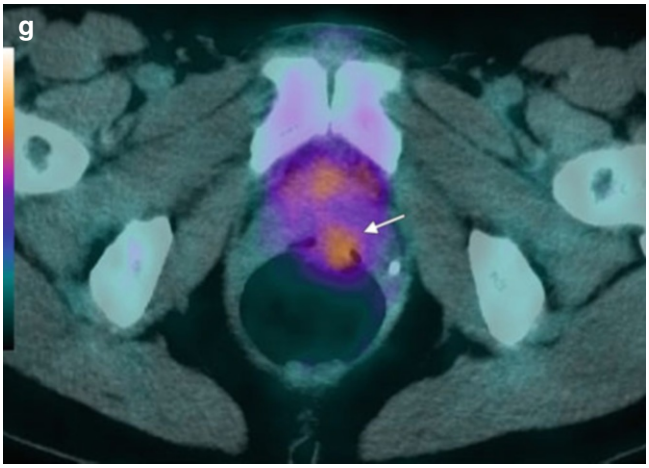

Fig. 6.11 (continued)

and are low for early-stage disease, up to stage 1A2 or 2A [9–11]. The primary advantage of FDG PET-CT is the detection of unknown distant metastases and lymph node metastases that are benign by mere size criteria (Fig. 6.14). The use of FDG PET imaging for routine staging prior to radical hysterectomy and pelvic lymph node dissection is still controversial, though the high specificity and negative predictive value of PET may be helpful in appropriate treatment planning [12, 13]. Low-volume disease and micrometastasis are the most frequent causes for false negative FDG PET findings. The use of larger scanning areas can also detect extra-abdominal disease (Fig. 6.15) [14]. Involvement of para-aortic metastasis is linked to prognosis and progression-free survival [15].

FDG PET helps in early detection of recurrent disease, evaluation of distant lesions, and followup of treatment (Fig. 6.16). The overall sensitivity for detection of recurrence was reported to be as high as 86 %, with specificity of 94 %; the positive predictive value was 85.7 % and the negative predictive value was 86.7 % [16]. It also is useful for assessing response to chemoradiation therapy (Fig. 6.17). Early metabolic response can be assessed, whereas anatomic changes may lag or may be difficult to assess.

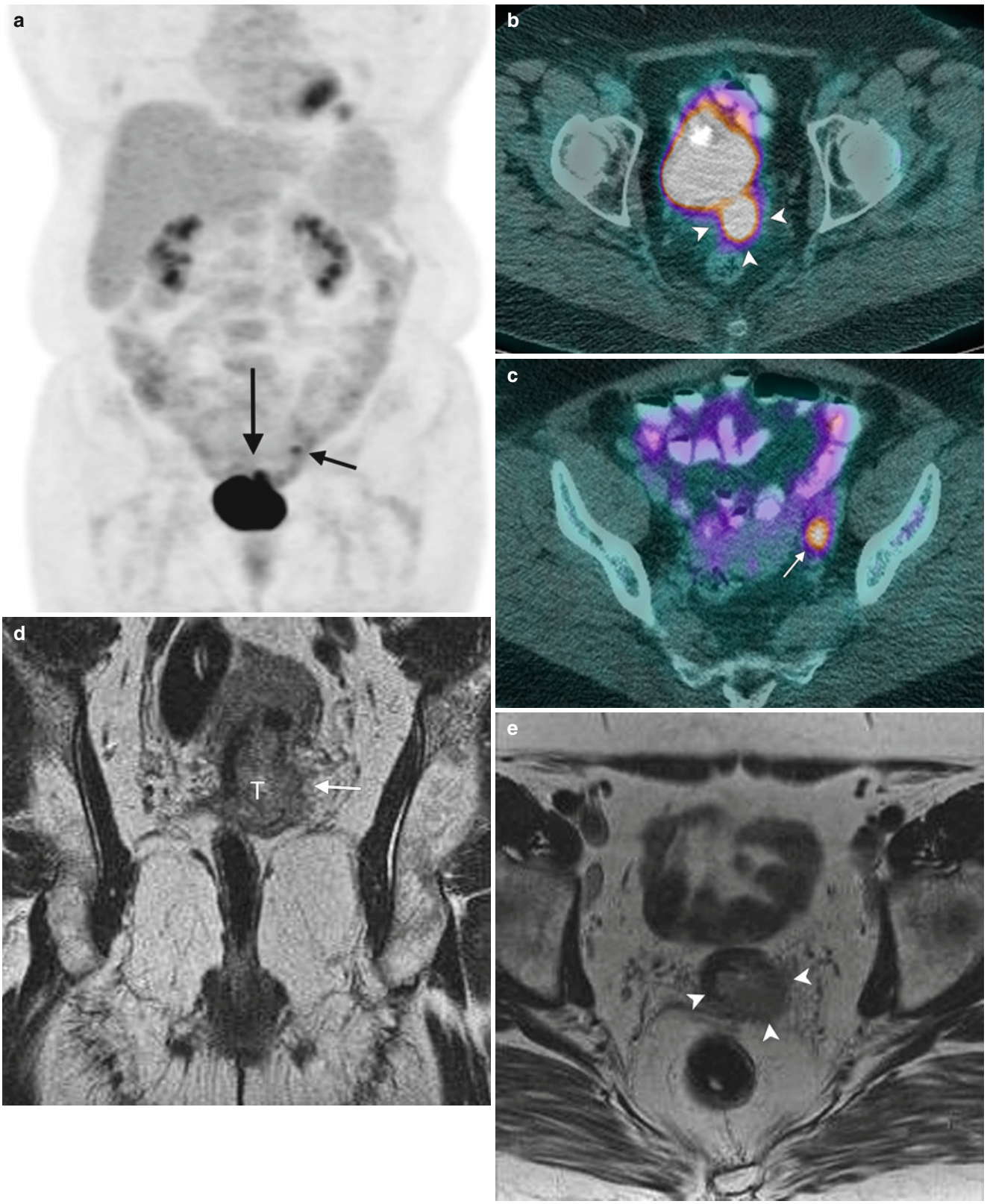

Fig. 6.12 Increased FDG uptake in primary cervical cancer with parametrial involvement and nodal uptake. In a 55-year-old woman with cervical carcinoma, FDG PET was performed for staging. A MIP image (**a**) shows a small area of activity beyond the superior aspect of the bladder (*long arrow*), and fused images confirm uptake in the primary tumor (*arrowheads*) (**b**), corresponding to the lesion on MRI (**c**). FDG uptake is also seen in a lymph node (**d**) as also seen on MRI (**e**). No uptake was seen in the endometrium or ovaries (**d**). MRI also shows tumor (*arrow*) involving the parametrium (**f**). The patient underwent laparoscopic dissection. Pathology revealed poorly differentiated, high-grade adenosquamous carcinoma of the cervix and metastatic disease in the left external iliac node

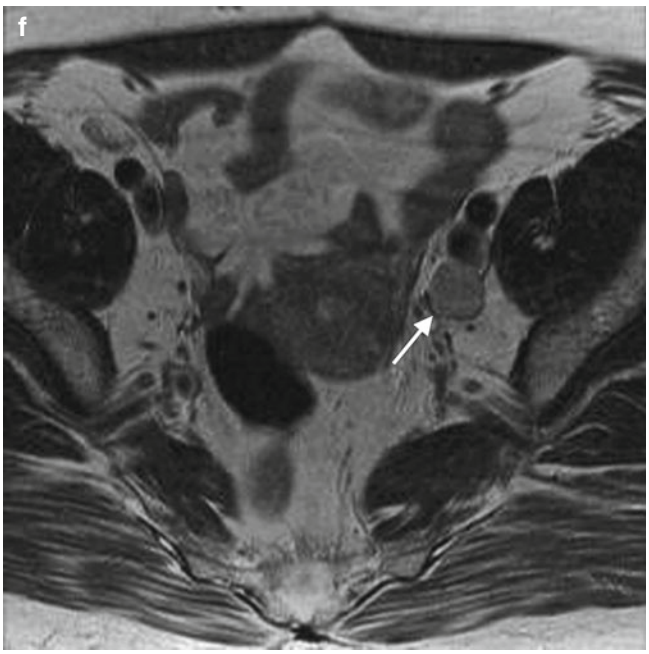

Fig. 6.12 (continued)

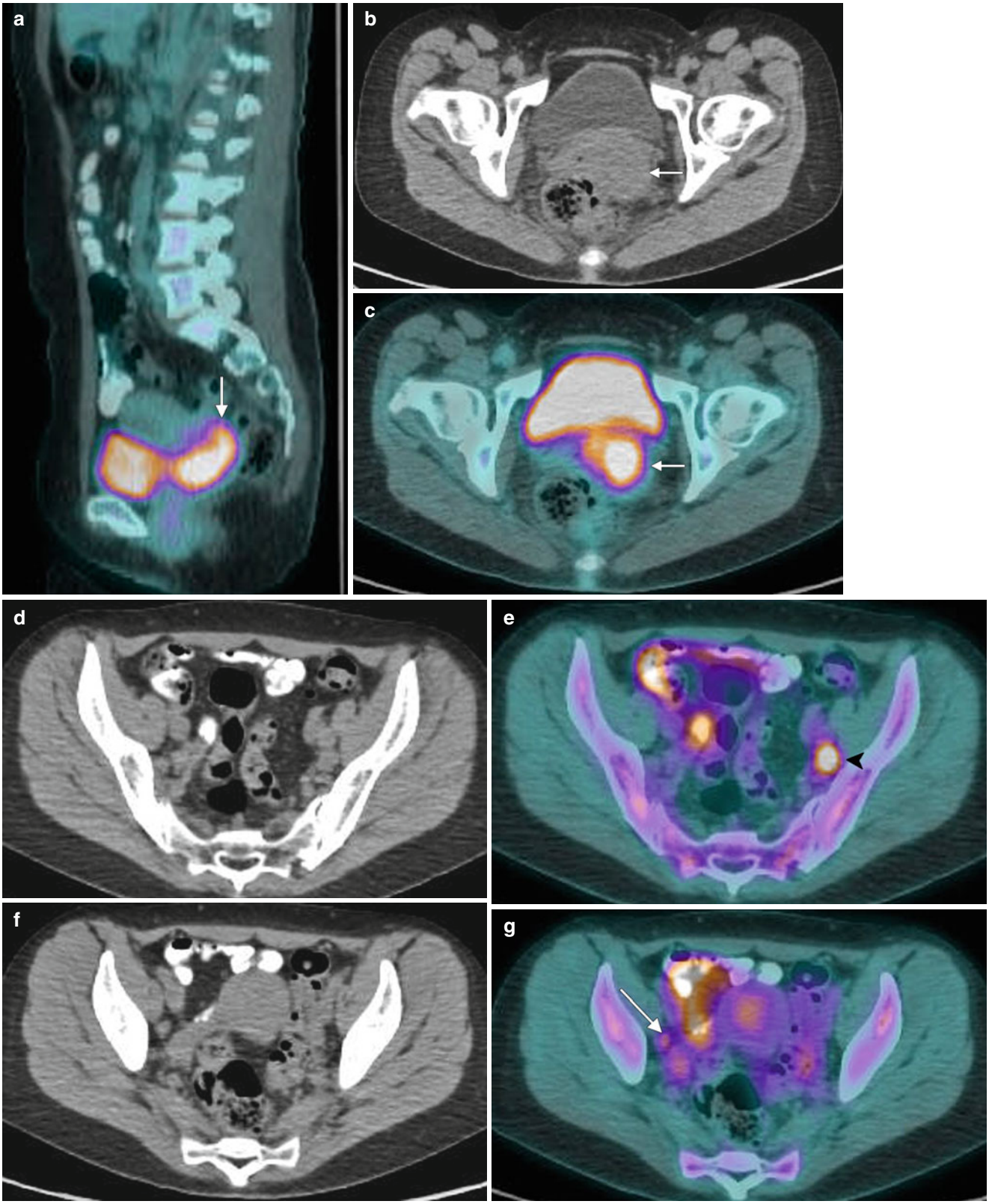

Fig. 6.13 Cervical cancer with bilateral nodes. In a 34-year-old woman with cervical cancer, FDG PET was performed for staging. Sagittal (**a**) and axial CT (**b**) and PET CT (**c**) images show increased uptake in the cervical mass. Intense uptake is also seen in a left external iliac node (**d**) (*arrowhead*), which was enlarged (**e**) Mild increased uptake is also seen in the right external iliac region with standardized uptake value (SUV) of 2.9 (*long arrow* in **f**) corresponding to a 9-mm node (**g**)

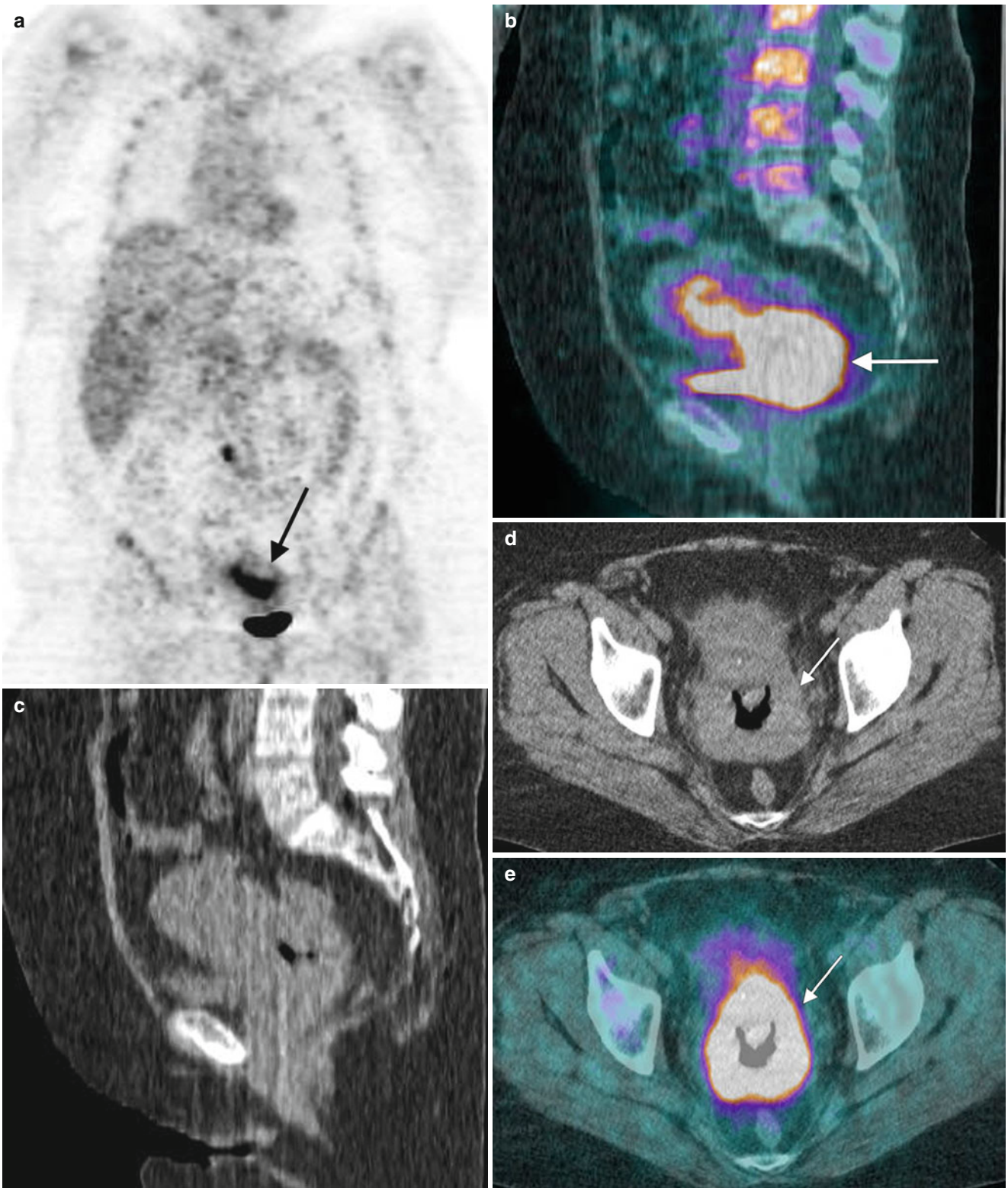

Fig. 6.14 Primary cervical cancer with extrapelvic nodal metastasis. A 53-year-old woman with high-grade squamous cell carcinoma of the cervix was imaged with FDG PET for staging and evaluation of extrapelvic nodes. MIP (**a**) shows increased uptake superior to the bladder (*long arrows*). Sagittal and axial fused images (**b**, **c**), show uptake the cervical mass as seen on corresponding CT images (**d**, **e**) with a standardized uptake value (SUV) of 19.5. Additionally FDG avid 1.2-cm node (*short arrow*), anterior to the inferior vena cava just proximal to the aortic bifurcation (**f**, **g**)

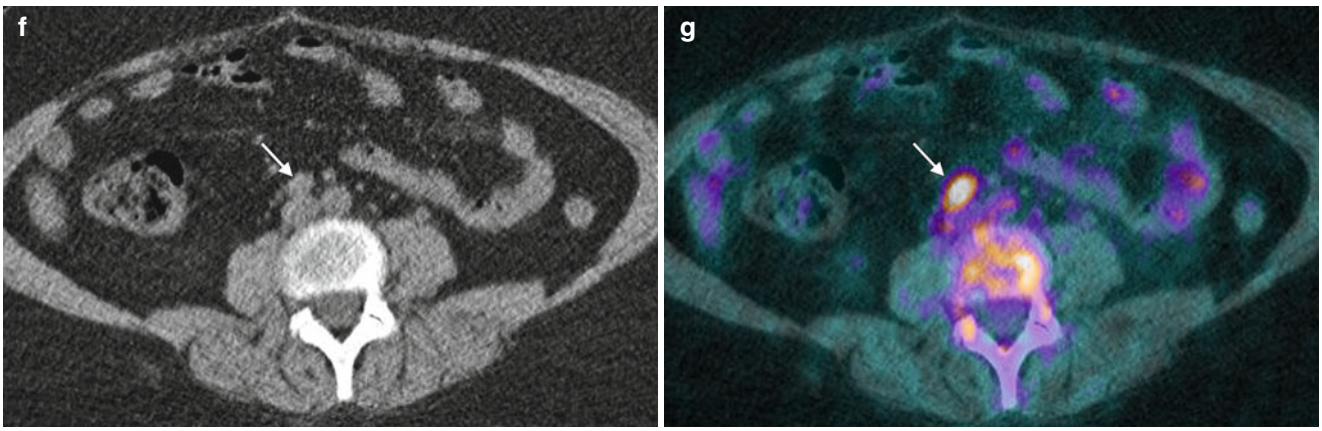

Fig. 6.14 (continued)

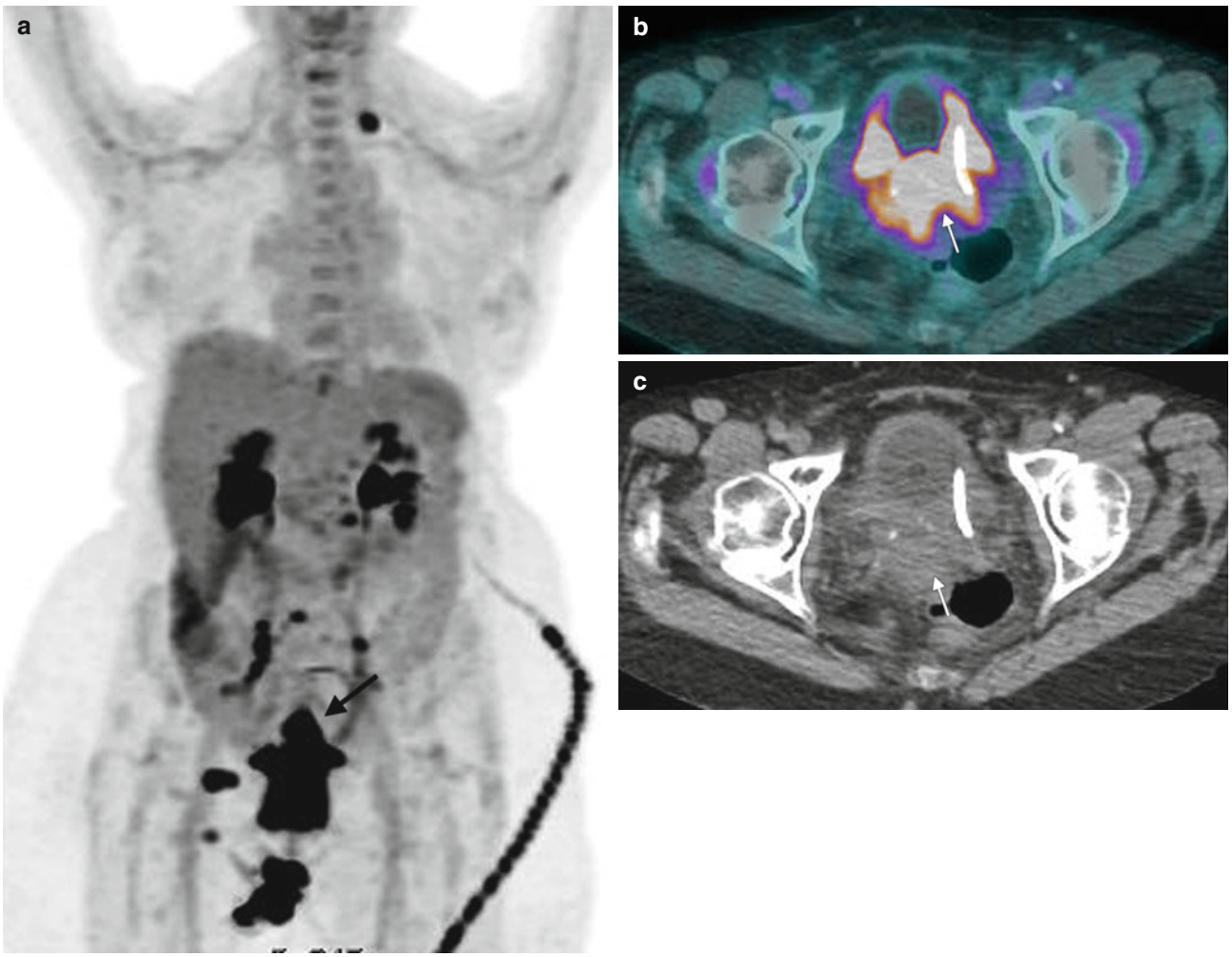

Fig. 6.15 Carcinoma of the cervix with distant metastasis in the left supraclavicular region. In a 58-year-old woman with cervical carcinoma, a MIP image (**a**) shows intense uptake in the pelvis (*arrow*), localizing to a cervical mass on axial CT and fused images (**b**, **c**). Additionally, uptake is seen in the retrocrural region (*arrow* in **d**) corresponding to a small node seen on CT (**e**) left retroperitoneal node (*short arrows* in **f** and **g**), right inguinal node (*arrow* in **h** and **i**), and supraclavicular node (*arrow* in **j** and **k**) seen on fused and CT images respectively, consistent with metastasis

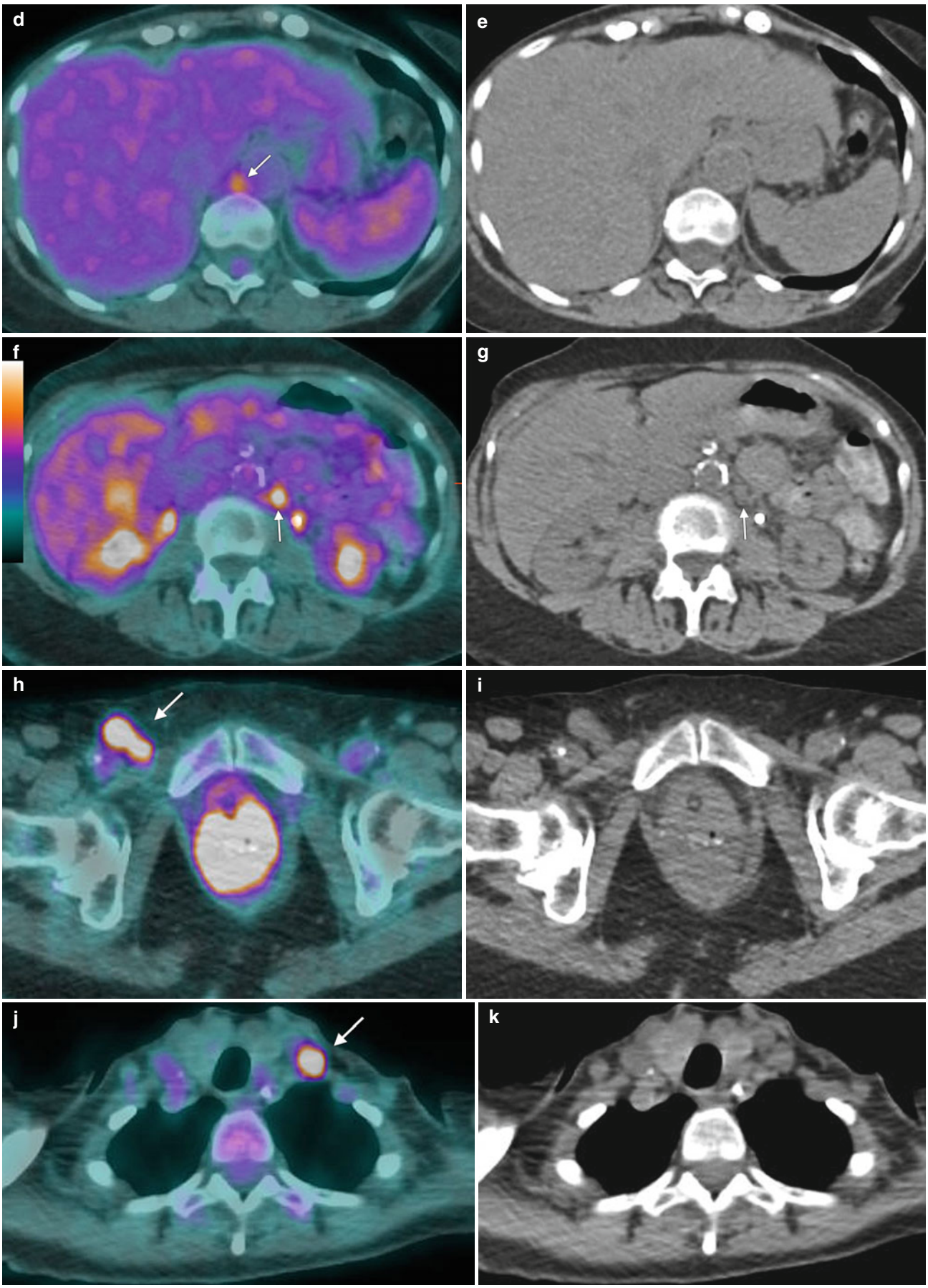

Fig. 6.15 (continued)

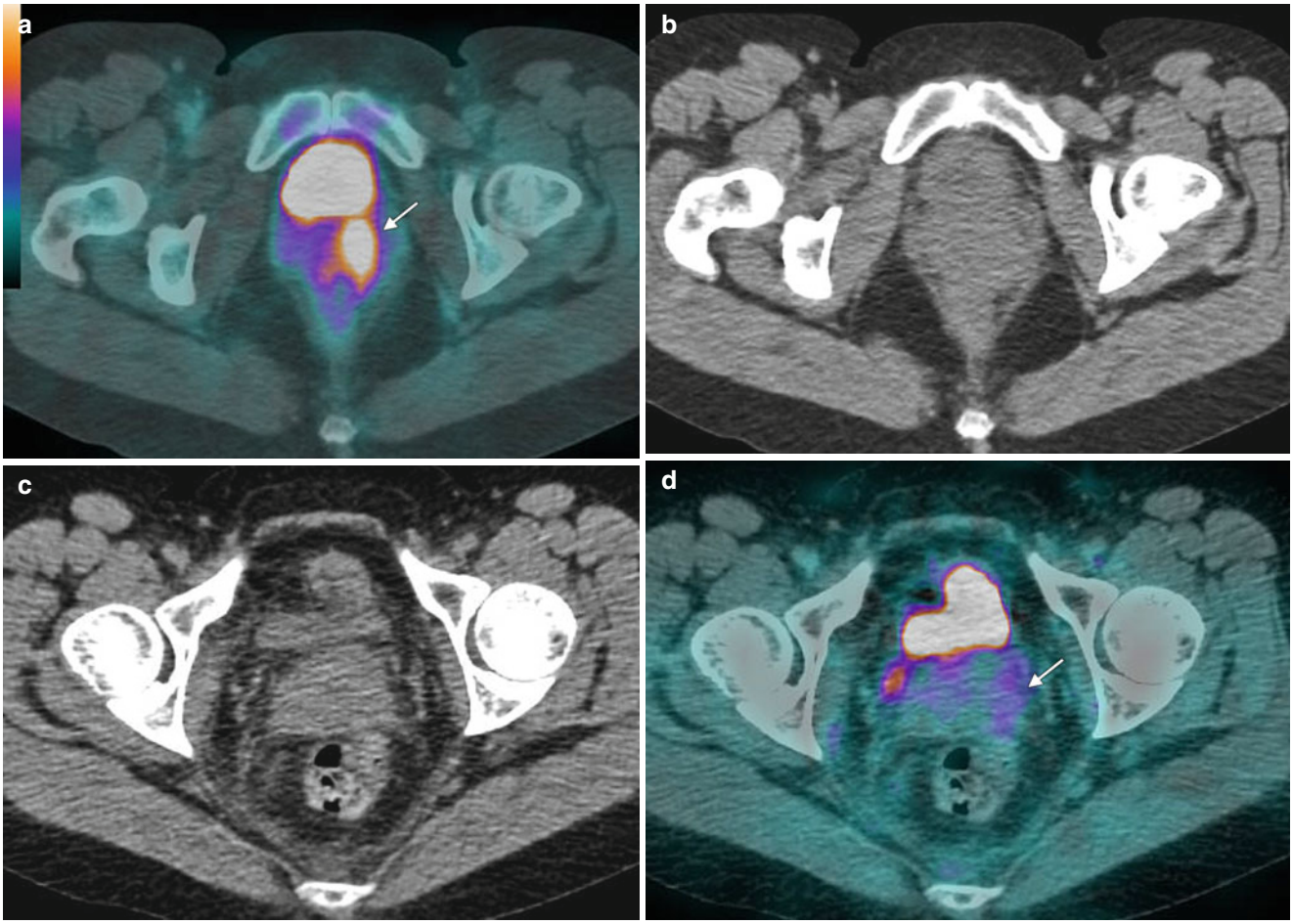

Fig. 6.16 Carcinoma of the cervix: serial imaging for followup of treatment response and evaluation of residual or recurrent disease. This 40-year-old woman had a history of adenocarcinoma of the cervix. Axial fused FDG PET-CT (**a**) and CT images (**b**) show uptake in the primary malignancy in the cervix (*arrow*), which was treated with chemoradiation therapy. A followup scan after treatment showed resolution of hypermetabolic uptake in cervix (**c**, **d**), suggesting metabolic response. A MIP FDG PET image (**e**) obtained a year later to evaluate for recurrence showed intense activity in the cervix (*long arrow* in **f**), corresponding to a lesion seen on MRI (**g**, **h**) consistent with recurrence. Increased FDG uptake is also seen in the mesenteric nodes (**i**, **j**) and internal iliac lymph node (**k**, **l**) consistent with metastatic disease (*arrowheads* in **c**)

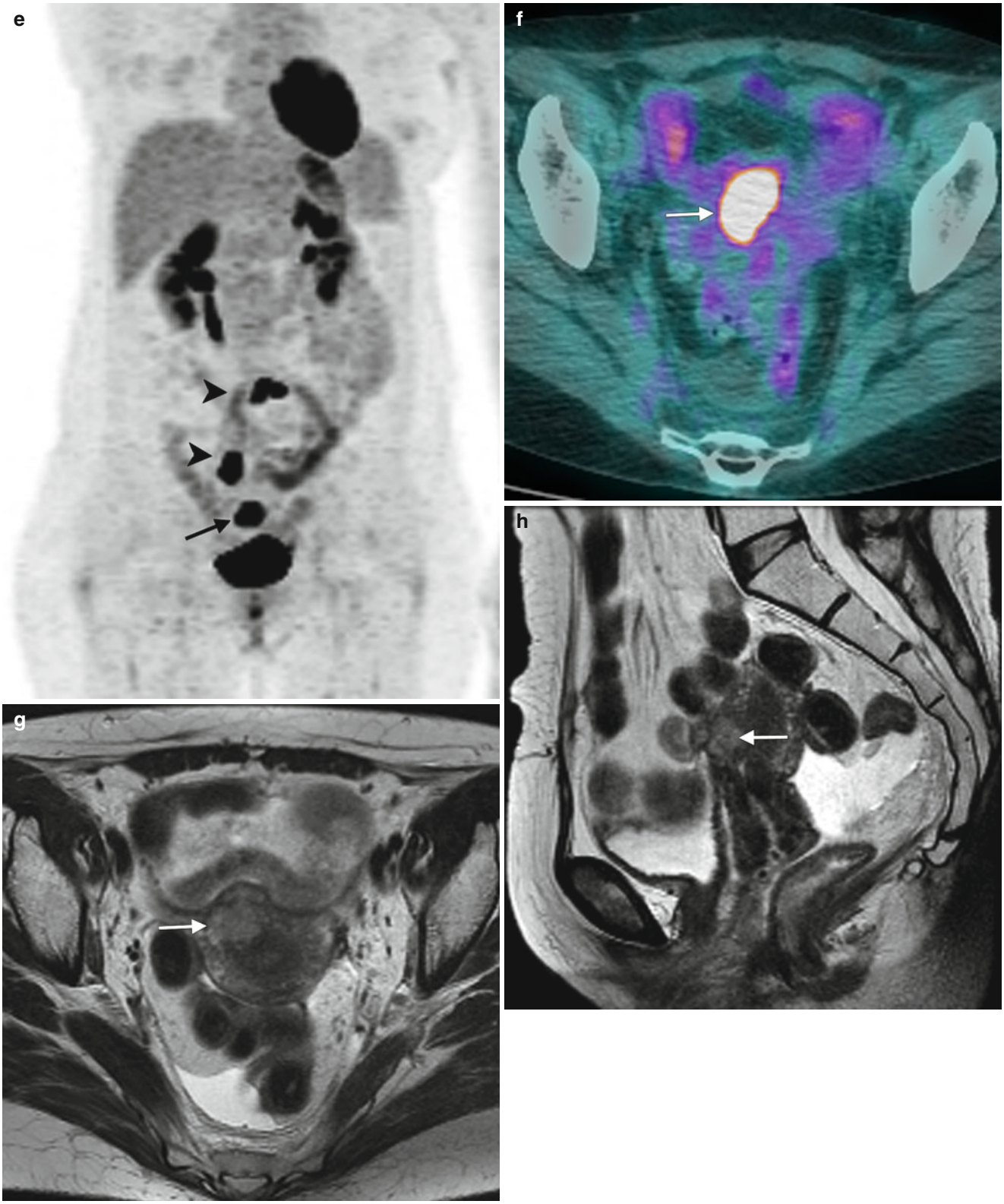

Fig. 6.16 (continued)

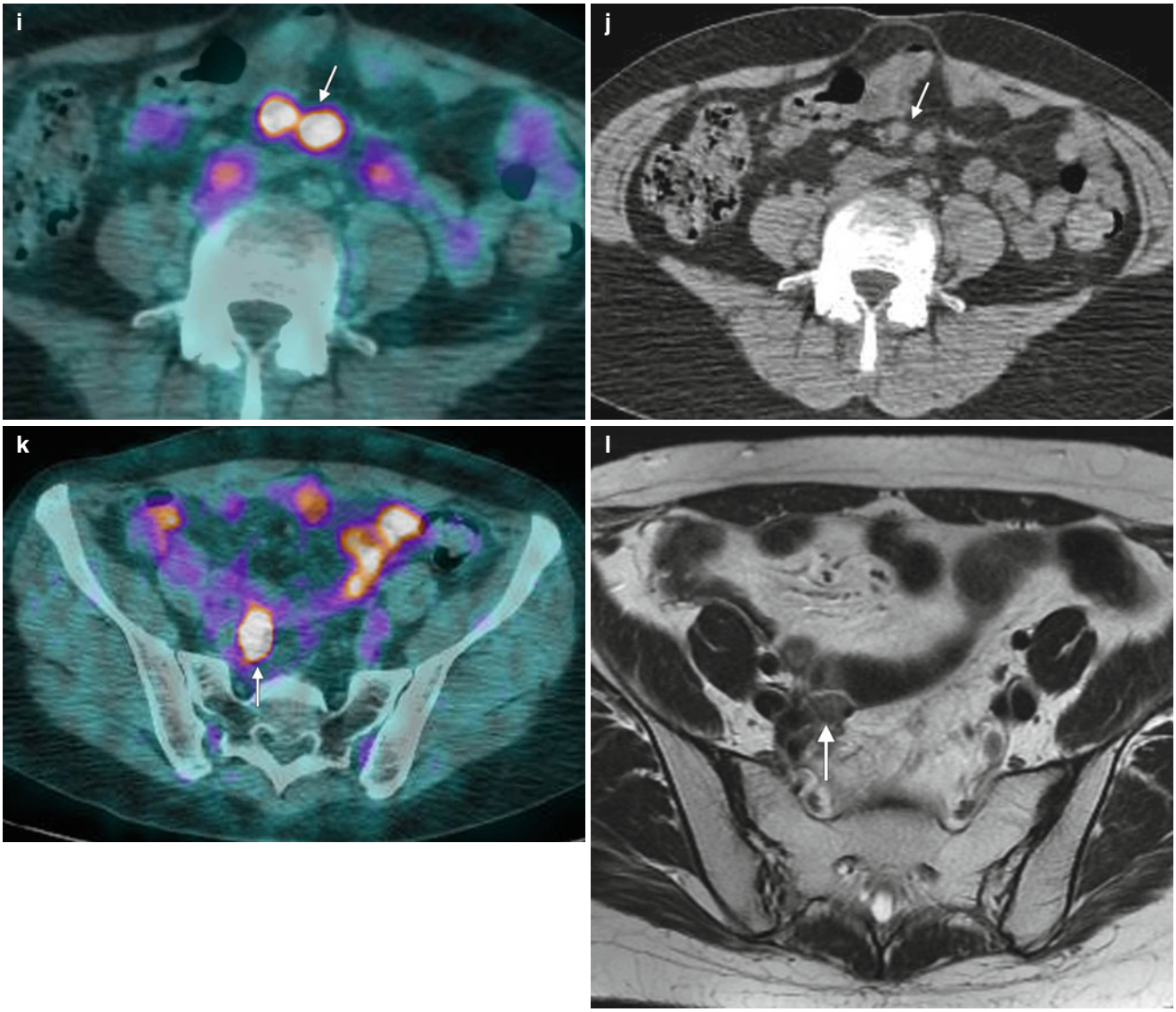

Fig. 6.16 (continued)

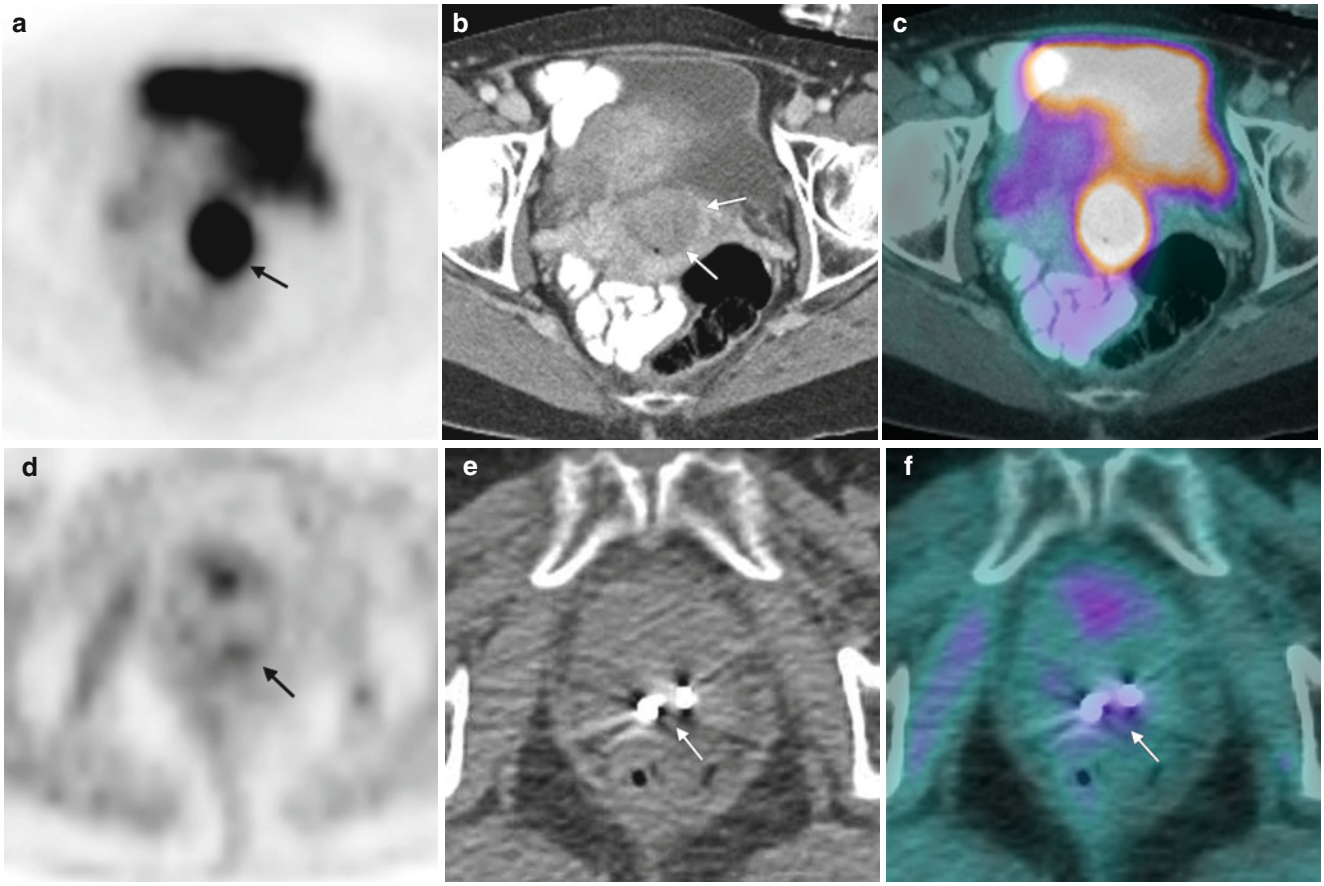

Fig. 6.17 Carcinoma of the cervix: assessment of response to radiation therapy. This 61-year-old woman underwent FDG PET-CT imaging for initial staging. (**a**–**c**) Scans showed a hypermetabolic lesion in the cervix. No other lesions were seen. The patient was subsequently treated with chemoradiation. (**d**–**f**) A followup study after the completion of treatment showed complete resolution of the hypermetabolic lesion in the cervix. (**e**, **f**) CT scans show the residual brachytherapy seeds in the cervix

6.3 Endometrial Cancer

Assessment of primary endometrial lesions for malignancy using FDG PET is limited because of size and resolution. Uterine malignancies can be detected by FDG (Fig. 6.18). The role of PET/CT in evaluation and management of uterine cancer is emerging. Currently, no data support routine presurgical imaging; instead, it is limited to selected cases with questionable or equivocal lesions that may be seen on other imaging. It is useful in confirming disease in nodes,

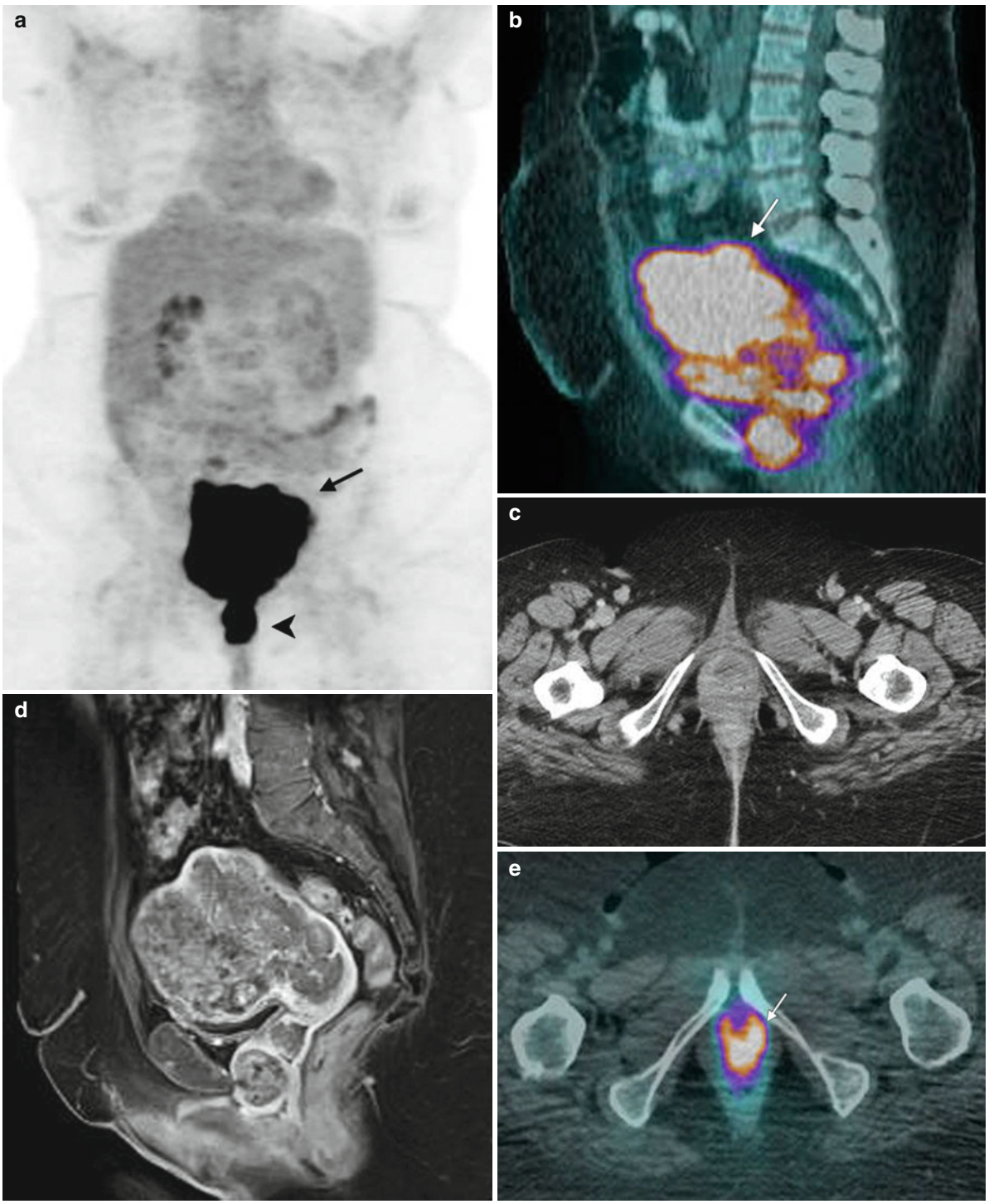

Fig. 6.18 FDG PET and primary endometrial cancer. A 55-year-old woman presented with irregular menorrhagia and metrorrhagia. Evaluation with ultrasound revealed a large pelvic mass. A dedicated CT scan, MRI, and PET-CT were performed for staging. MIP PET images (**a**) and a PET-CT sagittal image (**b**) show uptake (SUV 26.4) (*arrows*) in a large uterine mass measuring 13×9.8×9.7 cm (**c**), which pathology confirmed to be undifferentiated carcinoma. Inferiorly, the tumor extends to the periurethral region as seen on axial CT (**d**) and fused images (**e**) and MRI sagittal MRI image (**f**). There was invasion of serosa and extension to the pelvic side wall (**g**, **h**), with increased FDG activity (SUV 11.6) (**i**). There was extension to the bladder and involvement of the vagina (**j**, **k**). Uptake is also seen in pelvis anteriorly (**l**) along bowel serosa (**m**), consistent with an implant. No extrapelvic nodes or distant metastases were seen

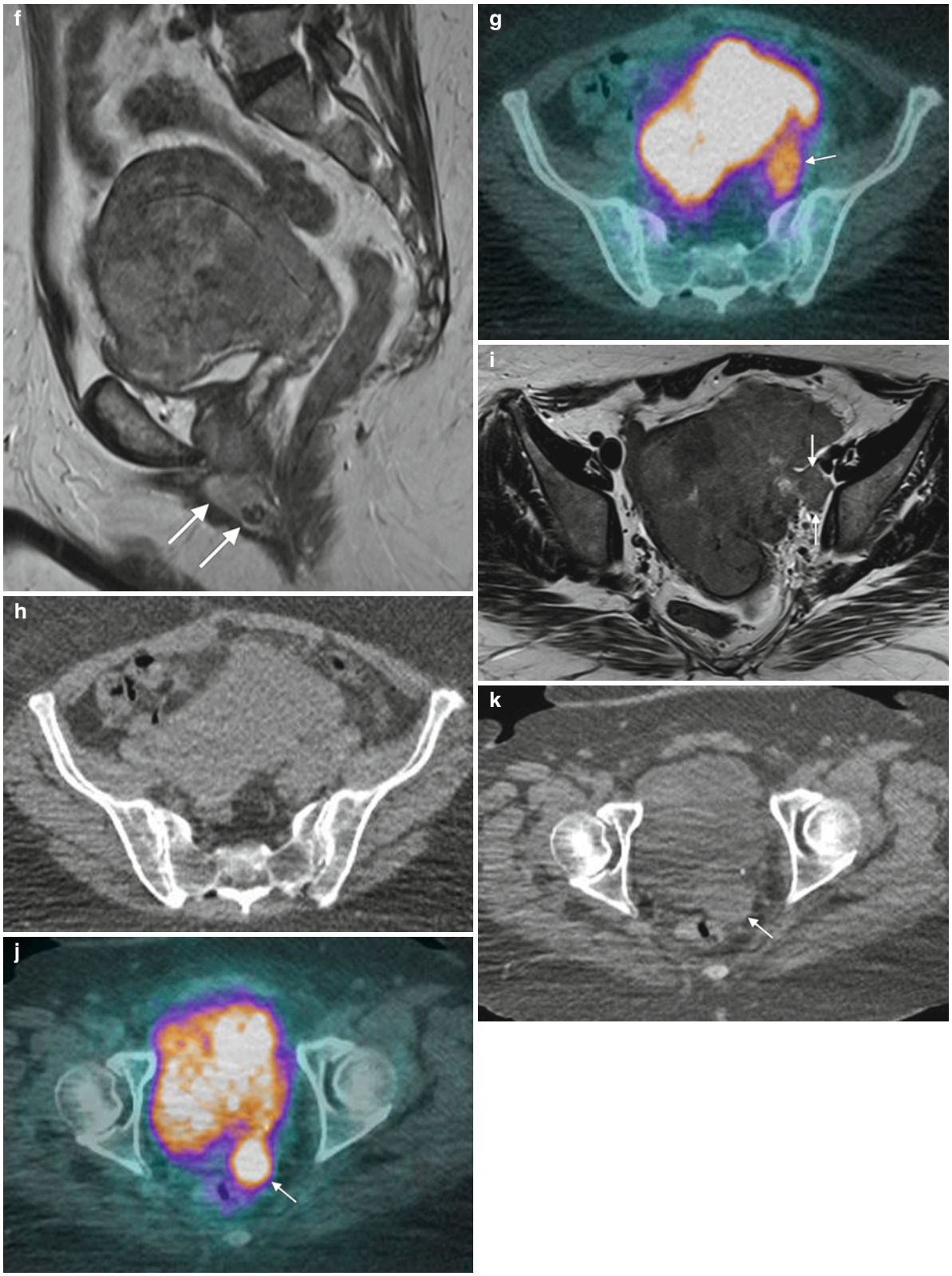

Fig. 6.18 (continued)

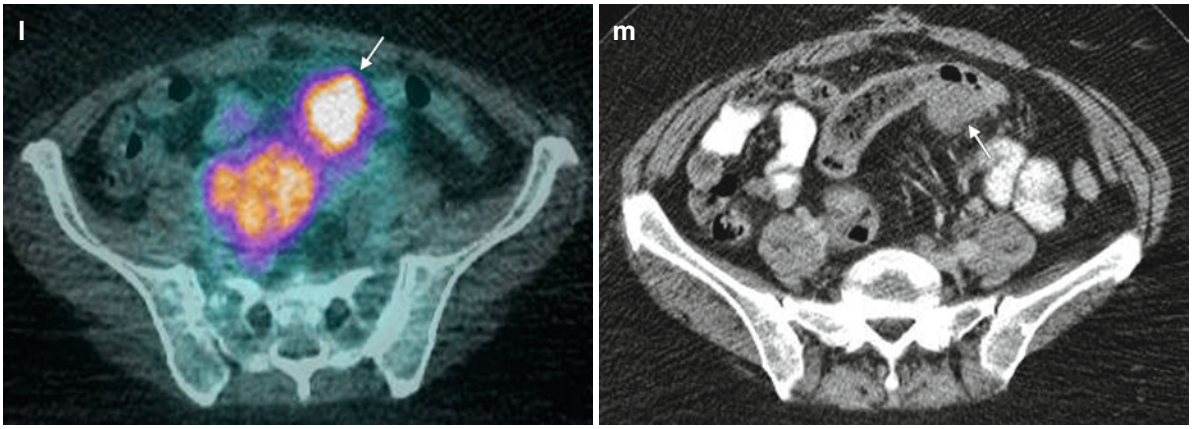

Fig. 6.18 (continued)

and it is possible to detect extrapelvic sites of disease in high-grade endometrial cancers with high sensitivity, though lower sensitivity has been reported in detecting nodal disease [17]. The uptake correlates with histologic grade and tumor size [18]. Extrapelvic and extra-abdominal sites of involvement can be detected in the evaluation of recurrent disease (Figs. 6.19 and 6.20). PET is useful for postsurgical monitoring and surveillance; high uptake has been linked to poor prognosis [19]. In followup of previously treated endometrial cancers in 34 women, Belhocine and colleagues detected unsuspected, asymptomatic recurrences in 4 women (12 %) and detected additional metastatic sites in 9 (35 %) of 26 patients with confirmed recurrences, significantly altering the treatment choice [20].

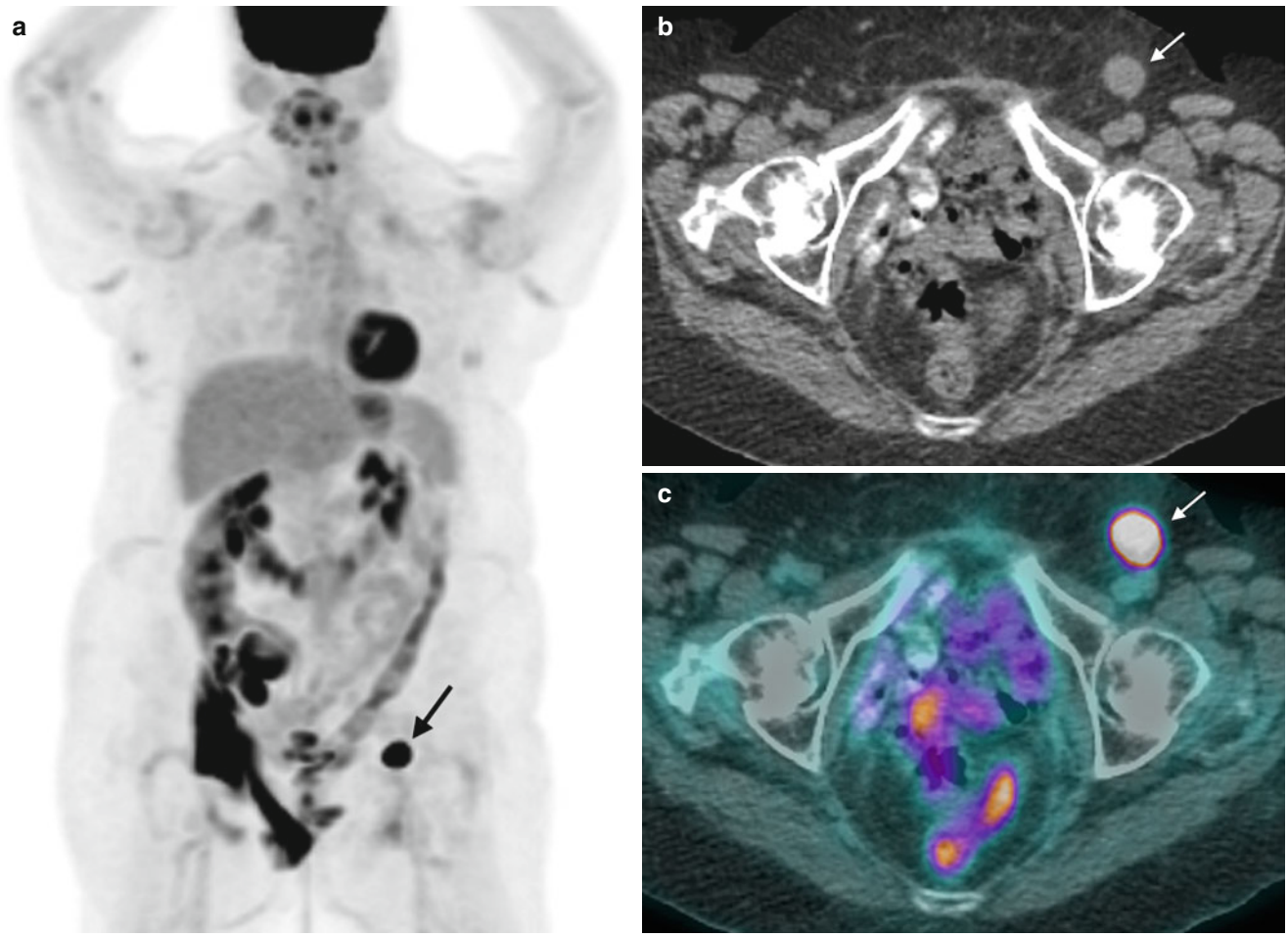

Fig. 6.19 Recurrent endometrial cancer with inguinal node metastasis. FDG PET-CT images were obtained in a 58-year-old woman referred for restaging of endometrial cancer. The patient had prior anterior pelvic exenteration for recurrent endometrial carcinoma. (**a**–**c**) PET images show a solitary inguinal lymph node metastasis (*arrow*), which was subsequently resected

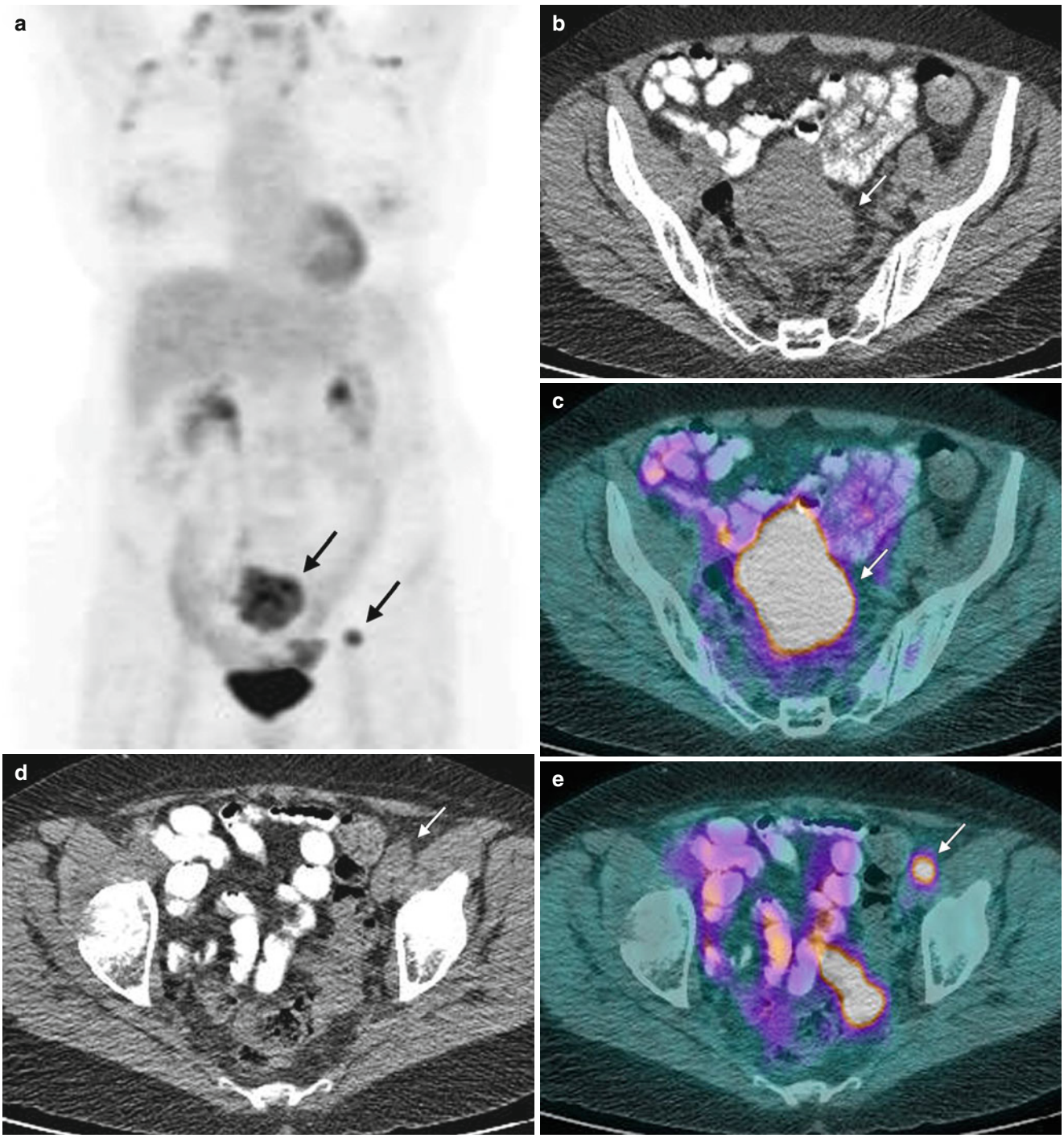

Fig. 6.20 Recurrent endometrial cancer with pelvic masses and perihepatic implant. A 73-year-old woman was referred for evaluation of the extent of endometrial cancer. MIP images (**a**) show a large area of uptake in the pelvis, which corresponded to the recurrent pelvic mass pelvic mass seen on transaxial CT and PETCT images (*arrow* in **b** and **c**) with an uptake of 12.7, consistent with recurrent disease. A hypermetabolic left external iliac node is seen with an SUV of 6.8 on transaxial CT and PETCT images (**d**, **e**). Additional sites seen on CT and fused PET CT images respectively included a subcentimeter right common iliac SUV 2.8 (**f**, **g**) and a perihepatic implant SUV 5.9 (**h**, **i**) consistent with metastatic disease

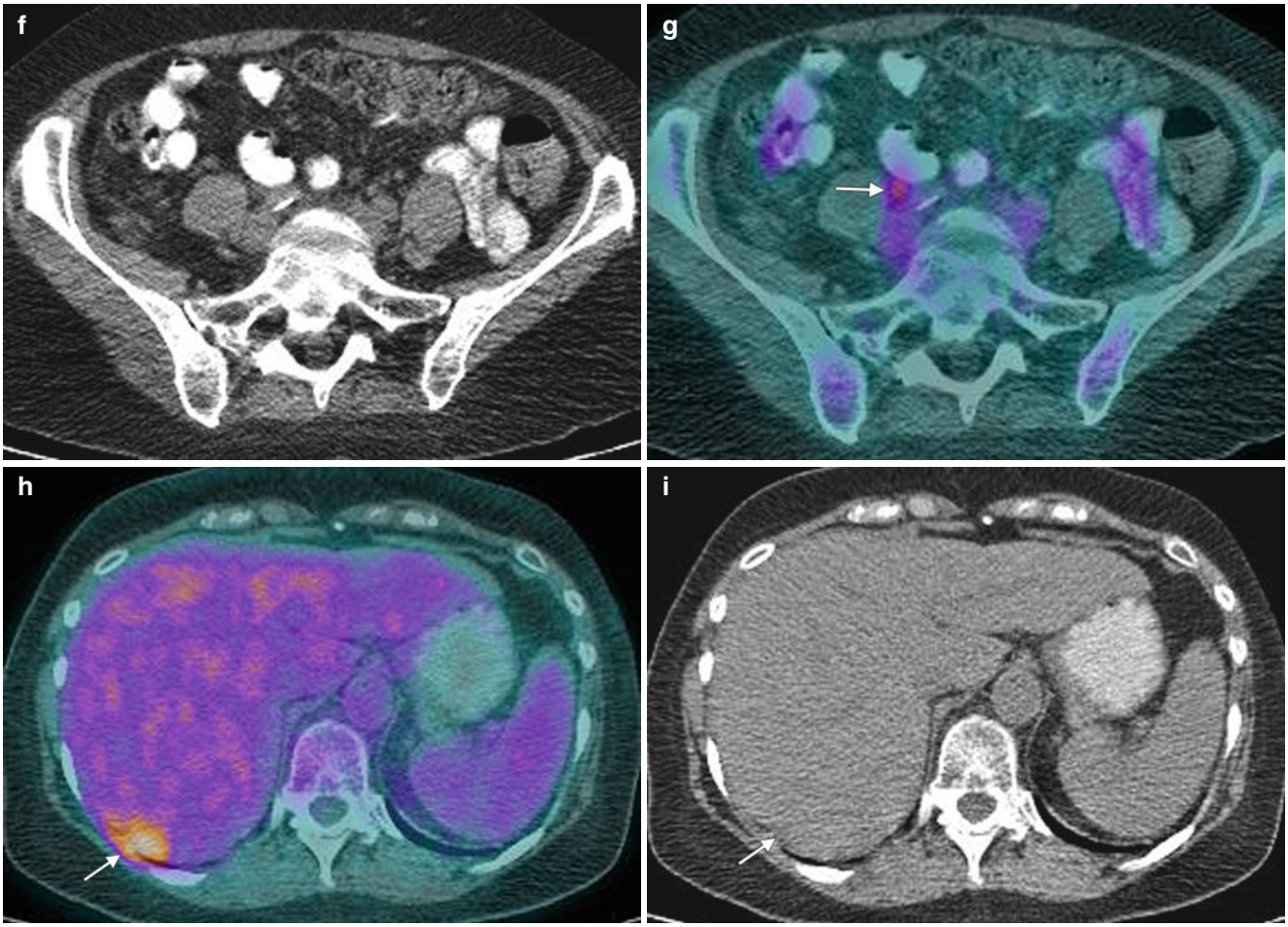

Fig. 6.20 (continued)

6.4 Ovarian Cancer

Most primary epithelial tumors show high FDG activity (Fig. 6.21) that correlates to tumor grade and cell proliferation [21]. PET-CT has a limited role in the primary diagnosis and staging of ovarian cancer, owing to lack of resolution and false negatives. Ultrasound, CT, and MRI remain the mainstay of initial evaluation and staging, but PET may add value in some cases. Although some studies have reported the detection of lesions smaller than

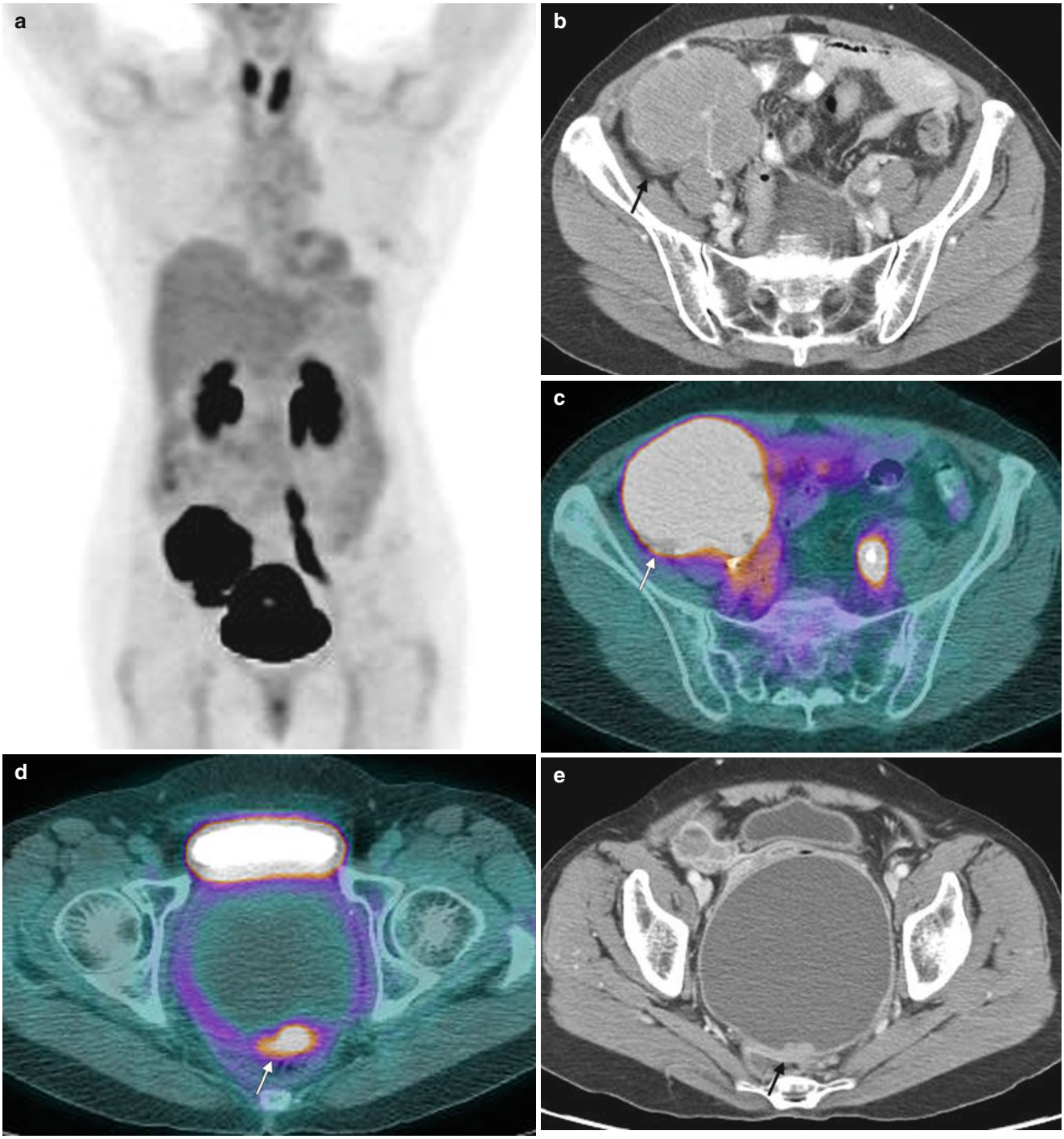

Fig. 6.21 Adnexal mass with large cystic lesions. A 60-year-old woman reported symptoms of pelvic pressure and urinary frequency. Evaluation showed a large pelvic cyst and a mass. FDG PET, performed for staging, showed intense activity in the pelvis (*arrow*) and dilated left ureter (*short arrow*) as seen on MIP image (**a**). The pelvic uptake is seen localizing to a right pelvic solid mass seen in transaxial CT (**b**) and fused PETCT (**c**) with a standardized uptake value (SUV) of 20.9). Peripheral uptake was seen in the cystic mass in the cul-de-sac with SUV 9.3 (**d**), more intense focus seen along the posterior thickening in the wall (**e**). Pathology showed high-grade serous carcinoma of the ovary. Small peritoneal carcinomatosis was not FDG-avid probably limited by size (**f**)

Fig. 6.21 (continued)

a centimeter, generally the detection of small lesions and peritoneal deposits is limited. In specific cases, PET may add incremental value to conventional imaging by detecting disease in normal-size or small-size lymph nodes and by confirming extra-abdominal or distant disease [22–25]. Because of the larger scanning area, unknown extra-abdominal disease, such as supradiaphragmatic metastases and supraclavicular lymph node metastases, can be detected (Figs. 6.22, 6.23, and 6.24). Uptake is lower in borderline mucinous tumors and germ cell tumors, leading to false negative results [26].

Recurrent disease is frequent in ovarian cancer and can present as pelvic masses, recurrence at the vaginal cuff, pelvic side wall recurrence, peritoneal tumor implants, malignant ascites, lymphadenopathy, or distant metastases in sites such as the lung, pleura, liver, or bone (Fig. 6.25). In general clinical practice, CT scans remain the first imaging modality in followup, and PET is used only when other imaging gives unclear results or is negative in the presence of rising tumor markers. The utility of FDG PET in recurrent ovarian cancer includes surveillance, assessment in patients with rising tumor markers, and help with management decisions. The reported sensitivity and specificity ranges 83–91% and 66–93% respectively. Sensitivity has been shown to be up to 83–91 % and its specificity has been reported to be 66–93 % [23–28].

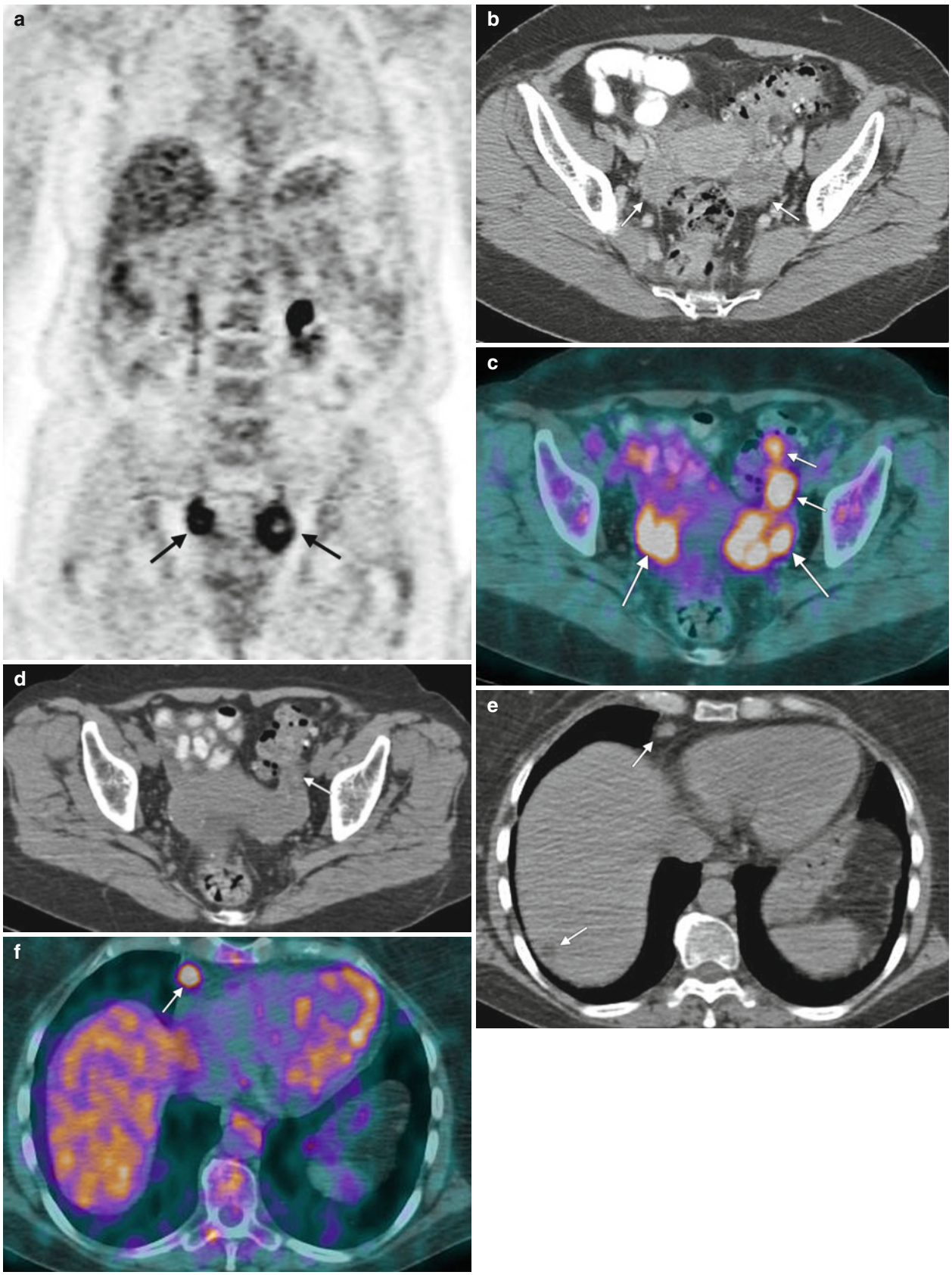

Fig. 6.22 Primary ovarian cancer with involvement of a diaphragmatic node. A 65-year-old woman presented with increasing abdominal distention with ascites, which was drained. Further workup revealed adnexal and pelvic masses. FDG PET was done at the time of initial evaluation, for staging that revealed intense uptake in bilateral adnexal masses (*arrows* in **a**–**c**) with a maximum standardized uptake value (SUV_{max}) of 8.9 and hypermetabolic uptake along bowel serosa in the left pelvis, with SUV of 10.2 (*short arrow* in **c** and **d**). Additionally, a hypermetabolic right anterior diaphragmatic node (SUV 7.2) was seen, consistent with metastasis (**e**, **f**). Pathology showed high-grade serous ovarian carcinoma. A non–FDG-avid hepatic low-attenuation lesion was consistent with a cyst and remained stable on followup

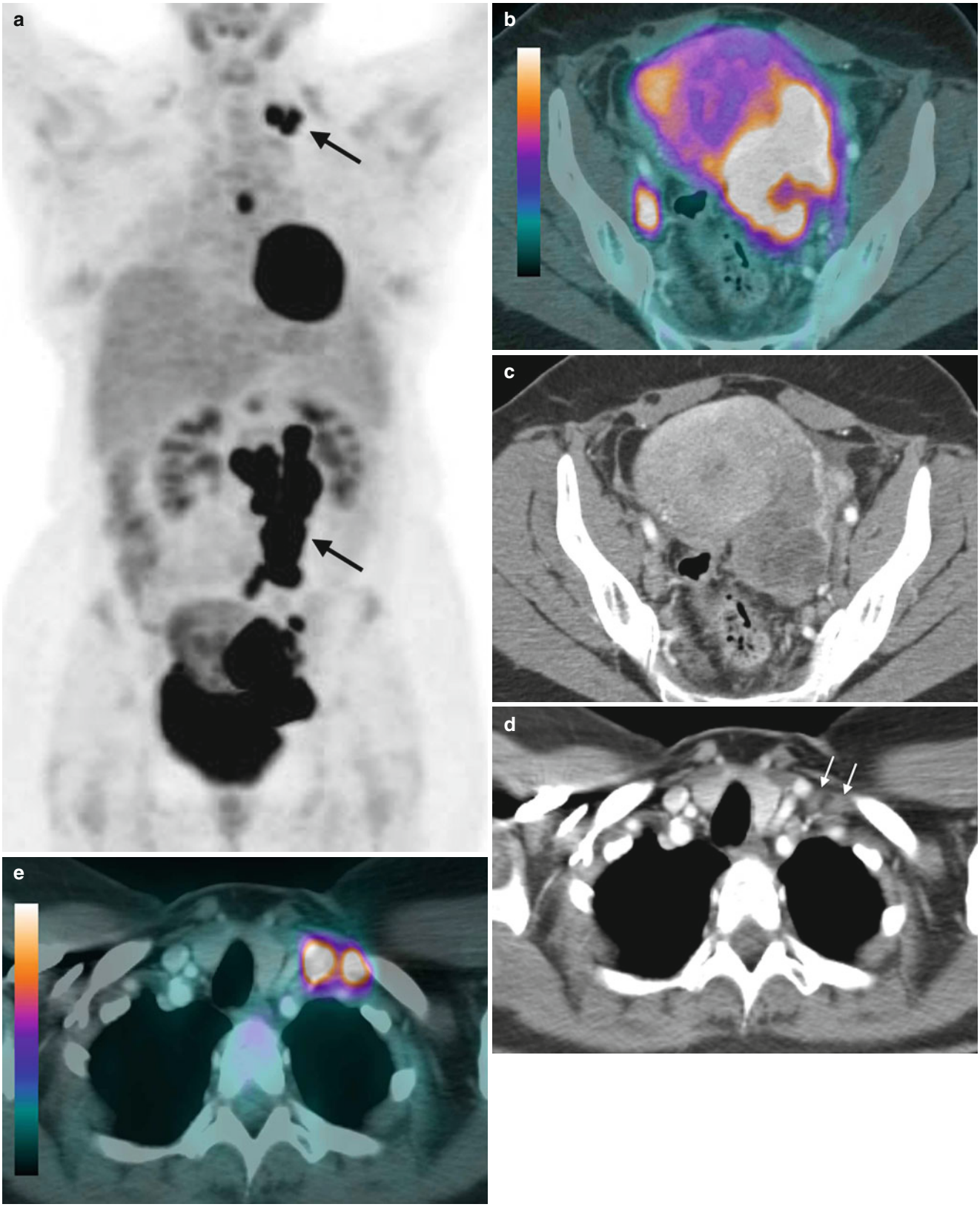

Fig. 6.23 Staging: detection of unknown distant metastatic sites. A 51-year-old woman with ovarian carcinoma was referred for FDG PET scan for staging. The scan showed intense uptake in the primary lesion in the left pelvis, seen superolateral to the bladder on (MIP) images (**a** in arrow) and on the fused images (**b**) and the CT image (**c**). Intense uptake is also seen in two supraclavicular lymph nodes (**d**, **e**) measuring up to 1.2 cm with standardized uptake value (SUV) of 8.2, multiple retroperitoneal nodes with SUV 12.4 (**e**) also seen on MIP images (*arrowhead in* **a**), and mediastinal nodes with SUV 6.5 (**f**), consistent with distant metastasis

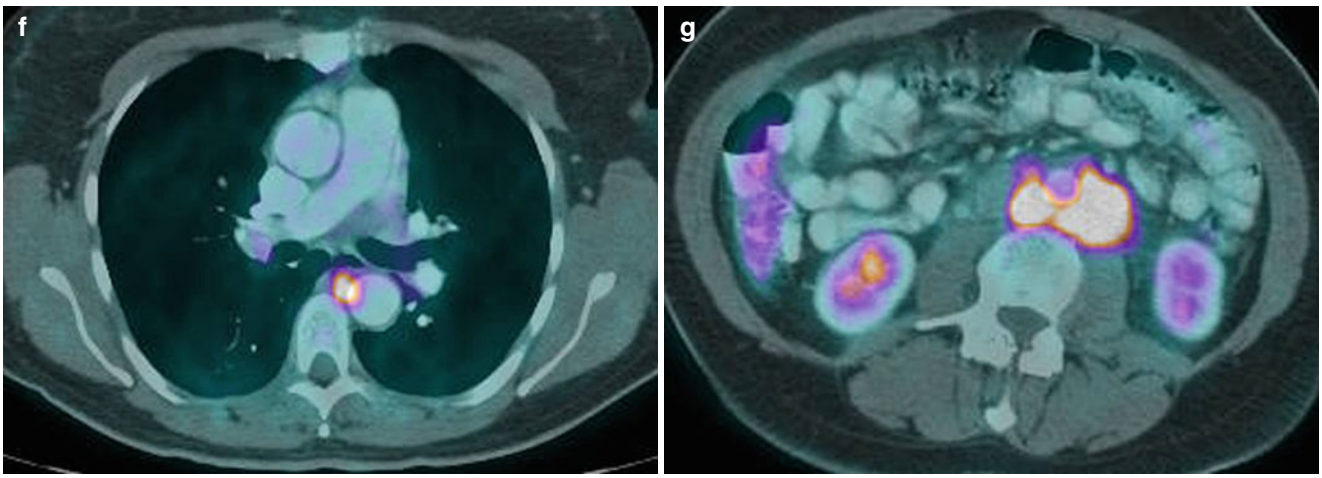

Fig. 6.23 (continued)

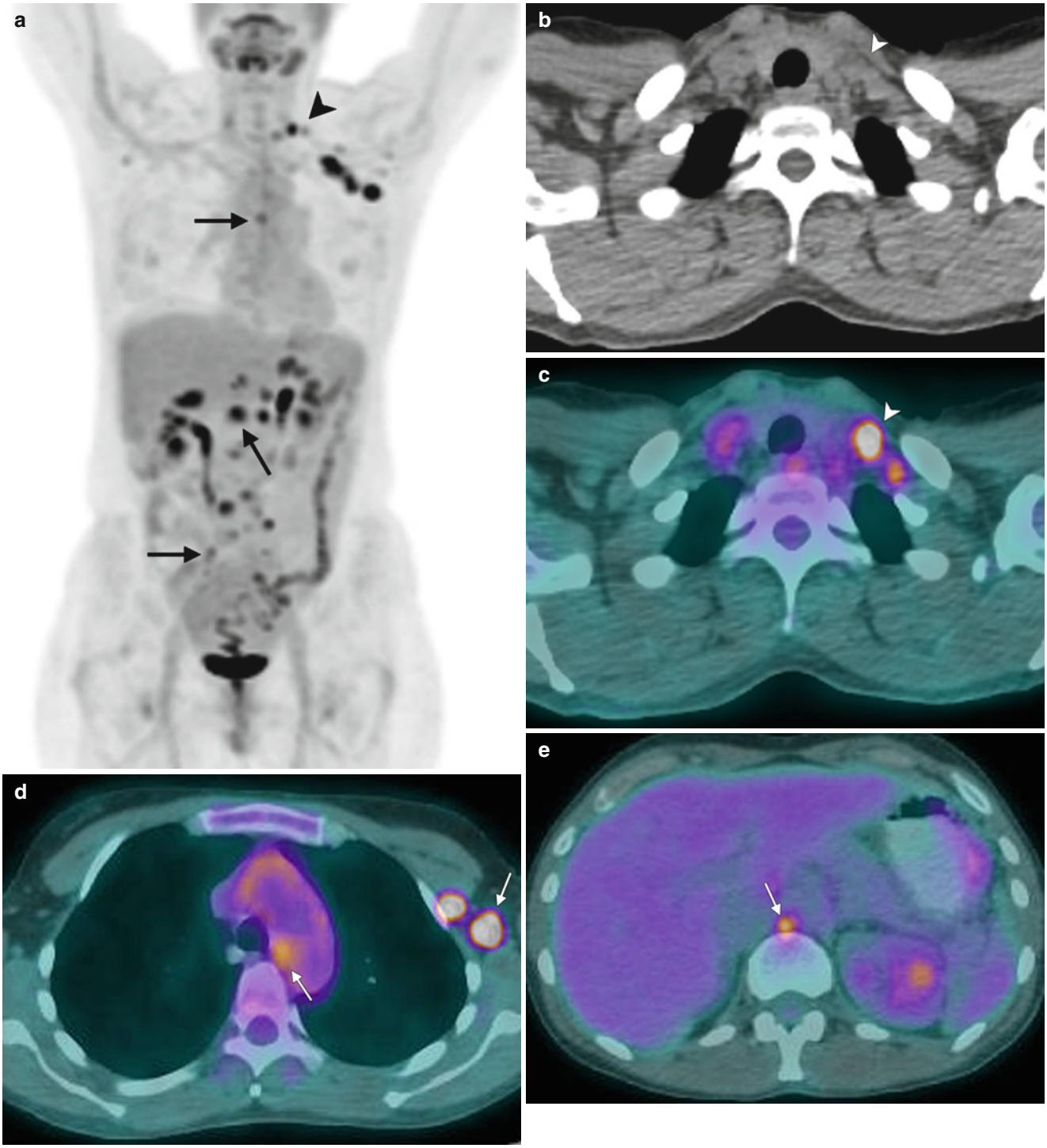

Fig. 6.24 Restaging: detection of extra-abdominal distant metastatic sites. FDG PET-CT scanning was performed in a 53-year-old patient with ovarian cancer being evaluated for recurrence. A MIP image (**a**) shows hypermetabolic nodal disease in the retroperitoneum and pelvis (*arrows*). Additional extra-abdominal sites were seen in the left supraclavicular region (**b**, **c**), a mediastinal node and multiple nodes in the left axilla (**d**), and a subcentimeter node in the retrocrural region (**e**), consistent with metastatic disease

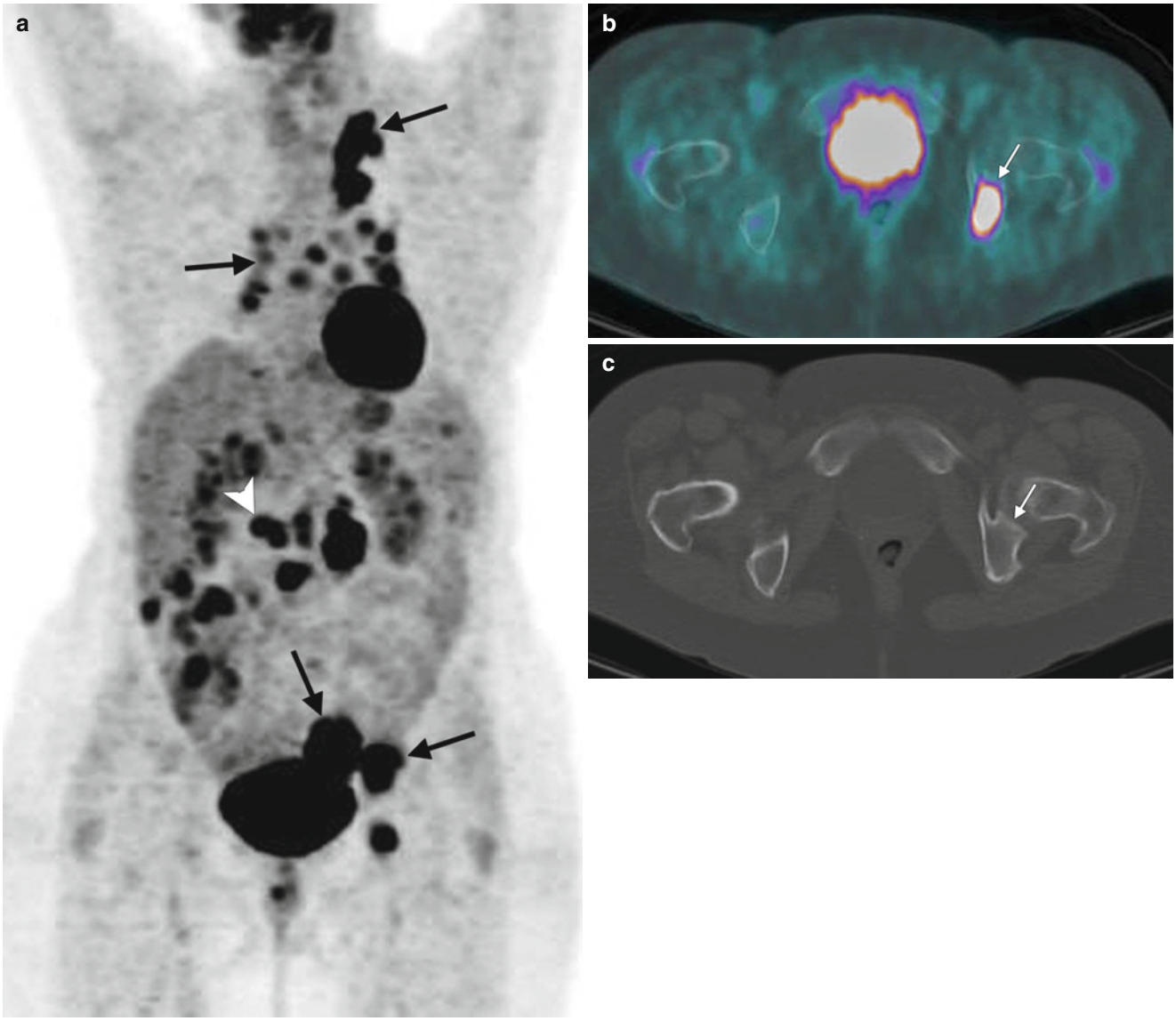

Fig. 6.25 Ovarian cancer: detection of unknown, extra-abdominal distant metastatic sites. A 63-year-old woman with poorly differentiated carcinoma of the left ovary was referred for FDG PET scanning for evaluation of the extent of disease. MIP images (**a**) show pelvic ovarian mass with peritoneal disease (*arrows*), retroperitoneal adenopathy (*arrowhead*), and mediastinal and left supraclavicular adenopathy (*arrows*). In addition, a left acetabular lesion was seen more clearly on PET (**b**) than on CT (**c**), consistent with metastatic disease

6.5 Vaginal and Vulvar Cancer

The role of FDG PET in patients with vaginal or vulvar cancer is generally limited to the assessment of nodal involvement, including pelvic and extrapelvic sites. It is not routinely used for staging and is generally obtained based on clinical need and findings on other imaging. The primary tumors do accumulate FDG avidly. Unilateral or bilateral involvement of pelvic or inguinal nodes or extrapelvic disease may be detected at primary staging or at recurrence (Fig. 6.26).

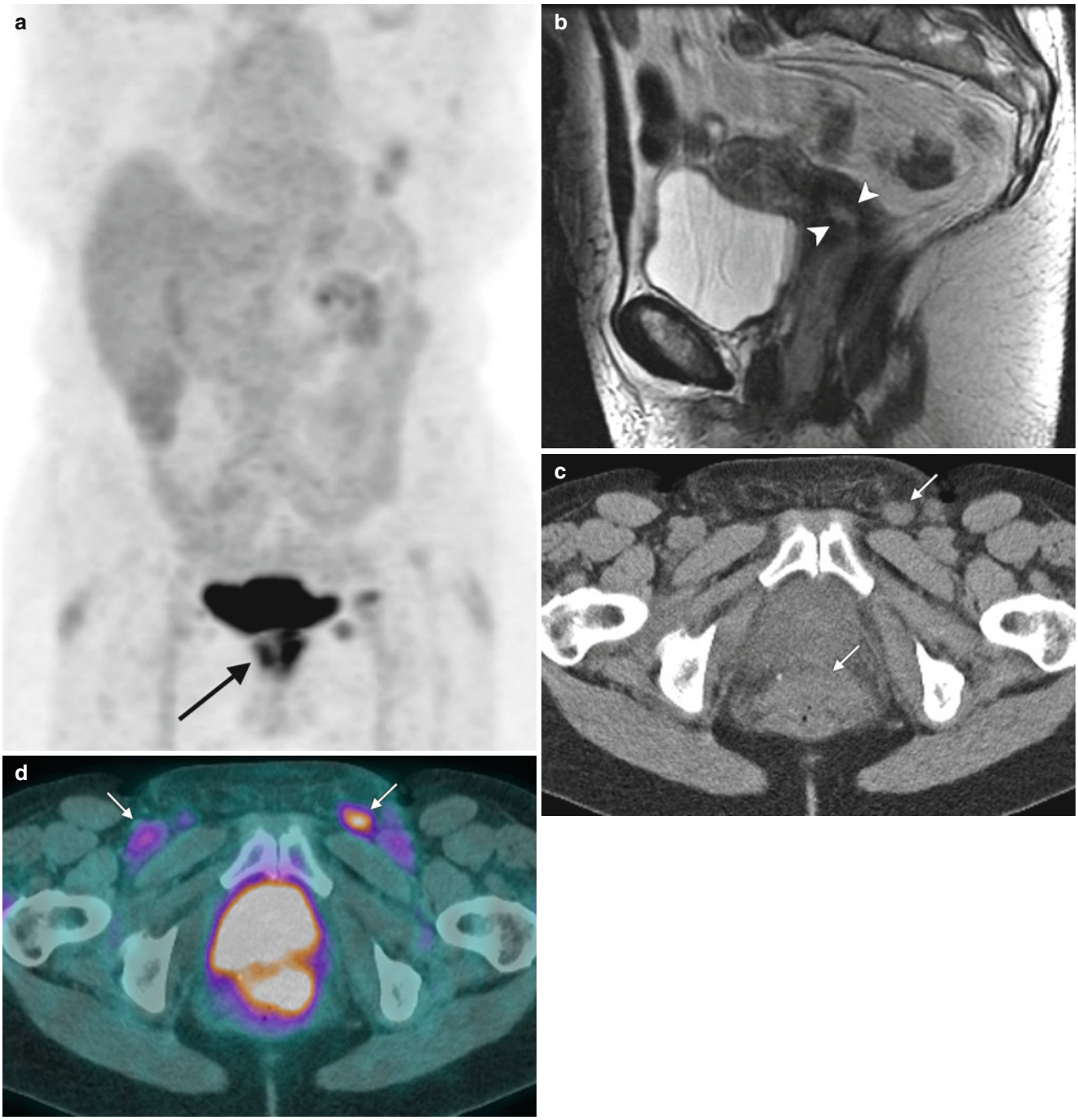

Fig. 6.26 Vaginal cancer. This 81-year-old woman with squamous cell carcinoma of the vagina was referred for evaluation prior to treatment. FDG PET-CT was performed for evaluation of the extent of disease. A MIP image (**a**) showed increased uptake in the vagina corresponding to abnormality on MRI (**b**) and also bilateral inguinal nodes (**c**, **d**)

References

1. Chander S, Meltzer CC, McCook BM. Physiologic uterine uptake of FDG during menstruation demonstrated with serial combined positron emission tomography and computed tomography. Clin Nucl Med. 2002;27:22–4.
2. Subhas N, Patel PV, Pannu HK, Jacene HA, Fishman EK, Wahl RL. Imaging of pelvic malignancies with in-line FDG PET-CT: case examples and common pitfalls of FDG PET. Radiographics. 2005;25:1031–43.
3. Nishizawa S, Inubushi M, Okada H. Physiological 18F-FDG uptake in the ovaries and uterus of healthy female volunteers. Eur J Nucl Med Mol Imaging. 2005;32:549–56.
4. Lerman H, Metser U, Grisaru D, Fishman A, Lievshitz G, Even-Sapir E. Normal and abnormal 18F-FDG endometrial and ovarian uptake in pre- and postmenopausal patients: assessment by PET/CT. J Nucl Med. 2004;45:266–71.
5. Grab D, Flock F, Stohr I, Nussle K, Rieber A, Fenchel S, Brambs HJ, Reske SN, Kreienberg R. Classification of asymptomatic adnexal masses by ultrasound, magnetic resonance imaging, and positron emission tomography. Gynecol Oncol. 2000;77:454–9.
6. Kitajima K, Murakami K, Yamasaki E, Kaji Y, Sugimura K. Standardized uptake values of uterine leiomyoma with 18F-FDG PET/CT: variation with age, size, degeneration, and contrast enhancement on MRI. Ann Nucl Med. 2008;22:505–12.
7. Nishizawa S, Inubushi M, Kido A, Miyagawa M, Inoue T, Shinohara K, Kajihara M. Incidence and characteristics of uterine leiomyomas with FDG uptake. Ann Nucl Med. 2008;22:803–10.
8. Burger IA, Scheiner DA, Crook DW, Treyer V, Hany TF, von Schulthess GK. FDG uptake in vaginal tampons is caused by urinary contamination and related to tampon position. Eur J Nucl Med Mol Imaging. 2011;38:90–6. doi:10.1007/s00259-010-1618-7.
9. Amit A, Beck D, Lowenstein L, Lavie O, Bar Shalom R, Kedar Z, Israel O. The role of hybrid PET/CT in the evaluation of patients with cervical cancer. Gynecol Oncol. 2006;100:65–9.
10. Choi HJ, Roh JW, Seo SS, Lee S, Kim JY, Kim SK, Kang KW, Lee JS, Jeong JY, Park SY. Comparison of the accuracy of magnetic resonance imaging and positron emission tomography/computed tomography in the presurgical detection of lymph node metastases in patients with uterine cervical carcinoma: a prospective study. Cancer. 2006;106:914–22.
11. Chou HH, Chang TC, Yen TC, Ng KK, Hsueh S, Ma SY, et al. Low value of [18F]-fluoro-2-deoxy-d-glucose positron emission tomography in primary staging of early-stage cervical cancer before radical hysterectomy. J Clin Oncol. 2006;24:123–8.
12. Loft A, Berthelsen AK, Roed H, Ottosen C, Lundvall L, Knudsen J, Nedergaard L, Højgaard L, Engelholm SA. The diagnostic value of PET/CT scanning in patients with cervical cancer: a prospective study. Gynecol Oncol. 2007;106:29–34.
13. Belhocine T, Thille A, Fridman V, Albert A, Seidel L, Nickers P, Kridelka F, Rigo P. Contribution of whole-body 18FDG PET imaging in the management of cervical cancer. Gynecol Oncol. 2002;87:90–7.
14. Yen TC, See LC, Lai CH, Tsai CS, Chao A, Hsueh S, Hong JH, Chang TC, Ng KK. Standardized uptake value in para-aortic lymph nodes is a significant prognostic factor in patients with primary advanced squamous cervical cancer. Eur J Nucl Med Mol Imaging. 2008;35:493–501.
15. Havrilesky LJ, Wong TZ, Secord AA, Berchuck A, Clarke-Pearson DL, Jones EL. The role of PET scanning in the detection of recurrent cervical cancer. Gynecol Oncol. 2003;90:186–90.
16. Belhocine TZ. 18F-FDG PET imaging in posttherapy monitoring of cervical cancers: from diagnosis to prognosis. J Nucl Med. 2004;45:1602–4.
17. Picchio M, Mangili G, Samanes Gajate AM, De Marzi P, Spinapolice EG, Mapelli P, Giovacchini G, Sigismondi C, Viganò R, Sironi S, Messa C. High-grade endometrial cancer: value of [(18)F]FDG PET/CT in preoperative staging. Nucl Med Commun. 2010;31:506–12.
18. Nakamura K, Kodama J, Okumura Y, Hongo A, Kanazawa S, Hiramatsu Y. The SUVmax of 18F-FDG PET correlates with histological grade in endometrial cancer. Int J Gynecol Cancer. 2010; 20:110–5.
19. Chung HH, Kim JW, Kang KW, Park NH, Song YS, Chung JK, Kang SB. Post-treatment [^{18}F]FDG maximum standardized uptake value as a prognostic marker of recurrence in endometrial carcinoma. Eur J Nucl Med Mol Imaging. 2011;38:74–80.
20. Belhocine T, De Barsy C, Hustinx R, Willems-Foidart J. Usefulness of (18)F-FDG PET in the post-therapy surveillance of endometrial carcinoma. Eur J Nucl Med Mol Imaging. 2002;29:1132–9.
21. Kurokawa T, Yoshida Y, Kawahara K, Tsuchida T, Okazawa H, Fujibayashi Y, Yonekura Y, Kotsuji F. Expression of GLUT-1 glucose transfer, cellular proliferation activity and grade of tumor correlate with [F-18]-fluorodeoxyglucose uptake by positron emission tomography in epithelial tumors of the ovary. Int J Cancer. 2004;109:926–32.
22. Iyer VR, Lee SI. MRI, CT, and PET/CT for ovarian cancer detection and adnexal lesion characterization. AJR Am J Roentgenol. 2010; 194:311–21.
23. Yoshida Y, Kurokawa T, Kawahara K, Tsuchida T, Okazawa H, Fujibayashi Y, Yonekura Y, Kotsuji F. Incremental benefits of FDG positron emission tomography over CT alone for the preoperative staging of ovarian cancer. AJR Am J Roentgenol. 2004;182:227–33.
24. Risum S, Høgdall C, Loft A, Berthelsen AK, Høgdall E, Nedergaard L, Lundvall L, Engelholm SA. Does the use of diagnostic PET/CT cause stage migration in patients with primary advanced ovarian cancer? Gynecol Oncol. 2010;116:395–8.
25. Kitajima K, Suzuki K, Senda M, Kita M, Nakamoto Y, Onishi Y, Maeda T, Yoshikawa T, Ohno Y, Sugimura K. FDG-PET/CT for diagnosis of primary ovarian cancer. Nucl Med Commun. 2011; 32:549–53.
26. Palomar A, Nanni C, Castellucci P, Ambrosini V, Montini GC, Allegri V, Pettinato C, Al-Nahhas A, Soriano A, Grassetto G, Rubello D, Fanti S. Value of FDG PET/CT in patients with treated ovarian cancer and raised CA125 serum levels. Mol Imaging Biol. 2012;14:123–9.
27. Nanni C, Rubello D, Farsad M, De Iaco P, Sansovini M, Erba P, Rampin L, Mariani G, Fanti S. (18)F-FDG PET/CT in the evaluation of recurrent ovarian cancer: a prospective study on forty-one patients. Eur J Surg Oncol. 2005;31:792–7.
28. Kim CK, Park BK, Choi JY, Kim BG, Han H. Detection of recurrent ovarian cancer at MRI: comparison with integrated PET/CT. J Comput Assist Tomogr. 2007;31:868–75.

Image-Guided Intervention in Gynecologic Oncology

7

Duan Li

Image-guided intervention in gynecologic oncology includes biopsy, aspiration and drainage, transcatheter treatment, and intraoperative guidance for surgical procedures. This chapter focuses on needle biopsy and aspiration, using ultrasound and CT guidance.

7.1 Indications and Contraindications

Needle biopsy is indicated when an undiagnosed abdominal or pelvic mass is detected, especially when malignancy (which may originate from the uterus, ovaries, peritoneum, omentum, pelvic lymph nodes, or vagina) is suspected. It is also appropriate for staging a previously identified malignancy [1]. There is significant controversy regarding the role of needle aspiration in diagnosis and treatment of cystic lesions of the ovaries and adnexa. The major concerns are potential false-negative diagnoses, tumor seeding, and peritoneal contamination. The diagnostic accuracy of needle aspiration in the diagnosis of ovarian cystic lesions does remain controversial, but concerns about peritoneal contamination and tumor seeding remain theoretic and unsubstantiated [2–5]. If solid components can be demonstrated in cystic lesions, sampling of the solid components will be helpful in increasing diagnostic accuracy (*see* Fig. 7.1) [4, 6–8].

Needle biopsy and aspiration are contraindicated if there is no safe path for the introduction of the needle, if the patient is at high risk for bleeding because of uncorrectable coagulopathy, or if the patient is uncooperative to an extent that will detrimentally influence the biopsy outcome.

Ideally, the needle path should avoid the bowels, bladder, and large vessels, but it has been reported that biopsies using a 22-gauge needle can be performed safely if the small bowel cannot be bypassed. Passing through the large bowel should be avoided because of a high risk of infection from perforation. It has also been reported that biopsy can be safely performed through ascites [1]. Some authors have acknowledged that the presence of a small amount of ascites may be helpful for ultrasound-guided biopsy of small lesions, but if there is a large volume of ascites, it should be drained before the procedure, to reduce the risk of postbiopsy hemorrhage [5, 9].

To avoid high-volume bleeding, the bleeding history of the patient and the patient's family should be carefully reviewed. Patients should be screened for the recent use of blood-thinning agents such as warfarin, heparin, adenosine diphosphate (ADP) inhibitor, and aspirin. If such a medication is currently being taken, biopsy should be delayed until the blood-thinning effect of the medication has waned. Measurements of prothrombin time (PT), activated partial thromboplastin time (aPTT), and platelet count should be obtained before the biopsy is performed. Transfusion of appropriate blood products can be used in those with severe coagulopathy. For patients with platelet dysfunction, administration of desmopressin (DDAVP) is helpful [12, 14]. If biopsy must be performed immediately despite unresolved bleeding risks, embolizing the needle track has been shown to be helpful in controlling hemorrhage [1, 13].

Sedation may be required for uncooperative patients whose motion may make accurate needle placement and withdrawal difficult.

7.2 Image Modality

In most situations, both ultrasound and CT scanning can be used for percutaneous needle biopsy and aspiration. The choice will be influenced by tumor size, location, physician and patient preference, the skills of the doctor, and available equipment (*see* Fig. 7.2) [9–11].

D. Li, MD
Department of Radiology,
Memorial Sloan-Kettering Cancer Center,
1275 York Avenue, New York, NY 10065, USA
e-mail: lid1@mskcc.org

O. Akin (ed.), *Atlas of Gynecologic Oncology Imaging*, Atlas of Oncology Imaging,
DOI 10.1007/978-1-4614-7212-4_7, © Springer Science+Business Media New York 2014

Ultrasound-guided biopsy is more cost-effective than CT-guided biopsy because it usually requires less time to perform. The benefits of ultrasound guidance include the lack of radiation exposure, readily available and portable equipment, relatively low equipment cost, and flexibility as to the anatomic plane. The two outstanding features of ultrasound biopsy are real-time visualization of needle placement and color Doppler visualization of blood vessels, allowing the physician to avoid vessels in the needle path (*see* Fig. 7.3). The primary disadvantage is an inability to visualize lesions behind bone or gas-filled bowel [9].

CT can provide excellent spatial resolution of targeted lesions. CT offers accurate imaging of the needle tip and is able to visualize deep lesions that ultrasound cannot reach [10, 11]. Historically, CT guidance has not provided continuous visualization of needle insertion, but within the past decade, CT fluoroscopy has provided real-time needle-positioning guidance, reducing procedure time and patient radiation exposure [15].

7.3 Procedure Approach

Biopsies of gynecologic lesions can be percutaneous (transperitoneal or transgluteal) or transvaginal. Although a percutaneous approach is preferred, the vagina provides a less harmful point of entry when no safe path is available. Transvaginal entry provides the most direct path to the pelvic organs (*see* Fig. 7.3). The disadvantage is a relatively small field of vision and increased risk for infection because the vagina is at best a semisterile field. When biopsy of a predominantly cystic lesion is performed using transvaginal approach, the fluid components should be aspirated completely before solid tissue samples are obtained; this procedure will decrease the likelihood of superinfection of residual cystic contents and will also increase the yield of solid material with biopsy [5].

There are two basic kinds of needle biopsy: fine-needle aspiration (FNA) and core biopsy. FNA uses a 20- or 22-gauge needle and provides cells for cytology study. It is most commonly used for staging. Core biopsy uses trucut needles (commonly 18-gauge) and provides a greater amount of tissue. It is most often used for primary diagnosis. Whenever a core biopsy is performed, a tissue sample should be swabbed on the slide so that the on-site cytologist can evaluate the adequacy of the biopsy. This process is known as "touch-prep." [16]. Core biopsies are performed with a single needle or through an introducer needle, in a coaxial manner (*see* Fig. 7.4). Use of an introducer needle makes it possible to obtain multiple samples without repositioning the access. In patients with high risk of bleeding, the needle track can be embolized with foam gel via the introducer needle [13].

7.4 Technique

Biopsies are usually performed in an outpatient setting. Before the procedure, the benefits, alternatives, and risks should be explained to the patient and informed consent should be obtained. The patient's medical history, medication list, and coagulation studies should be carefully

reviewed. A planning briefing involving the performing physician, nurse, and technologist makes for an efficient procedure. Intravenous access should be established before the biopsy procedure so that fluid or medication can be provided as required. A sedative-analgesic combination such as midazolam and fentanyl is recommended for sedation. Local anesthesia can be administrated after the skin is cleaned and draped. The probe can be sterilized either by using a sterile probe cover or by directly sterilizing the probe with Betadine (povidone-iodine). Sterile gel is commonly used as an acoustic coupling agent for ultrasound guided procedures.

Both FNA and core biopsies can be performed freehand or using a needle-guidance device (*see* Fig. 7.5). With freehand technique, the needle is independently directed into the target under ultrasound visualization. This technique provides greater flexibility in making subtle adjustments to the needle path. It also makes it possible to coordinate needle placement with the patient's respiration. Needle guidance systems are designed to provide proper needle placement at preselected angles and depths. This can decrease the time required for needle placement, especially in the hands of an inexperienced operator [17].

Transvaginal biopsy is performed with patient in lithotomy position. Because the patient's discomfort during simple aspiration biopsy is minimal, most procedures can be performed without intravenous sedation. In our experience, however, providing sedation can decrease the patient's anxiety and discomfort, especially for core biopsy. It also can increase the patient's acceptance of the procedures. The perineum and vaginal vault are sterilely cleaned with Betadine. Intravenous antibiotics (1 g of ampicillin, 80 mg of gentamicin, and 1 g of clindamycin) can be administered prior to the procedure. Some authors have suggested that patients receive a 5-day course of clindamycin (30 mg every 6 h) after the procedure [5]. The probe should be covered with a sterile probe cover. A needle guidance device should be used to provide accurate needle insertion and to prevent injury of the vaginal wall (*see* Figs. 7.6 and 7.7).

When a transvaginal approach is used for biopsy, the ultrasound probe should be placed in the vaginal fornix as close to the lesion as possible. The space between the fornix and the lesion should be carefully examined to avoid penetrating other structures such as the bladder, the bowels, or vessels. Because it is usually not possible to adequately anesthetize the needle insertion site with local anesthesia, it is important to minimize needle manipulation while accessing the lesion. A short, rapid forward thrust of the needle is helpful in penetrating the vaginal muscle.

Seeing the needle clearly is the most important factor in the success of an ultrasound-guided biopsy. A combination of four techniques helps to make the needle visible: aligning the needle parallel to the center plane of the transducer (*see* Fig. 7.8); using a needle whose tip is especially visible under ultrasound; being careful to position the needle so that the bevel is pointed upward, increasing reflection; and using a single focal zone placed in near-field setting. Trumping all of these is experience, however.

Once the needle reaches the target area, jiggling the needle will trap the cellular material inside the lumen of the needle. Depending on the biopsy being performed, some doctors like to use a syringe to suck out a maximum amount of cellular material.

7.5 Complications

Image-guided needle biopsy is widely accepted as a safe method to obtain tissue diagnosis. Several multicenter reviews have reported major complication rates of 0.05–0.19 %. The mortality rate is reported at 0.008–0.038 % [18–20]. The difference between large-caliber needles and small-caliber needles in complication rates is not statistically significant [19].

Hemorrhage is the most common complication. If bleeding is suspected after biopsy in an otherwise hemodynamically stable patient, CT should be performed. Other major complications include infection, peritonitis, and needle track seeding. Even through needle track seeding after biopsy has been reported [18], it is so rare (0.003 %) that in most cases it should not influence the decision to perform biopsy. Minor complications often include pain and vasovagal reaction [18, 19, 21].

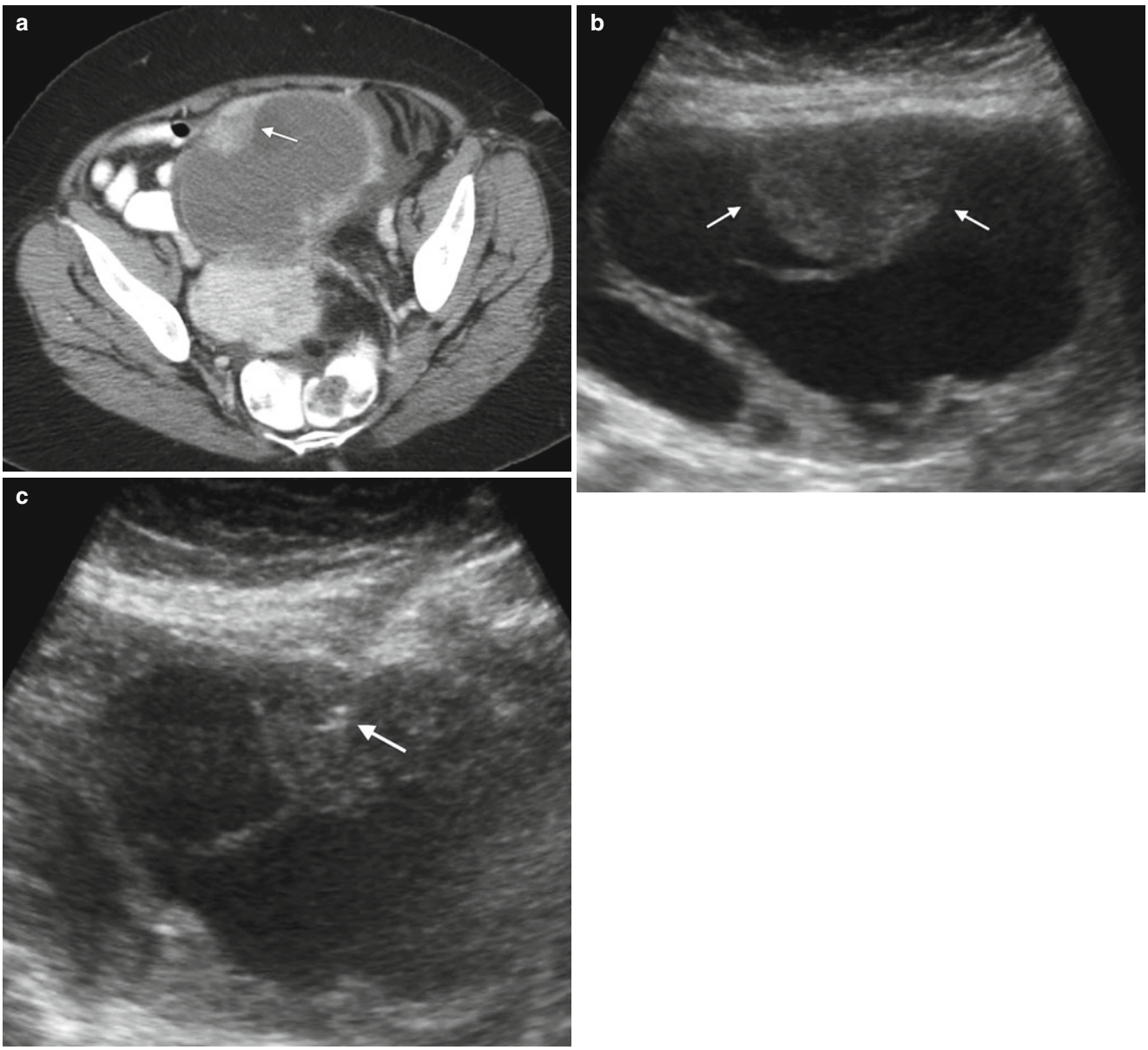

Fig. 7.1 A predominantly cystic pelvic mass containing mural nodularity is detected on contrast-enhanced CT (**a**) and ultrasound (**b**). For an accurate diagnosis, the needle must target the solid component of the mass (as shown in **c**), rather than the fluid component

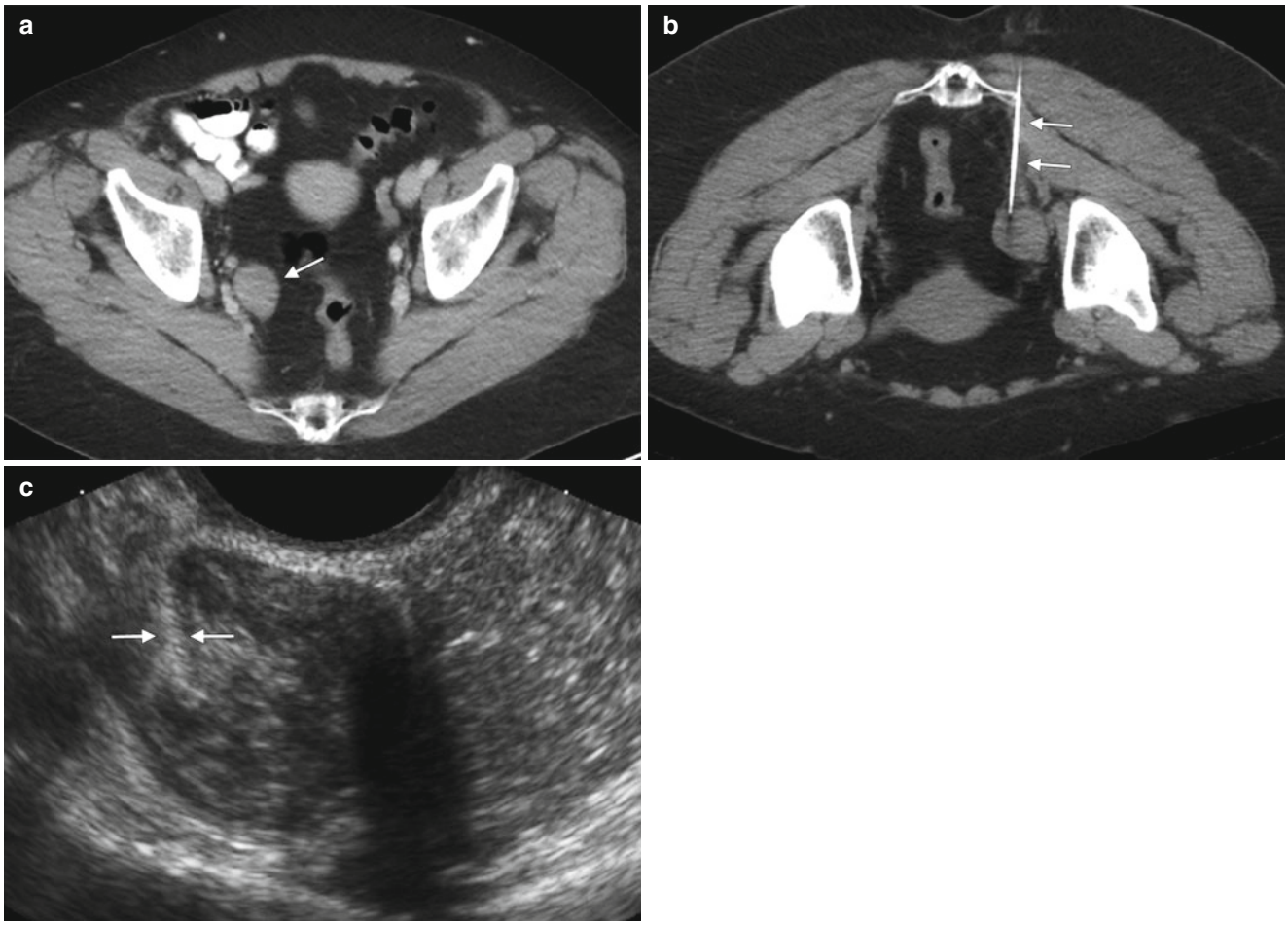

Fig. 7.2 (**a**) CT scan of a patient with ovarian cancer who previously underwent total abdominal hysterectomy and bilateral salpingo-oophorectomy. This followup CT scan demonstrates a right-sided pelvic mass. (**b**) In the same patient, CT-guided percutaneous biopsy is performed with the patient in a prone position. The needle is inserted via a posterior approach and is placed into the mass. (**c**) In the same patient, a transvaginal approach offers a more direct path to the mass. The needle track is seen between the *arrows*

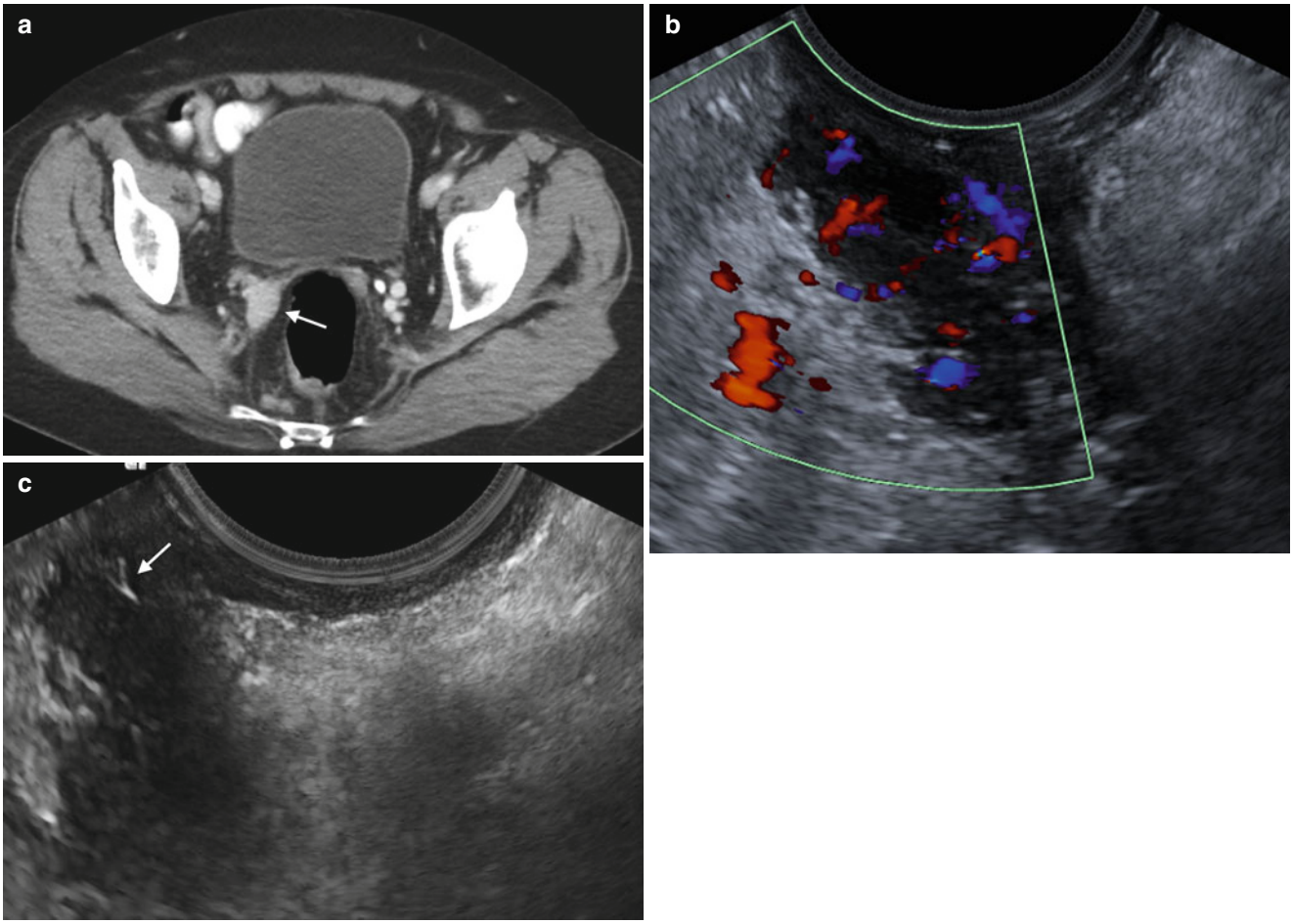

Fig. 7.3 (**a**) A contrast-enhanced pelvic CT scan shows a solid mass in the vaginal wall. (**b**) In the same patient, a transvaginal ultrasound shows a hypoechoic mass in the same location. A color Doppler image demonstrates increased internal vascularity. (**c**) This image of an ultrasound-guided transvaginal biopsy shows the needle inside the mass (*arrow*), which proved to be non-Hodgkin's lymphoma. The benefit of the transvaginal approach can be seen by comparing **a**, **b**, and **c**: A transvaginal biopsy avoids passage through the bowel and bladder with an anterior approach, and avoids the sciatic nerve and vessel with a posterior approach

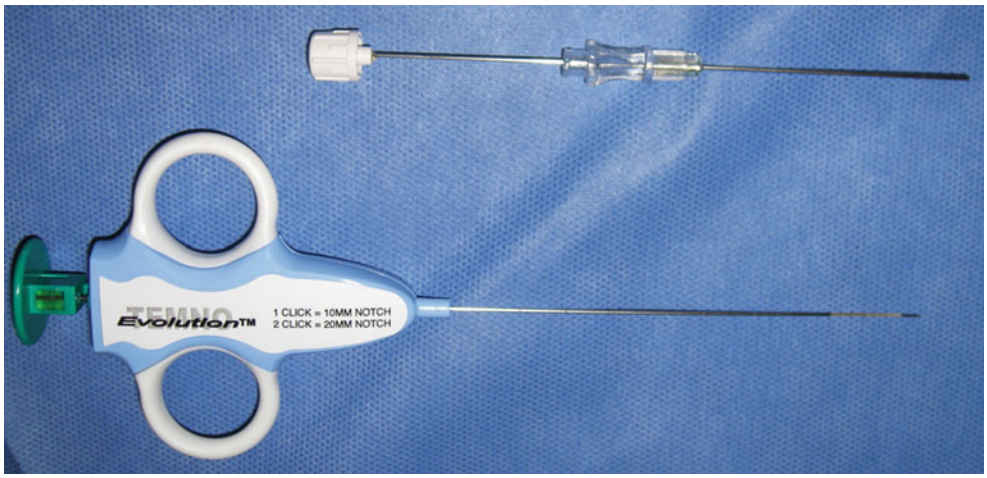

Fig. 7.4 The introducer needle for a core biopsy (*top*). Once the needle in inserted into the peripheral portion of the target, the stylet (the inner portion of the needle) is withdrawn and the longer needle (with handle, *bottom*) is inserted into the mass

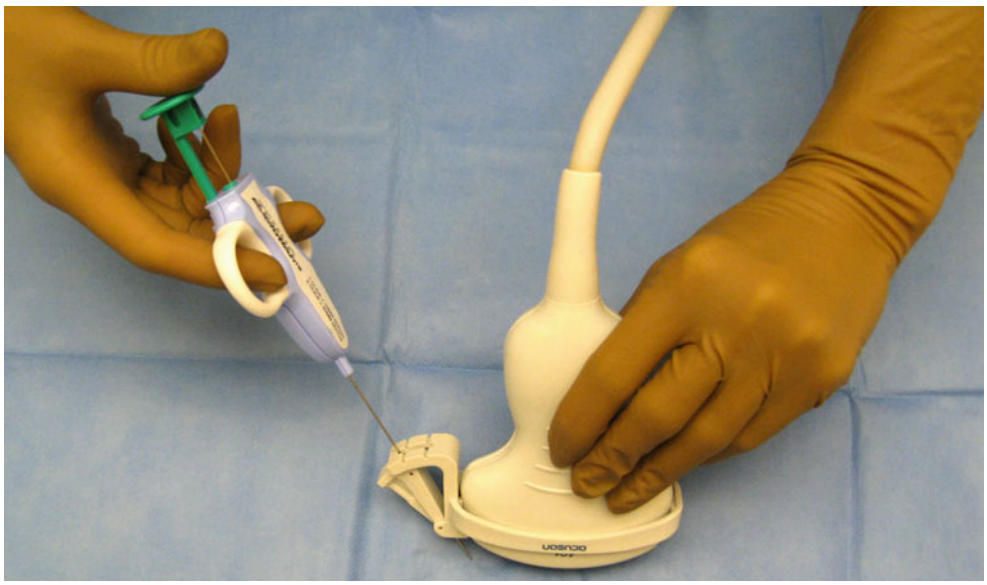

Fig. 7.5 Ultrasound-guided percutaneous biopsy. The core needle is passed through the needle guide attached to the transducer

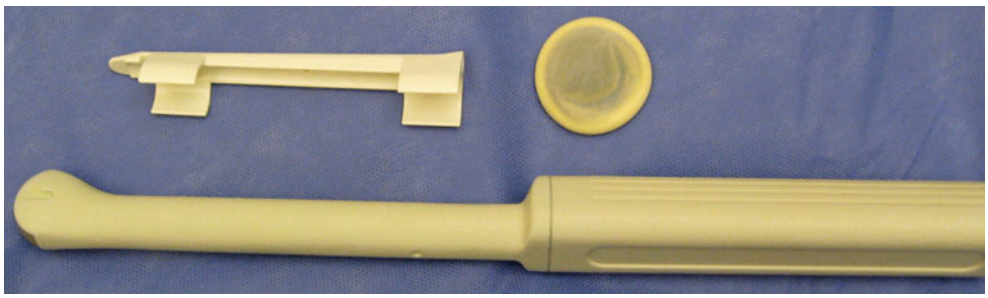

Fig. 7.6 A transvaginal transducer, with needle guide and probe cover

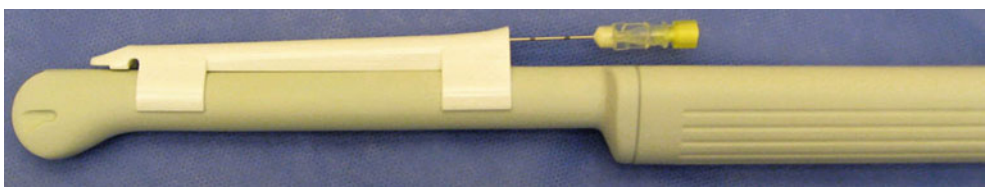

Fig. 7.7 After the guide is attached to the transducer, the transducer is inserted into the vagina; then the needle is inserted into the guide

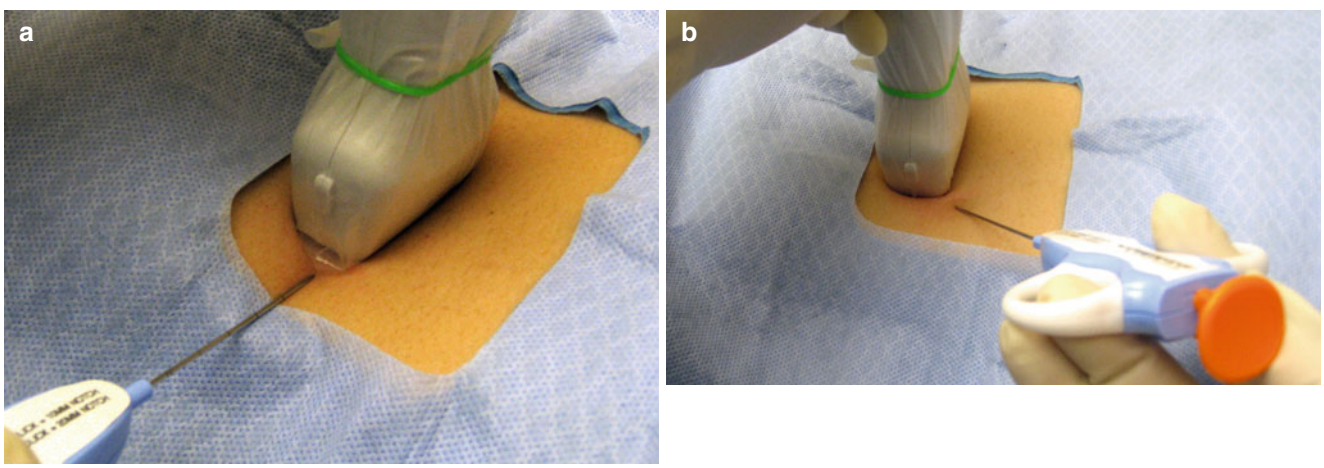

Fig. 7.8 (**a**) Accurate alignment of the needle with the transducer. (**b**) Inaccurate alignment: the needle is off center relative to the transducer. (**c**) Inaccurate alignment: the needle is in the center of the transducer, but angled off to one side

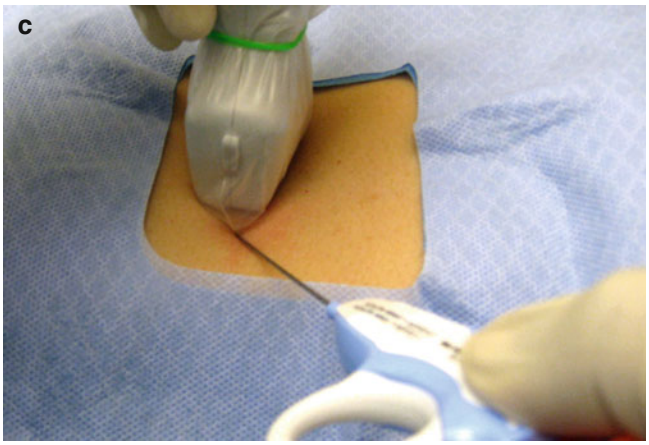

Fig. 7.8 (continued)

References

1. Thomas DA, et al. Ultrasound-guided biopsy and drainage of the abdomen and pelvis. In: Rumack CM, Wilson SR, Charboneau JW, et al., editors. Diagnostic ultrasound. 3rd ed. Philadelphia: Elsevier/Mosby; 2005. p. 625–55.
2. Ganjei P, Dickinson B, Harrison T, Nassiri M, Lu Y. Aspiration cytology of neoplastic ovarian and non-neoplastic ovarian cysts: is it accurate? Int J Gynecol Pathol. 1996;15:94–101.
3. Wojcik E. Fine needle aspiration cytology of cystic ovarian lesions. Diagn Cytopathol. 1994;11:9–14.
4. Zanetta G, Lissoni A, Franchi D, Pittelli MR, Cormio G, Trio D. Safety of transvaginal fine needle puncture of gynecologic mass: a report after 500 consecutive procedures. J Ultrasound Med. 1996;15:401–4.
5. O'Neill MJ, Rafferty EA, Lee SI, Arellano RS, Gervais DA, Hahn PF, Yoder IC, Mueller PR. Transvaginal interventional procedures: aspiration, biopsy, and catheter drainage. Radiographics. 2001;21:657–72.
6. Belinson JL, Lynn JM, Papillo JL, Lee K, Korson R. Fine needle aspiration cytology in management of gynecologic cancer. Am J Gynecol. 1981;19:148–53.
7. Hajdu SI, Melamed MR. Limitations of aspiration cytology in the diagnosis of primary neoplasms. Acta Cytol. 1984;28:337–45.
8. Bandyopadhyay A, Chakraborty J, Chowdhury AR, Bhattacharya A, Bhattachrya P, Chowdhury M. Fine needle aspiration cytology of ovarian tumors with histological correlation. J Cytol. 2012;29:35–40.
9. Griffin N, Grant LA, Freeman SJ, Jimenez-Linan M, Berman LH, Earl H, et al. Image-guided biopsy in patients with suspected ovarian carcinoma: a safe and effective technique? Eur Radiol. 2009;19:230–5.
10. Hewitt MJ, Anderson K, Hall GD, et al. Women with peritoneal carcinomatosis of unknown origin: efficacy of image-guided biopsy to determine site-specific diagnosis. BJOG. 2007;114:46–50.
11. Layfield LJ, Gopez EV. Percutaneous image-guided fine needle aspiration of peritoneal lesions. Diagn Cytopathol. 2003;28:6–12.
12. Silverman S, Mueller P, Pfister R. Hemostatic evaluation before abdominal interventions: an overview and proposal. AJR Am J Roentgenol. 1990;154:233–8.
13. Smith TP, McDermott VG, Ayoub DM, et al. Percutaneous transhepatic liver biopsy with tract embolization. Radiology. 1996;198:769–74.
14. Peter FW, Benkovic C, Muehlberger T, Vogt PM, Homann HH, Kuhnen C, et al. Effects of desmopressin on thrombogenesis in aspirin-induced platelet dysfunction. Br J Haematol. 2002;117:658–63.
15. Sheafor DH, Paulson EK, Kliewer MA, DeLong DM, Nelson RC. Comparison of sonographic and CT guidance techniques: does CT fluoroscopy decrease procedure time? AJR Am J Roentgenol. 2000;174:939–42.
16. Hahn PF, Eisenberg PJ, Pitman MB, et al. Cytopathologic touch preparation (imprints) from core needle biopsies: accuracy compared with that of fine needle aspirates. AJR Am J Roentgenol. 1995;165:1277–9.
17. Phal PM, Brooks DM, Wolfe R. Sonographically guided biopsy of focal lesions: a comparison of freehand and probe-guided techniques using a phantom. AJR Am J Roentgenol. 2005;184:1652–6.
18. Smith EH. Complications of percutaneous abdominal fine-needle biopsy. Radiology. 1991;178:253–8.
19. Welch T, Sheedy PI, Johnson C, et al. CT-guided biopsy: prospective analysis of 1,000 procedures. Radiology. 1989;17:493–6.
20. Nolsoe C, Nielsen L, Torp-Pedersen S, et al. Major complications and death due to interventional ultrasonography: a review of 8,000 cases. J Clin Ultrasound. 1990;18:179–84.
21. Livraghi T, Damascelli B, Lombardi C, Spagnoli I. Risk in fine-needle abdominal biopsy. J Clin Ultrasound. 1983;11:77–81.

Index

O. Akin (ed.), *Atlas of Gynecologic Oncology Imaging*, Atlas of Oncology Imaging,
DOI 10.1007/978-1-4614-7212-4, © Springer Science+Business Media New York 2014